ALMA MATER STUDIORUM - UNIVERSITÀ DI BOLOGNA

FACOLTA' DI INGEGNERIA

CORSO DI LAUREA IN INGEGNERIA CIVILE

DISTART

Dipartimento di Ingegneria delle Strutture, dei Trasporti,
delle Acque, del Rilevamento, del Territorio

TESI DI LAUREA

in

PROGETTO IN ZONA SISMICA

MODELING OF CONDUCTORS IN ELECTRICAL EQUIPMENT & SENSITIVITY STUDIES

CANDIDATO:
Benassi Andrea

RELATORE:
Chiar.mo Prof. Ing. **Tomaso Trombetti**

CORRELATORI:
Prof. Ing. **Andrei M. Reinhorn**
Dr. Ing. **Stefano Silvestri**

Anno Accademico 2008/09

Sessione III

ABSTRACT

It has been reported that the presence of flexible conductors between electrical equipment during an earthquake might be responsible for generating destructive forces at the top of such apparatus. The purpose of this study is to investigate the effect of interaction between two equipment items connected by a cable conductor, through a finite-element model describing the dynamic behavior of flexible conductors interconnecting electrical equipment items.

The first part of this study consists in modeling previous experimental tests of a cable conductor only, already present in literature. The sensitivity of the modeling to the various parameters affecting the solution is specifically checked. The initial compression in the cable coming from the static loads is found to be the most significant parameter to evaluate the accuracy of the model for the dynamic analysis. If the analytical and actual values are close, it is reasonable that the finite-element model will provide an adequate approximation of the dynamic behavior of the cable. The biggest errors related to the initial compression are directly caused by overestimated values of the bending stiffness. Compression can shift the natural frequencies, changing the dynamic properties of the cable. The model implementing an adequate variable bending stiffness reproduces the experimental results with an average error of 4.8%: the model simply considering a constant bending stiffness shows an average error of 16.2%.

The second part of this report aims to model the dynamic behavior of a flexible conductor interconnecting two electrical equipment items modeled through equivalent beams: a very large range of interconnected systems can be analyzed simply changing the structural properties of these beams. Some ground motions are applied to the base of the structure, and different initial shapes of the cable are assumed. The cable is redistributing the horizontal forces from the more affected element to the less affected. In the vertical direction both the equipment items are more severely tested in the interconnected configuration, due to the vertical inertia provided by the cable. The moment at the base of the two cantilevers generated by the axial force in the cable has the same order of magnitude of the moment due to the seismic response of the equipment itself.

It is suggested to design flexible connections so that the range of natural frequencies at which they are likely to be excited are different from those of the equipment they are interconnecting, in order to avoid the risk of dynamic interaction and resonance between them.

AKNOWLEDGEMENT

The author greatly appreciates the essential support of Boneville Power Administration and the California Energy Commission (California Institute for Energy and Environment for the California Energy Commission) for the financial support provided to University at Buffalo – the State University of New York during the development of this project. This entire work has been developed and completed at the State University of New York at Buffalo, under the supervision of local professorial staffs and making use of its laboratories and facilities.

The support of Prof. M. Sivaselvan from University of Colorado at Boulder is also gratefully acknowledged. Special thanks are due to Mr. J.-B. Dastous of Hydro-Québec Research Institute for providing a large number of information on his previous studies and results, and for invaluable assistance in the use of his subroutine for the finite-element program FEAP. The writer expresses his sincere appreciation to Prof. A. Filiatrault of State University of New York at Buffalo, for his assistance in looking insight some specific issues regarding the cable dynamics. Special thanks must be also given to all the graduate students of State University of New York at Buffalo that supplied information and data about the qualification tests and other studies on the high-voltage substation electrical equipment items.

TABLE OF CONTENTS

LIST OF FIGURES

LIST OF TABLES

CHAPTER 1

INTRODUCTION

1.1 Introduction

1.1.1 Background

Cables forming tension-loaded structural members are found in nearly all branches of engineering. They are widely used in structural engineering: they cannot be only used singularly, but also composing different and more complex systems. Cables structures are mainly divided into two categories: suspended structures and braced structures. Suspended structures can be subdivided into single curvature structures (all the cables are parallel), double cable structures (cables with different curvature in the same plane) and double curvature structures (or anticlastic, with cables owning different curvatures crossing each other). Braced structures typically use either vertical or inclined compressed columns, to which straight cables bearing the deck are attached.

Suspended cables can be used to cover very big distances, thus they are commonly used for suspension bridges, where they have to stand the deck and the traffic loads. Since the traffic loads are very variable, in order to avoid changes of configuration in the cables, the deck is a rigid plane; therefore the load transmitted to the cables remains constant. Other suspended cable structures are used for suspended roofs, especially for big spans.

Another fundamental field where cable are widely used is electrical engineering: they are the transmission lines with which the electricity is carried from the power plants to the single users, passing through electrical substations. An electrical substation consists of a complex set of equipment items that are interconnected through conductor buses or cables. Many equipment items in electrical substation are connected to each other by flexible conductors, typically cables made of braided aluminum wire strands. These flexible conductors are single cables, just like those used for suspension bridges or suspended roofs: therefore, the same calculation methods

can be applied. As well as for the other cable structures, they can be either pre-stressed or non-prestressed: in this case, we will talk about either slack or tight cables.

1.1.2 Purpose of the Study

It has to be noted that the classical theory of cables, which calculation methods are based on, completely neglects their bending rigidity, and takes account only for the axial internal forces. Despite the low values of their bending rigidity, in comparison with the axial stiffness, the cables are capable of transmitting moments too, indeed. Since this aspect has been neglected up to now by most of the researchers, the influence of bending stiffness in the static and dynamic behavior of cables has not been fully investigated. The present work aims to achieve a more realistic description of the mechanics of cables, thanks to accounting for the bending stiffness of the cable. This means that the behavior is something intermediate between the classical beam theory and the classical cable theory.

It has been reported that the presence of flexible conductors between equipment experiencing a differential displacement during an earthquake might be responsible for generating destructive forces at the top of such apparatus. Since these events, many works have been involved to investigate the effect of dynamic interaction between two equipment items connected by a cable conductor. In order to understand it, this work aims to take fully account for the dynamic behavior of single cables, also considering their bending stiffness, even if relatively low.

The purpose of this study is to describe the dynamic behavior of flexible conductors owning some bending stiffness and interconnecting electrical equipment items, in specific configurations under given boundary conditions and base motions. To do this, we want to reproduce through finite-element models experimental tests already done in the past, as well as experimental tests not yet done, but likely to be done in the future.

1.1.3 Organization of the Present Work

The first part of this study presents the classical theory of flexible cables owning no bending stiffness. A generic survey about cables is provided, as well as an historical background about them. Some case studies are developed providing both the theoretical approach and numerical examples. This first part is necessary in order to create a theoretical background on which basing

the further developments that are the inclusion of some bending stiffness and the extension of the study from the statics to the dynamics of cables.

The second part of this study is based on the specific problems involving dynamics of flexible wrapped cables used as conductors in electrical substations. The first step consists in modeling previous sine-start and frequency-sweep experimental tests of a cable conductor only, already present in literature. After the model is validated by comparing its results with the experimental ones, the sensitivity of the modeling to the various parameters affecting the solution is specifically checked: through these analyses, it's possible to understand what the cable dynamics depends primarily on. Therefore, a benchmark model common for all the experimental tests wanted to be reproduced can be built by setting all the parameters equal to the values that are found to guarantee a stable and accurate solution under any specific configuration. Owning this tested and reliable model, the second part consists of reproducing the dynamic behavior of two electrical equipment items interconnected at their tops by a flexible wrapped conductor, subjected to different ground motions. Every equipment item, as well as the cable, is modeled through equivalent beam: since the flexibility of the model, a very large range of interconnected systems can be analyzed simply changing the structural properties of the equivalent beams representing the equipment items. Some ground motions are applied to the base of the structure, and the response of the system is computed. Different initial shapes of the cable are assumed for different tests experienced: depending on the ground motion, the cable can be either slack or straight, in order to accommodate or not the required displacement at the two ends of the cable. For all these tests, comparison are made between the response of the two equipment items in the interconnected and in the standalone configuration, to understand the influence of the presence of the flexible connection on the forces generated and the displacements experienced.

CHAPTER 2

GENERAL DISCUSSION ABOUT FLEXIBLE CABLES

2.1 Introduction

Cables are one-dimensional supporting system: such systems can also be called line supporting structures. They are large in one dimension and small in the other two. The material is concentrated along either a straight or a curved line. A flexible cable is such a line supporting system. The required cross section tends to zero as the tensile strength of the material increases. Due to their lack of rigidity in bending, all pure cable structures are subject to comparatively large ranges of deformation under varying loads. The reason for this is that a state of equilibrium can only be achieved through finite deformations. In contrast to conventional structures, primarily subject to bending, it must be considered equilibrium of deformed structures.

A cable can be idealized as a continuous series of discrete elements bounded each other through hinges, just like a chain. Every element of the cable is free to rotate under a load, but no bending moments can be transmitted from one element to another. An element with pure cable behavior, that means without any bending stiffness, can only be subject to traction forces. In a section of the cable, the shear due to the external loads is equilibrated by the vertical component of the internal traction force; the external moment is balanced by the internal moment provided by the horizontal component of the internal traction force times the vertical distance between the section and the restraints.

Components subjected either to bending or compression must be first be given a shape. Flexible tension-loaded components automatically assume an equilibrium shape most suited to transmission of forces and moments. Shape and structure are largely one entity in such a flexible tension-loaded system. A cable is understood to be any support system that can be loaded by tension but is very flexible. A cable is a linear (one-dimensional) supporting system, large in one direction and small in the other two. Cables are deformable structural elements. The shape assumed under external loads depends on the type and intensity of the load itself. When a cable is simply undergoing a traction force at its ends, it assumes a straight configuration. When a

cable undergoes a series of concentrated loads, it assumes a deformed shape consisting of a series of straight segments. When a cable undergoes a distributed load, the deformed shape is a continuous curve. A cable under its dead weight assumes the so-called catenary curve. For uniformly distributed loads, the following shapes are possible: catenary shape (for vertical loads uniformly distributed along the cable), parabolic shape (for vertical loads uniformly distributed along the horizontal axis), cubic shape (for vertical loads linearly distributed along the horizontal axis) and circular shape (for loads at right angles to the curve formed by the cable, uniformly distributed along the cable axis). This physically explains the relationship between the geometrical shape and the applied loads; the cable automatically assumes a natural shape under every applied load.

Different forces either coplanar or forming a spatial system can act on a cable. In the former case the cable lies in the plane; in the latter, the cable forms a three-dimensional curve.

A cable is able to transmit load to the restraints only thanks to change of its shape, since it doesn't own any shear of bending stiffness; therefore, a cable can also be called a variable geometry element. The significant changes of geometry, due to load variations, are mainly responsible for the non-linear geometrical behavior of cables. This non-linear behavior is a hardening type, where the stiffness increases with the displacements. Suspended structures can be divided into two different classes: discrete structures (cables) and continuous structures (membranes). Cable structures can be subdivided in three more classes: single cables (mono-dimensional structures coplanar with the loads), cable beams (pre-tensioned cables, with different curvatures, coplanar with the loads) and cable nets (pre-tensioned cables, with different curvatures, and perpendicular loads).

The entire mechanics of cable structures is influenced by the sag/span ratio. For high values of the sag/span ratio, the internal forces are only slightly influenced by sag variations. For small values of the sag/span ratio, the internal forces are highly influenced by sag variations. The forces inherent the cable depend on the central sag and the span of the system, as well as the value and position of the applied loads. The higher the central sag value is, the less the forces at the ends of the cable are. A catenary cable always changes its deformed shape when the external load varies. If the shape of the cable undergoing its dead weight differs from the catenary shape,

there will always be bending moments inherent the structure. It is obvious that it's possible only if the cable owns some bending stiffness.

In order to take advantage of the optimal characteristics of suspended cables, it is mandatory limiting the displacements by means of geometrical stabilization methods. Cable structures can be stabilized in different ways: introducing rigid elements, introducing permanent weights bigger than the accidental ones, introducing secondary cables providing a pre-tension state. Simple slack cables are, in view of their greatly variable deformations, used in structural engineering as supporting elements only if stabilized by supporting members rigid in bending or by large permanent loads in comparison with which the useful loads are negligible. A non-pretensioned structure usually requires a comparatively high constant load for stabilization, in order to maintain the shape of the structure in the presence of negative loads (wind suction) or reduce the deformations to a minimum.

Cables are widely used in structural engineering, since suspended cable structures can cover big spans. Given the span and the loads, all the problems involved in the design of their geometry are related to the sag/span ratio. Furthermore, simple suspended cables are particularly sensitive to vibrations due to wind effect; therefore, specific measures have to be taken. For example, the traction forces inherent the cable can be checked, since the eigenfrequencies of the cable depend on its internal traction, or bracing system can be added. Double cable structures are primarily designed to control the vibrations due to wind effect, which can be extremely dangerous for simple cable structures. A double cable structure usually consists of two pre-tensioned cables bounded each other through either tensioned or compressed trusses. These structures create big traction forces on the restraints that have to be carefully designed. The dynamic behavior of such structures is extremely interesting. Since the eigenfrequencies of the cables depend on the internal traction, and the two cables have different internal forces due to the external loads and their geometry, they have slightly different natural frequencies too. When an external force induces vibrations in both cables matching the first natural frequency of one cable, the other will damp this effect, since it has a different eigenfrequency. This implies that every vibration is damped, because neither cable can be excited in resonance thanks to the damping effect of the other. Nevertheless, the system consisting of the two connected cable will have its own

eigenfrequencies. The first natural frequency of the total system is function of the two single frequencies, and is higher than both.

Many common cable structures, used both for building and bridges, include also rigid beams and columns. A series of straight cables stand a horizontal rigid beam, and they are attached to one or more compressed columns. This structural system can cover big span without any curve cable. The load is divided between the straight cables and the rigid beam, whose length covers the whole span. The number of cables depends on the dimension and flexural stiffness of the rigid element. The cables have to be very close each other if the rigid beam is slender, otherwise a less number of them can be used if the beam is stiffer. In such a system, cables are always subject to tension. Too small angles between the cables and the rigid beam must be avoided, because they could involve extremely high forces inherent the cables.

2.2 Historical Development of Tension-Loaded Structures

Through the human history, men have always been inspired by nature: every achievement in scientific progress has been possible observing the natural examples found around us. The same process governed the historical development of light tension-loaded structures built by men, which can be seen in living structures owning a much higher performance level.

In nature, tension-loaded systems are found in animal bodies: such systems are sinews, muscles and skins. Therefore, the first ever human-made tension-loaded structures were probably tent-like, made of animal skins or thin wood branches. Soon after, the first improvements were available thanks to the invention of knotting and weaving: these techniques made possible fabric more complex and resistant tents, as well as fishing nets and sails. Nets and fabrics were made of vegetal fibers extracted from plants for thousands of years: their strength has been surpassed only in the 20^{th} century by the introduction of steel cables.

The first surface tension-loaded structures were tents: their mechanics is based on the flexible animal skins they are made of, which can stand large stresses. The first type of tent was the pointed tent, consisting of a central mast, surrounded by a membrane with a conical shape. A

different version consists of two masts and looks like a gable roof. Over the centuries only simple variations of these basic types have been used.

Large circus tents achieved their classical shape only relatively late, at the end of the 19th century. In their most common version, they have four large masts distributed along the edge of the arena, from which the center of the circular tent is attached, with inclined beams supporting the membrane above the arena. The large spans covered and the high membrane stresses developed make necessary the reinforcement of the fabric at the critical point by sewn-on ropes.

Ship sails were studied and improved separately from tents and net structures: fundamental impulse to the development of sail-making became possible only thanks to achievements in aerodynamics and in the design of membranes. However, apart from yacht racing, incentives for further developments are lacking since the end of the 19th century, due to the introduction of engine-powered ships.

Only few available data and records have survived until nowadays, but it can be assumed that important designs of net and membrane structures were already known in ancient times. Unfortunately, no significant progress has been attained in this state of technology since the Middle Ages. In contrast to compression- and bending-loaded structures, tension-loaded structures are a development of the second half of 20th century.

Another engineering field where cables have been used are suspension bridges. Long ago, the ropes of these bridges required to be renewed very frequently, since they were made of plant fibers, thus with a limited service life. The introduction of steel cables made possible to overcome this problem related to service life of suspension bridges. The first cable suspension bridges of this kind appeared in Great Britain around 1816, using wrought-iron chains.

The further development in bridge building was the switch from single cable to multi-cable suspension bridges. Two different solutions could be adopted for the pathway: it was following along the catenaries, but it could either placed directly on the cables or suspended underneath them.

Later on in the 19th century, the early level roadways were built, with the roadway separated from the main structure: the structure design was quite different, since the roadways didn’t

follow along the catenaries, but were suspended from the cables. This design allowed spans much larger than before.

The large-span suspension bridges have been built for a long time until now, with only slight variations. One of the first most important designers of gravity suspension bridge was John Roebling, whose main works are the Ohio Bridge in Cincinnati and the Brookling Bridge in New York. His technique consisted of cable nets forming vertical surfaces connecting the suspension cables (not pre-assembled but spun in place) and a rigid roadway. The perfection achieved by Roebling influenced all the other designers of large suspension bridges.

Only in the late 1960s suspension bridges were designed with a newer technique: from three up to four cables were used to form a three-dimensional pre-stressed system, useful to reinforce highly-stressed bridges and reduce the deformations. This pre-stressed three-dimensional cable system was also designed to brace laterally the bridges and to prevent lifting and twisting due to wind suction.

In the 20th century cable structures began to be used for a completely new kind of buildings: roofs were suspended from cables, just like bridges. Suspended roofs gave start to a research field quite different from suspension bridges. Their main problems were related to the much lighter weight, due to the smaller loads acting on them. As a matter of fact, they are much more sensitive to lifting and twisting by wind suction than heavy bridge, because of their low dead weight. Nevertheless, they are much less affected by danger of aerodynamic instability than suspension bridges.

One of the first master in suspended roofs design was Shuchov: his works in Nizhni Novgorod have been the first surface structures in which roof membrane and main structure cooperate forming one unit. Shuchov can be considered as the father of the structural-steel method that extended the secular technique used to build tents during the last centuries.

In the early 1930s in Paris Lafaille designed sheet-metal shell structures, as well as tension-loaded roofs some years later. At the same time, in various U.S. states (New York state, Missouri, …) modern tension-loaded surface structures were developed attempting to roof large grain silos with steel sheeting of simple curvature.

A new phase of development was represented by pneumatic membranes, arches stabilized by pre-tensioned cable nets, edge cables and edge supports used for non-prestressed cable structures: the main examples of these structures are Nowicki's Raleigh Arena (1950) and the works of Severud and Deitrick in 1953. All these structures, as well as pre-stressed centrally supported surface structures were surveyed by Otto Frei in the early 1950s for the first time.

Soon after, the design of suspended roofs received a further noticeable impulse. Since 1960 large tension-loaded surface structures were built all over the world. Among them, the most significant examples are the Schwarzwald Hall (Karlsruhe), the swimming pool in Wuppertal and the Westphalian Hall (Dortmund) in Germany, the Rio Grande do Sul Pavilion (Sao Paulo, Brazil), the Olympic gymnasiums (Tokyo, Japan), the Sydney Meyer Music Bowl (Melbourne, Australia) and the Yale Hockey Rink (New Haven), the Dulles Airport (Washington D.C.) and the auditorium in Utica in the U.S.A.

CHAPTER 3

CASE STUDIES AND NUMERICAL EXAMPLES

In this chapter, three numerical examples are shown. The first is about a classical cable, without any flexible stiffness, undergoing a concentrated load at the middle of its span and a pre-tension force at its ends. The deflection caused by the external force and the pre-tension is investigated. The second consists of a classical cable undergoing its dead weight: this kind of structural element is also called as "catenary". The third example shows a possible approach to study the interaction between a so-called "beam effect" and a "cable effect" that can address the problem of a cable owning some bending stiffness, as well as the influence of the axial elongation for a beam. In this case, the interaction between the two effects is investigate for a double-hinge beam undergoing a constant distributed load. The fourth and last example shows the sensitivity of the natural frequencies of a double supported continuous beam to its axial tension.

3.1 Evaluation of Internal Forces and Spans in a Pre-tensioned Cable Subject to a Vertical Concentrated Load at the Middle of its Span

A cable made of steel is pre-tensioned between two hinges. It is subject to a concentrated load at the middle of its span.

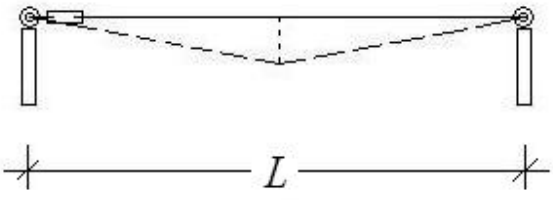

Figure 3-1: Geometry of the steel cable

3.1.1 Glossary

- P = external vertical load applied at the middle of the span;
- N_{tot}= traction force inherent the cable (sum of two components: the first, $N_{pretension}$, due to the pre-tension in the cable and the second, N_{sag}, due to the sag caused by the vertical load P);
- H = horizontal force at the end of the cable;

- V = vertical force at the end of the cable;
- $N_{pretension}$ = pre-tension force;
- $L = 2l$ = distance between the two hinges (span of the cable);
- $L_0 = 2l_0$ = initial length of the cable before the pre-tension;
- $L_1 = 2l_1$ = final length of the cable after the pre-tension;
- $\Delta L_{pretension} = L_1 - L_0$= change of length caused by the pre-tension;

3.1.2 Cable Stress and Strain

The pre-tension force necessary in order to avoid the slackness of the cable is assumed to be $N_{pretension}$ = 0.80 kN.

Considering the elastic modulus of steel, the cross-section area of most of the cable usually adopted in the industry, and the relatively low value of the pre-tension force, the deformation of the cable caused by the pre-tension is assumed to be negligible for engineering purposes.

$$L_0 \cong L_1 \equiv L$$

$$\Delta L_{pretension} \cong 0$$

The cable is assumed to have a linear elastic behavior up to the failure.

Under a vertical concentrated load P at the middle of the span, the deformed shape of the cable is shown in the figure below:

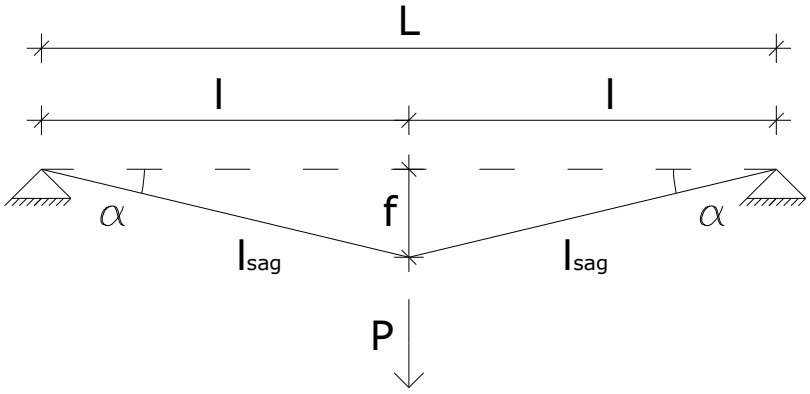

Figure 3-2: Geometry of a cable undergoing a vertical concentrated load

where the data of the problem are:

- A_{eff} = effective cross-section area of the cable;
- E = elastic modulus;

- $L = 2l$ = distance between the two hinges (span of the cable) = length of the cable after the pre-tension, but before applying the concentrated load P;
- $l = L/2$ = half distance between the two hinges (half span of the cable) = half length of the cable after the pre-tension, but before applying the concentrated load P;
- $N_{pretension}$ = traction force due to the pre-tension inherent the cable;
- $\varepsilon_{pretension}$ = cable strain due to the pre-tension inherent the cable;
- P = external vertical concentrated load applied at the middle of the span of the cable;

while the unknowns are:

- f = sag at the middle of the span due to the load P;
- α = angle between the horizontal axis and the deformed shape of the cable;
- $L_{sag} = 2l_{sag}$ = length of the cable in the deformed configuration, due to the load P;
- $l_{sag} = \frac{L_{sag}}{2}$ = half length of the cable in the deformed configuration, due to the load P;
- $\Delta L_{sag} = L_{sag} - L$ = cable elongation in the deformed configuration, due to the load P;
- $\Delta l_{sag} = l_{sag} - l$ = half cable elongation in the deformed configuration, due to the load P;
- ε_{sag} = cable strain due to the load P;
- N_{sag} = traction force due to the load P;
- $N_{tot} = N_{pretension} + N_{sag}$ = traction force in the deformed configuration of the cable, due to both the pre-tension inherent the cable and the load P.

The equilibrium of node C' (correspondent to the middle of the cable in the deformed configuration) at the middle of the span is:

$$N_{tot} = \frac{P}{2 \cdot sin\alpha} \tag{1}$$

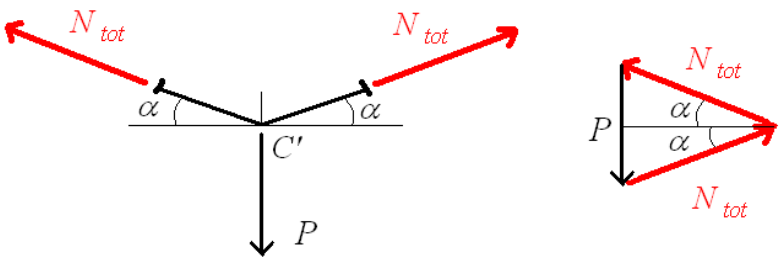

Figure 3-3: Equilibrium of the middle node

Equilibrium conditions:

$$N_{tot} = N_{pretension} + N_{sag} \tag{2}$$

Elasticity conditions:

$$N_{tot} = \varepsilon_{pretension} \cdot E \cdot A_{eff} + \varepsilon_{sag} \cdot E \cdot A_{eff}$$

$$\varepsilon_{sag} = \frac{N_{sag}}{E \cdot A_{eff}} = \frac{N_{tot} - N_{pretension}}{E \cdot A_{eff}} \tag{3}$$

Cable elongation:

$$\Delta l_{sag} = \varepsilon_{sag} \cdot l \tag{4}$$

$$\Delta l_{sag} = \frac{N_{sag} \cdot l}{E \cdot A_{eff}} = \frac{\left(N_{tot} - N_{pretension}\right) \cdot l}{E \cdot A_{eff}} \tag{5}$$

From simple geometric considerations:

$$sin\alpha = \frac{f}{l_{sag}} = \frac{f}{l + \Delta l_{sag}} \tag{6}$$

and:

$$f = \sqrt{\left(l + \Delta l_{sag}\right)^2 - l^2}$$

$$f = \sqrt{l^2 + 2l \cdot \Delta l_{sag} + \Delta l_{sag}{}^2 - l^2}$$

$$f = \sqrt{\Delta l_{sag}\left(2l + \Delta l_{sag}\right)} \tag{7}$$

Using Δl_{sag} as the only unknown of the problem, substituting (1) into (4):

$$\Delta l_{sag} = \frac{\left(\frac{P}{2 \cdot sin\alpha} - N_{pretension}\right) l}{E \cdot A_{eff}}$$

$$\Delta l_{sag} = \frac{\left(P - 2 \cdot sin\alpha \cdot N_{pretension}\right) l}{2 \cdot sin\alpha \cdot E \cdot A_{eff}}$$

$$\Delta l_{sag} = \frac{P \cdot l}{2 \cdot sin\alpha \cdot E \cdot A_{eff}} - \frac{N_{pretension} \cdot l}{E \cdot A_{eff}}$$

$$\Delta l_{sag} = \frac{P \cdot l}{2 \cdot sin\alpha \cdot E \cdot A_{eff}} - \varepsilon_{pretension} \cdot l \tag{8}$$

and substituting (6) into (8):

$$\Delta l_{sag} = \frac{P \cdot l}{2 \cdot \frac{f}{l + \Delta l_{sag}} \cdot E \cdot A_{eff}} - \varepsilon_{pretension} \cdot l$$

$$\Delta l_{sag} = \frac{P \cdot l \cdot \left(l + \Delta l_{sag}\right)}{2 \cdot f \cdot E \cdot A_{eff}} - \varepsilon_{pretension} \cdot l \tag{9}$$

and substituting (7) into (9):

$$\Delta l_{sag} = \frac{P \cdot l \cdot \left(l + \Delta l_{sag}\right)}{2 \cdot \sqrt{\Delta l_{sag}\left(2l + \Delta l_{sag}\right)} \cdot E \cdot A_{eff}} - \varepsilon_{pretension} \cdot l \tag{10}$$

This last equation has Δl_{sag} as the only unknown.

Solving (10) by analytical or numerical way, Δl_{sag} can be obtained.

Substituting (4) into (10):

$$\varepsilon_{sag} \cdot l = \frac{P \cdot l \cdot \left(l + \Delta l_{sag}\right)}{2 \cdot \sqrt{\varepsilon_{sag} \cdot l \cdot \left(2l + \Delta l_{sag}\right)} \cdot E \cdot A_{eff}} - \varepsilon_{pretension} \cdot l$$

$$\varepsilon_{sag} \cdot l = \frac{P \cdot l^2 \cdot \left(1 + \varepsilon_{sag}\right)}{2 \cdot \sqrt{\varepsilon_{sag} \cdot l^2 \cdot \left(2 + \varepsilon_{sag}\right)} \cdot E \cdot A_{eff}} - \varepsilon_{pretension} \cdot l$$

$$\varepsilon_{sag} = \frac{P \cdot \left(1 + \varepsilon_{sag}\right)}{2 \cdot \sqrt{\varepsilon_{sag} \cdot \left(2 + \varepsilon_{sag}\right)} \cdot E \cdot A_{eff}} - \varepsilon_{pretension} \tag{11}$$

whence:

$$\varepsilon_{sag} = \left(\frac{P}{2 \cdot E \cdot A_{eff}}\right) \frac{\left(1 + \varepsilon_{sag}\right)}{\sqrt{\varepsilon_{sag} \cdot \left(2 + \varepsilon_{sag}\right)}} - \varepsilon_{pretension} \tag{12}$$

The last equation has ε_{sag} as the only unknown. Solving (12) by analytical or numerical way, ε_{sag} can be obtained.

From (2) the total traction force inherent the cable is obtained:

$$N_{tot} = N_{pretension} + \varepsilon_{sag} \cdot E \cdot A_{eff} \tag{13}$$

From (6) the angle between the horizontal axis and the deformed shape of the cable is obtained:

$$\alpha = arcsin\left(\frac{P}{2 \cdot N_{tot}}\right) \tag{14}$$

Equations (12), (13) e (14) show that ε_{sag}, N_{tot} and α only depend on the vertical applied load P, the elastic modulus E, the cable effective cross-section area A_{eff} and the pre-tension force $N_{pretension}$.

From (4) the elongation of half cable Δl_{sag} is obtained:

$$\Delta l_{sag} = \varepsilon_{sag} \cdot l \tag{15}$$

From (7) the sag f is obtained:

$$f = \sqrt{\Delta l_{sag}\left(2l + \Delta l_{sag}\right)} \tag{16}$$

Finally, from (16) and (15) the sag/span ratio $\frac{f}{L}$ is obtained:

$$\frac{f}{L} = \frac{1}{2}\sqrt{\varepsilon_{sag}\left(2 + \varepsilon_{sag}\right)} \tag{17}$$

3.1.3 Forces (H e V) Transmitted to the Ends

The total traction force N_{tot} inherent the cable is split into an horizontal H and a vertical forces V:

$$H = N_{tot} \cdot cos\alpha \tag{18}$$

$$V = N_{tot} \cdot sin\alpha \tag{19}$$

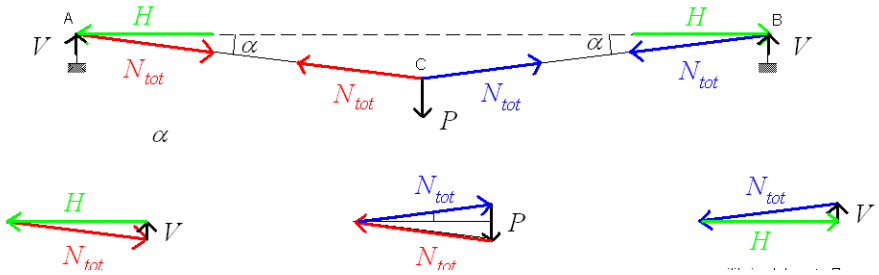

Figure 3-4: Equilibrium of the deformed cable

3.1.4 Numerical Example

Making reference to a steel cable consisting of 19 wrapped strands, the geometrical and mechanical data of the cable are:

$$\Phi = 8\ mm$$

$$E = 10800\ kN/cm^2$$

$$A_{eff} = 0.34\ cm^2$$

The pre-tension force inherent the cable is:

$$N_{pretension} = 0.80\ kN$$

whence:

$$\varepsilon_{pretension} = \frac{N_{pretension}}{E \cdot A_{eff}} = \frac{0.80}{10800 \cdot 0.34} = 2.18 \cdot 10^{-4}$$

The value of span and external load are assumed to be:

$$L = 800\ cm$$

$$l = \frac{L}{2} = 400\ cm$$

$$P = 12\ kN$$

The solving equation of the problem is:

$$\varepsilon_{sag} = \left(\frac{P}{2 \cdot E \cdot A_{eff}}\right) \frac{(1 + \varepsilon_{sag})}{\sqrt{\varepsilon_{sag} \cdot (2 + \varepsilon_{sag})}} - \varepsilon_{pretension} = 0.0109261$$

implementing the equations in Mathematica 3.0:

```
P = 12;                          (* kN *)
EA = 10800 * 0.34;               (* kN/cm^2 * cm^2 = kN *)
Npretensione = 0.80;             (* kN *)
epretensione = Npretensione / EA;
efreccia = .;
Solve[efreccia == (P / (2 * EA)) * (1 + efreccia) / Sqrt[efreccia * (2 + efreccia)] - epretensione, efreccia]
```

{{efreccia → −2.}, {efreccia → 0.0109261}}

Knowing the strain ε_{sag}, all the other unknowns can be obtained.

From (13) the total traction force inherent the cable is obtained:

$$N_{tot} = N_{pretension} + \varepsilon_{sag} \cdot E \cdot A_{eff}$$

$$N_{tot} = 0.80 + 0.0109261 \cdot 10800 \cdot 0.34 = 40.92\ kN$$

From (14) the angle between the horizontal axis and the deformed shape of the cable is obtained:

$$\alpha = arcsin\left(\frac{P}{2 \cdot N_{tot}}\right)$$

$$\alpha = arcsin\left(\frac{12}{2 \cdot 40.92}\right) = 0.1472\ rad = 8.431°$$

From (15) the elongation of half cable Δl_{sag} is obtained:

$$\Delta l_{sag} = \varepsilon_{sag} \cdot l$$

$$\Delta l_{sag} = 0.0109261 \cdot 400 = 4.37\ cm$$

From (16) the sag f is obtained:

$$f = \sqrt{\Delta l_{sag}(2l + \Delta l_{sag})}$$

$$f = \sqrt{4.37(2 \cdot 400 + 4.37)} = 59.29\ cm$$

From (17) the sag/span ratio $\frac{f}{L}$ is obtained:

$$\frac{f}{L} = \frac{1}{2}\sqrt{\varepsilon_{sag}(2 + \varepsilon_{sag})}$$

$$\frac{f}{L} = \frac{1}{2}\sqrt{0.0109261(2 + 0.0109261)} = 0.074 = \frac{1}{13.49}$$

From (18) the horizontal force transmitted at the end of the cable is obtained:

$$H = N_{tot} \cdot cos\alpha$$

$$H = 40.92 \cdot 0.9892 = 40.48\ kN$$

From (19) the vertical force transmitted at the end of the cable is obtained:

$$V = N_{tot} \cdot sin\alpha$$

$$V = 40.92 \cdot 0.1466 = 6\ kN$$

3.1.5 Parametric Study: Influence of the Vertical Load *P*

Making reference to a steel cable consisting of 19 wrapped strands, the geometrical and mechanical data of the cable are:

$$\Phi = 8\ mm$$

$$E = 10800\ kN/cm^2$$

$$A_{eff} = 0.34\ cm^2$$

$$L = 800\ cm$$

The pre-tension force inherent the cable is:

$$N_{pretension} = 0.80\ kN$$

whence:

$$\varepsilon_{pretension} = \frac{N_{pretension}}{E \cdot A_{eff}} = \frac{0.80}{10800 \cdot 0.34} = 2.18 \cdot 10^{-4}$$

the four following figures show respectively the influence of the vertical load P on the strain inherent the cable ε_{sag}, the total traction force N_{tot}, the angle α between the horizontal axis and the deformed shape of the cable and the sag/span ratio $\frac{f}{L}$.

It has to be noted that the results shown are independent from the total span L, since, as shown before, they depend only on the vertical applied load P, the elastic modulus E, the effective cross-section area A_{eff} and the pre-tension force $N_{pretension}$.

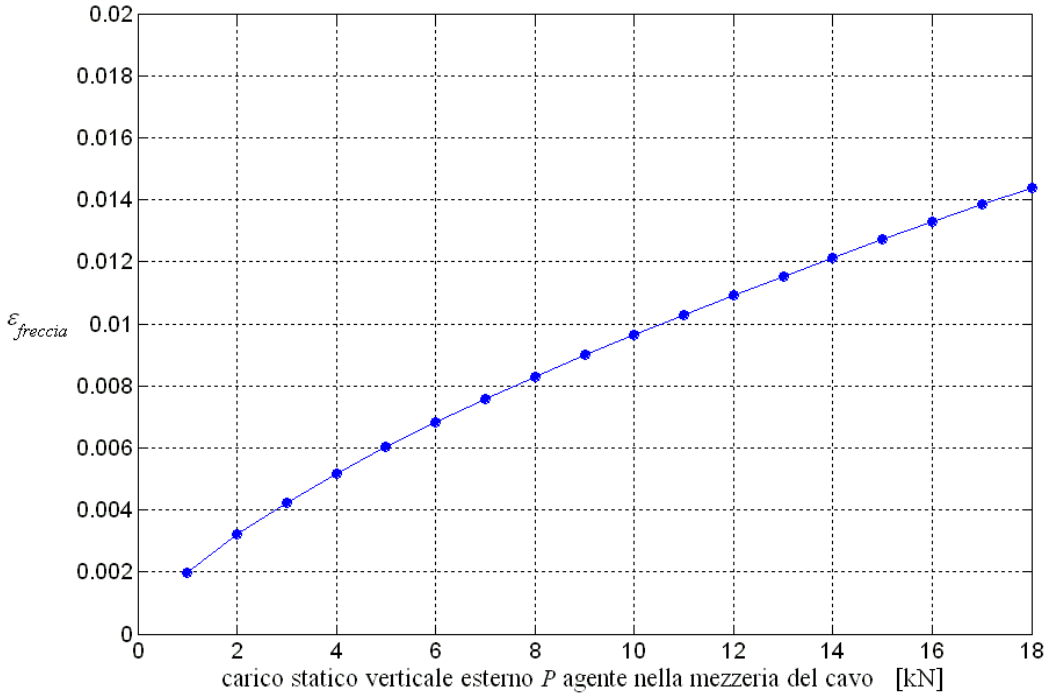

Figure 3-5: Strain due to the vertical concentrated load *P*

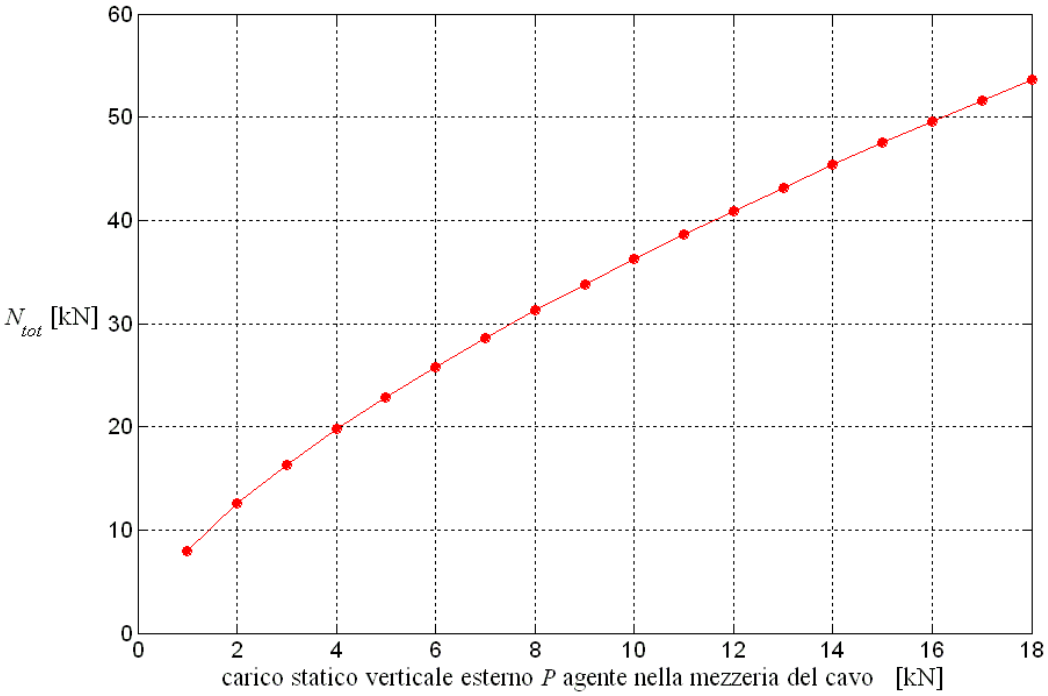

Figure 3-6: Total traction inherent the cable

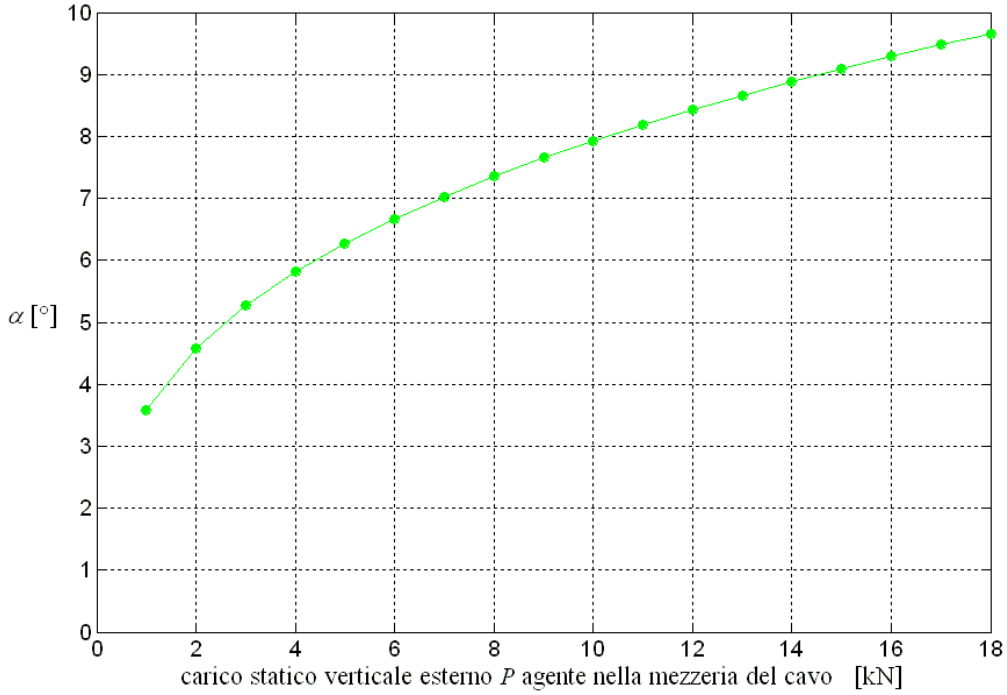

Figure 3-7: Angle between the deformed cable and the horizontal axis

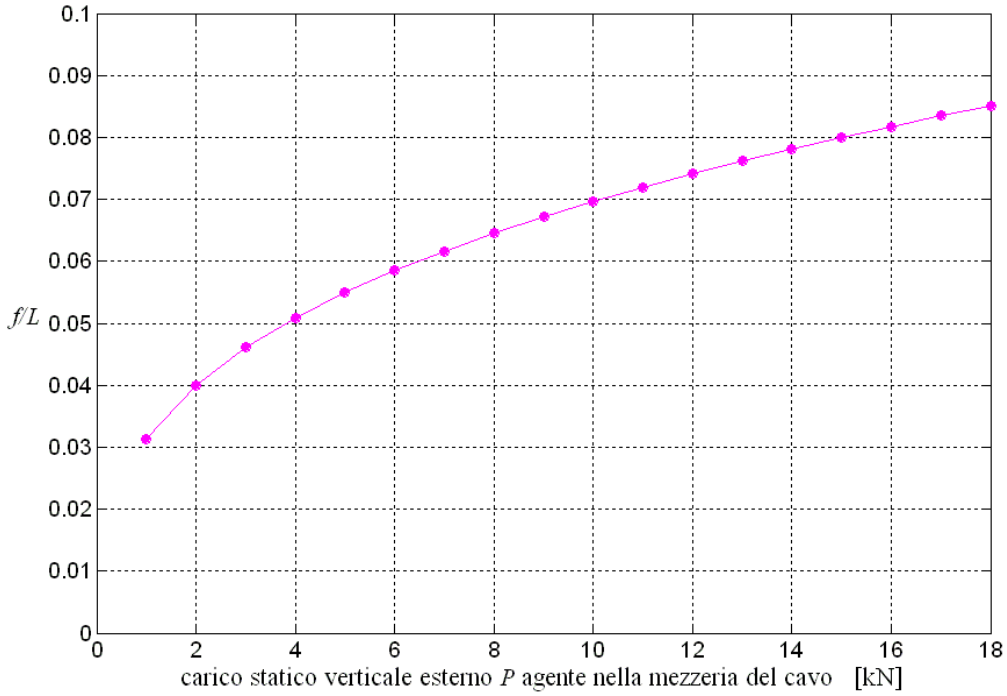

Figure 3-8: Sag/span ratio

3.1.6 Table resuming the Influence of the Vertical Load *P* on N_{tot}, *H* and *V*

Making reference to a steel cable consisting of 19 wrapped strands, the geometrical and mechanical data of the cable are:

$$\Phi = 8\ mm$$

$$E = 10800\ kN/cm^2$$

$$A_{eff} = 0.34\ cm^2$$

$$L = 800\ cm$$

The pre-tension force inherent the cable is:

$$N_{pretension} = 0.80\ kN$$

whence:

$$\varepsilon_{pretension} = \frac{N_{pretension}}{E \cdot A_{eff}} = \frac{0.80}{10800 \cdot 0.34} = 2.18 \cdot 10^{-4}$$

the following table shows the values of the total traction force inherent the cable N_{tot} and the horizontal as well as the vertical forces transmitted at the end of the cable to the restraints (*H* and *V*) for different values of the static vertical external load *P*, applied at the middle of the span. Particularly interesting are two values, *P* = 6 kN and *P* = 12 kN.

P	$\varepsilon_{freccia}$	N_{tot}	α	*f/L*	*L/f*	*H*	*V*
[kN]		[kN]	[°]			[kN]	[kN]
1.00	0.20%	8.00	3.584	0.031	31.93	7.98	0.50
2.00	0.32%	12.54	4.575	0.040	24.99	12.50	1.00
3.00	0.42%	16.35	5.264	0.046	21.71	16.28	1.50
4.00	0.52%	19.76	5.810	0.051	19.66	19.66	2.00
5.00	0.60%	22.89	6.269	0.055	18.20	22.76	2.50
6.00	**0.68%**	**25.83**	**6.670**	**0.058**	**17.10**	**25.65**	**3.00**
7.00	0.76%	28.60	7.029	0.062	16.22	28.39	3.50
8.00	0.83%	31.25	7.354	0.065	15.50	30.99	4.00
9.00	0.90%	33.79	7.652	0.067	14.89	33.49	4.50
10.00	0.97%	36.25	7.929	0.070	14.36	35.90	5.00
11.00	1.03%	38.62	8.188	0.072	13.90	38.22	5.50
12.00	**1.09%**	**40.92**	**8.431**	**0.074**	**13.49**	**40.48**	**6.00**
13.00	1.15%	43.16	8.662	0.076	13.13	42.67	6.50
14.00	1.21%	45.35	8.880	0.078	12.80	44.80	7.00
15.00	1.27%	47.48	9.088	0.080	12.50	46.89	7.50
16.00	1.33%	49.57	9.287	0.082	12.23	48.92	8.00
17.00	1.38%	51.62	9.478	0.083	11.98	50.91	8.50
18.00	1.44%	53.63	9.661	0.085	11.75	52.87	9.00

Table 3-1: Table Resuming the Influence of the Vertical Load *P* on N_{tot}, *H* and *V*

3.2 Evaluation of Internal Forces and Shape of an Inextensible Cable Subject to its Dead Weight: the Catenary Case

An inextensible cable is suspended between two hinges and it is subject only to its dead weight, without any external additional load. Such a cable is also known as catenary.

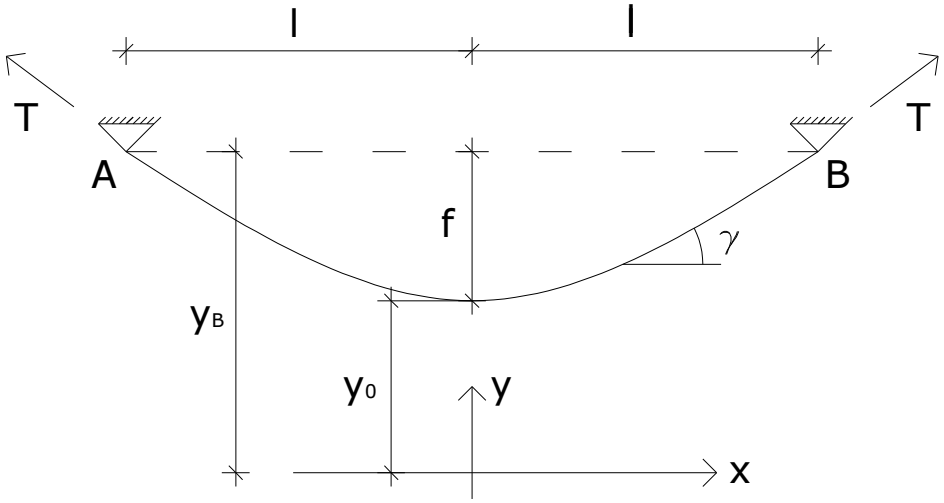

Figure 3-9: Geometry of the catenary

3.2.1 Glossary

- p = dead weight of the catenary, equal to the mass per unit of length of the cable times the gravity acceleration;
- T = traction force inherent the catenary (it has to be noted that has the same slope of the cable);
- γ = angle between the catenary and the horizontal axis;
- $2L$ = total length of the catenary;
- $2l$ = span of the catenary (distance between the two hinges);
- y_0 = y-coordinate of the middle of the catenary;
- y_B = y-coordinate of the hinges;
- f = central sag of the catenary;

3.2.2 Evaluation of the Shape and the Internal Tension

The cable is assumed to have a homogeneous density, therefore it is subject to a homogeneous dead weight: this dead weight is constant along the direction of the cable itself.

The data of the problem are:

- p = dead weight of the catenary, equal to the mass per unit of length of the cable times the gravity acceleration;
- γ_B = angle between the catenary and the horizontal axis at the ends of the cable;
- $2L$ = total length of the catenary;
- $2l$ = span of the catenary (distance between the two hinges);

while the unknowns are:

- T = traction force inherent the catenary (it has to be noted that has the same slope of the cable);
- T_0 = horizontal component of the traction force inherent the catenary;
- γ = angle between the catenary and the horizontal axis;
- y = shape of the catenary;
- y_0 = y-coordinate of the middle of the catenary;

The differential equilibrium equation governing the mechanics of the cable is:

$$\frac{dT(s)}{ds} = p(s) \tag{1}$$

Since the only load is in the vertical direction, separating the differential equilibrium equation in the two perpendicular directions we obtain:

$$\begin{cases} \frac{d(T \cdot cos\gamma)}{ds} = 0 \\ \frac{d(T \cdot sin\gamma)}{ds} = p \end{cases} \tag{2}$$

Integrating the first of the two, we have that the horizontal component of the tension is always constant, and can be called T_0:

$$T \cdot cos\gamma = T_0 \tag{3}$$

Substituting (3) into the second equation of (2) we have:

$$\frac{d(T_0 \cdot tg\gamma)}{ds} = p \tag{4}$$

From geometrical consideration we know that:

$$\frac{dy}{dx} = tg\gamma \tag{5}$$

and:

$$ds = \sqrt{1 + (y')^2}dx \tag{6}$$

Substituting (5) and (6) into (4), and considering that T_0 is constant, we obtain:

$$\frac{T_0 \cdot d(tg\gamma)}{ds} = p$$

$$T_0 \cdot \frac{d(\frac{dy}{dx})}{\sqrt{1 + (y')^2}dx} = p$$

$$\frac{d(\frac{dy}{dx})}{dx} = \frac{p}{T_0} \cdot \sqrt{1 + (y')^2}$$

$$y'' = \frac{p}{T_0} \cdot \sqrt{1 + (y')^2} \tag{7}$$

This is the second grade differential equation governing the shape of the catenary.

One possible solution is:

$$y = \frac{T_0}{p} \cdot cosh\frac{p \cdot x}{T_0} \tag{8}$$

This equation can be rewritten in a different way, from considering it for the middle of the catenary:

$$y(0) = \frac{T_0}{p} \cdot cosh\frac{p \cdot 0}{T_0} = \frac{T_0}{p}$$

$$y_0 = \frac{T_0}{p} \tag{9}$$

Substituting (9) into (8) we can rewrite:

$$y = y_0 \cdot cosh\frac{x}{y_0} \tag{10}$$

It has to be noted that the shape of the catenary is still unknown, since we don't know either T_0 or y_0 that depends on the choice of the position of the y-axis.

Deriving (8) in the x-direction, we obtain:

$$\frac{dy}{dx} = sinh\frac{p \cdot x}{T_0}$$

$$tg\gamma = sinh\frac{p \cdot x}{T_0} \tag{11}$$

Writing (11) for the one of the two hinges, we have:

$$tg\gamma_B = sinh\frac{p \cdot l}{T_0} \tag{12}$$

Knowing the dead weight of the material (p), the angle formed by the catenary and the horizontal axis in the end points (γ_B) and the span of the cable ($2l$), we can evaluate the horizontal tension T_0 from (12).

Alternatively, T_0 can be obtained knowing the total length of the catenary ($2L$).

As a matter of fact, the total length of half cable is:

$$L = \int_0^l ds \tag{13}$$

Substituting (6) into (13), we have:

$$L = \int_0^l \sqrt{1 + (y')^2}dx \tag{14}$$

Substituting (8) into (14), we have:

$$L = \int_0^l \sqrt{1 + \left(sinh\frac{p \cdot x}{T_0}\right)^2}\,dx = \int_0^l \sqrt{\left(cosh\frac{p \cdot x}{T_0}\right)^2}\,dx = \int_0^l cosh\frac{p \cdot x}{T_0}\,dx$$

$$L = \frac{T_0}{p} \cdot sinh\frac{p \cdot l}{T_0} \tag{15}$$

Knowing the dead weight of the material (p), the total length of the catenary ($2L$) and the span of the cable ($2l$), we can evaluate the horizontal tension T_0 from (15).

Substituting (12) into (15) we have:

$$L = \frac{T_0}{p} \cdot tg\gamma_B \tag{16}$$

Knowing the dead weight of the material (p), the total length of the catenary ($2L$) and the angle formed by the catenary and the horizontal axis in the end points (γ_B), we can evaluate the horizontal tension T_0 from (16).

Inserting the value of T_0 in (9), we can evaluate y_0 that is the ratio of the horizontal tension and the dead weight of the material.

We can also determine the shape of the catenary from either (8) or (9).

In order to know the total sloped tension T inherent the cable, we must first determine the equation of the angle γ. Substituting (9) into (5), we have:

$$sinh\frac{x}{y_0} = tg\gamma$$

$$\gamma = arctg\left(sinh\frac{x}{y_0}\right) \tag{17}$$

Knowing γ, the tension T can be evaluated from (3).

It has to be noted that, whether the horizontal tension T_0 is sufficiently high, the shape of the catenary can be approximated with a parabola, since the terms over the second grade in the series expansion of (8) can be neglected.

$$y = \frac{T_0}{p} \cdot cosh\frac{p \cdot x}{T_0} \cong \frac{T_0}{p} \cdot \left(1 + \frac{p^2 \cdot x^2}{2 \cdot {T_0}^2} + \frac{p^4 \cdot x^4}{24 \cdot {T_0}^4} + \cdots\right) \tag{18}$$

3.2.3 Forces (*H* e *V*) Transmitted to the Ends

The total traction force T inherent the catenary can be split at the restraints into a horizontal H and a vertical reaction V:

$$H_B \equiv T_0 = T(l) \cdot cos\gamma_B \tag{19}$$

$$V_B = T(l) \cdot sin\gamma_B \tag{20}$$

3.2.4 Numerical Example

Making reference to the same steel cable of the previous example, consisting of 19 wrapped strands, the geometrical and mechanical data of the cable are:

$$\Phi = 8\,mm$$

$$A_{eff} = 3.4 \cdot 10^{-5}\,m^2$$

$$\rho = 7.87 \cdot 10^{3}\,kg/m^3$$

$$p = 7.87 \cdot 10^{3} \cdot 3.4 \cdot 10^{-5} \cdot 9.81 = 2.62\,N$$

The span and the total length of the cable are assumed to be respectively:

$$2l = 800\,cm = 0.8\,m$$

$$2L = 1000\,cm = 1\,m$$

The cable is let under the dead weight: therefore, it will assume the catenary shape.

The solving equation of the problem, knowing p, l and L, is:

$$L = \frac{T_0}{p} \cdot sinh\frac{p \cdot l}{T_0}$$

It has to be noted that this equation can't be directly solved (e.g., using Mathematica) since it is transcendental. Therefore, it has to be solved with an iterative procedure, for different trial values of T_0, until the equation is satisfied. Below the procedure is showed, with the value of T_0 that, substituted into the solving equation, was found to give the best approximation of the total length L.

implementing the equations in Mathematica 3.0:

```
l = 0.4;                                   (*m*)
L=.;                                       (*m*)
p = 2.62;                                  (*N/m*)
T0 = 0.8861;                               (*N*)
Solve[L == T0/p * Sinh[p*l/T0], L]
{{L→ 0.499997325642781209`}}
```

The correct value of the horizontal tension is therefore:

$$T_0 = 0.8861\,N$$

Knowing T_0, all the other unknowns can be evaluated.

The shape of the catenary is:

$$y = \frac{T_0}{p} \cdot cosh\frac{p \cdot x}{T_0} = \frac{0.8861}{2.62} \cdot cosh\frac{2.62 \cdot x}{0.8861} = 0.338 \cdot \cosh\,(2.956 \cdot x)$$

Knowing the expression of the shape of the catenary, one meaningful parameter is the central sag *f* that is the difference between y_0 and y_B.

The parameter y_0 is:

$$y_0 = \frac{T_0}{p} = \frac{0.8861}{2.62} = 0.338\ m$$

The y-coordinate y_B is:

$$y_B = y(l) = \frac{T_0}{p} \cdot cosh\frac{p \cdot x}{T_0} = \frac{0.8861}{2.62} \cdot cosh\frac{2.62 \cdot 0.4}{0.8861} = 0.604\ m$$

Therefore, the central sag f is:

$$f = y_B - y_0 = 0.604 - 0.338 = 0.266\ m$$

The sag/span ratio is:

$$\frac{f}{2l} = \frac{0.266}{0.8} = 0.3325$$

The angle between the catenary and the horizontal axis is:

$$\gamma = arctg\left(sinh\frac{x}{y_0}\right) = arctg(\sinh\,(2.956 \cdot x))$$

At the end of the cable, this angle is:

$$\gamma_B = \gamma(l) = arctg(sinh(2.956 \cdot 0.4)) = 55.92°$$

The reactions at the restraints are respectively:

$$H_B \equiv T_0 = 0.8861\ N$$

$$V_B = T(l) \cdot sin\gamma_B = \frac{T_0}{cos\gamma_B} \cdot sin\gamma_B = T_0 \cdot tg\gamma_B = 0.8861 \cdot tg55.92° = 1.309\ N$$

3.2.5 Parametric Study: Influence of the Length of the Cable *2L*

Making reference to the same steel cable of the previous example, consisting of 19 wrapped strands, the geometrical and mechanical data of the cable are:

$$\Phi = 8\ mm$$

$$A_{eff} = 3.4 \cdot 10^{-5}\ m^2$$

$$\rho = 7.87 \cdot 10^3\ kg/m^3$$

$$p = 7.87 \cdot 10^3 \cdot 3.4 \cdot 10^{-5} \cdot 9.81 = 2.62\ N$$

The span between the two hinges is assumed to be:

$$2l = 800\ cm = 0.8\ m$$

Some cables, with different length, are supposed to be installed between the two hinges, and let under the dead weight: therefore, they will assume the catenary shape.

The five following figures show respectively the influence of the total length $2L$ of the catenary on the horizontal traction T_0, on the vertical reaction V_B of the hinges, on the angle γ_B at the end of the cable, on the central sag f and on the sag/span ratio $\frac{f}{L}$.

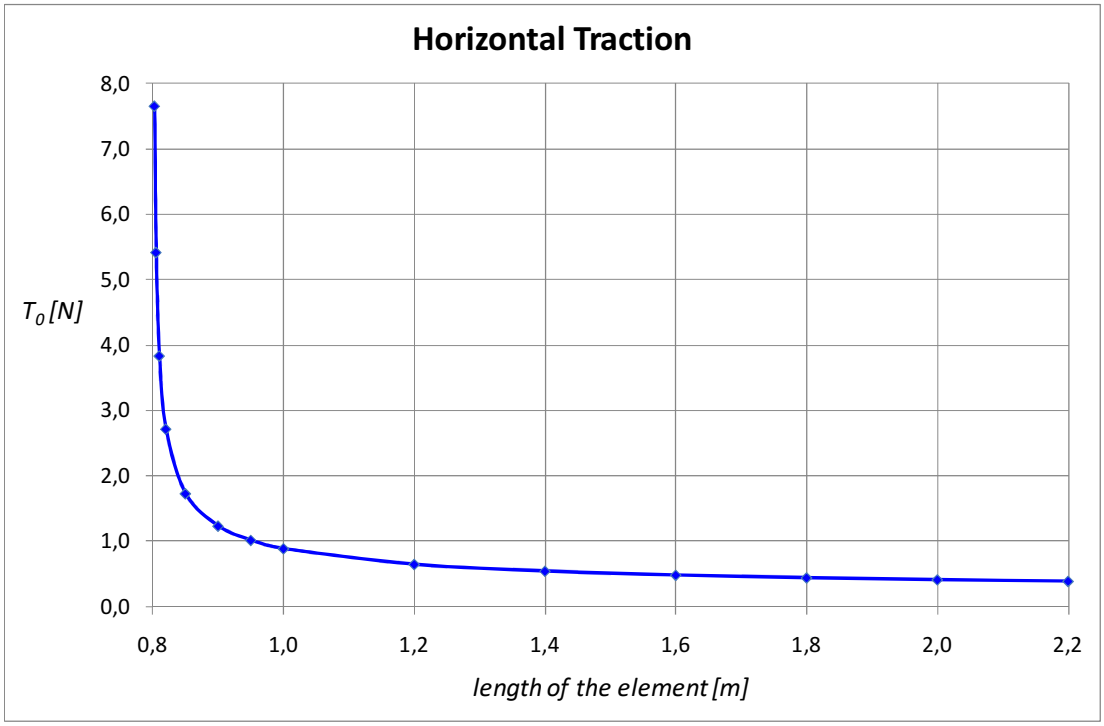

Figure 3-10: Horizontal traction for different values of the length *2L*

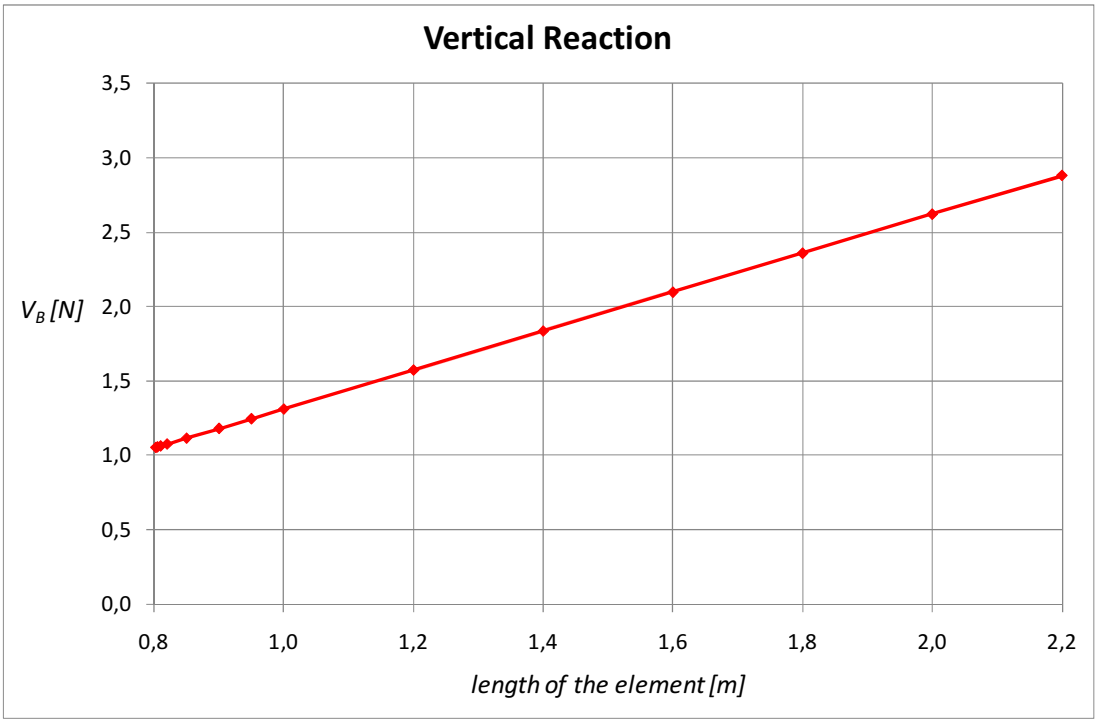

Figure 3-11: Vertical reaction for different values of the length *2L*

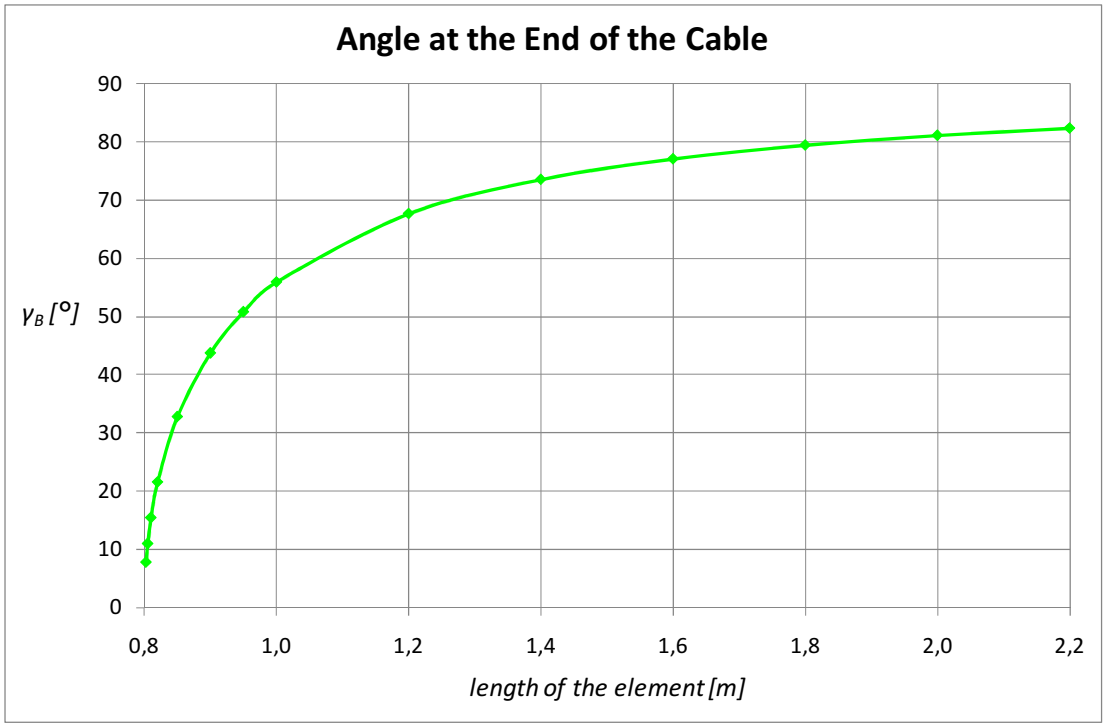

Figure 3-12: Angle at the end of the cable for different values of the length *2L*

Figure 3-13: Central sag for different values of the length *2L*

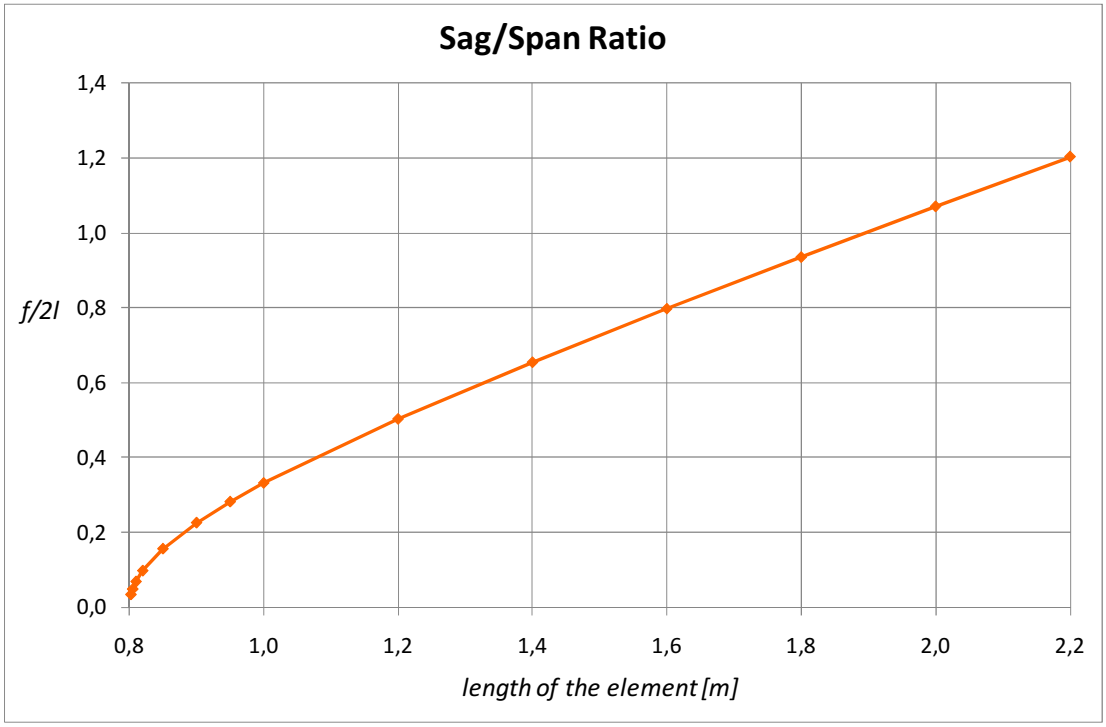

Figure 3-14: Sag/span ratio for different values of the length *2L*

3.2.6 Table resuming the Influence of the Length of the Cable *2L* on T_0, V_B, γ_B, f and $\frac{f}{L}$

Making reference to the same steel cable of the previous example, consisting of 19 wrapped strands, the geometrical and mechanical data of the cable are:

$$\Phi = 8\ mm$$

$$A_{eff} = 3.4 \cdot 10^{-5}\ m^2$$

$$\rho = 7.87 \cdot 10^{3}\ kg/m^3$$

$$p = 7.87 \cdot 10^{3} \cdot 3.4 \cdot 10^{-5} \cdot 9.81 = 2.62\ N$$

The span between the two hinges is assumed to be:

$$2l = 800\ cm = 0.8\ m$$

Some cables, with different length, are supposed to be installed between the two hinges, and let under the dead weight: therefore, they will assume the catenary shape.

The following table shows the values of the horizontal traction T_0, the vertical reaction V_B of the hinges, the angle γ_B at the end of the cable, the central sag *f* and the sag/span ratio $\frac{f}{L}$ for different values of the total length *2L* of the catenary.

2L	T_0	V_B	γ_B	y_0	y_B	*f*	*f/2l*
[m]	[N]	[N]	[°]	[m]	[m]	[m]	
0.8025	7.6560	1.0513	7.82	2.922	2.950	0.027	0.034
0.805	5.4170	1.0545	11.02	2.068	2.106	0.039	0.049
0.81	3.8340	1.0611	15.47	1.463	1.518	0.055	0.069
0.82	2.7160	1.0742	21.58	1.037	1.115	0.078	0.098
0.85	1.7272	1.1135	32.81	0.659	0.784	0.125	0.156
0.90	1.2322	1.1790	43.74	0.470	0.651	0.181	0.226
0.95	1.0147	1.2445	50.81	0.387	0.613	0.226	0.282
1.00	0.8861	1.3100	55.92	0.338	0.604	0.265	0.332
1.20	0.6461	1.5719	67.66	0.247	0.649	0.402	0.503
1.40	0.5422	1.8339	73.53	0.207	0.730	0.523	0.654
1.60	0.4813	2.0961	77.07	0.184	0.821	0.637	0.796
1.80	0.4404	2.3580	79.42	0.168	0.916	0.747	0.934
2.00	0.4105	2.6205	81.10	0.157	1.012	0.856	1.070
2.20	0.3876	2.8817	82.34	0.148	1.110	0.962	1.202

Table 3-2: Table Resuming the Influence of the Length of the Cable *2L* on T_0, V_B, γ_B, f and $\frac{f}{L}$

3.3 Interaction between "Beam Effect" and "Cable Effect" in a Simply Supported Element undergoing Uniform Vertical Distributed Load

A horizontal element is simply supported by two fixed hinges, and is subject to an uniform vertical distributed load.

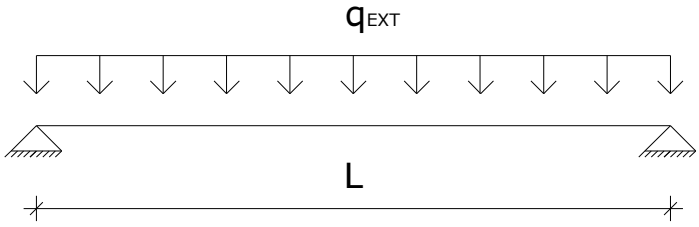

Figure 3-15: Simply supported element undergoing a vertical distributed load

3.3.1 Glossary

- q_{EXT} = uniform vertical distributed load applied to the beam;
- q_B = part of the external vertical distributed load carried by the "beam effect";
- q_C = part of the external vertical distributed load carried by the "cable effect";
- N = horizontal traction force inherent the cable;
- L = distance between the two hinges (span of the element);

3.3.2 Evaluation of the Axial Stress Arising in the Element

The total external distributed load on the element is supposed to be carried by two different complementary effects, one being a "beam effect" (moment + shear), the other being a "cable effect" (axial force).

First, we assume one restraint to be a roller, and the other to be a hinge: in this way, the horizontal translation of one end are allowed.

The element is subject to an uniform vertical distributed load, and the deformed shape is assumed to be a parabolic curve, as shown in the pictures below:

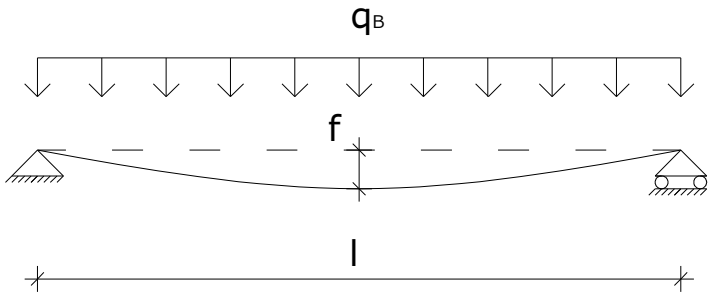

Figure 3-16: Deformed shape of the element due to the "beam effect"

Then, the element is considered to be a cable subject to horizontal traction *N*, with a span equal to *L* and a central sag equal to *f*.

The horizontal traction *N* is arising from the necessity of respecting the fixed hinges that don't allow the horizontal translation of the ends of the element.

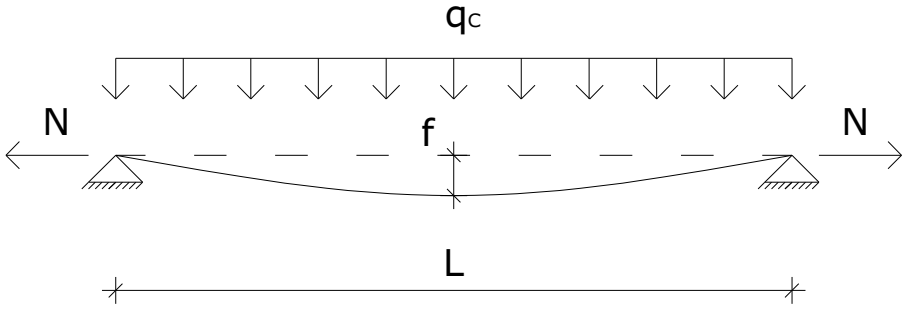

Figure 3-17: Mechanics of the element due to the "cable effect"

where the data of the problem are:

- *A* = cross-section area of the element;
- *I* = moment of inertia of the element;
- *E* = elastic modulus of the material the element is made of;
- *L* = distance between the two hinges (span of the element);
- q_{EXT} = external vertical distributed load applied to the element;

while the unknowns are:

- q_B = part of the external vertical distributed load carried by the "beam effect";
- q_C = part of the external vertical distributed load carried by the "cable effect";
- *f* = sag at the middle of the span due to the load q_B;

- l = span assumed by the element, supported by a fixed hinge and a roller, under the load q_B;
- N = horizontal force arising in the element to respect the restraints (fixed hinges);
- α = coefficient representing the part of the total external load carried by the "beam effect".

The central sag is evaluated through the classical beam theory:

$$f = \frac{5}{384} \cdot \frac{q_B \cdot L^4}{EI} \tag{1}$$

The subscript "$_B$" stands for "beam": it means that the sag is supposed to be caused only by a percentage of the total external load.

As a matter of fact, the "beam effect" of the element will stand for a percentage of the total external load, and the "cable effect" will stand for the complementary part.

In the following calculations, q_B is obtained applying a coefficient to the external load:

$$q_B = \alpha \cdot q_{EXT} \tag{2}$$

Assuming a parabolic shape for the deformed beam, and considering there are no axial forces, the axis of the beam should not vary its length.

Therefore, due to the deflection of the beam, the roller will translate shortening the span.

The value of the translation of the roller is evaluated by subtracting the span achieved under the external load from the initial length of the beam, which is equal to the length of the parabolic curve:

$$L = l\left(1 + \frac{8}{3}\frac{f^2}{l^2}\right) \tag{3}$$

It has to be noted that this formula is valid only under the assumption of small sag/span ratios.

The horizontal displacement of the roller is then equal to:

$$\Delta L = \frac{8}{3}\frac{f^2}{l^2} \cdot l = \frac{8}{3}\frac{f^2}{l} \tag{4}$$

Since both restraints at the ends of the cable are fixed hinges, an horizontal force necessary to prevent this translation has to be developed.

This force is evaluated from elasticity conditions:

$$N = E \cdot A \cdot \frac{\Delta L}{L}$$

(5)

Substituting (4) into (5):

$$N = E \cdot A \cdot \frac{8}{3}\frac{f^2}{l \cdot L}$$

(6)

Considering the deformed shape of the element, it has a deflection that can be intended as a slack cable.

Therefore, the horizontal force N is able to equilibrate, through a "cable effect", the complementary part of q_B that is the part of external load supported by the "beam effect".

In a cable, the horizontal force, multiplied by the sag, is necessary to equilibrate the central moment arising from the external distributed load.

From the equilibrium condition of a cable, we have:

$$q_C = 8 \cdot \frac{f}{L^2} \cdot N$$

(7)

Substituting (6) into (7):

$$q_C = 8 \cdot \frac{f}{L^2} \cdot E \cdot A \cdot \frac{8}{3}\frac{f^2}{l \cdot L} = \frac{64}{3} \cdot E \cdot A \cdot \frac{f^3}{l \cdot L^3}$$

(8)

Substituting (1) into (8):

$$q_C = \frac{64}{3} \cdot \frac{E \cdot A}{l \cdot L^3} \cdot \frac{5^3}{384^3} \cdot \frac{{q_B}^3 \cdot L^{12}}{E^3 \cdot I^3}$$

(9)

From the total equilibrium of the system, since the load carried by the "cable effect" is complementary to that carried by the "beam effect":

$$q_C + q_B = q_{EXT}$$

(10)

Substituting (2) into (10):

$$q_C = (1 - \alpha) \cdot q_{EXT}$$

(11)

The solving equation from which evaluating the coefficient α, representing the part of total external load carried by the "beam effect", is obtained substituting (11) into (9):

$$(1-\alpha)\cdot q_{EXT} = \frac{64}{3}\cdot\frac{E\cdot A}{l\cdot L^3}\cdot\frac{5^3}{384^3}\cdot\frac{{q_B}^3\cdot L^{12}}{E^3\cdot I^3} \tag{12}$$

Simplifying we obtain:

$$(1-\alpha)\cdot q_{EXT} = \frac{125}{2654208}\cdot\frac{L^9\cdot A}{E^2\cdot I^3\cdot l}\cdot {q_B}^3 \tag{13}$$

Substituting (2) into (13) we obtain the final solving equation, where α is the only unknown:

$$(1-\alpha)\cdot q_{EXT} = \frac{125}{2654208}\cdot\frac{L^9\cdot A}{E^2\cdot I^3\cdot l}\cdot \alpha^3\cdot {q_{EXT}}^3 \tag{14}$$

This third grade equation can be solved in numerical way (e.g., using Mathematica).

It has to be noted that l is an unknown too, depending on α.

Since for small sag/span ratios the difference between L and l has no engineering meaning, it is possible to assume $l \cong L$.

Otherwise, if a better approximation is wanted, it is possible to substitute the exact expression of l into (14):

$$l = \frac{L+\sqrt{L^2-{}^{32}/_3\cdot f^2}}{2} \tag{15}$$

3.3.3 Numerical Example

Making reference to a steel element IPE 120, the geometrical and mechanical data of the cross-section are:

$$A = 1320\ mm^2$$

$$\mathrm{I} = 3.18\cdot 10^6\ mm^4$$

$$\mathrm{E} = 2.06\cdot 10^5\ N/mm^2$$

The element is assumed to be subject only to the gravity load and no external additional loads:

$$\rho = 7.71\cdot 10^{-5}\ N/mm^3$$

$$q_{EXT} = \rho\cdot A = 7.71\cdot 10^{-5}\cdot 1320 = 0.10\ N/mm$$

The span of the element is assumed to be:

$$L = 5000\ mm$$

implementing the equations in Mathematica 3.0:

```
A = 1320;                                   (* mm^2 *)
J = 3.18 * 10^6;                            (* mm^4 *)
El = 2.06 * 10^5;                           (* N/mm^2 *)
qext = 0.10;                                (* N/mm *)
L = 5000;                                   (* mm *)
f = 5/384 * alpha * qext * L^4 / (El * J);
l = (L + Sqrt[L^2 - 32/3 * f^2]) / 2;
alpha = .;
Solve[(1 - alpha) * qext == 125/2654208 * A * L^9 / (El^2 * J^3 * l) * alpha^3 * qext^3, alpha]
{alpha → 0.999822146853347426`}
```

Now we know the two parts of the total external load carried respectively by the "beam effect" and the "cable effect", and it we can evaluate every other unknown of the problem.

From (2), the distributed load carried by the "beam effect" is:

$$q_B = \alpha \cdot q_{EXT} = 0.0099982\ N/mm$$

From (11), the distributed load carried by the "cable effect" is:

$$q_C = (1 - \alpha) \cdot q_{EXT} = 1.8 \cdot 10^{-5}\ N/mm$$

From (1), the sag is:

$$f = \frac{5}{384} \cdot \frac{\alpha \cdot q_{EXT} \cdot L^4}{EI} = 1.24\ mm$$

Expressing (7) in terms of *N*, the horizontal traction arising in the element is:

$$N = \frac{q_C \cdot L^2}{8 \cdot f} = 45.36\ N$$

Finally, we have to check the sag/span ratio to ensure the validity of the initial assumption of low sag/span ratio, necessary for the hypothesis of parabolic deformed shape:

$$\frac{f}{L} = \frac{1.24}{5000} = 2.48 \cdot 10^{-4}$$

This shows that the initial assumption is valid; therefore the presented approach can be applied for this numerical problem.

It has to be noted that for the element considered in this numerical example and its span, the presence of the "cable effect" is absolutely negligible.

The "cable effect" can play a bigger role in the mechanical behavior of the element when the span arises, but is still under the assumption of small sag/span ratios.
Let's consider the same element, under gravity load, but with a different span:

$$L = 12000\ mm$$

In this case we have:

implementing the equations in Mathematica 3.0:

```
A = 1320;                          (* mm^2 *)
J = 3.18 * 10^6;                   (* mm^4 *)
El = 2.06 * 10^5;                  (* N/mm^2 *)
qext = 0.10;                       (* N/mm *)
L = 12000;                          (* mm *)
f = 5/384 * alpha * qext * L^4 / (El * J);
l = (L + Sqrt[L^2 - 32/3 * f^2]) / 2;
alpha = .;
Solve[(1 - alpha) * qext == 125/2654208 * A * L^9 / (El^2 * J^3 * l) * alpha^3 * qext^3, alpha]
{alpha → 0.870699871331925479`}
```

Now we know the two parts of the total external load carried respectively by the "beam effect" and the "cable effect", and it we can evaluate every other unknown of the problem.
From (2), the distributed load carried by the "beam effect" is:

$$q_B = \alpha \cdot q_{EXT} = 0.08707\ N/mm$$

From (11), the distributed load carried by the "cable effect" is:

$$q_C = (1 - \alpha) \cdot q_{EXT} = 0.01293\ N/mm$$

From (1), the sag is:

$$f = \frac{5}{384} \cdot \frac{\alpha \cdot q_{EXT} \cdot L^4}{EI} = 35.88\ mm$$

Expressing (7) in terms of *N*, the horizontal traction arising in the element is:

$$N = \frac{q_C \cdot L^2}{8 \cdot f} = 6486.6\ N$$

Again, we have to check the sag/span ratio to ensure the validity of the initial assumption of low sag/span ratio, necessary for the hypothesis of parabolic deformed shape:

$$\frac{f}{L} = \frac{35.88}{12000} = 2.99 \cdot 10^{-3}$$

Under this span, the sag/span ratio is one order of magnitude bigger than in the previous case, but the initial assumption can still be considered valid.

It has to be noted how, for span values common in the practice (12 m), the "cable effect" cannot be considered negligible, inducing important traction forces in the element, when the horizontal translations of the ends are prevented.

3.3.4 Parametric Study: Influence of the Span *L*

Making reference to a steel element IPE 120, with the following geometrical and mechanical data of the cross-section:

$$A = 1320\ mm^2$$

$$\mathrm{I} = 3.18 \cdot 10^6\ mm^4$$

$$\mathrm{E} = 2.06 \cdot 10^5\ N/mm^2$$

and considering the element undergoing the gravity load:

$$\rho = 7.71 \cdot 10^{-5}\ N/mm^3$$

$$q_{EXT} = \rho \cdot A = 7.71 \cdot 10^{-5} \cdot 1320 = 0.10\ N/mm$$

the four following figures show respectively the influence of the span *L* on the coefficient α, the central sag *f*, the horizontal traction inherent the element *N* and the sag/span ratio *f/L*.

The span is assumed varying in a range of feasible common values, from 1 up to 20 m.

All the pictures show that a different behavior is observed over the span equal to 12 m; therefore, over this span, the sag/span ratio *f/L* is not sufficiently small to completely validate the initial assumption of the presented approach.

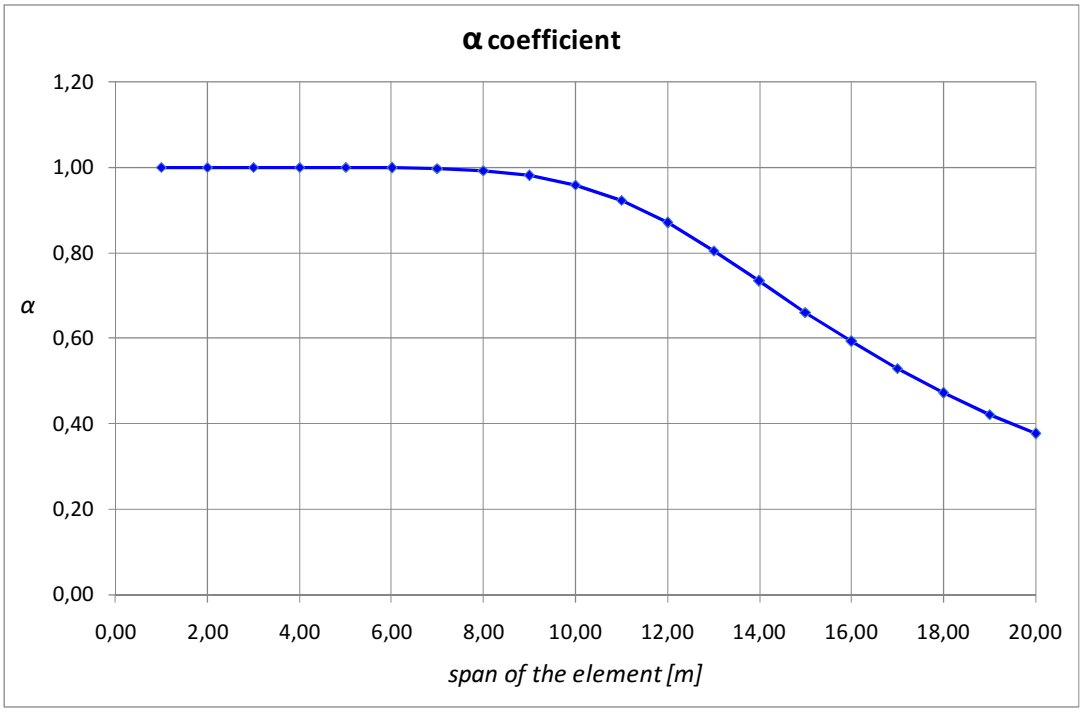

Figure 3-18: α coefficient for different values of the span

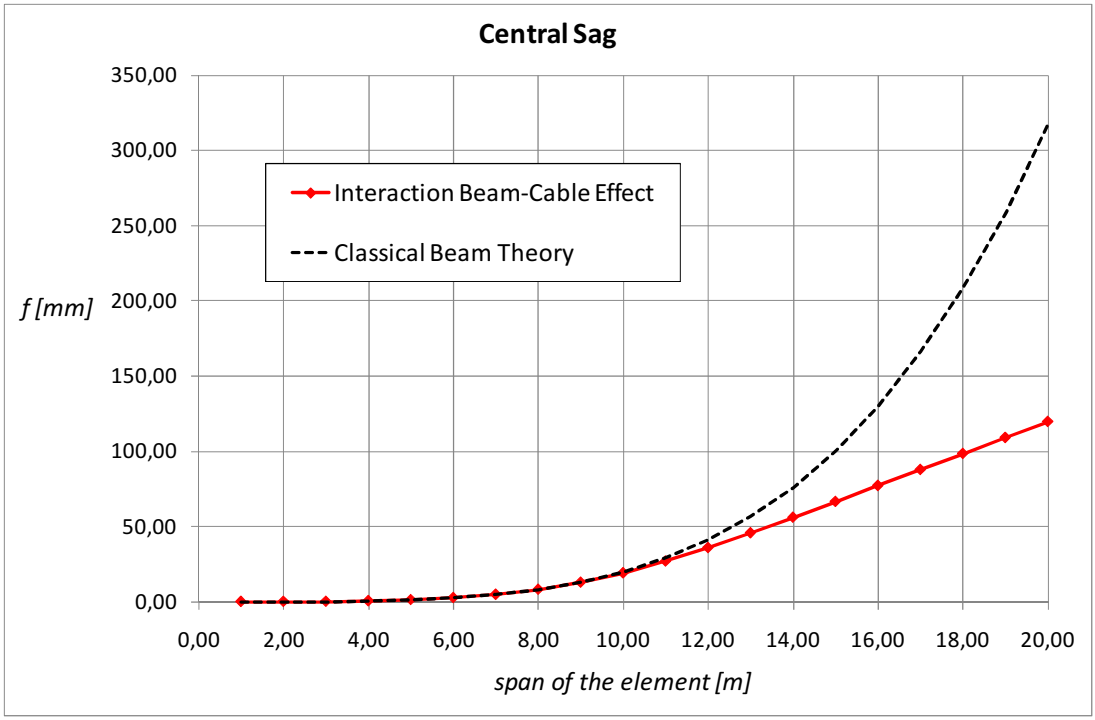

Figure 3-19: Central sag for different values of the span

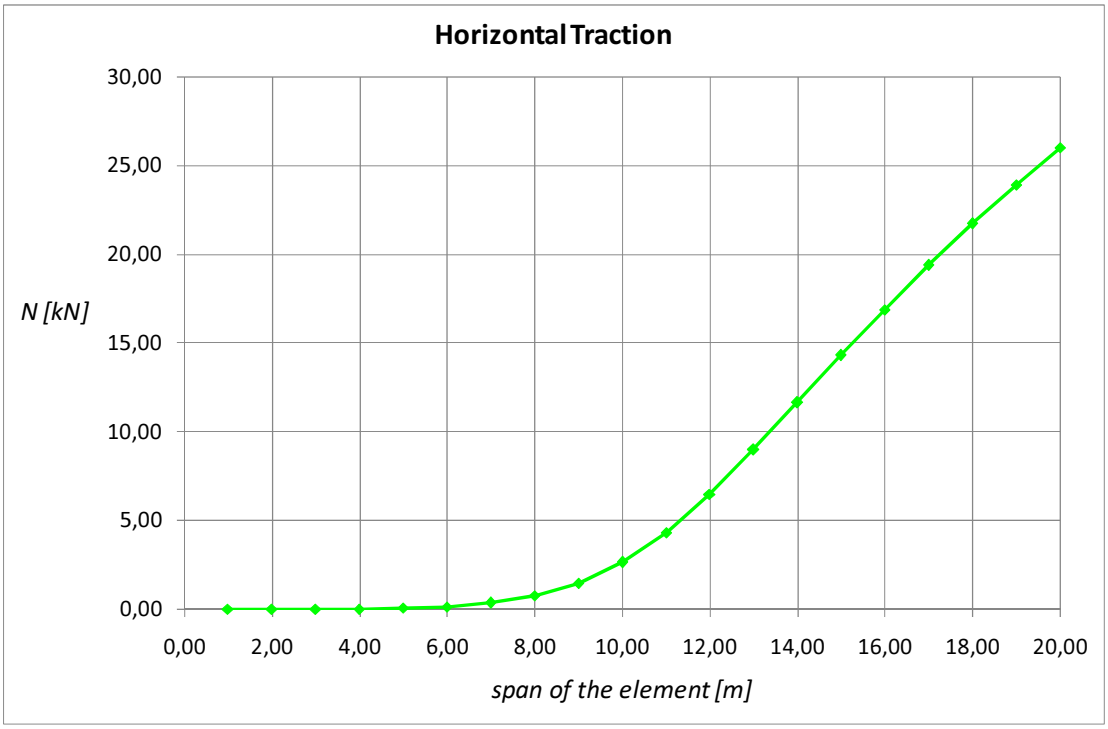

Figure 3-20: Horizontal traction for different values of the span

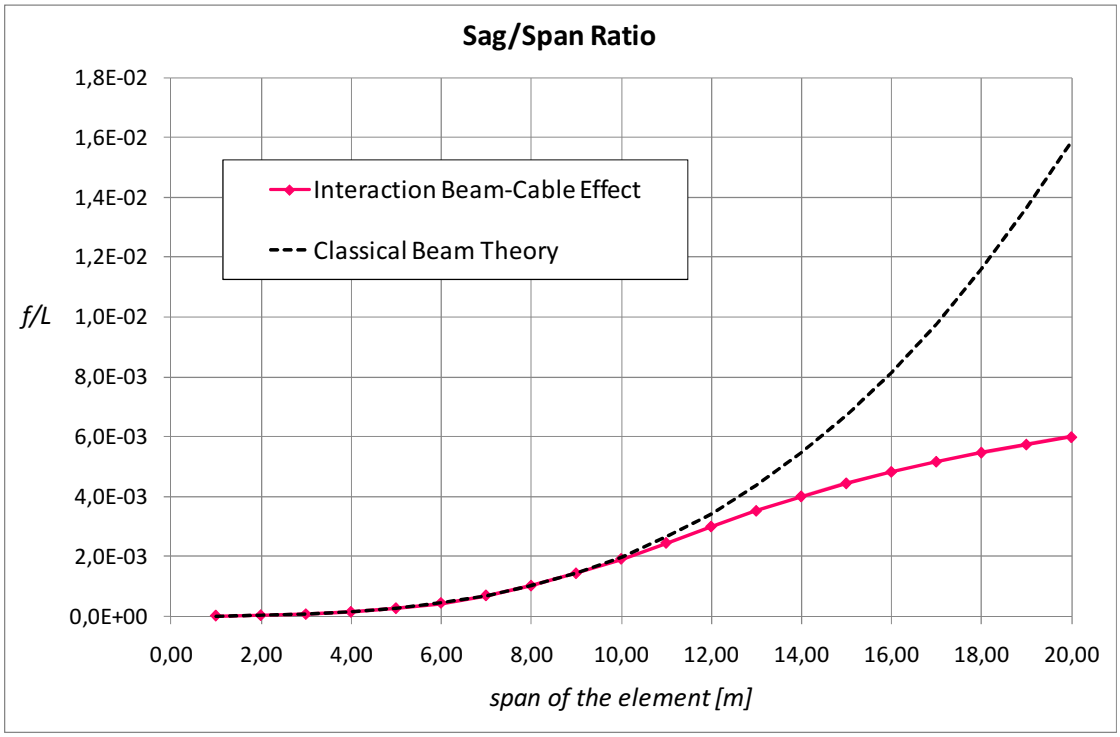

Figure 3-21: Central sag for different values of the span

3.3.5 Table Resuming the Influence of the Span L on $\alpha, f, N, \frac{f}{L}$

Making reference to a steel element IPE 120, with the following geometrical and mechanical data of the cross-section:

$$A = 1320\ mm^2$$

$$\mathrm{I} = 3.18 \cdot 10^6\ mm^4$$

$$\mathrm{E} = 2.06 \cdot 10^5\ N/mm^2$$

and considering the element undergoing the gravity load:

$$\rho = 7.71 \cdot 10^{-5}\ N/mm^3$$

$$q_{EXT} = \rho \cdot A = 7.71 \cdot 10^{-5} \cdot 1320 = 0.10\ N/mm$$

the following table shows the values of the α coefficient, the central sag f, the horizontal traction inherent the element N and the sag/span ratio f/L for different values of the span L.

The span is assumed varying in a range of feasible common values, from 1 up to 20 m.

L	α	f	N	f/L
[m]		[mm]	[N]	
1.00	1.000000	0.00	0.00	1.99E-06
2.00	1.000000	0.03	0.00	1.59E-05
3.00	0.999997	0.16	2.10	5.37E-05
4.00	0.999970	0.51	11.79	1.27E-04
5.00	0.999822	1.24	44.78	2.48E-04
6.00	0.999237	2.57	133.39	4.29E-04
7.00	0.997394	4.76	335.33	6.80E-04
8.00	0.992527	8.08	739.84	1.01E-03
9.00	0.981461	12.80	1466.54	1.42E-03
10.00	0.959730	19.08	2638.75	1.91E-03
11.00	0.923171	26.87	4325.37	2.44E-03
12.00	0.870699	35.89	6485.40	2.99E-03
13.00	0.805663	45.74	8975.96	3.52E-03
14.00	0.734064	56.05	11623.92	4.00E-03
15.00	0.661710	66.59	14289.09	4.44E-03
16.00	0.592666	77.20	16883.65	4.83E-03
17.00	0.529147	87.84	19363.18	5.17E-03
18.00	0.472017	98.49	21711.15	5.47E-03
19.00	0.421321	109.14	23926.71	5.74E-03
20.00	0.376675	119.79	26016.77	5.99E-03

Table 3-3: Table Resuming the Influence of the Span L on $\alpha, f, N, \frac{f}{L}$

3.3.6 Parametric Study: Influence of the External Load q_{EXT}

Making reference to a steel element IPE 120, with the following geometrical and mechanical data of the cross-section:

$$A = 1320\ mm^2$$

$$\mathrm{I} = 3.18 \cdot 10^6\ mm^4$$

$$\mathrm{E} = 2.06 \cdot 10^5\ N/mm^2$$

and considering a fixed span equal to:

$$\mathrm{L} = 5000\ mm$$

the four following figures show respectively the influence of the vertical external distributed load q_{EXT} on the coefficient α, the central sag *f*, the horizontal traction inherent the element *N* and the sag/span ratio *f/L*.

The external load q_{EXT} is assumed from the dead weight of the IPE 120 beam up to 1 t/m, because for bigger values the sag/span ratio seems to be not sufficiently low to respect the initial hypothesis of parabolic deformed shape.

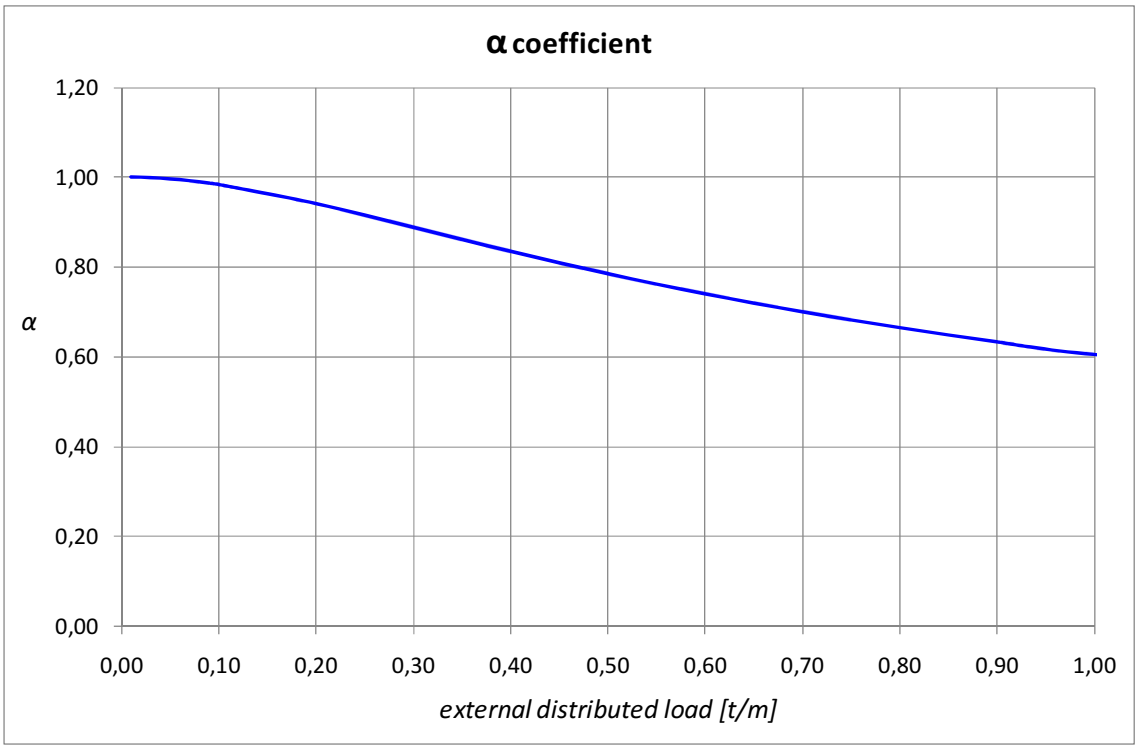

Figure 3-22: α coefficient for different values of the span

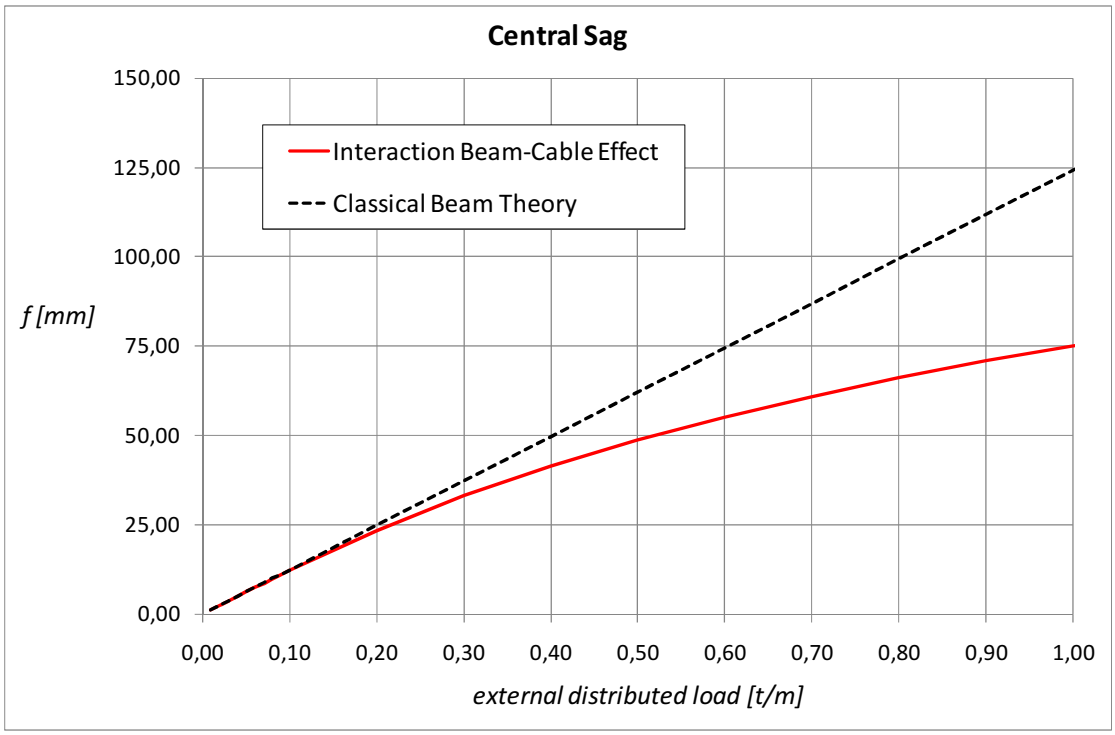

Figure 3-23: Central sag for different values of the span

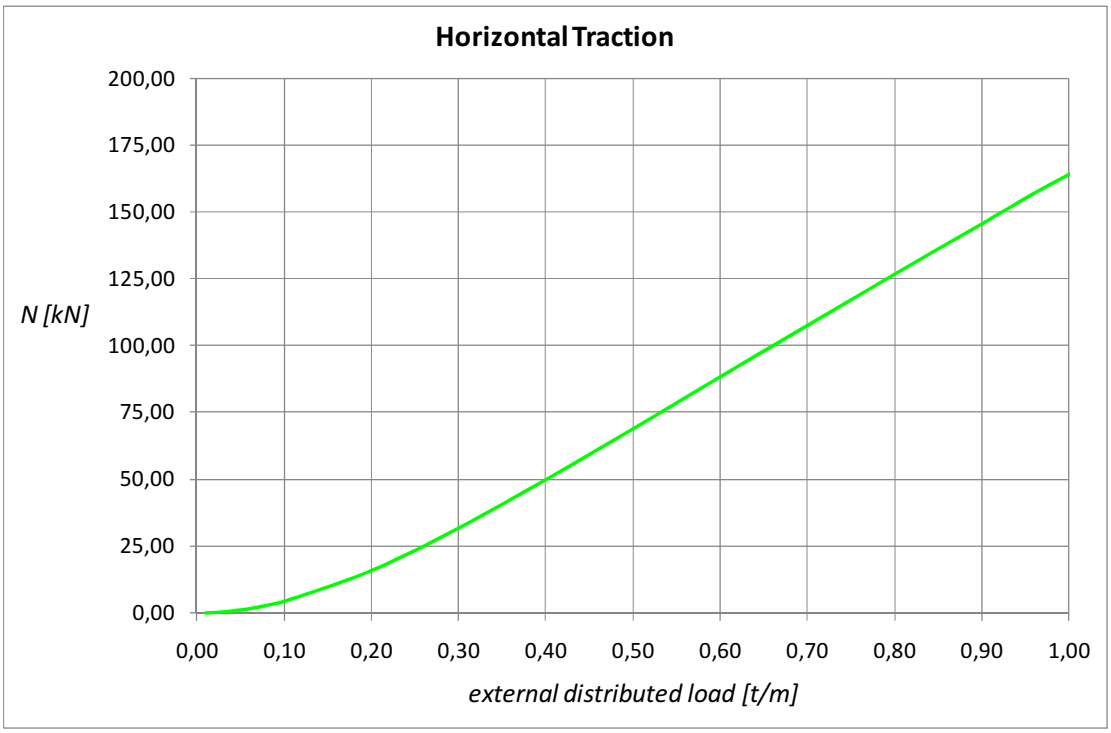

Figure 3-24: Horizontal traction for different values of the span

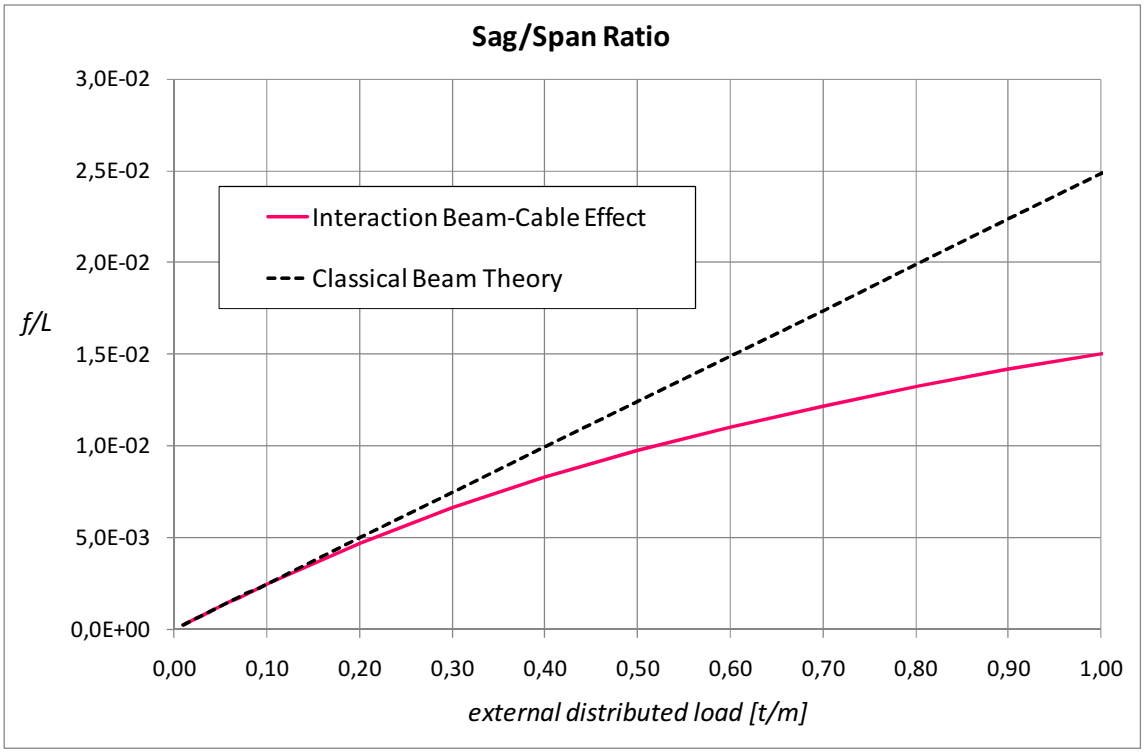

Figure 3-25: Central sag for different values of the span

3.3.7 Table Resuming the Influence of the External Load q_{EXT} on $\alpha, f, N, \frac{f}{L}$

Making reference to a steel element IPE 120, with the following geometrical and mechanical data of the cross-section:

$$A = 1320\ mm^2$$

$$\mathrm{I} = 3.18 \cdot 10^6\ mm^4$$

$$\mathrm{E} = 2.06 \cdot 10^5\ N/mm^2$$

and considering a fixed span equal to:

$$\mathrm{L} = 5000\ mm$$

the following table shows the values of the α coefficient, the central sag f, the horizontal traction inherent the element N and the sag/span ratio f/L for different values of the vertical external distributed load q_{EXT}.

The external load q_{EXT} is assumed from the dead weight of the IPE 120 beam up to 5 t/m, even if for values bigger than 1 t/m the sag/span ratio seems to be not sufficiently low to respect the initial hypothesis of parabolic deformed shape.

q_{EXT}	α	f	N	f/L
[t/m]		[mm]	[kN]	
0.01	0.999822	1.24	0.04	2.48E-04
0.02	0.999290	2.48	0.18	4.97E-04
0.03	0.998406	3.72	0.40	7.44E-04
0.04	0.997177	4.96	0.71	9.91E-04
0.05	0.995610	6.18	1.11	1.24E-03
0.06	0.993714	7.41	1.59	1.48E-03
0.07	0.991501	8.62	2.16	1.72E-03
0.08	0.988983	9.83	2.80	1.97E-03
0.09	0.986176	11.03	3.53	2.21E-03
0.10	0.983092	12.21	4.33	2.44E-03
0.20	0.940737	23.37	15.85	4.67E-03
0.30	0.887886	33.09	31.76	6.62E-03
0.40	0.834506	41.47	49.89	8.29E-03
0.50	0.784860	48.75	68.95	9.75E-03
0.60	0.740158	55.17	88.31	1.10E-02
0.70	0.700352	60.90	107.63	1.22E-02
0.80	0.664971	66.09	126.74	1.32E-02
0.90	0.633445	70.82	145.56	1.42E-02
1.00	0.605238	75.19	164.07	1.50E-02
2.00	0.430682	107.01	332.52	2.14E-02
3.00	0.344433	128.37	478.78	2.57E-02
4.00	0.291704	144.95	610.80	2.90E-02
5.00	0.255550	158.73	732.80	3.17E-02

Table 3-4: Table Resuming the Influence of the External Load q_{EXT} on $\alpha, f, N, \frac{f}{L}$

3.4 Influence of the Axial Tension on the Natural Frequencies of a Simply Supported Beam

A horizontal beam is simply supported by a fixed hinge and a roller, and is subject to an axial load.

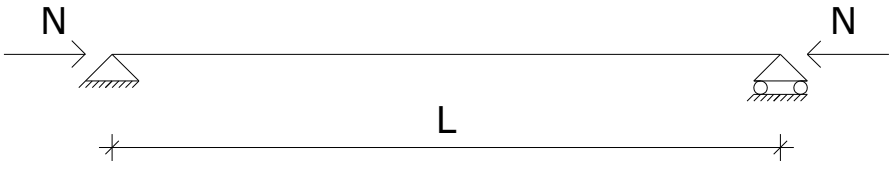

Figure 3-26: Simply supported beam undergoing an axial load *N*

3.4.1 Glossary

- N = axial load applied to the beam (positive values correspond to compression);
- L = length of the beam;

3.4.2 Evaluation of the Natural Frequencies under the Influence of an Axial Load

The data of the problem are:

- A = cross-section area of the beam;
- I = moment of inertia of the beam;
- E = elastic modulus of the material the beam is made of;
- L = distance between the hinge and the roller (length of the beam);
- N = axial load applied to the beam;
- m = mass per unit of length of the beam;

while the unknowns are:

- ϕ_n = n-th natural mode of the beam;
- ω_n = n-th natural frequency of the beam;

The fundamental equilibrium equation of a continuous beam considering the influence of the axial stress is, and in absence of any vertical external load is:

$$EI\frac{\partial^4 v}{\partial x^4} + N\frac{\partial^2 v}{\partial x^2} + m\frac{\partial^2 v}{\partial t^2} = 0 \tag{1}$$

Let the solution v be product of two separate functions, respectively depending only on the space and the time:

$$v(x,t) = \phi(x) \cdot Y(t) \tag{2}$$

Substituting (2) into (1), and dividing by $\phi(x) \cdot Y(t)$:

$$EI\frac{\phi^{IV}}{\phi} + N\frac{\phi^{II}}{\phi} = -m\frac{\ddot{Y}}{Y} = m\omega^2 \tag{3}$$

This single equation can be divided into a system of two separate equations, one depending only on the space, and one on the time:

$$\begin{cases} EI\phi^{IV} + N\phi^{II} - m\omega^2\phi = 0 \\ \ddot{Y} + \omega^2 Y = 0 \end{cases} \tag{4}$$

Solving the first equation of (4), the natural modes of the beam are obtained:

$$\phi^{IV} + \frac{N}{EI}\phi^{II} - \frac{m\omega^2}{EI}\phi = 0 \tag{5}$$

Let it be:

$$\begin{cases} g^2 = \dfrac{N}{EI} \\ a^4 = \dfrac{m\omega^2}{EI} \end{cases} \tag{6}$$

Substituting (6) into (5):

$$\phi^{IV} + g^2\phi^{II} - a^4\phi = 0 \tag{7}$$

The solution of (7) gives the natural modes of the beam:

$$\phi(x) = D_1 sin\delta x + D_2 cos\delta x + D_3 sinh\varepsilon x + D_4 cosh\varepsilon x \tag{8}$$

being:

$$\begin{cases} \delta = \sqrt{\left(a^4 + \dfrac{g^4}{4}\right)^{1/2} + \dfrac{g^2}{2}} \\ \varepsilon = \sqrt{\left(a^4 + \dfrac{g^4}{4}\right)^{1/2} - \dfrac{g^2}{2}} \end{cases} \tag{9}$$

D_1, D_2, D_3, D_4 are constants determined by the boundary conditions.

Considering a simply supported beam, the boundary conditions imply:

$$x = 0: \ \begin{cases} \phi(0) = 0 \\ EI\phi''(0) = 0 \end{cases} \xrightarrow{yields} D_2 = D_4 = 0 \tag{10}$$

$$x = L: \ \begin{cases} \phi(L) = 0 \\ EI\phi''(L) = 0 \end{cases} \xrightarrow{yields} \begin{cases} D_1 sin\delta L + D_3 sinh\varepsilon L = 0 \\ -\delta^2 D_1 sin\delta L + \varepsilon^2 D_3 sinh\varepsilon L = 0 \end{cases} \tag{11}$$

A solution is obtained only if the matrix is singular:

$$\begin{cases} sin\delta L \cdot sinh\varepsilon L = 0 \\ sinh\varepsilon L > 0 \end{cases} \xrightarrow{yields} sin\delta L = 0 \xrightarrow{yields} \delta \cdot L = n \cdot \pi \tag{12}$$

Substituting (9) into (12), the natural frequencies of the beam are extracted:

$$\omega_n = \frac{n\pi}{L}\sqrt{\frac{EI}{m}}\left(\frac{n^2\pi^2}{L^2} - \frac{N}{EI}\right)^{\frac{1}{2}} = \frac{\pi^2}{L^2}\sqrt{\frac{EI}{m}}\left(n^4 - \frac{n^2 N L^2}{\pi^2 EI}\right)^{\frac{1}{2}} \tag{13}$$

Since the buckling load for the beam is:

$$N_{cr} = \frac{\pi^2 EI}{L^2} \tag{14}$$

Substituting (14) into (13) the natural frequencies can be expressed in terms of N_{cr}:

$$\omega_n = \frac{\pi^2}{L^2}\sqrt{\frac{EI}{m}}\left(n^4 - n^2\frac{N}{N_{cr}}\right)^{\frac{1}{2}} \tag{15}$$

When N goes to N_{cr}, ω_1 tends to zero.

3.4.3 Numerical Example

Making reference to a steel beam IPE 120, the geometrical and mechanical data of the cross-section are:

$$A = 1.32 \cdot 10^{-3}\ m^2$$

$$\mathrm{I} = 3.18 \cdot 10^{-6}\ m^4$$

$$\mathrm{E} = 2.06 \cdot 10^{11}\ N/m^2$$

$$\mathrm{m} = 10.0\ kg/m$$

The length of the beam is assumed to be:

$$L = 5\ m$$

The buckling load for this beam, under this length, is from (14):

$$N_{cr} = \frac{\pi^2 EI}{L^2} = \frac{\pi^2 \cdot 2.06 \cdot 10^{11} \cdot 3.18 \cdot 10^{-6}}{5^2} = 258.6\ kN$$

Therefore, the natural frequencies of the beam are obtained from (15):

$$\omega_n = \frac{\pi^2}{L^2}\sqrt{\frac{EI}{m}}\left(n^4 - n^2\frac{N}{N_{cr}}\right)^{\frac{1}{2}} = 101.0\left(n^4 - n^2\frac{N}{258.6}\right)^{\frac{1}{2}}$$

In absence of any external axial load, the first natural frequency is:

$$\omega_n = \frac{\pi^2}{L^2}\sqrt{\frac{EI}{m}}\left(n^4 - n^2\frac{N}{N_{cr}}\right)^{\frac{1}{2}} = 101.0\left(1 - \frac{0}{258.6}\right)^{\frac{1}{2}} = 101.0\ rad/s = 16.0\ Hz$$

3.4.4 Parametric Study: Influence of the Axial Force *N*

Making reference to a steel beam IPE 120, the geometrical and mechanical data of the cross-section are:

$$A = 1.32 \cdot 10^{-3}\ m^2$$

$$\mathrm{I} = 3.18 \cdot 10^{-6}\ m^4$$

$$\mathrm{E} = 2.06 \cdot 10^{11}\ N/m^2$$

$$\mathrm{m} = 10.0\ kg/m$$

The length of the beam is assumed to be:

$$L = 5\ m$$

the following figure shows the influence of the axial load *N* on the first natural frequency ω_1.
The axial load *N* is assumed varying in a range from a traction equivalent to the buckling load, up to the buckling load in compression. As calculated before, for the present beam the buckling load is equal to 258 kN.

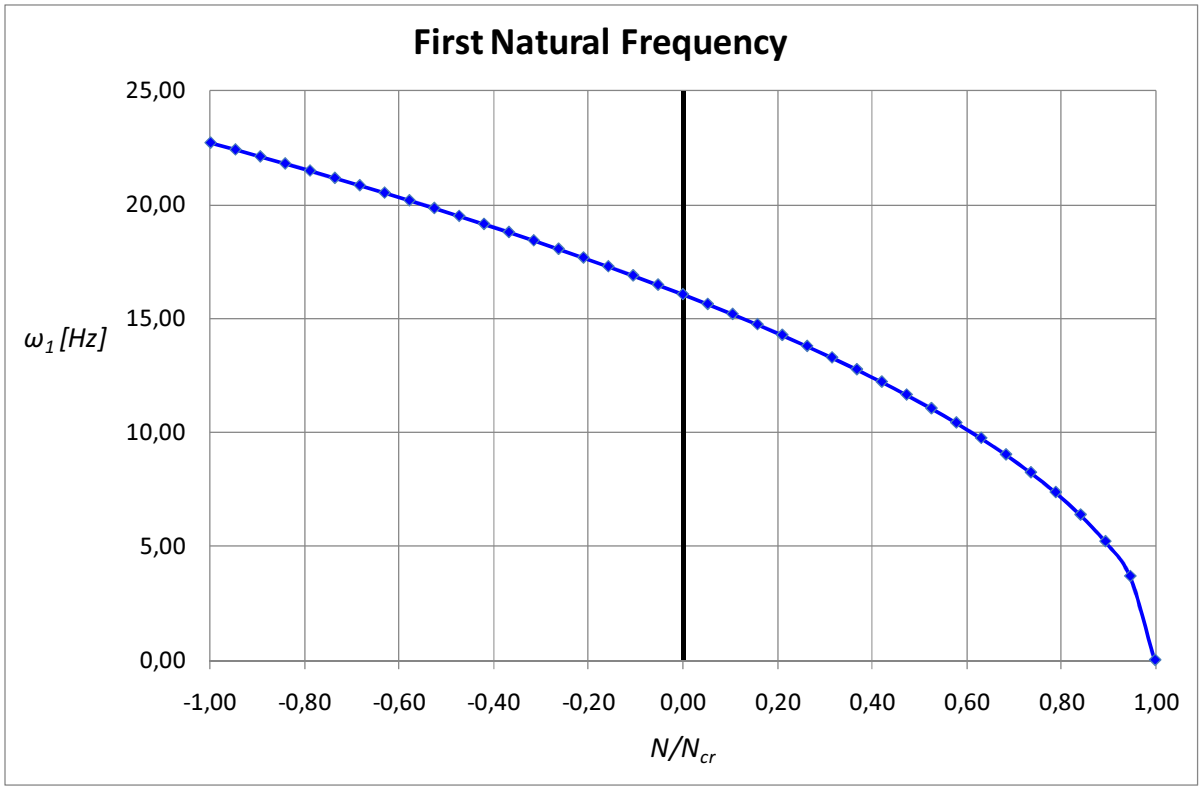

Figure 3-27: First natural frequency for different values of the axial load

3.4.5 Table Resuming the Influence of the Axial Force N on the Natural Frequencies ω_n

Making reference to a steel beam IPE 120, the geometrical and mechanical data of the cross-section are:

$$A = 1.32 \cdot 10^{-3}\ m^2$$

$$\mathrm{I} = 3.18 \cdot 10^{-6}\ m^4$$

$$\mathrm{E} = 2.06 \cdot 10^{11}\ N/m^2$$

$$\mathrm{m} = 10.0\ kg/m$$

The length of the beam is assumed to be:

$$L = 5\ m$$

the following table shows the values of the first natural frequency ω_1 for different values of the axial load *N*.

The axial load *N* is assumed varying in a range from a traction equivalent to the buckling load, up to the buckling load in compression. As calculated before, for the present beam the buckling load is equal to 258 kN.

N	N/N_{cr}	ω_1
[kN]		[Hz]
-258.00	-1.00	22.7
-244.42	-0.95	22.4
-230.84	-0.89	22.1
-217.26	-0.84	21.8
-203.68	-0.79	21.5
-190.11	-0.74	21.2
-176.53	-0.68	20.9
-162.95	-0.63	20.5
-149.37	-0.58	20.2
-135.79	-0.53	19.9
-122.21	-0.47	19.5
-108.63	-0.42	19.2
-95.05	-0.37	18.8
-81.47	-0.32	18.4
-67.89	-0.26	18.1
-54.32	-0.21	17.7
-40.74	-0.16	17.3
-27.16	-0.11	16.9
-13.58	-0.05	16.5
0.00	0.00	16.1
13.58	0.05	15.6
27.16	0.11	15.2
40.74	0.16	14.8
54.32	0.21	14.3
67.89	0.26	13.8
81.47	0.32	13.3
95.05	0.37	12.8
108.63	0.42	12.2
122.21	0.47	11.7
135.79	0.53	11.1
149.37	0.58	10.4
162.95	0.63	9.8
176.53	0.68	9.0
190.11	0.74	8.2
203.68	0.79	7.4
217.26	0.84	6.4
230.84	0.89	5.2
244.42	0.95	3.7
258.00	1.00	0.0

Table 3-5: Table Resuming the Influence of the Axial Force N on the Natural Frequencies ω_n

CHAPTER 4

FLEXIBLE STRANDED CONDUCTORS FOR ELECTRICAL PURPOSES

4.1 Introduction

An electrical substation consists of a complex set of equipment items that are interconnected through conductor buses or cables. Many equipment items in electrical substation are connected to each other by flexible conductors, typically cables made of braided aluminum wire strands. Stranded conductors are widely used structural components, in power engineering, in overhead transmission lines, and interconnections between substation equipment. Under some types of structural loading, these conductors may be subjected to large displacements that vary with time, leading to nonlinear behavior as a result of non negligible changes in geometry. Examples of such loading include conductor galloping, ice-shedding, short-circuit and interconnected substation equipment subjected to earthquakes. If the connections are not sufficiently flexible, significant dynamic interaction may occur between the connected equipment items during these loadings.

It has been reported that the presence of flexible conductors between equipment experiencing a differential displacement during an earthquake might be responsible for generating destructive forces at the top of such apparatus. For example, during the Miyagi earthquake of 1978, many units of interconnected equipment failed, even though individually qualified to withstand the effects of an event of this magnitude. Connections were then identified as one of the important causes of destruction. Similar conclusions were drawn after the 1986 North Palm Springs earthquake and after the 1988 Saguenay earthquake of magnitude 6.2, which caused severe damage to several substations.

Since these events, many works have been involved to investigate the effect of interaction between two equipment items connected by a cable conductor. Analytical as well as large-deformation finite-element analyses have been used to determine the nonlinear response of the cable-connected system to selected ground motions. The sensitivity to various parameters, such the cable geometry and its axial extensibility, flexural stiffness, and inertia on the interaction effect have been considered. As a matter of fact, several authors studied the effect of interaction

in interconnected equipment items when the flexible conductor is considered to be an extensible cable with either negligible or significant flexural rigidity and inertia effects. In addition, since the bending stiffness of a stranded conductor may vary during motion as a function of its inherent tension, curvature and deformation history, and specific studies have been carried on for taking account of variable bending stiffness for the wrapped conductors.

All these studies found that the interaction may amplify significantly the responses of the equipment items relative to their stand-alone responses when the cable lacks sufficient slack, but there's also amplification, despite smaller, for cable with large slack values. In particular, the amplification can be particularly large for the higher frequency equipment item.

The purpose of this study is to develop a reliable finite-element model to describe the dynamic behavior of flexible conductors interconnecting electrical equipment items, in specific configurations under given boundary conditions and base motions. To do this, we want to reproduce through finite-element models experimental tests already done in the past, as well as experimental tests not yet done, but likely to be done in the future.

The first part of this study consists in modeling previous sine-start and frequency-sweep experimental tests of a cable conductor only, already present in literature. Reproducing previous tests is needed in order to be able of validating the current model, understanding the sensitivity to the different parameters and having a benchmark on which basing further analysis. After reaching this understanding, the sensitivity of the modeling to the various parameters affecting the solution is specifically checked: through these analyses, we understand what the cable dynamics depends primarily on. Then, all the parameters are set to the values that are found to guarantee a stable and accurate solution for each configuration, building a benchmark model common for all the experimental tests wanted to be reproduced.

The second part of this report aims to model the dynamic behavior of two electrical equipment items interconnected by a flexible wrapped conductor, subjected to different ground motions. A feasible configuration of interconnected electrical equipment items is individuated: an electrical component (equipment #1) is mounted in the top of a steel post, and an insulator (equipment #2) is installed on top of a support frame structure consisting of steel beams (simulating a second piece of electrical equipment), interconnected by a flexible stranded conductor, attached at the top of the two equipment items. Every equipment item, as well as the cable, is modeled through

equivalent beam, whose structural properties are specifically computed. The structural properties of equipment #1 are inspired to those of a current transformer, and equipment #2 to those of a transformer bushing. This is not a common configuration for high-voltage electrical substations, but it is just intended to represent a general possible system: since the flexibility of the model, a very large range of interconnected systems can be analyzed simply changing the structural properties of the equivalent beams representing the equipment items. Some ground motions are applied to the base of the structure, and the response of the system is computed. Different initial shapes of the cable are assumed for different tests experienced. When the input at the base of the two equipment items is an acceleration vector, the cable is assumed to be initially straight. Conversely, when the input at the two bases is a sinusoidal displacement, the cable is assumed to be initially slack, with certain sag, in order to accommodate the required displacement at the two ends of the cable. For all these tests, comparison are made between the response of the two equipment items in the interconnected and in the standalone configuration, to understand the influence of the presence of the flexible connection on the forces generated and the displacements experienced.

4.2 Glossary

A glossary is provided here since the terms are not too familiar to the structural dynamics engineers who need to develop or change some of the electrical devices as done in this report.

Electrical Substation: high-voltage facility used to switch generators, equipment, and circuits or lines into and out of a system. Substations can also be used to change AC voltages from one level to another, or for the purposes of inversion. In these facilities, direct current is changed to alternating current or alternating current is changed to direct current. Some substations are small with little more than a transformer and associated switches, while others are very large with several transformers and dozens of switches and other equipment. There are a number of distinct types of substations.

Distribution Substation: it is located near to the residential, commercial, or light industrial end-users, and changes the transmission voltage to lower levels. Typical distribution voltages vary from 19,920 volts to 2400 volts.

Collector Substation: it merges electricity from multiple point sources before delivery to the grid. Collector substations are found in at locations where multipoint power generation systems such as wind farms are used to augment grid capacity.

Transmission Lines: Power lines that typically have a voltage of 69 kV or higher. These lines are often protected from lightning strikes by shield wires or surge arresters.

Distribution Lines: power lines with a voltage lower than 69 kV.
Electrical Clearance: physical separation needed for the air gaps between conductors and nonconductors to provide safe working conditions and prevent flashovers. Minimum clearances can be found in the National Electric Safety Code (NESC 2007).

Rigid Bus System: buswork system in which the conductor is an extruded metal bar, typically an aluminum tube.

Cable Bus System: buswork system in which the conductors are low tension flexible wires supported on insulators.

Potential Transformer: it changes the magnitude of the primary voltage to a lower secondary value that can be used with various equipment measuring voltage. In substations, these devices are typically supported on a single pedestal.

Equipment #1: it is the same device as the potential transformer, but it measures current.

Bushing: it isolates energized components from supporting structures. Suspension bushings transfer tensile forces from the suspended conductor to the supporting structure. Station post bushings have the ability to transfer compressive and tensile forces to the structure as well as bending moments. They are constructed in a wide variety of both shapes and sizes, and may be formed using porcelain, glass, or composite materials.

4.3 Common Seismic Design of Substation Equipment

According to the previous introduction, the effects of connections made of wrapped flexible conductors must be included in the seismic design of substation equipment. At the present time, the most common practice is to take account of their effects as static loading only, providing

sufficient slack to let the expected relative displacement between interconnected equipment items during an earthquake, without generating destructive forces. More specifically, substation equipment is generally qualified on an individual basis to withstand the loads generated by an earthquake, with the effect of flexible conductors taken into account as a static force. For example, a static force of 1000 N/conductor is currently used in Hydro-Quebec's specification on the seismic qualification of substation equipment.

The other primary requirement is that all the connections between equipment are able to accommodate the large relative displacements that might occur, without generating impact forces, as specified in many standards. For example, a study performed after the Miyagi earthquake established some criteria for evaluating the required conductor slack for differential displacements of the interconnected equipment to have no significant impact. The study was primarily based on finite-element computer analyses of interconnected equipment items, without mentioning dynamic behavior of the conductors. However, other authors mentioned that the dynamic behavior of flexible connections might generate significant forces on interconnected equipment.

Various works presented different approaches developed to investigate the influence of the dynamic behavior of flexible conductors interconnecting electrical equipment under earthquake excitation. It has been found that they can be excited in resonance and generate significant forces on the equipment they are interconnecting, even when is provided sufficient slack to accommodate the expected relative displacement between interconnected equipment items. Therefore, the dynamic reactions of these connections must be considered for the proper design of substation equipment, and the substations must be designed not only to permit relative displacement between equipment, but also to avoid dynamic interaction.

One possible way to forecast whether the flexible connections are likely to be excited during an earthquake, consists of establishing their natural frequencies. Knowing these, possible resonances are avoided ensuring the connections have natural frequencies different from those of the interconnected equipment. Guidelines for seismic design of substation recommend experimental measurement of the natural frequencies rather than analytical studies, because of the uncertainty and inaccuracy regarding the mechanical properties of conductors made of

wrapped strands, due to highly nonlinear behavior as well as axial and flexural coupling. Next, some of these approaches will be presented and discussed.

4.4 Bending of Stranded Conductors

Before describing experimental tests and modeling of electrical equipment items interconnected by flexible stranded conductors, it's essential to fully understand the peculiarity of bending behavior of cable made of wrapped strands [7]. Generally speaking, a stranded conductor consists of a certain number of layers of wires helically wrapped around a central core. Typically, for overhead transmission line conductors, the core and some of the inner layers may be made of steel, while the outer layers are usually aluminum. Conversely, conductors typically used in electrical substations to interconnect equipment items are composed by aluminum wires of the same diameter, including the core. Each wire belonging to a given layer is centered on a radius r_i normal to the conductor axis, and each layer is wrapped over the core at an angle β_i with the same axis. Each layer comprises $n_i$wires of diameter δ_i, section $A_i$and Young's modulus E_i.

The tensile force, to which each individual wire of a given layer is subject, under the conductor's axial tension, is the same and it's given by [7]:

$$T_i = \frac{E_i \cdot A_i \cdot cos^2\beta_i}{\sum_i E \cdot A \cdot cos^3\beta} \cdot T$$

When in addition to an axial force, a wire in a given layer is also bent to a constant curvature of the conductor neutral axis, its bending stress consists of two terms. The first term is the stress arising from the bending of the wire around in its own neutral axis. This stress is the same for all wires belonging to a given layer, and varies linearly over the wire section from $-\sigma_{MIN,i}$ to $+\sigma_{MIN,i}$, being null on the wire neutral axis, with $\sigma_{MIN,i}$given by:

$$\sigma_{MIN,i} = E_i \cdot \frac{\delta_i}{2} \cdot \kappa$$

Therefore, this stress component is always present as a function of the actual curvature κ, thus independently of the history of deformation.

Conversely, the second stress term is due to the value of the friction between the wire and those in the adjacent layers. For the sake of simplicity, it is assumed that the friction forces between adjacent wires in the same layer are negligible. The friction forces between the layers depend on

the tension in the conductor and the helical wrapping, causing radial forces. When the bending reaches small values, these radial forces are sufficient high to prevent relative interlayer slipping; in this state, the wire sticks to the wires in the adjacent layers and is thus also bent around the conductor neutral axis. This 'sticking' stress, is therefore a function of the distance from the wire neutral axis to the conductor neutral axis, depending on the helical angle. When the wire is first bent from initially zero curvature, $\sigma_{STICK,ij}$ is given by:

$$\sigma_{STICK,ij} = E_i \cdot h_{ij} \cdot (cos^2\beta_i) \cdot \kappa$$

As mentioned earlier, this stress component is constant over the wire cross section and is equal for wires at the same distance above and under the conductor neutral axis. As the bending increases, at a certain point the friction forces acting on the wire are no longer high enough to prevent slipping and this stress component remains always equal to the maximum value reached before slipping. Obviously, this stress component will remain constant until there is a reversal in the sign of the rate of curvature change; then, the wire sticks again and the sticking stress will first decrease to zero, and then increases again in the opposite direction until slipping is reached again.

It's noteworthy that there's a big similarity between the variation in the sticking/slipping stress and the elasto-plastic material behavior. As a matter of fact, there are two stress regimes. The first is the elastic regime, when the stress increases or decreases linearly around a reference value, always with the same slope; the second is the plastic regime, when the wire is slipping. As mentioned earlier, the value of the elastic (sticking) stress must be computed according to the history of deformation, and therefore it depends on the curvature at the point of reversal in the sign of the rate of change of curvature in the plastic regime; thus, this value changes at every reversal in the sign of this rate in the plastic regime. The required change of curvature from the state of zero stress to the slipping state in either direction in the elastic regime is the absolute difference between the curvature at the point of reversal and the reference curvature. This value is a function of the tension in the conductor; therefore it changes according to the variation in tension. It is to be noted that the sticking/slipping stress component can become negative even while the curvature of the neutral axis is still positive, and vice versa, since it doesn't depend on the current curvature, but its rate of change.

4.5 Experimental Investigation on the Dynamic Behavior of Flexible Conductor

An experimental research program was initiated in 1996 by Dastous and Hydro-Québec's Research Institute [4] to investigate the influence of the dynamic behavior of connections, despite little information was available at that time. The scope of the study was to determine whether the flexible conductors have natural frequencies likely to be excited during an earthquake, and to take insight into their dynamic behavior. A method of establishing those natural frequencies was proposed, and it was described the dynamic phenomena as well as conditions, such as resonances, that might cause additional forces during such an event.

The method of establishing natural frequencies of flexible connections was proposed since they are difficult to determine analytically for many reasons. First, these elements are highly geometrically nonlinear, that means their properties and behavior depend on their current configuration; thus, a flexible connection subject to differential displacement of its ends has natural frequencies varying during the motion itself. Next, it's difficult to determine their mechanical properties, such as axial and bending stiffness, since they may change according to the level of tension in the conductor, the geometry and during time. As a matter of fact, for connections consisting on short conductor lengths, their tension can vary significantly during a differential displacement at their ends. Therefore, it could not be meaningful to try to analytically evaluate their natural frequencies, considering their variation during motion. For this study, the natural frequencies likely to be excited were determined by means of a frequency-sweep test performed at low amplitude, since the natural frequencies of the standalone electrical equipment are generally low.

Furthermore, since the natural frequencies of the cables depend on the amplitude of vibration because of their geometrically nonlinear properties, the tests were performed at amplitudes representative of those expected during an earthquake for the interconnected equipment items. The excitation was applied in the horizontal direction along the span of the connection. Two different variants of excitation were used: the first where a connection is installed between two equipment items oscillating out of phase, corresponding to the most extreme case, the second corresponding to a conductor connected between oscillating equipment and a fixed or not excited

one. The measured values were the horizontal reactions applied at both ends together with the frequency of excitation.

It is noteworthy that the excitation applied at the ends of a flexible connection is the motion at the top of the interconnected equipment excited at their base by the earthquake.

Since the substation equipment can be analytically modeled as linear single or multi-degree-of-freedom, the ground motion is filtered by it and the oscillation is mostly at its natural frequency, thus the motion at the top of the equipment is something close to a sinusoidal excitation of varying amplitude. Therefore, a frequency-sweep test at expected amplitudes allows investigating the dynamic behavior of flexible connections during an earthquake and their possible resonances. However, continuous excitation at constant amplitude during the frequency-sweep test, like those in the experimental tests, may have amplified the response at levels higher than those actually expected. The forces measured during resonance therefore provided an upper-bound estimate of those expected in practice.

In order to obtain a first evaluation of the severity of the results measured from the frequency-sweep test, sine-start tests were also performed. In this case, the motion consisted in the application at the ends of a sinusoidal excitation characterized by constant amplitude and fixed frequency; this scope was to evaluate how many cycles were required to obtain the same level of forces as those measured during the frequency-sweep tests. Finally, static tests were performed, consisting in applying a cyclic quasi-static differential displacement to the ends of the cable, in order to investigate the corresponding behavior.

4.5.1 Test Parameters

The amplitudes for the frequency-sweep tests were selected on frequency bands whose upper frequency was related to the amplitude used [4]. Both the amplitudes and corresponding upper frequencies were determined using validated seismic response spectrum for substations, for an acceleration of 0.34 g; in addition, a value of 2% was assumed for the critical damping. Selected values of amplitudes and related frequencies from the spectrum for these conditions are presented in Table 4-1.

Table 4-1: Spectrum Displacements and Accelerations

Frequency (Hz)	Displacement (mm)	Acceleration (g)
0.5	0.28	0.28
1	0.15	0.60
2	0.076	1.2
3	0.035	1.3
5	0.015	1.5
10	0.0045	1.8

In the case of substation equipment, the value of the displacement obtained from the response spectrum corresponds to the displacement at its centre of gravity, whose position depends on its mass distribution. Since the equipment in a substation are pretty different, direct use of the displacements obtained from the response spectrum was made. This approach is consistent with the goal of performing tests using realistic amplitudes.

The natural frequencies of standalone substation equipment typically vary between 0.5 and 10 Hz, but rarely exceed 5 Hz. Furthermore, since displacements corresponding to frequencies higher than 5 Hz are negligible, the higher upper-band frequency for the frequency-sweep tests was limited to 5 Hz. The lowest frequency for each band was assumed as 0.5 Hz. The values of amplitudes and frequencies adopted for each test are summarized in Table 4-2 and Table 4-3.

Table 4-2: Amplitudes and Frequencies for Sine-Start Experimental Tests

Test ID	Cable	Amplitude (mm)	Frequency (Hz)
#134	1796-MCM	150	1
#135	1796-MCM	80	2
#136	1796-MCM	40	3
#137	1796-MCM	20	3
#138	1796-MCM	20	5
#139	1796-MCM	20	1
#140	1796-MCM	20	2

Table 4-3: Amplitudes and Frequencies for Frequency-Sweep Experimental Tests

Test ID	Cable	Amplitude (mm)	Lowest Frequency (Hz)	Highest Frequency (Hz)
#130	1796-MCM	20	0.5	5
#131	1796-MCM	40	0.5	3
#132	1796-MCM	80	0.5	2
#133	1796-MCM	150	0.5	1
#156	4000-MCM	20	0.5	5
#157	4000-MCM	40	0.5	3
#158	4000-MCM	80	0.5	2
#160	4000-MCM	150	0.5	1

4.5.2 Test Specimens

Hydro-Québec substations were used for the tests; as mentioned above, since the present study was interested only in understanding the general behavior of cable dynamics, only one kind of configuration was modeled, and therefore presented hereafter [4]. Most of the tests were experienced on the 1796-MCM electrical conductor, while few of them on the 4000-MCM conductor, less common in electrical substations. In Table 4-4 the mechanical properties of the 1796-MCM cable conductor are summarized.

Table 4-4: Mechanical Properties of Cables 1796-MCM and 4000-MCM

Property	**1796-MCM**	**4000-MCM**
Material	aluminum	aluminum
Young's Modulus (MPa)	5.72e4	5.72e4
N° of Layers	5	10
N° of Strands	61	271
Strand Diameter (mm)	4.36	3.09
Overall Diameter (mm)	39.2	58.6
Cross Section Area (mm^2)	910	2027
Mass per Unit Length (kg/m)	2.509	5.698

The configuration of the cable was a catenary type with both ends clamped horizontally. The span was assumed in an interval from 5.0 to 5.6 m. In particular, for the tests shown and discussed hereafter, a total length of 5.52 m and an initial span of 5.00 m for the 1796-MCM conductor, and a total length of 5.64 m and an initial span of 5.15 m for the 4000-MCM were adopted. The effect of the sag/span ratio on the natural frequencies and the dynamic behavior was studied: ratios of 0.08, 0.12, 0.16 and 0.20 were used by varying the span for conductors of fixed lengths. One support was moveable, in order to obtain the desired span and sag / span ratio. It has to be noted that the National Electrical Safety Code [1] doesn't provide specific limit about the range of sag / span ratio for flexible cable conductors, but only absolute reference values for the clearances between the cable, or its lowest point, and other facilities, depending on external conditions. Since a specific range for sag / span ratio is not defined, it was decided to use a feasible one. This range, whose boundary values are 2% and 20%, has been confirmed and validated for year 2009 by Ansell Schiff [26].

The sinusoidal excitation applied to the ends of the cable was transmitted by a rotating disk coupled with a sliding mechanism; the required amplitude was set by attaching this mechanism at different radii on the disk, and the frequency of excitation during the frequency-sweep was adjusted by a frequency controller. The load cell used to measure the horizontal reactions generated at the ends of the conductors had a 4500N capacity, and the capability of measuring only axial forces (both compression and traction) and insensitive to loads in other directions (vertical, lateral or rotational).

4.5.3 Static Tests

In the static tests, quasi-static cyclic differential displacement at large amplitude was applied to the cable connection [4]. A significant sudden change in traction was observed, as the flexible connection was stretched to a span close to its total length: this confirms the need to accommodate the differential displacement providing sufficient slack to the cable. For large sag, compression forces were observed, highlighting the importance of bending stiffness on the behavior of conductors for short span at low tension. It was also observed that the conductor behavior varies as its tension increases and decreases, with the traction following a hysteresis cycle; this means that the mechanical properties of conductors change during a cycle, confirming the material nonlinear behavior of short conductors.

4.5.4 Frequency-Sweep Tests

All the frequency-sweep test were performed only for amplitudes that allowed the corresponding differential displacement without generating impact forces [4]. Since the cable experiences large displacements and its behavior is highly nonlinear, it is not completely correct to reason in terms of natural frequencies, but rather in terms of frequencies likely to be excited during an earthquake. These resonant frequencies, that means those likely to be excited during an earthquake, were identified using spectra built measuring the minimum and maximum values of horizontal forces for the corresponding frequency. During the sweep tests three predominant behaviors were observed.

First, cable oscillating in a stable way around its equilibrium position, without any abrupt change of amplitude or forces: this can be called dynamic stability. This behavior is characterized by the forces varying cyclically between two extremes, corresponding to the minimum and maximum spans reached for a given amplitude and frequency of sinusoidal input. It is noteworthy that the minimum and maximum levels of the forces increase monotonically with the frequency; this indicating that no natural frequencies are significantly excited. It was also observed that the forces generated dynamically can be of compression and considerably higher than those developed statically. In particular, the results showed that a high sag/span ratio favors dynamic stability over a wider range of amplitudes and frequencies. It was observed that the highest forces were typically developed at low amplitudes, at frequencies close to the upper limit of the test band, from which can be concluded that dynamic effects play a key role in generating horizontal forces, depending more on frequency than on amplitude.

Resonance was the second observed behavior. In this case, there was a sudden amplification of the forces at the cable ends; sometimes, the resonance led to a large oscillation of the conductor that lashed back and forth generating big impact forces, closely to a dynamic instability behavior. Also, there was often a lateral motion, highlighting that modes in two orthogonal directions can be coupled during dynamic excitation in only one direction. In some cases, the tests were stopped to avoid damage to the testing setup, due to the severity of the resonances. This evidenced that the natural frequencies of a flexible connection vary during motion that means a given configuration can be excited in resonance over a range of frequencies rather than at one specific frequency alone. This is why it's not completely correct to reason in terms of classical natural frequencies. It was observed that the level of forces reached for both types of excitation

was of the same order of magnitude: since excitation at one end only is less idealistic than out-of-phase excitation, this means that significant forces can be developed in resonance, even if only one end of a connection is excited in the proper frequency range. The resonances frequencies varied according to the sag/span ratio, as well as the amplitude of excitation; generally, higher frequencies were excited at smaller amplitudes and vice versa.

The third meaningful observed behavior was compression in the cable. It was showed that big compression forces may be generated during motion, and were higher for the higher sag/span ratio, according to the fact that traction in the cable can be very low for large sag, due to the low bending stiffness of the cable and the short span used. The magnitude of the compression forces measured was lower than the traction ones, but although impressive in resonance. Therefore, the reactions at the end of the cable can oscillate from a high value of traction to a high value of compression during motion. This means that the resultant force applied to the top of equipment with connections on both sides can be the combination of forces in the same direction, since traction forces can be developed on one side while compression forces can be developed on the other.

4.5.5 Sine-Start Tests

The scope of the sine-start tests at fixed frequencies was to investigate the number of cycles of oscillation required to obtain the same level of horizontal forces measured during the sweep tests [4]. The tests were performed both at frequencies characterizing dynamic stability and resonance; for all the tests performed, 3 to 5 cycles were necessary to reach the same level of force obtained during the sweep tests. This means that the level of forces obtained during the sweep tests could be achieved also during an earthquake, when the equipment is excited for a few cycles only.

4.5.6 Conclusions

This study showed the big importance of dynamic behavior of flexible connections in response to the excitation generated by an earthquake [4]. Frequency-sweep tests at realistic amplitudes on selected frequency bands were considered an appropriate way to evaluate the frequencies of connections likely to be excited during such an event. The final conclusions were the following.

Almost all the results showed that such forces might be dynamically generated, even when sufficient slack is provided to account for the differential displacement between the interconnected equipment items. Flexible connections interconnecting substations equipment are highly geometrically nonlinear systems, characterized by frequencies likely to be excited in the range 0.5 to 5 Hz during a ground motion; due to their nonlinear behavior, these frequencies vary according to their current configuration. Furthermore, large forces, both of traction and compression, can develop at the ends of cables excited in resonance. The maximum forces measured in resonance were achieved for small amplitudes of excitation, indicating that it is not sufficient to seismically design connections on a static basis only, in terms of allowing for the differential displacement expected at their ends; nevertheless, a large sag/span ratio tends to promote the dynamic stability, avoiding the risk of resonances.

Therefore, it is important to design flexible connections so that the range of natural frequencies at which they are likely to be excited are different from those of the equipment they are interconnecting, in order to avoid the risk of dynamic interaction and resonance between them.

4.6 Constant Bending Stiffness Studies

Studies on the dynamic behavior of flexible conductor typically interconnecting high-voltage electrical substation equipment items, considering a constant bending stiffness for the cable itself, have been presented by A. Der Kiureghian, K. J. Hong and J. L. Sackman, 1999 [9].

A typical electrical substation consists of a complex set of interconnected electrical equipment items, such as transformers, circuit breakers, surge arresters, capacitor banks, disconnect switches, etc. As shown in various works of different authors, these equipment items are often connected to each other through flexible conductor cables: significant dynamic interaction between them may occur during seismic events, even whether the cable is sufficiently slack to accommodate for the relative displacement. This kind of interaction is likely to be responsible for some of the observed damage in electrical substations during past earthquake, also when the equipment items were qualified to stand for a ground motion of that severity.

Der Kiureghian's studies investigated, through a finite element model using frame elements and a Lagrangian formulation taking into account large displacements, the effect of interaction in two equipment items connected by a cable and subjected to a horizontal earthquake ground motion in

the plane of the cable. The influence of interaction was evaluated by calculating the ratios of the equipment responses in the connected system to their corresponding responses in their standalone configurations. For the sake of simplicity, since the study was more concerned on cables, each equipment item was modeled as a linear system with distributed mass, damping, and stiffness properties. Through the use of a prescribed displacement shape function, each equipment item was characterized by a single degree of freedom, neglecting the modes higher than the first. This assumption is consistent with the fact that the displacements at the ends of the cable have amplitudes and frequencies filtered by the interconnected equipment; since its mass proportional to the first mode was observed to be about 80%, it can be considered the only significant.

4.6.1 Catenary Cable

Actually, the shape of an extensible cable is not a catenary, because the strain along the cable varies according to the inherent tension force [10]. However, for cables generally used in the power industry and for overhead transmission, the axial deformation is significant only for extremely taut cables. But also in that case, the tension force in the cable is essentially a constant, generating an uniform strain along the cable and, thus, a catenary shape.

In the first part of the study, the connecting cable was modeled as an extensible catenary cable, neglecting both its flexural stiffness and inertia. Under these assumptions, it was possible to derive a closed form expression for the stiffness of the cable, and there was no need to model the cable by finite elements with a formulation capable to account for large deformations. Two equipment items with distributed mass, damping, and stiffness properties, with a vertical separation of the supports and connected by an extensible catenary cable were considered; the system was then subjected to a horizontal base motion. For the sake of simplicity, each equipment item was modeled as a linear, single-degree-of-freedom system by describing only its horizontal displacement at the point of attachment. Also damping coefficients were included to take into account energy dissipation in the equipment items; their values were computed on the basis of an estimated modal damping ratio for each of them. It is noteworthy that energy dissipation also occurs in the cable due to slippage of the strands one other under friction forces; actually this is a very complicated phenomenon, for which several simplified models have been presented in literature. Nevertheless, the contribution of the cable damping to the energy dissipation in the total system can be considered negligible: therefore, it’s a conservative

approach to neglect the cable damping. In order to compute the nonlinear response of the interconnected system, the classical Newmark step-by-step time integration algorithm was adopted, together with a Newton iteration scheme at each step to solve these equations; this required to compute the tangent stiffness matrix at each time step.

As measures of interaction between the two equipment items, the ratio of the equipment responses in the connected system to their corresponding responses in their standalone configurations was adopted. Therefore, if the ratio is > 1, the response of equipment in the interconnected system is amplified on account of the interaction effect, whereas if the ratio is < 1 it is de-amplified. It is also noteworthy that, since the equipment items are linear and described by a single displacement shape function, all internal forces are linearly proportional to the corresponding displacement responses. Therefore, the same response ratios can be considered for the maximum internal forces in each equipment item. The seismic demand on the interconnected system can be measured by the maximum relative displacement of the standalone equipment items away from one another; next, based on this a parameter to predict the effect of interaction can be defined. This approach is particularly easy, since this value can be directly computed in terms of the response spectrum of the ground motion and properties of the standalone equipment items.

The responses in the interconnected system showed strongly peaks relative to their static equilibrium positions, with larger displacements occurring towards the side that slackens the cable. In particular, the amplification in the peak response of the higher frequency equipment was the most significant: this is absolutely not surprising, since this equipment tends to act as a restraint against the motion of the lower frequency one, which in turn tends to generate large motions on the higher frequency equipment item. The peak forces were more than two orders of magnitude greater than the initial cable force: these occurred when the cable was stretched to its utmost straight position. These results confirmed that, when the cable does not have sufficient slack, allowing the relative displacements, the interaction between the two equipment items develops large additional, in particular for the equipment with higher frequency. This was especially evident when the ends of the cable were attached at different heights, generating a vertical component of the forces in the cable. To avoid all these adverse effects, criteria for selecting the cable length to provide sufficient slack were found advisable.

4.6.2 Cable with Flexural Stiffness and Inertia

The cable inertia tended to cause further forces amplification, especially when the ends of the cable were attached at different heights [10]. The interest of the study was, thus, concerned on slack cables with axial and flexural stiffness undergoing large deformations under dynamic loading. Although a theory for the dynamics of taut cables experiencing small deformations developed by Irvine was available since 1981, the finite deformation problem was practically impossible to be solved analytically. Therefore, a numerical solution through the finite-element method had to be sought. A brief description of the section properties of the cable subjected to study is the following.

Cable conductors typically used either in the power industry or for overhead transmission are made of helically twisted strands of aluminum wire. If neglecting the small lay angle that the wires make with the axis of the cable, the cross-sectional area is simply the sum of the areas of the individual strands. The two ends of the cable are typically attached to the equipment items through welded connectors, so that is not allowed any unwrapping of the strands. When a tension force is applied to the cable, the wrapped wires will be tightened before the full axial stiffness of the cable can be developed. Conversely, when the cable is subjected to compression, the twisted wires can open, or even the outer strands can buckle. This means that the axial stiffness of the cable, either for a small tension force or a large compression force, could be smaller than the sum of the axial stiffnesses of the individual strands. For the sake of simplicity, and considering these effects negligible, the analyses were made ignoring these effects and assuming that the axial stiffness of the cable section was constant and described by EA, where A is the sum of the areas of the individual strands, and E is the elastic modulus of the cable material (typically aluminum).

The flexural stiffness of the cable section was given by the product EI, where I denoted the effective moment of inertia of the section; in this case, the choice of I was not univocal. As a matter of fact, the value of I depended on whether the strands at the cross section remain attached or slide with respect to one another during the cable motion. The minimum value of the inertia was obtained under the assumption that all the strands were freely sliding against one another. In the actual system, when the cable was subjected to high tension, significant friction may be generated between the strands; this may prevent sliding of some of the strands and let a larger effective moment of inertia develop. The maximum value of I, obtained by assuming that all strands remained attached, was calculated considering the solid cross section of the strands

forming the cable. Actually, the effective moment of inertia of the cable at each cross section was somewhere between the above two extremes: unfortunately the two bounding values are widely apart for typical cables. For example, for the modeled hereafter 1796-MCM cable, consisting of 61 strands divided in five layers, the upper bound is about 80 times the lower bound. IEEE guidelines (IEEE 1999) directly recommend an approximation based on experimental tests conducted in the 1990s, where the value of I is computed by multiplying the inertia of a single strand times the number of layers increased by 1. It was assumed a constant moment of inertia throughout the length of the cable at all times, and equal to the approximation of the IEEE guidelines.

For the finite-element analyses, the cable was modeled by 100 frame elements having uniform length and cross-sectional properties as described above. Geometric nonlinearity due to large displacements and rotations was fully taken into account by using a Lagrangian deformation formulation based on the Cosserat rod theory. The finite-element program FEAP [28] was used for the analyses.

It is to be noted that the dynamic analysis of a cable undergoing large displacements and rotations is a highly nonlinear elasto-dynamic problem without known analytical solution, and even numerical solutions of this problem are challenging. During the dynamic response, since the cable is undergoing severe compression and traction forces, the axial stiffness dominates the flexural behavior, generating significant high frequency effects; these high frequencies, in addition to the spatial discretization employed in the finite-element model, may give rise to inaccuracy and instability in the numerical computations. Therefore, under these conditions, the Newmark time integration algorithm, which obviously can be successfully used for the catenary cable, does not lead to stable and accurate results. Furthermore, the classical Newmark family of algorithms typically has no capability to conserve the total energy and angular momentum for nonlinear elasto-dynamic problems. Since conservation of the energy and momentum through the numerical time integration algorithm was essential to achieve a sort of stability, a numerical algorithm that does preserve the total energy and angular momentum was needed: one algorithm with these capabilities is presented in Simo et al., 1992 [27]. The finite-element computer program FEAP provides a modified version of this algorithm (Simo et al., 1995), that introduces numerical damping to stabilize the computations, while only slightly compromising on the conservation of energy and angular momentum. Experience showed [10] that this modified

algorithm with parameter values $\alpha = 0.55$, $\beta = 0.5$, and $\gamma = 1$ and time step $\Delta t = 0.0005\ s$ worked successfully for the dynamics of this kind of cables. Conversely, parameter values of $\alpha = 0.5$, $\beta = 0.5$, and $\gamma = 1$ would have corresponded to the energy conserving algorithm with no artificial numerical damping.

The first step of the analysis consisted in understanding the initial shape of the cable, clamped at its two ends and under its own weight. Due to the flexural stiffness, the shape of this kind of cable was considerably different from the catenary shape. It is noteworthy that a cable having flexural rigidity and held between two fixed supports is a statically indeterminate system, since the horizontal support force for such a system cannot be determined from equilibrium considerations alone. Therefore, an approach different from the classical equilibrium method was needed, in order to get the initial shape and the initial internal forces inherent the cable. For the present analysis, the cable was assumed initially straight, with the two ends distant one another the total length of the cable. After fixing both ends, the gravity load was applied and the right support was then moved horizontally towards the left support until the initial span was reached. Only in the case the configuration of the cable showed also a vertical separation of its support points, the right end of the cable was moved vertically by consequence. Both cables with and without vertical separation between their ends were tested, obtaining different responses.

Only the horizontal component of the ground motion in the plane of the cable was considered in the analysis. The cables with no vertical separation experienced almost only vertical motions, therefore the inertia forces in these cables were primarily vertical, despite resulting from the horizontal motions of their end points. The cables with vertical separation experienced significant motions in both the horizontal and vertical directions, since they had significant inertia forces in their transverse direction.

Because of these effects, significant interaction between the interconnected equipment items can be expected, even when the cable has sufficient slack. By way of comparison with the same systems with the catenary cable, the response ratios were found to be primarily influenced by the cable inertia and flexural stiffness: it means that cable inertia can further amplify this interaction effect. This amplification can be especially significant for the equipment item that has the higher frequency. Obviously, since the cable behavior is highly nonlinear, it's not completely correct speaking of natural modes of vibration in the usual sense for linear systems. Nevertheless, when

the dominant frequency content of the excitation matches certain critical frequencies with appropriate amplitudes, then a dynamic instable behavior can be observed in the cable, just like a resonance. This is the same phenomenon observed in the experiments on cables subjected to imposed harmonic end displacements made by Dastous and Pierre, 1996 [4].

The results of this study provided new insight into the strongly nonlinear behavior of the electrical system interconnected by cable and the effect of interaction, through a reliable finite-element method; this method of analysis had been also used to develop a design criterion for the required cable slackness for electrical substation equipment.
Furthermore, this same numerical computational approach had also been used for dynamic analysis of overhead transmission cables subjected to wind forces, or other dynamic excitations.

4.7 Variable Bending Stiffness Studies

Studies on the dynamic behavior of flexible conductor typically interconnecting high-voltage electrical substation equipment items, considering a variable bending stiffness for the cable itself, have been presented by J-B. Dastous, 2005 [7].

In addition to the geometrical nonlinearity of stranded flexible conductor mentioned above, its bending stiffness can vary during motion according to its tension, curvature and history of deformation, this resulting in a material nonlinear behavior also. In order to fully understand the dynamic behavior of such a cable, a calculation method capable of taking into account both material and geometrical nonlinearities must be used. This was the purpose of Dastous' (2005) analytical study [7], following his experimental work [4]. The geometric nonlinearity due to large displacements experienced by the conductors can be successfully handled by finite-element analysis with the capability of an adequately beam element formulation. Most of commercial and research finite-element programs have such elements available in their library. The most delicate issue is adequately handling the variable bending stiffness of the flexible cable, and therefore the material nonlinearity arising from it, since this capability is not widely spread in commercial programs. This difficulty comes in particular from the mandatory requirement that the bending stiffness vary with the inherent deformation history and variation in tension. Nevertheless, an abundant literature on the bending stiffness of conductors was available, and the scope of Dastous' study was therefore to implement one of those formulations, in order to fully cover also

this particular aspect of the cable dynamics. It was chosen to adopt and implement the work of Papailiou [25], since it was a practical model of variable bending stiffness completely adaptable to finite-element formulation. This model presented the complete capability of taking into account the phenomena of the interlayer friction force and the slipping of the strands one another in the conductor during motion, by building a variable secant bending stiffness that changes with the variation of curvature and tension. Before implementing it for dynamic analyses, it had been validated experimentally on initially straight conductors subjected to static transverse force, at tensions representative of overhead transmission lines. For the purpose of this study this model was implemented in a classical finite-element program based on the tangent stiffness method, expressly designed to taking into account the specific loading used in the experimental tests; furthermore, it was adapted to treat arbitrary types of dynamic loading and to address both material and geometrical nonlinearities, as these are typical of many applications regarding stranded conductors. The choice of using the tangent bending stiffness instead of the secant tangent stiffness was made because it is the base for nonlinear finite element formulation used in most general-analysis computer programs. This formulation was implemented in the finite-element program FEAP, specifically dedicated to research purposes [28].

4.7.1 Bending Stiffness Calculation

In the general finite-element formulation of equilibrium was implemented the proposed model making use of the tangent stiffness matrix of the structure under analysis [7]. The tangent value is the actual slope of the moment-curvature relationship for a given curvature. The tangent bending stiffness can be calculated by summing the contribution of the core and each layer. The tangent bending stiffness of layer can be decomposed by summing the contribution of each wire in the layer according to its actual state, sticking or slipping. More specifically, the bending stiffness of a wire in the sticking state is composed of the contribution of its bending around its own neutral axis and the bending of its section around the conductor neutral axis. For a wire in the slipping state, the contribution of tangent stiffness from the bending of the wire section around the conductor neutral axis is lost as soon and as long as the wire is slipping; consequently, it is reduced to the contribution from the wire bending around its own neutral axis only. For a given layer, the tangent bending stiffness is thus obtained by summing the contribution of the sticking bending stiffness and the slipping bending stiffness, according to the state of each wire. When all wires in all layers are in the sticking state, the value of the tangent

bending stiffness is therefore maximum; conversely, when all wires slip, is minimum. The substantial difference between the secant and tangent bending stiffness is that the tangent bending stiffness varies in a staircase way, while the secant bending stiffness varies in a smooth monotonous way. This is because the tangent bending stiffness is based on the contribution of the different wires in the conductor section that are slipping at different curvatures; furthermore, the tangent stiffness reaches its minimum value at the curvature when the last wire slips. It is noteworthy that the secant and tangent stiffness methods are equivalent and lead to the same results.

4.7.2 Internal Moment Calculation

As for the tangent bending stiffness, the internal moment in each element has to be calculated at every iteration, and the contribution from every layer can be computed by summing the contribution of each wire in the layer according to its state [7]. Because of the two stress components present during bending mentioned above, the contribution of each wire can also be decomposed into two components, as the contribution from the stress arising from the bending of the wire around its own neutral axis and the contribution of due to the state of friction between the wire and those in adjacent layers, depending on whether the wire is in the sticking or slipping state. This computation requires not only the current curvature but also the reference value that has to be updated for every wire every time there is a reversal in the sign of the rate of change of curvature; this means monitoring the state of every wire at every moment, which in turn will slow down the computational process.

For the sake of simplicity, it was found more practical to use the average slip criterion for each layer: this implies that all the wires in a layer slip simultaneously at a single average curvature change. For a layer, this can be easily computed by equating the moment for the layer in the fully slipped state to the average moment in the sticking state at the onset of slipping, under the approximations that all wires slip simultaneously. By comparison on the same model analyzed with the implementation of either the tangent stiffness based on the average slip criterion or the real tangent stiffness, it was observed that the calculated moments presented very small difference. Therefore, this criterion provides a reliable and acceptable approximation for the tangent stiffness, with much less computational effort.

4.7.3 Implementation in a Finite-Element Formulation

During the time integration of the dynamic problem, the tangent bending stiffness and the internal moment must be computed at every iteration [7]. As mentioned earlier, the bending stiffness is obtained by summing the contribution of each layer, as well as the internal moment from every layer is calculated and counted to obtain the element total internal moment that will be used for calculating the internal-load vector. Since these quantities change according not only to the current curvature, but also to the deformation history, a material constitutive law must be developed to adequately compute the bending stiffness during the iterative process.

The moment-curvature relationship for a layer is bilinear when making use of the average slip criterion, with the tangent bending stiffness oscillating between the maximum value, when all wires are sticking, and the minimum, when all wires are slipping. It is noteworthy that the variation of bending stiffness for the sticking/slipping component is completely analogous to that of an elasto-perfectly plastic material. In the iterative process, the constitutive equation must therefore determine which state a given layer is in, through a specific test. The test on the layer state consists in checking whether the difference between the curvature at a given iteration and the reference curvature at the beginning of the same time step is smaller or larger than the average curvature change required to pass from the sticking to the slipping state. Actually, at every iteration a tentative reference curvature must be calculated and, at the last iteration after convergence is achieved, this will become the new reference curvature for layer for the beginning of the next time step. When in the slipping state, the tentative reference curvature is updated at every iteration, while at the beginning of a new time step, when a layer is found in the slipping state at the end of the previous step, the initial position of the converged curvature is at the point of onset of slipping on the sticking/slipping curve. Obviously, all the elements need to implement this variable tangent bending stiffness in the general material-constitutive equation that the beam element routine calls when forming the element tangent stiffness and its residual at the required iterations.

4.7.4 Time Integration Method

Since the cable dynamics is affected by geometrical and material highly nonlinear behavior, a particular class of time integration methods was needed to achieve accurate results [7]. For either static or dynamic problems, the nonlinear solution was obtained step by step through an iterative

process: numerous methods exist for this, but the most popular one is the Newton–Raphson method and its variations. It consists in evaluating the tangent stiffness matrix of every element at regular iteration steps during the search for a solution for each step; at the same time, it also calls for evaluation of the internal forces, in order to compute the internal-load vector.

For a dynamic problem, this finite-element equilibrium problem must be extended to a second-order problem involving inertial effects, requiring a time-stepping algorithm to calculate the dynamic solution for each time step. In most commercial finite-element programs the time-stepping schemes used is the implicit Newmark–Beta algorithm, belonging to the Newmark family of algorithms [23]. Nevertheless, this class of algorithms is not capable of achieving accurate solution for the cable dynamics problems, because of two main reasons. First, this family of algorithms generally fails to conserve total angular momentum for nonlinear systems, losing the accuracy of the results obtained when the system is subjected to significant angular motion. Next, the axial stiffness in the cable dynamics can introduce artificial high-frequency oscillations contaminating the response of the system; therefore an algorithm providing high-frequency numerical dissipation, like the Wilson-method [2], is needed. In the finite-element program FEAP, used for this study, is implemented a time-stepping scheme preserving angular momentum and capable of numerical dissipating high-frequencies, thus able to accurately treat cable dynamics problems [28]. As a matter of fact, a light numerical damping was introduced in order to avoid the high-frequency oscillations discussed above, at the expense of compromising just slightly on the conservation of energy.

4.7.5 Modeling of Experimental Tests

The tangent stiffness model was used to model some previous experimental tests on short-span flexible conductors used to interconnect substation equipment; the level of tension in the conductor was generally so low that compressive forces could be generated [4]. The tests were performed in a general study whose purpose was evaluating the additional end forces generated at the attachment point of interconnected substation equipment during dynamic motions. More specifically, they consisted in cyclically stretching / compressing a conductor in a catenary configuration at circular frequency at fixed amplitude around an average span, while measuring the horizontal traction forces generated at the cable ends. Two different types of conductors were

used, the 1796 MCM and the 4000-MCM conductor. The mechanical properties of those two conductors have already been shown in Table 4-4.

The modeling was done through the finite-element program FEAP, due to its advantages discussed above, with a user element subroutine consisting of a custom- modified frame element with the variable tangent bending stiffness constitutive equation described earlier. The axial rigidity EA was considered constant through the length of the cable, and a value of 69900 MPa was used for the elastic modulus. A friction coefficient of 0.5 was used for the building of the variable bending stiffness matrix. The conductor was subdivided into a finite number of elements, with their properties assumed constant over their length: to model each element, a large displacement / small deformation beam element formulation was adopted, in order to take care of the geometrical nonlinearity present. A relatively large number of elements was therefore required: an adequate number was found to be 100 to lead to accurate results. For the sake of simplicity, coupling between bending and either torsion or tension was neglected. Obviously some type of damping was needed in the model, in order to accurately reproduce the experimental tests. Since accurate modeling of damping is a very complex issue and many forms of damping are actually present, and furthermore it is indeed a function of frequency and amplitude, it was decided to use an equivalent viscous form of damping, calibrated with experimental results. The damping was modeled in FEAP using single-degree-of-freedom viscous dashpot dampers connected to all the internal nodes of the finite-element conductor model: since the damping is directly related to the slipping of the layers over each other, that means to the bending process, the best way to model such damping was to make it proportional only to the rotational degree of freedom. Nevertheless, it was found that this simple approach was sufficiently adequate to lead to a good approximation. Since the damping was to be applied at every node, it was decided to use a single value of damping by unit length, equally divided among all the nodes for a conductor of given length. After calibration, these values were found to be for the two types of conductors:

1796 MCM $\quad c_\theta = 10\ N \cdot s$

4000 MCM $\quad c_\theta = 35\ N \cdot s$

These values of rotational damping were then multiplied by the length of the cable, and divided by the number of nodes in which the cable was subdivided, to find the value to be applied at each

node. Furthermore, a mass was lumped at each end, in order to represent the mass of the load cell and the conductor clamp: after comparisons, a mass of 7.1 kg was used for the 1796-MCM conductor, and a mass of 12 kg for the 4000-MCM conductor.

The first step consisted in the calculation of the static equilibrium position of the conductor before applying cyclic displacement at both ends. Since the shape of the cable under its own weight cannot be computed by only equilibrium considerations, it was decided to start with an initially straight conductor without mass, and then linearly increment its weight from zero to the full value, as a distributed dead load. Then, one end was horizontally moved until reaching the desired span with a linear increment. Using a relatively small step increment, the equilibrium at each step is usually reached within an average of 3–4 iterations.

4.7.6 Results

For the quasi-static cycling tests, conducted with low circular frequency applied displacement, measuring the horizontal traction at one end, it was first observed that the level of tension predicted by the model was in excellent agreement with the experiments, especially considering the large nonlinearities present [7]. As a matter of fact, it is noteworthy that these tests corresponded to relatively large displacements of the conductors, since they were stretched almost to horizontal and then back to a relatively high sag; therefore large variations in their axial tension during the cycling were observed, corresponding to very strong nonlinearities. It was also observed that the hysteresis predicted by the model was much less than that obtained experimentally, also despite varying the friction coefficient, trying to better match the experimental results. One possible explanation was found to be the significant backlash in the mechanism used to transmit the motion at both ends, since it was observed during the experimental tests that there was a little slipping of the mechanism when the maximum span was achieved. It was also found that the model was able to adequately reproduce the shape of the cable under its own weight: this aspect didn't surprise, since the finite-element programs based on the displacement method provide more accurate displacements than forces.

The same comparisons were made also for the dynamic tests: the only difference with the quasi-static tests was that the displacements were applied dynamically at frequencies representative of the standalone natural frequencies of substation equipment. In particular, two different types of tests were developed, the first being the frequency-sweep tests at given amplitudes over a range

of frequencies, and the second being the sine-start tests at fixed amplitude and frequency. For the frequency-sweep, it was observed that the model predicted the measured traction with acceptable accuracy, despite a little smoothing of the model response over some frequencies as opposed to the experimental results: probably this can be related to the wrong approximation assumed for the damping. As expected, compression forces were also developed, due to the bending stiffness, which was more significant since the conductor had short length. Other comparisons between the model and the experimental results were made on the difference between the maximum and minimum horizontal traction force measured for a given cycle of applied displacement at a fixed amplitude and frequency. It was observed that the model reproduced with good accuracy the experimental results, with a maximum error of 20% and an average error of 7% for the 17 tests compared. Therefore, it could be concluded, from both the static and dynamic comparisons, that the presented model was completely adequate to representatively predict the dynamic response for short-span flexible conductors, typically connecting high-voltage substation electrical equipment.

4.8 Framework of the Present Study

The study presented in this report aims first to reproduce some of the mentioned above experimental tests through finite-element models, in order to try to match their results, thus providing a reliable model to describe the dynamics of flexible conductors. The experimental tests used for the comparisons are those described earlier in this report, since they had already been modeled successfully by other authors, thus they can be considered a reliable benchmark. Different models are investigated, some of them based on Der Kiureghian's studies [10], while others on Dastous' approach [7]. This aims to better understand the differences between these two approaches, their advantages and disadvantages, in order to be able to knowingly choose the most suited model for the further development.

Two different finite-element programs are used. The first is ABAQUS, a popular general-purpose analysis finite-element software, with the capability to take into full account the geometrical nonlinearity risen from the large displacements of the cables. It is chosen thanks to its characteristics of flexibility and easily adaptability to various changes in the model and in the type of the analysis. Therefore, it can be successfully used for static analyses as well dynamic ones, both with displacement control input and acceleration input, the last the most suited for

typical seismic analyses and earthquake simulations. The second finite-element computer program used is FEAP [28], a specific software committed to research purposes, thanks to the advantages described above. First, it allows recalling user-defined subroutine to build and consider the variable tangent bending stiffness, thus fully accounting for the material nonlinearity stemming from the interlayer friction due to the slipping of the strands over each other. Second, as most of finite-element programs, in its regular library are available beam formulations providing the capability of large displacement / small deformation, mandatory to take into account the geometrical nonlinearity affecting the response for dynamics of cables.
Next, contrary to ABAQUS, which only time integration method available is a classical HHT-alpha method [2], belonging to the Newmark method family [23], FEAP provides more recent energy-conserving methods, such as that presented by Simo, Tarnow and Wong, specifically designed for highly nonlinear dynamics [27]. As already discussed, such a method is necessary in order to lead to an accurate and stable solution, also when the response is affected by meaningful nonlinearities, both mechanical and geometrical. The Newmark family algorithms lack all these requirements, thus they need to use very small time steps as well as small values of the half-time step residual tolerance, that is the limit on residual forces at which the current solution is accepted for the time step, and the integration process moves to the next one. Since it's not possible to correctly speaking of stability for the nonlinear dynamics, it's not possible to set specific values for those parameters, but their setting is left to the experience and sensitivity of the user. In the following, their values are decided analysis by analysis, according to the different characteristics of each of them.

FEAP also requires the setting of some parameters for its integration method: it is decided to let these values equal to those already used by previous studies, like Der Kiureghian's [10] and Dastous' [7], since they were already found to be acceptable. The biggest disadvantage of FEAP is the unavailability of imposing acceleration input at the ends of the cable; as a matter of fact, the only available boundary conditions are either forces or displacements, but not accelerations.

Generally, in this work ABAQUS is used for analyses based on Der Kiureghian's approach, since they don't utilize and, thus, require the variable tangent bending stiffness. Nevertheless, particular attention must be focused on the correct and reliable choice of the parameters for the time integration method, in order to lead to a sufficient accuracy of the solution. Conversely, FEAP is used for the analyses based on Dastous' model, in addition with the user-defined

subroutine for the variable tangent bending stiffness. Thanks to the literature on these two models [7, 10] and the experimental results reproducing, it is possible to make some changes and validate other models, by direct comparison between the results obtained.

4.9 Scope of the Present Study

The purpose of this study is to understand the dynamic behavior of flexible conductors interconnecting electrical equipment items, in specific configurations under given boundary conditions and base motions. To do this, we want to reproduce through finite-element models already available experiments as well as of experimental tests not yet done, but scheduled to be done in the future. The importance of achieving a reliable model lays in the fact that it was widely observed that the interconnection between electrical equipment items made by flexible conductors can negatively affect their dynamic response. As a matter of fact, additional forces are generated since the cable can be excited in a sort of resonance when its ends are subjected to displacement with certain amplitudes and frequencies. This can turns in failures of equipment items, also for seismic events lower than those they were certified to stand for. Reproducing previous tests is needed in order to be able of validating the current model, understanding the sensitivity to the different parameters and having a benchmark on which basing further analysis. After reaching this consciousness, it is possible to specifically check the sensitivity of the modeling to the various parameters affecting the solution: through these analyses, it's easier to understand what the cable dynamics depends primarily on. Once achieved this, it is possible to set all the parameters in order to seek for a stable and accurate solution for each of the tests, building a benchmark model common for all the experimental tests going to be reproduced.

The second part of this report aims to model the dynamic behavior of two electrical equipment items interconnected by a flexible wrapped conductor, subjected to different ground motions. Before proceeding with experimental tests, it's absolutely useful to know in advance which forces and displacements have to be expected, through a finite-element model analysis of the specimens subjected to a given input. After a feasible and meaningful configuration of interconnected electrical equipment items is individuated, some ground motion are chosen and then applied to the base of the structure. The structure consists of equipment #1 mounted on the top of a steel post, and equipment #2 installed on top of a support frame structure consisting of steel beams. Actually, the steel post and the support structure are supposed to represent the other

equipment parts connecting the electrical equipment #1 and #2 to the ground: their characteristics are chosen in order to match the dynamic properties of those. Equipment #1 and equipment #2 are interconnected by a flexible stranded conductor, attached at the top of the two equipment items; the span of the cable, that means the distance between the two highest points of the two items, is based on the usual lengths of cable in electrical substations. The initial shape of the cable is assumed to be different depending on the kind of test experienced. When the input at the base of the two equipment items is an acceleration vector, the cable is assumed to be initially straight. Conversely, when the input at the two bases is a sinusoidal displacement control, the cable is assumed to be initially slack, with a certain sag: this is needed to accommodate the required displacement at the two ends of the cable. For all these tests, comparison are made between the response of the two equipment items in the interconnected and in the standalone configuration, to understand the influence of the presence of the flexible connection on the forces generated and the displacements experienced. Some parametric studies are also carried on, to check the sensitivity of the response to the configuration of the interconnected structure, such as the distance between the two equipment items and the vertical separation between the two attachment points of the cable.

4.10 Further Studies

Possible development of this are to be intended for minimizing the influence of the flexible conductor on the interconnected equipment, when subjected to strong ground motions. Since the cable is excited by the displacements experienced at its ends, corresponding to the motion of the attachment points on the top of the two equipment items, its response will be minimized when these displacements will assume the smallest values. According to this, classical approaches trying to minimize the acceleration experienced by the two equipment items through an elongation of their natural period are no more valid. This appears obvious from the spectrum of a general structure. For the same ground motion, increasing the natural period, that means increasing the flexibility of the structure itself, the relative acceleration experienced by the structure will decrease, but the displacement will increase. Therefore, trying either to increase the flexibility of the equipment items or to introduce classical base isolation, the displacement at the top of them will increase indeed. Despite reducing the severity of the response for the equipment in the standalone configuration, in the interconnected configuration this means the cable will

experience bigger displacements at both ends, resulting in a stronger dynamic input. In this case, the cable is more likely to be excited at frequencies close to a sort of resonance: this will cause large additional forces at the top of the two interconnected equipment items, resulting in possible failures.

One possible solution is introducing a pendulum system base isolation, allowing the base of the structure to slide on a circular trajectory. The scope is making the structure behaves like a rigid body rotating around a fixed point: this take advantage that the center of rotation doesn't translate. The goal of this approach is to set the pendulum system base isolation to match the center of rotation of each electrical equipment with the attachment point of the cable. If doing so, the two ends of the cable will only rotate but won't translate, strongly reducing its contribution to the dynamic response of the total interconnected structure.

CHAPTER 5

MODELING OF CONDUCTORS IN ELECTRICAL EQUIPMENT & SENSITIVITY STUDY

5.1 Bending Stiffness

The bending stiffness is a basic parameter to understand cable dynamics. Since the response of a geometrically nonlinear system depends on its current deformed shape, a big importance is based on how to accurately calculate these displacements. Obviously, from basic mechanics of structures, when the external loads are given, the displacements depend on the global stiffness matrix. This matrix is formed through the stiffness of the singular elements, and the global geometry of the system. While the geometry is automatically calculated at each step, the stiffness of the elements composing the cable depends on the parameters of the flexural stiffness that is plugged for them. Different approaches are available, and have been developed in previous studies [7, 10].

A traditional approach considers a constant value of flexural stiffness that is calculated through the boundary conditions of the element, its length, the elastic modulus of the material it's consisting of, and the second inertia area of the cross section. This approach is the simplest, and it's endorsed by the IEEE standard [21]. Conversely, the choice of a more accurate evaluation of the second inertia area of the cross section to be used is much more critical, and requires a more detailed discussion. Since the cable consists of strands wrapped together, the value of the second inertia area can be evaluated with different formulas, taking into account its dependence on the rate of curvature: then, since it changes during the motion and along the cable, the second inertia area is variable throughout the length of the cable and the time.

One of the most basilar and important issue in cable dynamics is choosing which kind of flexural stiffness has to be used, either the constant or the variable one. Therefore, these two possible approaches are completely different: both are separately described hereafter. Furthermore, it's also necessary to assign a value to the elastic modulus of the material. Despite the IEEE

guidelines [21] recommend E = 5.72e5 MPa, a value of E = 6.99e5 MPa has been adopted for these analyses, since it is believed to be closer to the real value for aluminum, and not too conservative.

5.1.1 Constant Bending Stiffness

In order to develop a finite element model of the flexible cable, it is necessary to describe the axial and bending rigidity of the conductor at each section. As mentioned earlier, the flexible conductor is generally a cable made of wrapped strands of aluminum wires. The two ends of the cable are usually attached to the equipment items through welded aluminum connectors, so that no unwrapping of the strands is possible. When the cable is subjected to a tension force, it's possible that some tightening of the strands will occur before the full axial stiffness is developed. Likewise, when a segment of the cable is subjected to compression, opening of the strands or even buckling of the outer may occur. This imply that the axial stiffness of the cable for small tension forces or a large compression force could be smaller than the sum of the axial stiffnesses of the individual strands. For the sake of simplicity, the simplest approach is to ignore these effects, and consider that the effective cross sectional area of the cable throughout its length is a constant: it's assumed to be equal to the sum of cross sectional areas of the strands.

The flexural rigidity of a cable at a cross section is given by the product EI, where I denotes the section moment of inertia. The value of I depends on whether the strands at the cross section remain attached or slide with respect to one another as the cable is subjected to bending. The minimum value of the moment of inertia is obtained by assuming that the strands are free to slide one another. In this case, the moment of inertia is simply the sum of the moment of inertia of the individual strands:

$$I_{min} = \frac{n \cdot \pi \cdot d^4}{64}$$

where d is the diameter of the single strand, and n is the number of strands in the cable.

In the real system, significant friction forces may develop between the strands, particularly at location where the cable has a strong curvature and is under elevate tension. These friction forces may prevent sliding of some of the strands and, hence, a larger effective moment of inertia may develop. Therefore, the maximum value of I is obtained when all strands are attached:

$$I_{max} = \sum_{i=1}^{n} \frac{\pi \cdot d^2}{4} \left(\frac{d^2}{16} + y_i^2 \right)$$

where y_i is the distance of the i-th strand from the neutral axis of the cable.

The actual moment of inertia of the cable is somewhere between the two extreme values. Unfortunately, the two bounding values are widely apart for typical cables used in the power industry. For example, for a 1796-MCM cable consisting of 61 strands placed in 5 layers, the upper bound is about 80 times the lower bound. For the following discussion, let n denote the number of strands and d the diameter of each strand. Based on specific experiments conducted by BC Hydro, the IEEE 2006 guideline [21] recommends the use of the approximation:

$$I \cong (1 + N) \cdot I_{min}$$

for short length aluminum conductors, where N denotes the number of layers. In the following analyses, when a constant value for the bending stiffness is used, this recommended approximation is employed. Furthermore, it's assumed that the moment of inertia remains constant throughout the length of the cable at all times.

5.1.2 Variable Bending Stiffness

More realistically, the bending stiffness of a stranded cable may vary during motion, depending on its internal tension, curvature and history of deformation. This results in a material nonlinear behavior as well, that has to be added to the geometrical nonlinearity of the system. Therefore, a finite element analysis capable of handling both material and geometrical nonlinearities needs to be used. While the geometrical nonlinearity is easily handled by most of commercial finite element programs, and beam elements with large displacement capabilities are implemented in their libraries, the material nonlinearity due to the variable flexural stiffness is usually not implemented, since it must depend on the variation in tension, curvature and history of deformation. As a matter of fact, quite an abundant literature on mechanical models of helical strands is available, but most theoretical approaches are not adaptable to finite element formulation, thus they don't find a place in commercial and research programs.

One practical model of variable flexural stiffness, adaptable to classical finite-element formulation, has been developed by Papailiou [25]. This well refined model takes into account the interlayer friction force and interlayer slipping in the cable during the bending process,

leading to a variable flexural stiffness that changes with the variation of curvature and tension, but neglecting the friction between wires in the same layer. This model has been experimentally validated on initially straight cables, at usual tension levels, under applying a static transverse force. This approach can be implemented in a finite-element custom-made program based on the secant stiffness method, designed to address the required external loading.

Through the work of J-B. Dastous [7], described in the next paragraphs, became available the compatibility of the iterative formulation used to obtain equilibrium for a given load step with equilibrium methods used in classical finite-element formulations, and the adaptation of that model to a general program able to treat arbitrary types of loading, as well as considering dynamic problems. Dastous extended Papailiou's work implementing the bending model in a more classical finite-element formulation, with capabilities to handle both material and geometrical nonlinearities for dynamic problems. Conversely of Papailiou's variable secant flexural stiffness approach, Dastous used a tangent bending stiffness adapted to a classical nonlinear finite-element formulation based on the tangent stiffness method, that is the most widely used in commercial computer programs as far as now. The calculation of the tangent flexural stiffness for the cable elements, and its difference with the secant flexural stiffness is well described in his work. Comparisons with both static as well as dynamic experimental tests for short cables interconnecting electrical equipment show that this model computes a very representative and realistic bending stiffness for such cases, leading to accurate evaluations of the displacements of the cables and of tension generated at their ends.

5.1.3 Comparisons

Some comparisons between these two different approaches are shown. For each comparison, the same model is used; therefore, the same loading process is employed. The analyses were run with FEAP, since it provides both the capabilities of accounting for variable and constant flexural stiffness. The comparisons are shown for two different sine-start tests, with different amplitudes. Figure 5-1 presents the results with the two different flexural stiffnesses for sine-start test #138 (amplitude = 20 mm, frequency = 5 Hz).

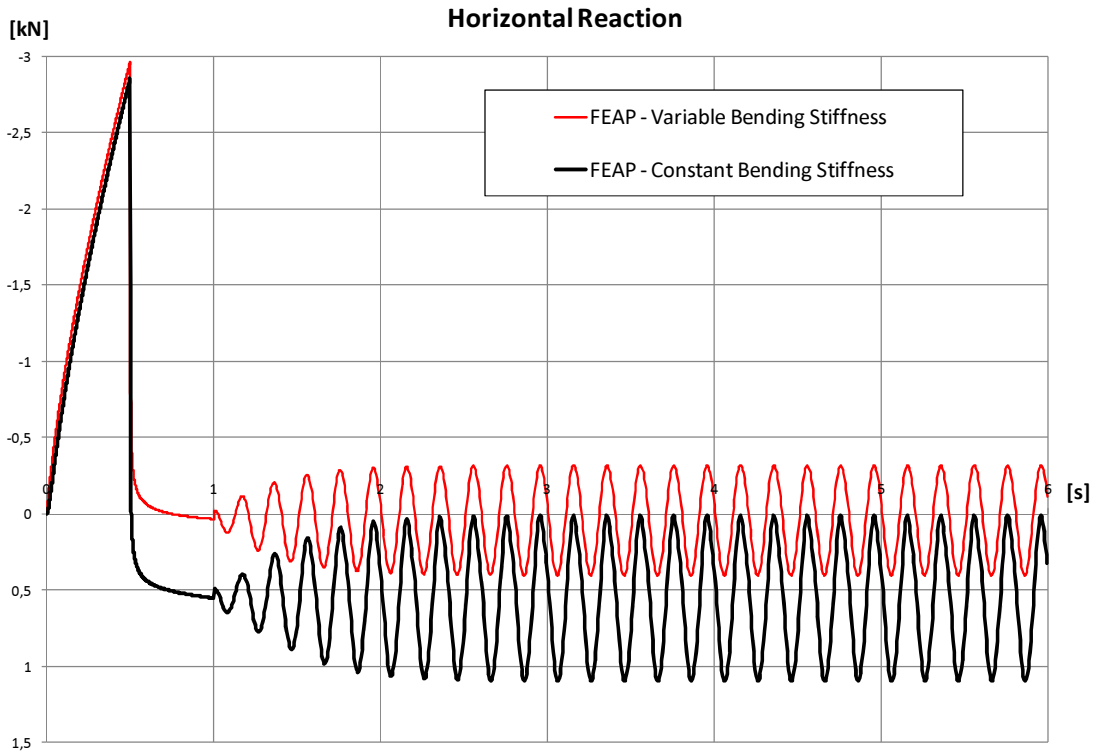

Figure 5-1: Test #138, horizontal reaction

In the graph, the positive values correspond to compression, accordingly to the positive orientation of the axes.

From 0 to 0.5 s, the own weight of the cable is linearly increasingly applied as a dead load on the cable in the vertical direction, with a quasi-static procedure consisting of 1000 steps. In this part, the cable is initially straight, with both ends fixed.

The vertical dead load will be left for all the time of the analysis. It can be seen that the horizontal reactions are increasing, reaching a value of 3 kN of traction: this is due to the geometrical nonlinearity, that requires the satisfaction of equilibrium in the deformed configuration of the structure. Therefore, horizontal tractions are generated to equilibrate the moments caused by the vertical external forces, the internal transverse forces and the internal moments. In this case, the results confirm what is expected from physical intuition. Since the deflection of the cable is quite small under its own weight, and the rate of curvature is quite low, there is no important slippage of the individual strands over each other. Therefore, the flexural stiffness of the cable doesn't change during time, and both the forces and the displacements

obtained with the constant and the variable flexural stiffness are similar. The difference between the two peaks is less than 4%.

Then, from 0.5 to 1 s, the two ends of the cable are linearly moved one toward the other, until the desired span is reached, with a quasi-static process consisting of 1000 steps. In this case, the cable experiences very big deflections. As a matter of fact, for this test the total length of the cable, that means the initial span of the straight conductor, was 5.52 m, while the desired span was 5.00 m. Moving each end by 0.26 m, the central sag obtained was about 0.85 m: this shows how relatively small horizontal displacements generate relatively big vertical deflections. This effect involves big rate of curvature, also when the procedure is quasi-static, and generates strong slippage of the individual strands over each other. This causes a very important and sudden decrease in the flexural stiffness of the cable, and can be easily observed in the graph. From 0.5 to 1 s, there is a big and sudden change in the tangent of the curve, that represents the stiffness of the system, and it is quite different for the two different models. This explains the big influence of considering the variability of the bending stiffness also for a static analysis, whether big rate of curvature, that means big vertical deflections, are involved. Furthermore, the decrease of the flexural stiffness is concentrated in the first instants right after the beginning of the horizontal displacements, because the vertical deflection is bigger, and it accumulates the biggest part of the difference between the two models. After this first deflection, the rate of curvature is smaller, thus the slippage in the cable ends and there are no big further changes in the bending stiffness. This physical aspect is confirmed by the graph, where it can be seen that the two curves have the same slope of their tangents, after the first instants subsequent to 0.5 s, where all the big differences are lumped.

After 1 s the dynamic sinusoidal input is applied at both ends. First of all, it can be observed that there are no resonance effects in the system, since no sudden amplifications are visible: this means that the natural frequencies of this cable are not close to 5 Hz, that is the fixed frequency of the input. Furthermore, other meaningful differences between the two models are clear. The model with variable bending stiffness shows the same general behavior, but the peaks and the difference between the minimum and maximum horizontal reaction assume smaller value than the model with constant bending stiffness. This is due to the fact that, experiencing big rate of curvature, the variable bending stiffness decreases, thus the cable is less stiff and the forces

generated in the system are smaller: it is to be noted that the horizontal displacements are the same, because the input is displacement controlled and not force controlled. This confirms again the physical intuition: therefore, the model that best represents the real dynamics of the cable is that accounting for variable flexural stiffness. Otherwise, the flexural stiffness is highly overvalued, when meaningful displacements are applied.

5.2 Loading Steps

In order to model past and future experimental tests on cable dynamics, it's necessary to understand the initial geometry and conditions of the cable, considered as standalone or interconnecting different equipment items. Therefore, the first goal of this study is to understand the shape achieved by the cable under its own weight, and the consequent internal forces. As shown hereafter, both are heavily influencing the dynamic behavior of the cable. Due to a low flexural stiffness, the cable experiences very big displacements under some types of structural loading; these large displacements lead to nonlinear behavior as a result of non negligible changes in geometry, and therefore a nonlinear analysis is needed to maintain the accuracy of the results obtained. The geometric nonlinearity deriving from large displacements of cables can be adequately addressed by choosing beam elements with large displacement and rotation formulation; these elements are provided in most of the commercial and research finite-element programs. Since a nonlinear analysis is performed, and the solution of each step depends on the current displacements, it's not possible to superimpose the effects of different external loads.

The initial shape is sensitive to various parameters, such as:

- properties of the cable (flexural stiffness)
- external forces acting on the cable
- boundary conditions

Furthermore, the initial geometry and condition are sensitive to how the external forces and the boundary conditions are applied. It is noteworthy that a cable having flexural rigidity and held between two fixed supports is a statically indeterminate system. This is because the horizontal support force for such a system cannot be determined from equilibrium considerations alone. This indeterminacy in the initial shape of the cable with flexural rigidity can lead to possible

quantitatively discrepancies between the experimental and the finite-element model results. Therefore, the first step in the analysis process is to compute the static equilibrium position of the cable, before the dynamic input is applied at its ends. To do this, the cable is assumed to be initially straight and without any mass, and it is incrementally subjected to its own weight from zero to the full value. Next, the two ends are moved one toward the other until the desired span is reached. Using a relatively small step increment, correspondent to applying the load and the linear displacement in 1000 steps for each, the equilibrium position at each step is achieved within an average of 3-4 iterations of calculations.

Two main different approaches have been developed from previous studies. One of them, developed by A. Der Kiureghian [10], consists in two separated steps. In the first step, the cable is considered to be straight, and the dead load of its own weight is applied; then, the two ends are moved one toward the other, until the initial span is reached. In the second step, all the internal forces are removed, so to have an initial deformed shape without any compression or traction in the cable, and then the dynamic input is applied to the fixed ends. The other approach has been developed by J-B. Dastous [7]: its main characteristic consists in the possibility to apply directly all the loads, without either dividing them in different steps or removing the internal forces. Following this order, the own weight is applied to the straight cable, then the two ends are moved one toward the other until reaching the desired value of the span, and finally the dynamic input is applied to the two ends. In this case, the cable will have a certain value of compression or traction at the end of the statically applied displacement, and the internal forces it experiences don't come only from the dynamic displacements, but have also a static contribution. Both these approaches are described more deeply hereafter. It is noteworthy that, for all the analyses presented and discussed in this report, a clear reference to one of these two approaches will be made, since its choice directly affects the results obtained.

5.2.1 Dastous' Model

For this model, the cable is assumed to be initially straight, and without any mass, so that its geometry is completely known. Next, after fixing both ends, the gravity load is applied from zero to the full value; then, the two ends are moved one toward the other. Due to flexural rigidity, the shape of the cable is considerably different from the catenary shape. In addition, the support will

develop a certain amount of horizontal forces. This means that the cable develops non negligible internal forces after the static step, before applying the dynamic input.

Contrary to common thinking, the cable can experience not only traction but also compression forces under its own weight. As mentioned above, this is due to the flexural stiffness, and can be explained easily with the following example. Let assume an initially straight cable, with two rollers at its ends, and without any mass and any load. Then, applying a vertical distributed load and allowing the two rollers to move in the horizontal direction, it will deflect and assume a deformed shape. The span between the two rollers will have been decreased, and the cable will be subjected to traction indeed. This is the natural shape that it tries to achieve under that load: it is the same that happens for a catenary cable, with the only difference that the shape will be different because of the presence of the flexural stiffness. Now, let suppose to want to close the span between the two rollers, that means between the two ends of the cable: in order to do this, it's mandatory to introduce an external horizontal force of compression. The smaller the span is wanted, the higher this force must be.

This process is shown in Figure 5-2 for the kind of cable that was considered in the experimental tests. The cable has a total length of 5.52 m, that is equal to the initial span, when the cable is straight and doesn't carry any load. One end is fixed, and the other is attached to a roller; the flexural inertia is considered constant, and equal to the IEEE recommended value. Applying the vertical dead load, considered as a concentrated force of 1.359 N at each of the 99 internal nodes of the cable, it will assume a deflected shape with a span of 5.26 m. This explains the traction forces generated in the model, since both ends are fixed; as a matter of fact, the traction is the reaction developed to avoid the motion of one end. Therefore, if the desired span is shorter than 5.26 m, an external compression force will be require to move the roller; this is the case of the experimental tests, in which the desired span was 5.00 m. Conversely, if the desired span is bigger than 5.26 m, an external traction force will be needed.

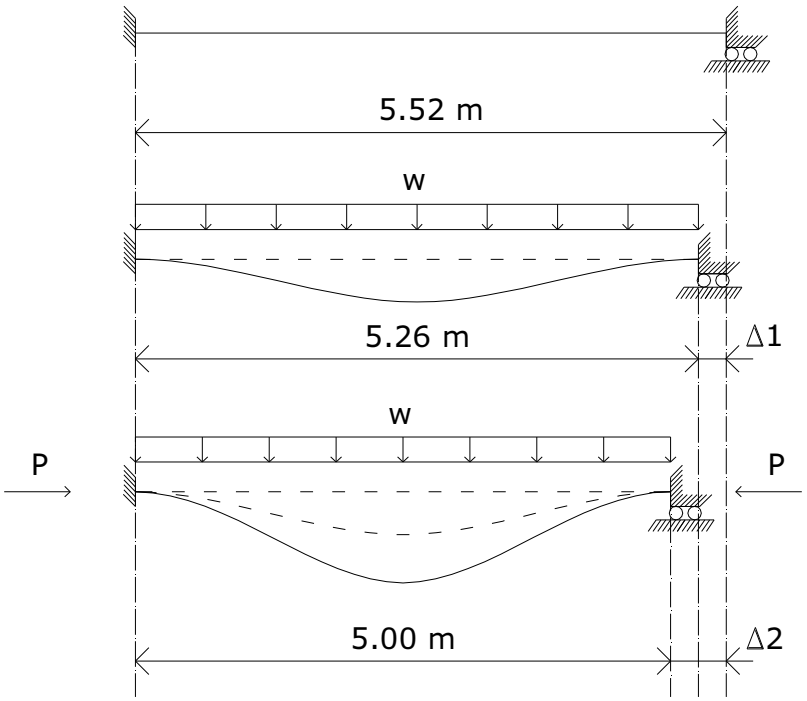

Figure 5-2: Loading Steps

If the desired span is much shorter than the one naturally assumed by the cable, the horizontal force can be so high, that the resultant of the initial traction and this force will assume the same direction of the introduced external force, that means compression in the cable. Therefore, the initial presence of traction or compression in the cable depends on its total length and on its span; this is equivalent to saying that it depends on the slackness ratio, defined as:

$$slackness = \frac{l_c - span}{span}$$

where l_c is the total length of the cable.

In particular, the support horizontal force was found to be in compression for slackness ratio bigger than 0.00275 (0.275%). For most of the analyses studied in this report, the slackness ratio is bigger than 0.00275, thus the cable is initially subjected to compression before the dynamic input.

5.2.2 Der Kiureghian's Model

For this model, as well as for Dastous' one, a finite element approach using frame elements with a Lagrangian strain formulation is used to take into proper account the geometric nonlinearity of the system. This model makes use of classical beam formulation available in the library of the most common finite-element programs. The only requirement, as mentioned above, is the capability to account for large displacements. Conversely, mechanical nonlinearity stemming from interlayer slipping and consequent friction is neglected: thus, the flexural stiffness is assumed to be constant over the total length of the cable.

For this model, the following steps have been used to set the initial shape of the cable. A straight cable of the required length is modeled with both its ends fixed. The weight of the cable is linearly applied as dead load, from zero to the full value, and the cable is allowed to deform. One end of the cable is then moved toward the other until the specified initial span length used in the experiments is achieved. The deformed shape of the cable in this position is computed: this shape is assumed to be the initial shape of the cable without any internal forces. It is particular noteworthy that removal the internal forces is typical of this model. As a matter of fact, considering a constant flexural stiffness for the cable, this value will be highly overestimated when the cable experiences big rate of curvature, actually causing large slippage and decrease in the interlayer friction. This effect is present in the motion of one end of the cable toward the other; due to the quite low bending stiffness of the cable, large deflection and, consequently, rate of curvature arises also for relatively small horizontal displacement. When making use of constant bending stiffness, this behavior of the real cable is completely lost. Therefore, the behavior of the model is more like the buckling of a beam, since the imposed displacement is in the same direction of the axis of the cable, and, having a constant flexural stiffness, it can be considered as a very slender beam. This means that, despite the vertical and horizontal displacements can be accurately evaluated, the internal forces will be highly overestimated, since they are computed by the product of the displacements times the flexural stiffness, that assumes an highly unrealistic value in this phase.

In order to avoid the presence in the cable of unrealistic internal forces through all the static and dynamic analyses, found to be likely bigger than the total forces arising from the dynamic input, the better choice is to completely ignore them. The correctness of this assumption has been

validated observing the internal forces in the cable measured in the experimental tests: since they were found to be quite low, comparing to those generated during the dynamic motion, they can be neglected without losing accuracy of the solution. The cable with this shape is now placed on the supports with fixed ends and the reaction forces under the dead load are calculated. Nevertheless, it is to be noted that the vertical forces representing the dead load of the cable will generate an horizontal initial tension force at each support. As described hereafter, because of the uncertainty in the initial conditions of the cable in the experiments as well as neglecting the internal forces arising from the horizontal displacement of the two ends, this horizontal force as well as the cable sag will be somewhat different from the initial conditions observed in the experimental tests.

5.2.3 Comparisons

The difference between these two approaches is shown in Figure 5-3.

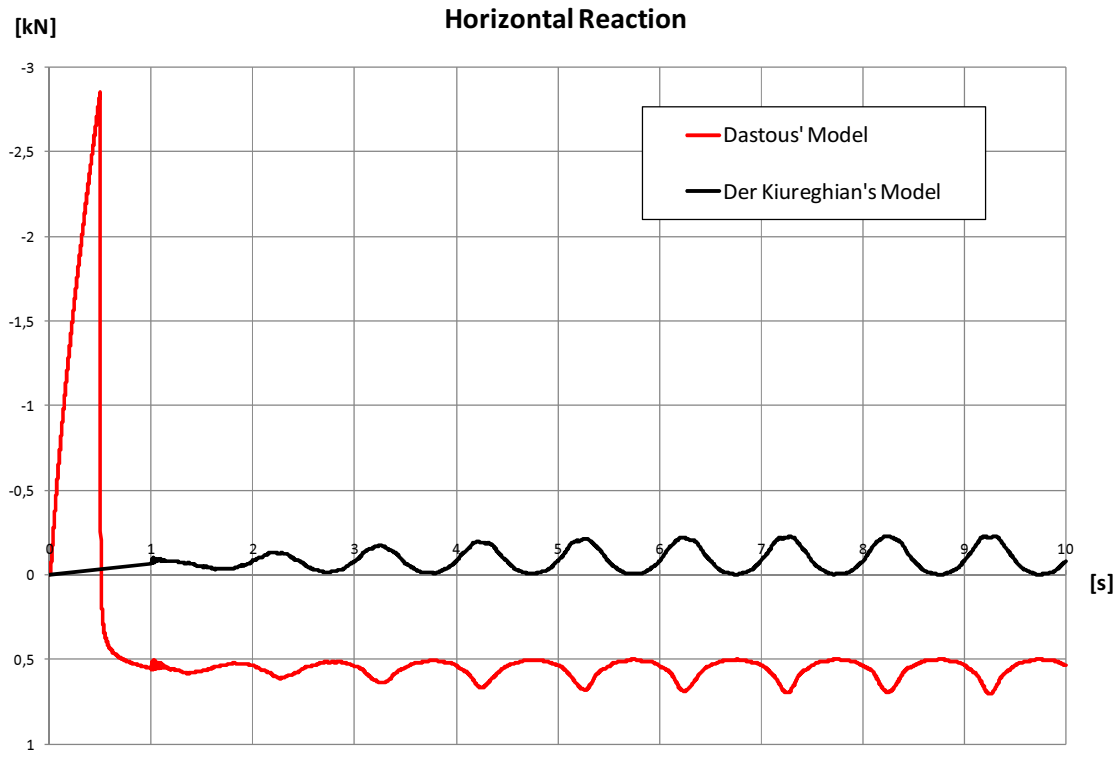

Figure 5-3: Test #134, horizontal reaction for Der Kiureghian's and Dastous' model

The horizontal reactions for sine-start test #134 are represented. Positive values correspond to compression, and negative to traction. One model has been studied with Dastous' loading step approach, and the other with Der Kiureghian's one: both have been run with ABAQUS. The same comparison for sine-start test #138 is shown in Figure 5-4.

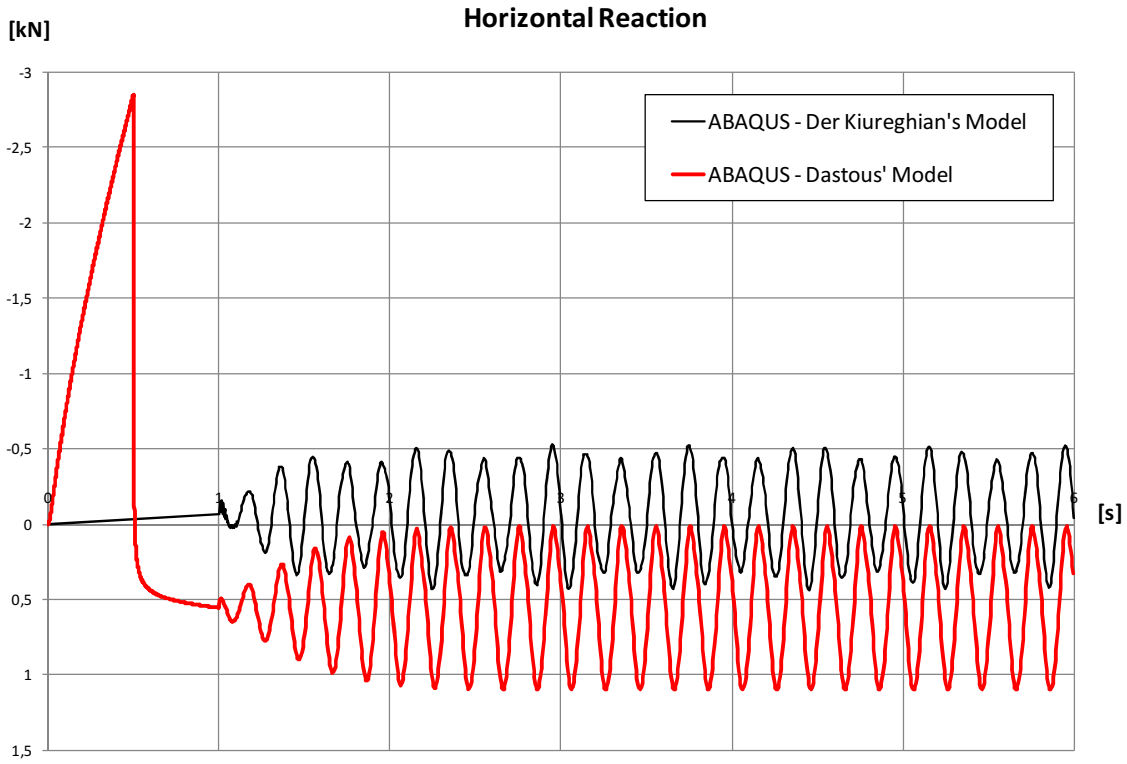

Figure 5-4: Test #138, horizontal reaction for Der Kiureghian's and Dastous' model

Again, positive values correspond to compression, and negative to traction. Also in this case, one model has been studied with Dastous' loading step approach, and the other with Der Kiureghian's one, and both have been run with ABAQUS.

In both the two graphs, it can be noticed that the biggest difference between the two models is in the static part. As a matter of fact, Dastous' model provides the dead load to the system from 0 to 0.5 s, and from 0.5 to 1 s the two ends are linearly moved one toward the other until the desired span is reached. Both the loads are applied quasi-statically. After the static part, the sinusoidal displacements are applied dynamically, without removing the internal forces. Therefore, the horizontal reactions in the dynamic part have a component due to the static part: this is clear

observing that the reactions are oscillating around a value shifted from the zero. Conversely, Der Kiureghian's model applies the dead load from 0 to 1 s on the already deflected and slack cable, in which all the internal forces due to the horizontal motion of the two ends, needed to reach the desired span, have been removed. In this case, the horizontal reactions generated in the dynamic part are oscillating around a value of initial traction, that is linearly achieved in the static part. This is the biggest difference between the two models. Dastous' model, depending on the sag / span ratio and the flexural stiffness of the cable, can show initial compression at the beginning of the dynamic input. This can be easily understood reasoning on the shape and the constraint of the cable. Let assume an initial straight cable, with rollers at both ends; applying its own weight, the cable will assume a deflected shape with the two rollers moving one toward the other, until a certain span is reached. Obviously, since the rollers allow horizontal displacements, no horizontal reactions are present at the two ends. If a different span from that obtained is wanted to be imposed to the cable, this will be possible only applying additional horizontal forces at the two ends. The value of the forces will depend on the change in span: in particular, whether the span is smaller than that obtained under the own weight, compression forces will be required. Since the deflected shape assumed by the cable under its own weight depends on the flexural stiffness, the value of the horizontal force will depend on the stiffness of the cable. Conversely, the application of a vertical dead load on a cable accounting for geometrical nonlinearity will generate traction reactions. For Dastous' model, if the traction due to the vertical dead load is smaller than the compression due to the horizontal displacements of the two ends, there will be initial compression at the beginning of the dynamic analysis. Conversely, since Der Kiureghian's model deletes all the internal forces due to the horizontal displacements of the two ends, and provides only the application of the vertical dead load in the static part, obviously there will be traction at the beginning of the dynamic analysis. The importance of the initial traction or compression in the cable will be clear in the following discussions.

The choice of showing two graphs for two different tests lays in the will of showing that the dynamic behavior is not directly influenced by the two different loading step models, but only indirectly, through the initial force discussed above. As a matter of fact, the two responses of the two models can be in-phase or out-of-phase. This doesn't depend directly on the model, but on the frequency of the sinusoidal input, due to a change in the natural frequency of the cable. This will be discussed more deeply hereafter.

5.3 Initial Conditions

The initial conditions of the cable, that means its initial shape and the inherent tension, are particular noteworthy for many reasons. First of all, as mentioned before, a cable having flexural rigidity and held between two fixed supports is a statically indeterminate system, since its horizontal support force cannot be determined from equilibrium considerations alone. Therefore, the initial shape of the cable and the consequent tension are not univocal, but depend on the loading process. Both of this aspect are absolutely non negligible, because of the nonlinearity of the system and its influence on the dynamic properties. As a matter of fact, the natural frequencies of the system depend on its stiffness, that depends indeed on the geometry. Despite it's not completely correct speaking of natural frequencies for a nonlinear system, the same logic is valid for the frequencies of the system more likely to be excited. This means that the dynamic properties of the cable, and thus its response to the dynamic input, depend on its initial geometry, assumed under its own weight and with both ends fixed.

Furthermore, also the initial inherent forces in the cable play an important role on its dynamic properties. As a matter of fact, since the value of initial compression can reach very high level in Der Kiureghian's model, this can change the frequencies more likely to be excited. This is similar to what happens to a straight beam: when it's subjected to a compression close to the critical buckling load, its natural frequencies decrease drastically. Therefore, since both the geometry and the internal forces of the cable before applying the dynamic input are unknown, and they have a large influence on the dynamic properties of the cable, specific studies are carried on about the sensitivity of the model to the initial conditions.

5.3.1 Compression in the Cable

First of all, it is to be noted that, due to the slackness ratio of the cable in most of the tests, the cable is often subjected to compression and not traction after the static step. This is particularly true when Der Kiureghian's model is used, for the reasons explained earlier. As a matter of fact, the flexural stiffness of the cable in the static step is highly overvalued, and this turns into very large value of compression forces at the supports. As well as for Dastous' model, the value of initial tension or compression depends on the configuration of the cable, more specifically on its

slackness ratio, thus is different for different tests. For some of the tests approached with Der Kiureghian's model, this initial compression was found to be so high that was close to the critical buckling load of the equivalent beam: this means, it was close to the critical buckling load of a beam with double fixed ends, span equal to the total length of the cable, and second inertia area of the cross section equal to that assumed constant for the cable. Strictly speaking, the equivalent beam corresponds to the initially straight cable with constant flexural stiffness. For a beam, such a high value of compression causes a strong decrease in the natural frequencies: something similar is found to affect the cable. It's not possible to fully develop a hand calculation of these changes for the cable, for two main reasons. First, as mentioned before, the cable doesn't have natural frequencies, but either a range of them or frequencies more likely to be excited: thus, it's not possible to reason about a specific value of frequency. Next, there's no available literature to compute the variation due to the compression for slack cable with non negligible flexural stiffness; it is possible to find some formulas only for either straight beams or cables with negligible bending stiffness and supporting only tension loads.

In the current discussion, it was decided to proceed with an approximate approach, applying the formula for straight beams to the frequencies extracted from the slack cable. As a matter of fact, the cable is believed to be closer to a straight beam that can experience bending and compression, than to a parabolic cable truss supporting only tension loads. Furthermore, when the cable is assumed to be straight and with a constant bending stiffness, it fully corresponds to a slender beam. Therefore, formulas for the influence of compression on the natural frequencies of a beam are used. Since natural frequencies for a geometrical nonlinear system don't exist, it is mandatory to work on something different. It is found to be noteworthy considering the natural frequencies extracted from a finite-element analysis of the cable in its initial shape, with a constant bending stiffness. This approach neglects the variability of the flexural stiffness, as well as the change of shape during the motion, but the frequencies obtained can be considered belonging to the range of frequencies more likely to be excited; the bound values of this range being the natural frequencies of the cable in its slackest and tightest configurations, both considering constant flexural stiffness. The first three natural frequencies of the cable with constant bending stiffness, computed with a finite-element computer program, are:

$$\omega_1 = 1.26\ Hz$$

$$\omega_2 = 4.28\ Hz$$

$$\omega_3 = 6.71\ Hz$$

The formulas adopted to evaluate the influence of the compression are extracted (Blevins, 1979 [3]):

$$\frac{\omega_{i|P\neq 0}}{\omega_{i|P=0}} = \left(1 + \frac{P}{|P_b|}\cdot\frac{\lambda_1^2}{\lambda_i^2}\right)^{1/2}$$

where $\lambda_1 = 4.73$, $\lambda_2 = 7.85$ and $\lambda_3 = 10.99$ for a clamped-clamped beam, P_b is the buckling load of the beam and P is the actual compression in the cable at the end of the static loading (found to be 554 N from the numerical solution). It is to be noted that positive values of P in the formula correspond to traction, therefore the compression has to be accounted for as negative: as a matter of fact, it reduces the values of the eigenfrequencies. For this case, the buckling load is evaluated for the cable in its initial straight position, with the constant flexural stiffness recommended by the IEEE guidelines [21]:

$$P_b = \frac{4\pi^2\cdot EI}{L^2} = \frac{4\pi^2\cdot 69900\cdot 6492}{5520^2} = 588\ N$$

Applying this method, the first three natural frequencies are found to be:

$$\omega_{1|P=554} = 1.26\left(1 - \frac{554}{588}\cdot\frac{4.73^2}{4.73^2}\right)^{1/2} = 0.3\ Hz$$

$$\omega_{2|P=554} = 4.28\left(1 - \frac{554}{588}\cdot\frac{4.73^2}{7.85^2}\right)^{1/2} = 3.5\ Hz$$

$$\omega_{3|P=554} = 6.71\left(1 - \frac{554}{588}\cdot\frac{4.73^2}{10.99^2}\right)^{1/2} = 6.1\ Hz$$

As mentioned earlier, those cannot be considered as the natural frequencies of the system in a classical view, but this approach is useful to understand how the compression in the cable deriving from the static part can heavily affect the dynamic response of the system.

The influence of the initial compression is shown in the following graphs. In Figure 5-5 are represented the horizontal reactions for the different values of initial compression in the cable, for the sine-start test #134. All the curves are obtained using the constant flexural stiffness.

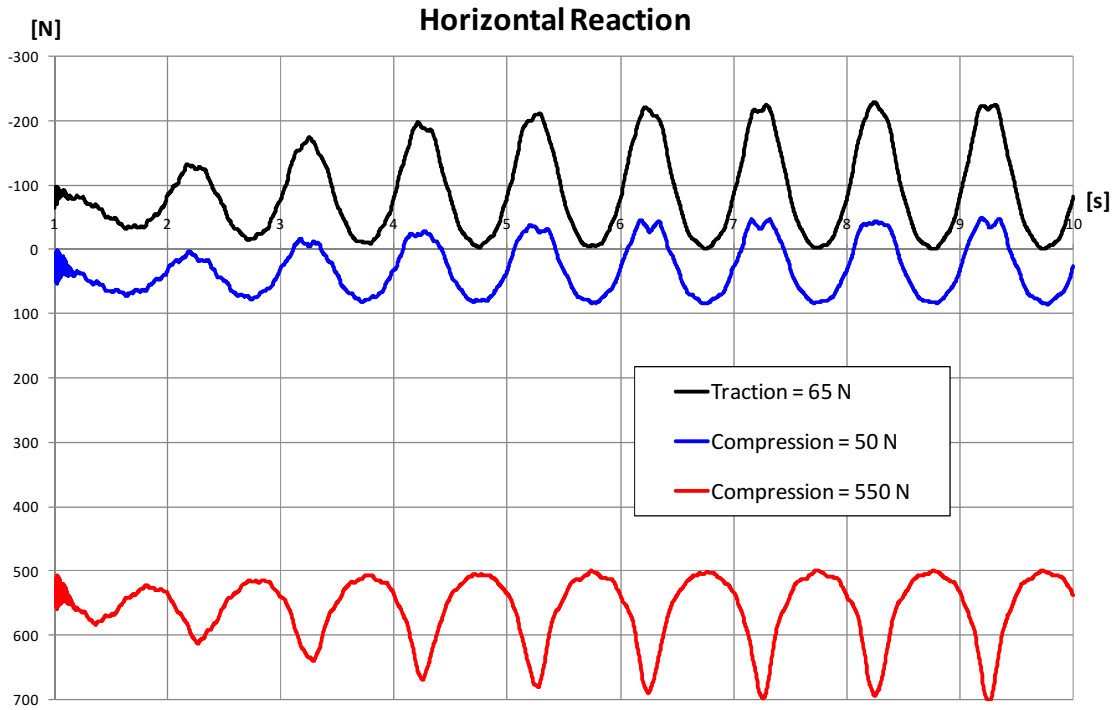

Figure 5-5: Test #134, horizontal reaction for different initial compressions

The value of initial traction equal to 65 N corresponds to the value obtained from the static procedure in Der Kiureghian's model. The value of initial compression equal to 550 N corresponds to the value obtained from the static procedure in Dastous' model. The value of initial compression equal to 50 N has been obtained introducing additional compression forces to the already deformed shape in Der Kiureghian's model. Comparing the different response of the three curves, and considering that all the other parameters are the same for each of them, it's clear the influence of the initial compression on the response.

As discussed earlier, the high value of compression present in the cable changes its natural frequencies, thus the fixed frequency of the input can be more or less close to the natural one. According to this, the response of the cable can be subjected to a big amplification if its natural frequency is shifted due to the compression to a value close to the given frequency of the input. It can be observed, introducing some compression forces to Der Kiureghian's model that the response is different, and in particular it's reduced: it means that the natural frequency closer to the sinusoidal input has been shifted. When the initial compression gets big enough, the first natural frequency of the cable crosses the fixed frequency of the applied displacements, and it

can be seen that the reaction of the cable goes in-phase with the acceleration input. This phenomenon physically agrees with the response of a single degree of freedom oscillator under harmonic motion: it undergoes a phase shift of 180 degrees between the displacement and the applied force when the excitation frequency crosses its natural frequency. Thus, the fact that the reaction curve for the initial compression equal to 550 N is out-of-phase with the other responses is the evidence that the first natural frequency of the system has been crossed, due to the compression force. The same change in natural frequencies is observed in Figure 5-6.

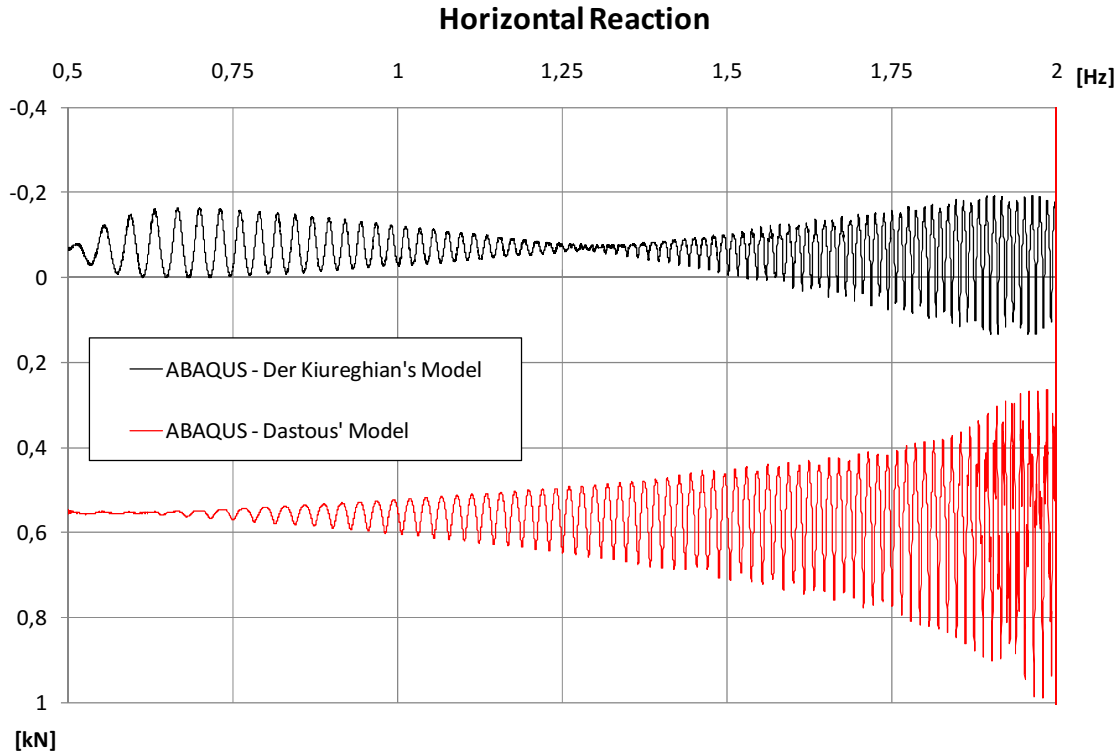

Figure 5-6: Test #130, horizontal reaction for Der Kiureghian's and Dastous' model

This graph shows the horizontal reactions measured in a frequency-sweep test from 0.5 Hz to 2 Hz. The black line represents Der Kiureghian's model, in which the dynamic input begins with internal traction equal to 63 N, due to the vertical dead load representing the own weight of the cable, applied to the already deformed shape. The red line represents Dastous' model, with an initial compression of 550 N, due to the traction generated by the vertical dead load applied to the straight cable, and the compression needed to move horizontally the two ends one toward the other. Both have been computed using a constant bending stiffness.

The response in Dastous' model is always increasing with the increase of frequency of the excitation, showing that no natural frequencies are crossed. In Der Kiureghian's response there's a clear beat, showing that the frequency of the harmonic input is matching the natural frequency of the system. The beat consists of a big decrease of the horizontal reactions, due to the sum of its out-of-phase components: these components are the forces generated by the lumped mass at the end times the acceleration input at the same node, and the dynamic response of the cable. As mentioned earlier, below the first natural frequency of the system, the dynamic response is out-of-phase with the input acceleration; therefore their sum turns out in a decrease of the total resultant reaction, since the two components are out-of-phase. The input acceleration increases its amplitude with the square of the frequency, since it is the second time derivative of the applied displacements; thus its shape is always increasing with the frequency. Conversely, the response of the cable fights this effect: therefore, the total horizontal reaction decreases when the response of the cable increases. The input acceleration is a fixed quantity, since it is given in input to the system. The resonance, when the excitation frequency matches the first natural frequency of the cable, affects only the cable response, amplifying it. Therefore, the beat is the biggest decrease in the total reaction, which corresponds to the biggest amplification of the cable response, summed with the out-of-phase acceleration input. Looking at this graph, the beat is around a frequency equal to 1.3 Hz. This agrees with the calculation of the first frequency of the cable with a constant bending stiffness equal to the IEEE recommendation, that was found to be equal to 1.26 Hz, in absence of internal forces. As a matter of fact, traction equal to 63 N seems to be a too small value to influence the natural frequencies of the cable. For Dastous' model, the absence of beats shows that no natural frequencies are crossed. Since the presence of compression decreases the value of the natural frequencies, it means that the first natural frequency has been shifted from 1.26 Hz to something less than 0.5 Hz, which is the lowest frequency of the frequency-sweep input. This confirms the hand calculation of the new first natural frequency of the system affected by the internal compression that was found to be about 0.3 Hz.

The frequency-sweep test is very effective to understand the big influence of initial compression on the dynamic properties of the cable, resulting in meaningful changes of the natural frequencies. This aspect is even more important for two reasons. First, the initial compression in the cable can reach very important values in the cable, and it's absolutely non negligible. As a

matter of fact, it depends on the model adopted, either Der Kiureghian's or Dastous' one, and on the type of flexural stiffness assumed for the cable. Next, the natural frequencies are shifted in a feasible range for electrical equipment. Since the motion applied to the two ends of the cable results from the ground motion filtered by the electrical equipment items, the frequency of that motion will have frequency content similar to the natural frequencies of the items, that are believed to lay between 0.5 and 10 Hz. Therefore, the cable design aims to avoid likely resonances for those frequencies. Using an unrealistic model, accounting for unfeasible compression forces resulting from the static loading, it is possible to lose completely the dynamic behavior of the cable, due to the shift of the eigenfrequencies.

5.3.2 Central Sag

Since the geometry of the system directly affects its stiffness, and thus its dynamic properties, the dynamic response of the cable can be significantly sensitive to its initial position. Furthermore, the shape of a cable having flexural rigidity and held between two fixed supports is statically indeterminate, and cannot be compared with the shape observed during the experimental tests, since unfortunately Dastous' paper [4] doesn't describe how the cables were shaped and put in their positions before starting the tests. Therefore, there's an indeterminacy of the initial shape of the cable in the analyses. This is why a parametric study on the sensitivity of the cable to its initial shape is developed. This is applied only to test analyzed with Der Kiureghian's model, because the initial shape is plugged in arbitrarily at the beginning of the second step without consequent internal forces. Therefore, a slightly different shape can be assumed for the test, without resulting in other changes. Conversely, in Dastous' model every shape corresponds to a specific value of initial tension, thus changing the initial shape also the tension should be changed accordingly.

The most meaningful parameter to be observed is found to be the central sag of the cable. Starting from the shape of the cable obtained through the static analysis under its own weight and with the linearly increasing motion of one end from the straight configuration to the desired span, the sag is shifted up and down, and the changes in the results are observed. Accordingly to the changes in the sag, linearly proportional changes are applied to all the nodes of the meshed cable, from a zero value for the two ends, to the biggest value at the middle point. The changes aren't completely arbitrary, but the total length of the cable is also computed, to be sure that the change

of the sag doesn't correspond to an unrealistic change in the total length of the cable. It is observed that a change of the central sag of 50 mm either up or down corresponds to a change of 1% in the total length of the cable. Since an error of up to 2% can be addressed to a lack of precision in the measurement of the length of the cable in the experimental tests, values of change of 50 and 100 mm are used for the central sag. It is to be noted that these two values correspond to a change of respectively 1% and 2% of the sag / span ratio. Considering that the initial value of sag / span ratio is about 19%, the modified initial sags still belong to the feasible range for slack cables interconnecting electrical equipment items.

Some results are presented hereafter. Figure 5-7 shows the shape assumed by the cable after applying the vertical dead load and moving the two ends horizontally to reach the desired span, measured for the sine-start test #135 (amplitude = 80 mm, frequency = 2 Hz). This shape, represented by the black line, is the same for all the sine-start and frequency-sweep test, since the configuration adopted is always the same. In particular, the cable is the 1796-MCM, with a total length equal to 5.52 m and a span equal to 5 m. The red line shows the different shape used to study the sensitivity of the response to the central sag, moving this down by 50 mm. It is to be noted that the scale on the two axes are different, thus the shape is only qualitatively. Figure 5-8 shows the horizontal reactions measured for the sine-start test #135 (amplitude = 80 mm, frequency = 2 Hz).

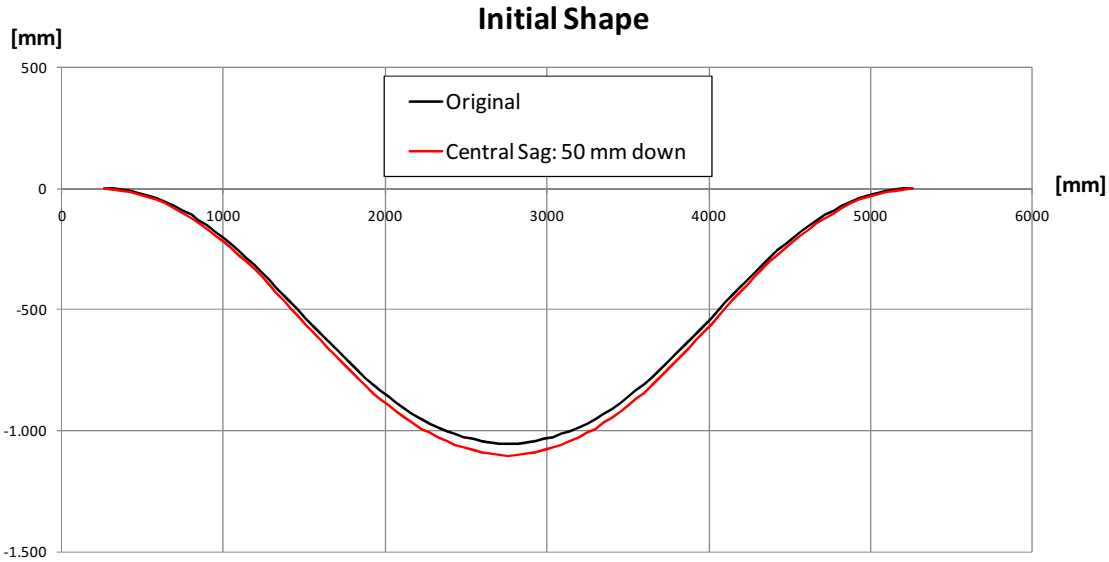

Figure 5-7: Test #135, shape of the cable with the central sag moved down by 50 mm

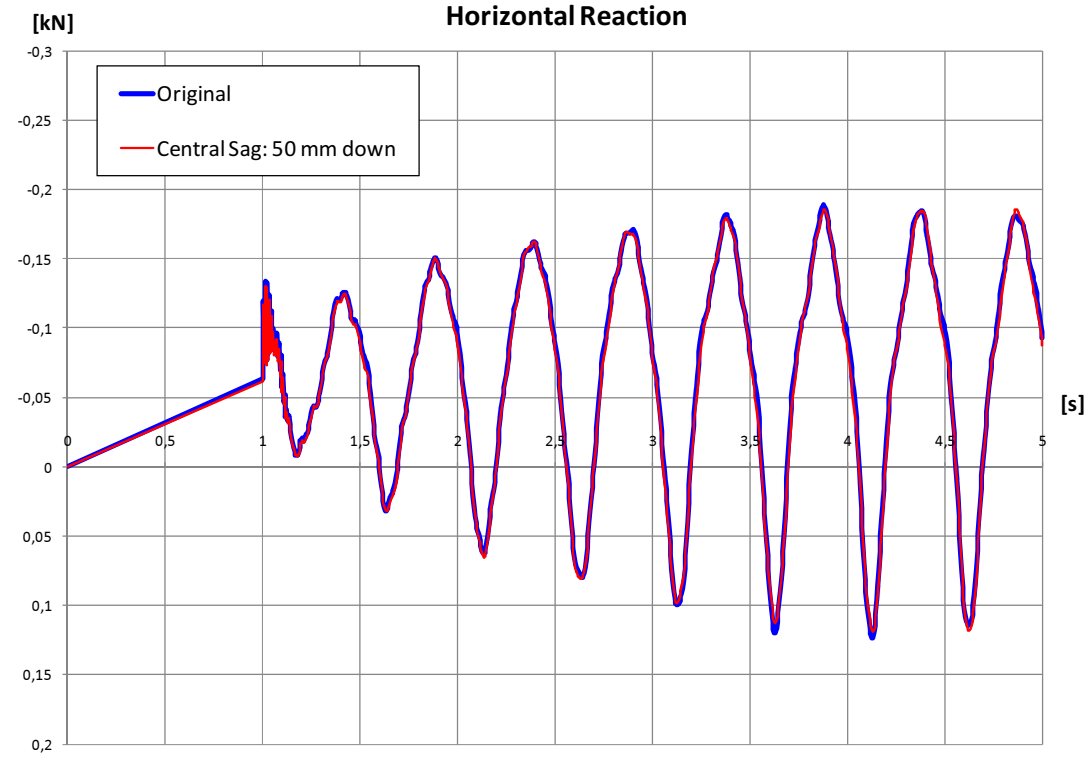

Figure 5-8: Test #135 with the central sag moved down by 50 mm, horizontal reaction

The horizontal reactions graph shows that there is a very small sensitivity to the initial central sag of the cable. The blue line represents the horizontal reaction for the original shape of the cable, while the red line, which is superimposed to the blue, represents the horizontal reaction for the cable in the slightly changed deflected configuration. It is noteworthy that the test is studied with Der Kiureghian's model, adopting the constant flexural stiffness. That is clear from the graph, where from 0 to 1 s there is a linear increase of traction, due to the vertical gravity load of the cable. The choice of using Der Kiureghian's model is justified by the fact that it uses an already deformed shape of the cable without internal forces; therefore it is easy to change this shape. For short, all the comparisons for the same test with different changes on the central sag are presented in the Appendixes. Figure 9-1 shows the comparison between the original deformed shape of the cable, and a variation equal to 50 mm up for the central sag value. Everything is equal to that described earlier, but for the value of the central sag. Figure 9-2 shows the horizontal reaction obtained with this new deformed shape of the cable. Also in this case, the two reaction time-histories are the same, that means that the dynamic response of the cable is not influenced by these values of difference in the initial central sag, either moved up or down. Finally, the results for a change of 100 mm up for the central sag are presented. As mentioned earlier, this is the biggest value of change studied, because otherwise it turns out into an unfeasible variation in the total length of the cable. In order to change the central sag without affecting the total length of the cable, it should be necessary to modify the span, but it is a fixed value known from the experimental setup. Figure 9-3 shows the shape assumed by the cable after applying the vertical dead load and moving the two ends horizontally to reach the desired span, in the original configuration and with a variation equal to 100 mm up for the central sag. Again, the scales of the two axes are different, thus the shapes are only qualitatively. For this new configuration, the horizontal forces are plotted in Figure 9-4, and compared with the original ones. In this case, there are slight differences between the horizontal reactions for the two initial configurations, but still very small. In particular, the general behavior is the same, and small changes are visible only for the peak values.

Therefore, meaningful changes in the initial geometry of the cable turn out into negligible variations in the response of the cable: this means that the influence of the dynamic behavior to the initial geometry of the system is very small, even negligible. This can be explained thinking that the displacements experienced by the cable during the motion are order of magnitude bigger

than the possible uncertainties in the initial position of the cable. It is to be noted that all the above analyses have been modeled in ABAQUS, using Der Kiureghian's model and constant bending stiffness.

5.4 Parameters

Since the cable dynamics is highly nonlinear, many parameters can address and affect the results. One of the most influencing parameter is the damping inherent the cable. It is practically impossible to predict the damping in the cable, which can be significant when the cable strands slide against one other under friction forces. Such damping would depend on the cable force and curvature at each location and would vary along the cable and in time. For this purpose, Noiseux [24] proposed a hysteretic damping model for cables, which is reported to well agree with experimental results and realistically describe the dissipation in the cable. Conversely, this class of model hasn't found place in commercial programs up to now, therefore it is not possible to take into account this model for the scope of this study. Since accurate modeling of the damping is a complex issue and doesn't belong to the scope of this study, it is decided to use an equivalent viscous type of damping that could be set to fit the experimental results. Furthermore, such type of damping is already available both in ABAQUS and FEAP, so that it is easier to proceed this way.

The damping is modeled using single-degree-of-freedom viscous dashpot dampers connected to all nodes of the finite element cable model. It is noteworthy that the best way to model this damping is to link it only to the rotational degree of freedom. This is physically consistent, since the damping is directly related to the bending process which in turn is related to slipping of the layers one other. It should be observe, however, that damping is indeed a function of frequency and amplitude. Nevertheless, it is found that the simple approach used is adequate and lead to good accuracy in results, as shown by comparison with experimental tests.

Another source of dissipation can arise from the Rayleigh damping that can be used to provide supplemental damping. Since damping in the cable stemming from the internal interlayer friction is already taken into account by the rotational velocity proportional dashpots, no additional Rayleigh damping is provided to the system. Nevertheless, some tests are run also including

some additional Rayleigh damping, just to understand its influence on the results and to check the validity of the assumption of neglecting it for most of the tests.

Next, another parameter has to be mentioned, also if it's not something directly regarding the physical issue of cable dynamics, but the computational method. One of the most common time integration method used for dynamic problems is the HHT-method [2]: in this study, it is used for the analyses run in ABAQUS. Since the system is highly nonlinear, solving each time step requires an iteration process, in this case being the Newton-Raphson method. This method consists of iteratively trying to solve the equilibrium equation reducing the residual forces: when the residual is less than a fixed value, the solution for that step is accepted, and the calculation shift to the next time step. ABAQUS lets the user choose between two different time stepping schemes. The first is the direct time stepping, which requires the user to explicitly define a fixed time step, that will be the increase of time between two subsequent solution instants. This direct user control over time stepping should be used only when the problem behavior is supposed to be well understood, or when the other option can't easily handle the problem. The second is the automatic time stepping, when the choice of the most suitable time step to be used is left to the program. The scheme used by ABAQUS is based on the maximum force residuals over each iteration: by comparing consecutive values of these quantities, it determines whether the convergence is likely to be reached in a relatively small number of iterations. Thus, the load increment is adjusted only if convergence is deemed to be unlikely, otherwise it will continue with the iteration process. Basically, the automatic time stepping is based on the concept of half-step residuals: the time stepping operator defines the velocities and accelerations at the end of the step in terms of displacement at the end of the step and conditions at the beginning of the step. Equilibrium is then established at the end of the step, thus ensuring an equilibrium solution at the beginning and end of any individual time step. The main problem is that this procedure doesn't guarantee equilibrium throughout the step; therefore another control is required in order to apply the automatic time stepping. The time step control consists then of measuring the force residuals at half step, by using the integration operator, together with the solution obtained at the end of the step, to interpolate within the time step. If the maximum entry in this residual vector is bigger than a user-specified tolerance, the time step is considered to be too large and is reduced. If the maximum half-step residual is sufficiently smaller than the user-specified tolerance, the time step will be increased by an appropriate factor for the next increment; otherwise, the time step is

considered adequate. This user-defined value governing the process is called “half-step residual tolerance”. Therefore, this parameter governs the dimension of the time steps adopted, and consequently the accuracy of the solution obtained by the time integration method. Some tests with different values of the half-time residual tolerance are analyzed, to understand the sensitivity of the time integration method adopted to this parameter. Usually, the stability of the solution decreases when the nonlinearity increases; thus, for cable dynamics the accuracy of the time integration method is one of the most important aspects.

5.4.1 Rotational Lumped Damping

As mentioned before, in the case of flexible conductors the determination of damping is very difficult, complicated by the fact that it’s a function of both amplitude and frequency of the input, therefore it may also vary during the motion itself. Since accurately evaluating all these aspects of damping is not a purpose of this study, it is decided to proceed with an approximate approach, thus considering the damping represented by lumped dashpots placed at every node of the cable. Since the damping is to be applied to every node, it is chosen to use a single value of damping by unit length, denoted by c_θ, which is divided equally among all the nodes for a cable of a given length. After calibration, the value for the cable subject to study is found to be:

$c_\theta = 10\ N \cdot s$ for the 1796-MCM

$c_\theta = 35\ N \cdot s$ for the 4000-MCM

In this model, distributed viscous damping is achieved by placing a dashpot at each node of the finite element model: viscosity is assumed to be proportional to the rotational velocity, since it is the best way to model a realistic damping depending on the curvature in the cable. Despite this model may not be realistic in describing energy dissipation by internal friction forces, it provides a preliminary estimation of the importance of the damping effect on the dynamic response of the cable. To apply this equivalent rotational damping to each node of the cable, the value by unit length is multiplied times the total length of the cable, and then divided by the number of the nodes of the mesh. For the cable 1796-MCM, adopted in the analyses, this value is:

$$10 \cdot \frac{5}{100} = 0.5\ N \cdot m \cdot s$$

The influence of this equivalent damping on the dynamic response is first studied on the sine-start test #137: two different analyses are conducted with and without this equivalent damping.

Figure 5-9 shows the horizontal reactions for the two different analyses. Both are based on Der Kiureghian's model with constant bending stiffness, and are run in ABAQUS.

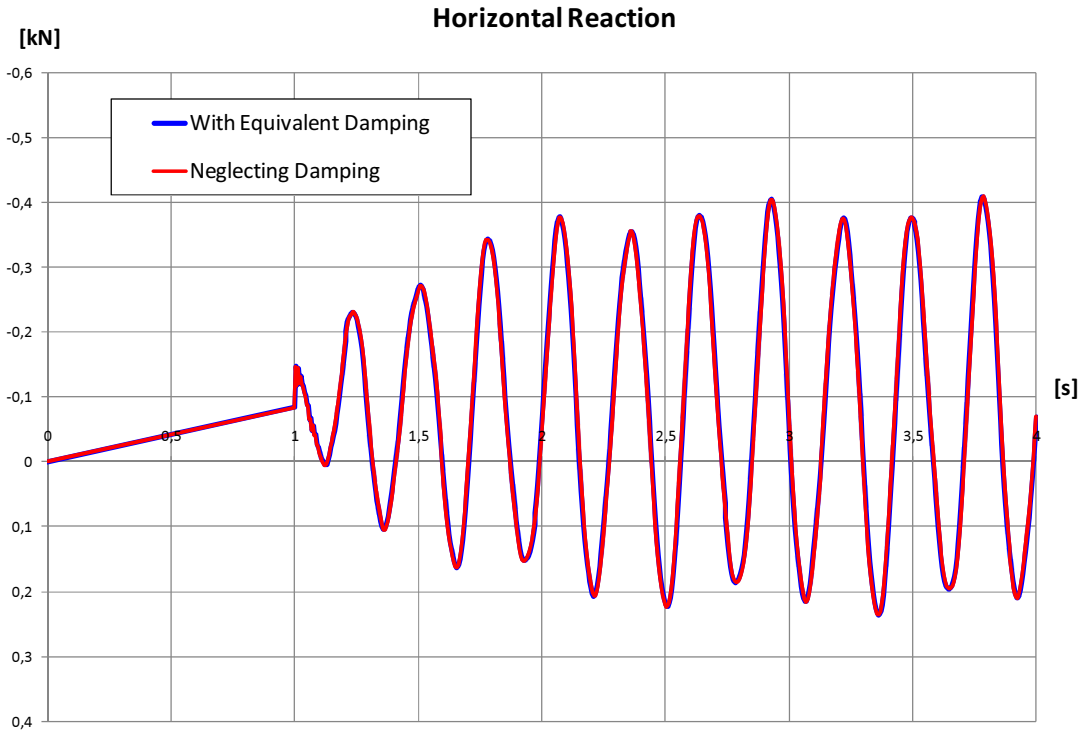

Figure 5-9: Test #137, horizontal reaction with and without equivalent dashpots

It is seen that there are no significant differences between the two models. This fact involves two aspects.

First, this is consistent with the small rotational velocities present in the cable: since the velocities are small, the damping proportional to them doesn't affect the solution. Next, this presents one of the limit of this approach: since the equivalent rotational damping doesn't affect absolutely the solution, it means that it doesn't represent in a realistic way the internal damping in the cable. This can be better shown in Figure 5-10, where are represented the horizontal reactions for frequency-sweep test #130, for the original value of equivalent rotational damping, and for a value multiplied by 100 times. This analysis is also based on Der Kiureghian's model with constant flexural stiffness, and has been modeled in ABAQUS.

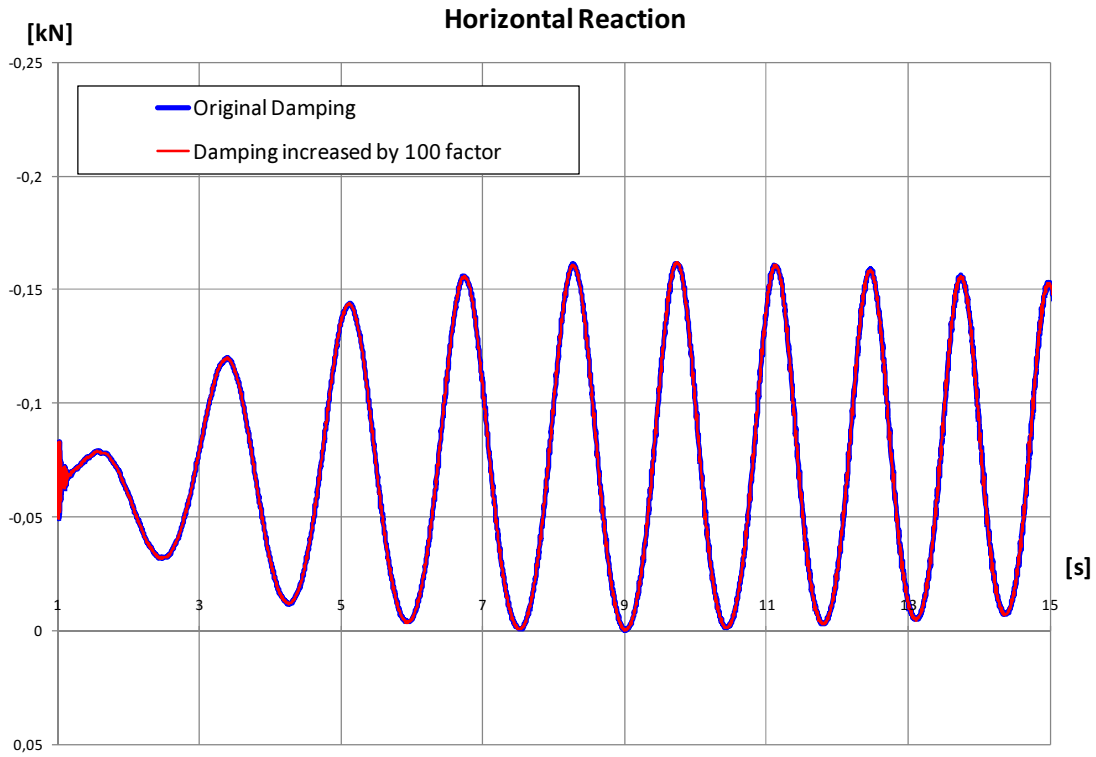

Figure 5-10: Test #130, horizontal reaction for different values of equivalent damping

Again, this kind of equivalent damping doesn't have any influence on the dynamic response: therefore, this model doesn't have the capability of accounting for the internal damping of the real system. One possible further development of the study could be the implementation of a more realistic damping behavior, with the capability of considering the damping due to the frictional interlayer forces.

5.4.2 Rayleigh Damping

Rayleigh damping is defined by a damping matrix formed as a linear combination of the mass and the stiffness matrices. With Rayleigh damping the eigenvectors of the damped system are the same as the eigenvectors of the system without damping: this means that, for a linear system, also the natural frequencies remain the same. Therefore, Rayleigh damping can be converted into critical damping fractions for each mode: this is why it's commonly used in commercial software, especially when the real behavior of the internal damping of a system is largely unknown, but just base on realistic assumptions. A form of Rayleigh damping can be also provided for nonlinear analysis. It is noteworthy that, in such a case, the stiffness matrix changes

during time, since it depends on the elastic or plastic state of the material: thus, being the Rayleigh factors fixed, the critical damping fractions will change too, according to the state of the material. This is why, when the problem is nonlinear, most of the finite-element computer programs allow the direct use of the mass damping factor: the stiffness damping factor is interpreted as creating visco-elastic behavior in which the viscosity is proportional to the elasticity, which gives exactly the stiffness proportional damping effect defined above for the linear case. It is to be noted that such an approach is very limited and approximated, especially for highly nonlinear systems.

In the following analyses, since the stiffness matrix of the system varies continuingly depending on the variable bending stiffness and the geometry of the cable, it is impossible to set the Rayleigh factors to achieve a certain critical damping, but it would change during motion, assuming very different values. Furthermore, the Rayleigh damping is based on the assumption of setting a critical damping ratio for a given mode: being the cable dynamics highly nonlinear, there are no given modes, and the basic assumption of Rayleigh damping cannot be satisfied. Because of all these reasons, and being rotational velocity proportional lumped dashpots available in both ABAQUS and FEAP, it is decided to completely neglect Rayleigh damping for most of the tests. For the sake of completeness, some tests are modeled also taking into account Rayleigh damping, just to see its influence on the response and to check the validity of the assumption of neglecting it. When using it, the procedure to set the two factors is the following. The given mode is assumed to be the first mode evaluated with a finite-element program, for the cable in its initial configuration, that means after the static steps, and without internal forces. The critical damping ratio is assumed to be 10%, evaluating the stiffness matrix for the elastic system: this is computed with the cable in its initial shape, after the static steps, and using the constant bending stiffness value extracted from the IEEE guidelines recommendations. Since only the first natural frequency is meaningful for the frequency content input used, the two parameters are set on the same frequency: this is equal to 1.26 Hz, as calculated earlier. The calculation is the following:

$$\alpha = 0.1\frac{2 \cdot (2\pi \cdot 1.26)^2}{2 \cdot (2\pi \cdot 1.26)} = 0.7917$$

$$\beta = 0.1\frac{2}{2 \cdot (2\pi \cdot 1.26)} = 0.0126$$

Figure 5-11 shows a comparison between the horizontal reactions obtained either considering or neglecting the Rayleigh damping, with the two parameters calculated above. The presented test doesn't belong to those experimentally tested, but is developed just for the analytical study: the sinusoidal input has an amplitude equal to 100 mm and a frequency equal to 0.6 Hz, the configuration of the cable is the same as for the other sine-start tests. Its ID is sine-start test #106. Both the models are considering also the same equivalent rotational damping. All the presented analyses are submitted in ABAQUS, and are based on Der Kiureghian's model with constant bending stiffness.

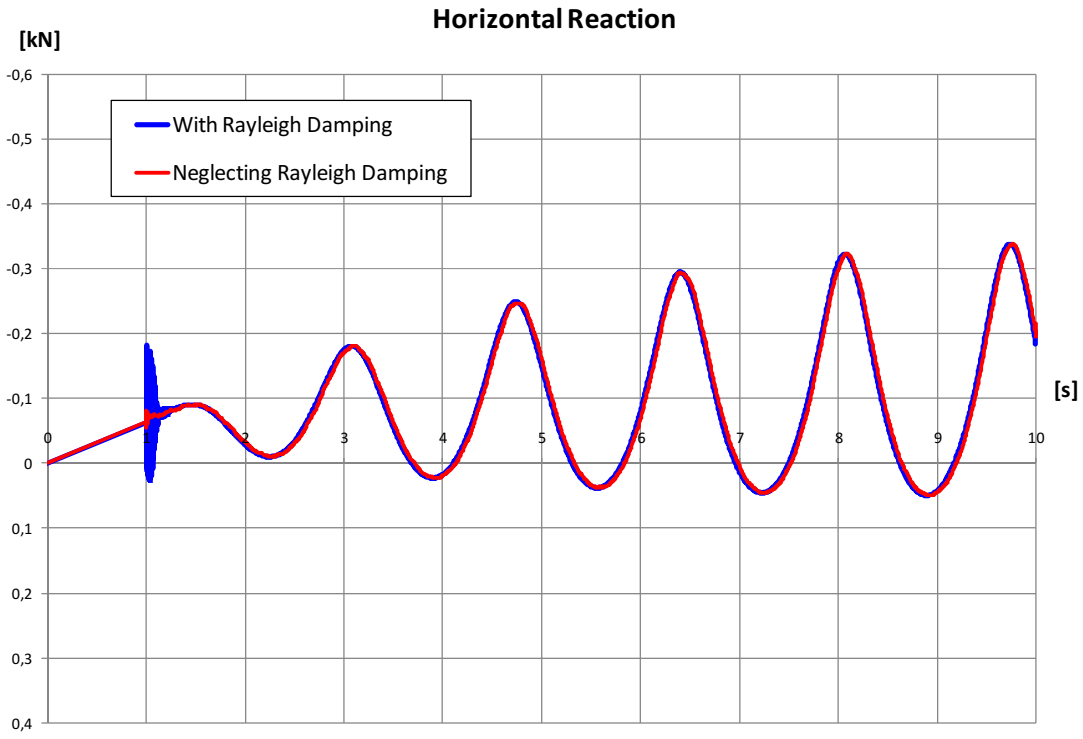

Figure 5-11: Test #106, horizontal reaction with and without Rayleigh damping

It is to be noted that there is just a numerical discrepancy at 1 s, at the beginning of the dynamic part. This numerical disturb ends after some steps, and then the two curves are superimposed. It shows that also this kind of representation of the damping is too less accurate to describe the real complex phenomenon. At the same time, it is noteworthy that the choice of the damping doesn't affect the solution, for the input considered in these analyses. In the further analysis, only the

rotational damping will be considered, since it's the only form of damping that has a physical explanation.

5.4.3 Half-Step Residual Tolerance

Since the highly nonlinear behavior of cables subjected to dynamic input, and the uncertainties regarding this kind of problem, it is decided to use the automatic time stepping for the analyses run with ABAQUS. As a matter of fact, before running the analyses there is no idea about what could be an adequate value of time step in order to achieve an accurate and stable solution. Therefore, the choice of automatic time stepping can lead to more stable results for the first analyses: then, once better understood the problem of cable dynamics and all its issues, the time steps computed by the program can be observed and an order of magnitude for the most suitable time stepping can be extracted. This aspect is particularly important, since the time integration method adopted by ABAQUS is already known not to be extremely accurate for highly nonlinear dynamic systems, as mentioned earlier. Conversely, FEAP doesn't provide the choice of automatic time stepping, but the better accuracy of the time integration method lets us think that a sufficiently stable and accurate solution will be obtained using a relatively very small time steps: the order of magnitude of the time steps can be evaluated by comparison with those used by ABAQUS for the same problems. In ABAQUS, since using the automatic time stepping, the accuracy of the solution is based on the maximum force residuals over each iteration, whose comparison on two consecutive values determines whether the convergence is likely to be reached in a relatively small number of iterations.

All the automatic time stepping scheme is based on the concept of half-step residuals. Since the time stepping operator defines the velocities and accelerations at the end of the step in terms of displacement at the end of the step and conditions at the beginning of the step, the equilibrium is established at the end of the step, thus establishing an equilibrium solution at the beginning and end of each time step. The main problem of this procedure consists of not ensuring equilibrium throughout the step: therefore another control is needed to guarantee sufficient approximate equilibrium for the entire solution path. The time step control consists then of measuring the force residuals at half step: if the maximum entry in this residual vector is bigger than a user-specified tolerance, the time step is considered to be too large and is reduced, otherwise, if the maximum half-step residual is sufficiently smaller, the time step is considered adequate. This

user-defined value governing the process is called “half-step residual tolerance”. Therefore, this parameter governs the dimension of the time steps adopted, and consequently the accuracy of the solution obtained by the time integration method, that is one of the most important issues for cable dynamics, since typically the stability of the solution decreases when the nonlinearity increases. The half-step residual tolerance has dimensions of force, and is usually chosen by comparison with typical actual force values, either applied forces or expected reaction forces. Value of half-step residual tolerance for obtaining reliable results can be very different. If the half-step residual tolerance is 1/10 of the forces, the solution will be highly accurate for elastic cases with little damping. In problems where considerable plasticity or other forms of dissipation are expected to be present and damp out the high frequency response, a tolerance this restrictive is not necessary. If the half-step residual tolerance is the same order of magnitude of the forces, the solution is moderately accurate for elastic cases with little damping and highly accurate for problems including plasticity or other damping effects. If the half-time step residual tolerance is about 10 times the forces, the solution is probably not sufficiently accurate for elastic problems with little damping, but could be still quite good for problems with dissipative effects. Furthermore, the half-step residual moment tolerance is the half-step residual tolerance times the characteristic element length calculated for a problem. Obviously, suitable values for the half-step residual tolerance depend on the unit adopted for the problem and plugged in the program.
Since the units adopted for the problem were N, mm, s and the geometry of the problem, the order of magnitude of the forces generated in the problem is up to 1e5 N. Thus, different tests are submitted with values for the half-step residual tolerance in a range of 1e3 to 1e7 N. It is noteworthy that, since this residual parameter governs the time stepping adopted and the number of iterations required over each time step, the use of a very small value will ensure an accurate solution, but will lead to a very large number of steps and iterations to achieve it. Thus, the user must decide which value is most suitable to guarantee a sufficient accurate numerical solution, without requiring a too big number of calculations and a too heavy computational effort to the program.

In addition, the user must provide the value of the maximum allowable time step: this will be the time step that the program will try to use in the first iteration, before computing the residual. Three factors should be considered when selecting this value: the rate of variation of the applied loading, the complexity of the nonlinear damping and stiffness properties, and the typical period

of vibration of the structure. Usually, a maximum increment equal to 1/10 of the first period of the structure is a good rule of thumb for obtaining acceptable results. Some tests with different values of the half-time residual tolerance have been analyzed, to understand the sensitivity of the time integration method adopted to this parameter. Figure 5-12 shows the horizontal reaction for two different values of the residual tolerance. The test presented doesn't belong to those subjected to laboratory experiments, but has been developed just for analytical studies: the ID is sine-start test #106. The harmonic input has an amplitude equal to 100 mm, and frequency of 0.6 Hz. The analysis is run in ABAQUS, using Der Kiureghian's model and accounting for constant flexural stiffness.

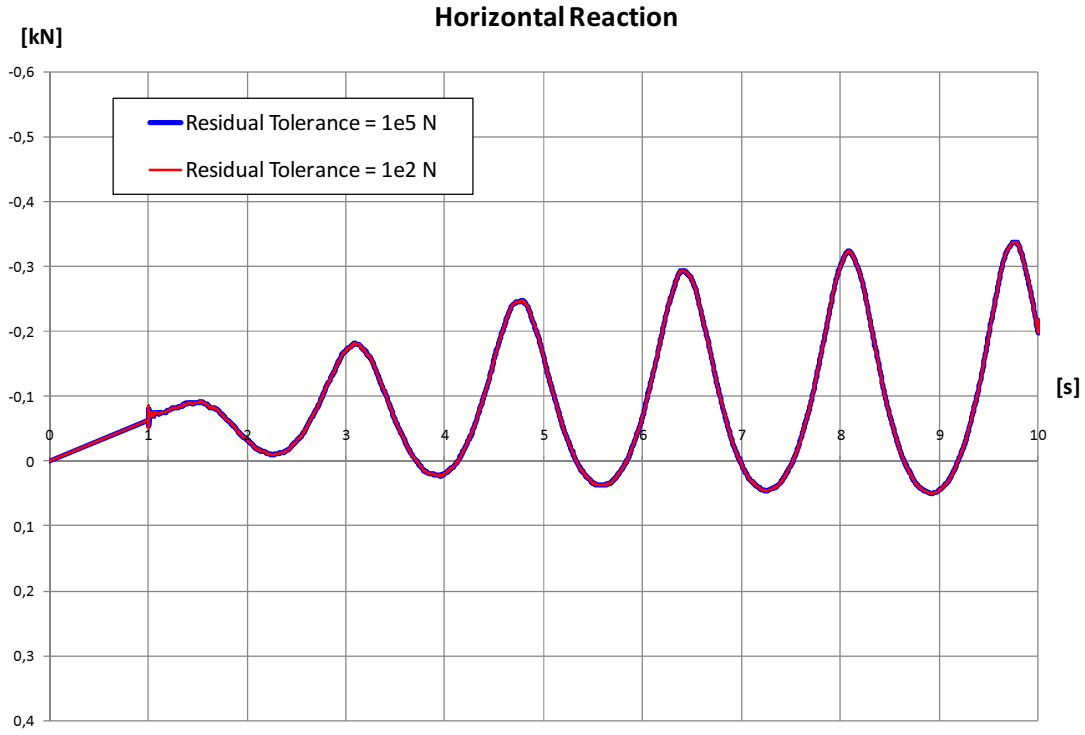

Figure 5-12: Test #106, horizontal reaction for different residual tolerance values

The blue curve corresponds to a given value of 1e5 N for the residual tolerance. Since the biggest peak of horizontal reaction is about 350 N, this residual tolerance value doesn't ensure a priori an high accuracy of the solution. The red curve represents a smaller value of residual tolerance, equal to 1e2 N: this is intend to be about 1/10 of the biggest force in the system, that corresponds to highly accurate solutions. No difference between the two curves is visible. This means that

both the two values allow obtaining stable and highly accurate solutions. Therefore, the bigger value is suitable for this kind of analyses with these inputs, and it can be used without the risk of unfeasible results. Since smaller values of residual tolerance require bigger computational efforts, in the following proceedings a half-step residual tolerance equal to 1e5 N or less will be adopted.

5.5 Element Formulation

Beam theory is the one-dimensional approximation of a three-dimensional continuum, resulting under the slenderness assumption that the dimensions of the cross-section are small compared to typical dimensions along the axis of the beam [30]. The axial dimension must be interpreted as a global dimension and not the element length, such as the distance between supports, the distance between significant changes in cross-section, or the wavelength of the highest vibration mode of interest. In out model a beam element is a one-dimensional line element in two-dimensional space that has stiffness associated with deformation of its axis. These deformations consist of axial stretch and curvature change (flexural bending): being in a two-dimensional space, torsion is not taken into account. Beam formulations can also offer additional flexibility associated with transverse shear deformation, but this aspect is negligible for slender beam, such as cables. The main advantage of using beam elements is that they are geometrically simple and with few degrees of freedom: this is achieved by assuming that the element deformation can be fully estimated from variables functions of position along the beam axis only. Thus, the key issue is to judge whether such one-dimensional modeling is appropriate. The fundamental assumption used is that the beam section cannot deform in its own plane. This assumption should be carefully considered using beam elements especially for cases involving large amounts of either bending or axial forces of non-solid cross-sections such as cables. A possible different choice consists of modeling the entire cross-section with shell elements, in order to take into account the in-plane deformations of the cross-section, but this means losing the simplicity of a one-dimensional approach for the element. After evaluating different options, the choice of beam element is deemed the best one, together with the use of a refined mesh; that means modeling the cable with a big number of elements. Beam elements are implemented for small or large displacements and

large rotations with small strains: this second option is used to properly take into account the geometrical nonlinearity of the cables.

For dynamic problems, also the rotary inertia of the beam cross-section plays a role: it is usually insignificant for slender beam structures, except for twist around the beam axis, but it is neglect in the following analyses, since they are two-dimensional. For Timoshenko beams the inertia properties are calculated from the cross-section geometry: the rotary inertia associated with the torsional mode is used for all rotational degrees of freedom. Different beam formulations are employed in ABAQUS, thanks to a vast library, and their differences are discussed below. For the analyses in FEAP, a specific beam formulation for large displacements and rotations with exact energy is used, since it has the capability to be handled by the energy and momentum conserving algorithm implemented in the program.

5.5.1 Timoshenko Linear Formulation

Timoshenko beams [29] allow for transverse shear deformation, thus can be used for thick as well as slender beams. For beams made from uniform material, this theory can provide useful results for cross-sectional dimensions up to 1/8 of typical axial distances or the wavelength of the highest natural mode that contributes significantly to the response. All the cable subjected to study are characterized by this dimensions, thus the Timoshenko theory is completely valid and provides adequate accuracy. The response of the cables is characterized mostly by the bending behavior than the transverse shear one, thus the Timoshenko theory is not necessarily required, but it is employed for these analyses because it provides the same efficiency of the Euler-Bernoulli and has no additional disadvantages. The transverse shear behavior of Timoshenko beams is assumed linear elastic with a fixed modulus and, thus, independent of the response of the beam section to axial stretch and bending. As mentioned before, since the bending behavior of the cable predominates the transverse shear due to the slenderness of the beam, there's no need of accuracy in the shear stiffness definition. The Timoshenko beams can be subjected to large axial strains. The linear Timoshenko beam elements use a lumped mass formulation with a 1/2, 1/2 distribution, while the quadratic Timoshenko beam elements in dynamic procedures use a 1/6, 2/3, 1/6 distribution: due to the very refined mesh used for modeling the cable, the lumped mass formulation is deemed to be sufficiently accurate.

5.5.2 Euler-Bernoulli Cubic Formulation

In order to check the importance of both transverse shear deformation and consistent mass formulation, some tests with a different beam formulation are analyzed. Instead of using a Timoshenko linear formulation, the Euler-Bernoulli cubic formulation is chosen [16]. These elements do not allow for transverse shear deformation, that means plane cross-sections initially normal to the axis of the beam remain plane and normal to it. This formulation is adequate only for modeling slender beams: the cross-sectional dimensions of the beam should be small compared to the significant distances along its axis. Typically, for beams made of uniform material the cross-section should be less than 1/15 of significant axial distances, in order to consider negligible the transverse shear flexibility: this ratio is usually called slenderness ratio. The geometry of the cable completely satisfies these requirements, therefore the Euler-Bernoulli formulation can be successfully used. The Euler-Bernoulli beam elements use cubic interpolation functions, which guarantee reasonable accuracy for cases involving distributed loading along the beam, such as the own weight of the cable, considered as a dead load. Therefore, they are well suited also for dynamic vibration studies, where the inertia forces provide additional distributed loading. The cubic beam elements have the capability of small-strain and large-rotation analysis, thus can successfully handle the geometrical nonlinearity of cable dynamics. They also use a consistent mass formulation, unlike the Timoshenko linear formulation. This should lead to an even better accuracy for the mass matrix.

5.5.3 Hybrid Formulation

A third possibility in ABAQUS is to use hybrid formulation elements [17]. The hybrid beam elements are designed to handle very slender situations, where the axial stiffness of the beam is very large compared to the bending stiffness. To do so a mixed method, where axial force is considered as an independent unknown, is required. For the Timoshenko theory hybrid beams, the transverse shear forces are also treated as independent unknowns. Hybrid beam elements are designed for use in cases where it is numerically difficult to compute the axial and shear forces in the beam by using common finite element displacement method. These problems usually arise for highly geometrically nonlinear analysis, when the beam undergoes large displacements and rotations and is very rigid in axial and transverse shear deformation: this is the case of a long flexible cable. More deeply, in such cases slight differences in nodal positions may generate very

large forces, causing large motions in other directions. This difficulty can be overcome by hybrid elements by using a more general formulation, treating the axial and transverse shear forces in the elements as primary variables, along with the nodal displacements and rotations. It is to be noted that this formulation makes these elements more computationally expensive, but they generally converge much faster for large beam rotations and, therefore, are more efficient overall.

5.5.4 Comparisons

Some comparisons between the different formulations adopted for the element constituting the cable are presented in Figure 5-13. The vertical axis shows the horizontal reactions measured for the frequency-sweep test #130, processed with ABAQUS using Der Kiureghian's model and the constant bending stiffness. For the sake of completeness, the horizontal reactions represented are only those generated in the dynamic part, without considering the traction due to the vertical dead load applied with a quasi-static process. This has been done, since the different element formulation was supposed to eventually only affect the dynamic part, but not the static one: for the static one, each of them is suitable to obtain trustworthy results.

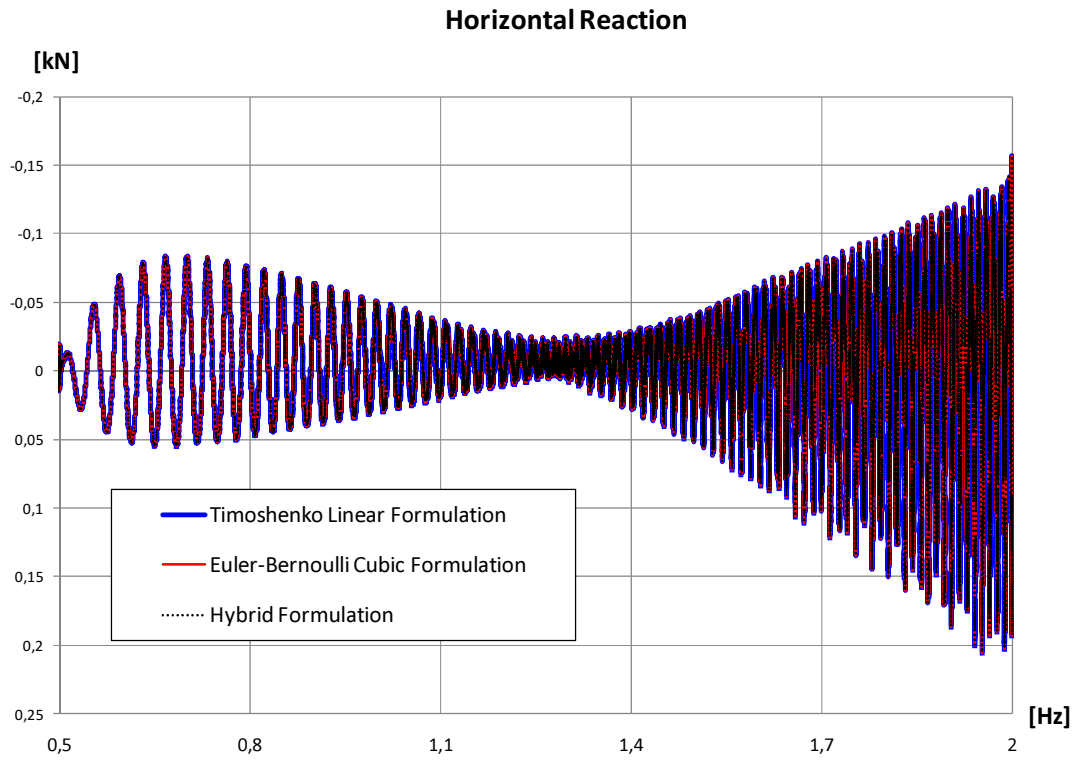

Figure 5-13: Test #130, horizontal reaction for different element formulations

The three curves, each representing a different formulation for the elements, are completely superimposed. This means that each of them is suitable to describe the cable dynamics, and to account for all the variables governing this kind of problem. As a matter of fact, the shear deformation is absolutely negligible in the cable that is an extremely slender structure. Furthermore, the axial force in the cable doesn't affect directly the node displacements of the elements, but its influence is limited to the change of eigenfrequencies. Thus, the use of hybrid formulation elements doesn't improve the solution with respect to the more classical either Timoshenko linear elements or Euler-Bernoulli cubic elements. In the next analyses, there is no difference considering one or another among these element formulations: they are all suitable for this kind of configuration, with these harmonic inputs.

5.6 Time Integration Method

Cables experience very large deformations and non negligible changes in geometry varying with time; this leads to nonlinear behavior that must be taken into account in the time integration

method. Since most of usual structural loading are in the field of nonlinear cable dynamics, a method that can adequate address this particular class of problems must be used. For a dynamic problem, the general finite-element problem described by the equilibrium equation must be extended to a second-order problem taking into account inertial effects. This requires a time-stepping algorithm capable to calculate the solution from the beginning of the time step to the end of it. One of most widely spread time-stepping schemes used in commercial finite-element programs is the implicit Newmark-Beta algorithm [2]. It is a particular sub-case of the general Newmark family of algorithms [23], but it's not completely suitable for cable dynamics for many reasons. First of all, this family of algorithms usually fails to conserve total angular momentum for nonlinear systems; since the cable elements are subjected to non negligible angular motion, this would jeopardize the accuracy of the results obtained. Next, the axial stiffness in the cable in the dynamic regime leads to spurious high-frequency oscillations that totally contaminate the response of the system. To limit such effects, many algorithms have been devised to incorporate high-frequency numerical dissipation. One of the most popular schemes is the HHT-alpha method [2], but it also fails to conserve angular momentum and energy.

A time-stepping scheme preserving angular momentum has been presented by Simo [27], and it's implemented in the finite-element program FEAP. It's highly recommended for adequately treating cable dynamics problems. Another example of its applications to seismic interaction in interconnected substation equipment has been presented by Der Kiureghian [10]. As pointed out by many authors, when this conserving algorithm is to be used for cable dynamics, it requires light numerical damping, in order to avoid the high-frequency oscillation discussed above. This slightly compromises the conservation of total energy, but it turns out to be acceptable. Recommended values for setting the algorithm parameters accordingly found to be adequate in the presented simulations.

5.6.1 HHT-alpha Method

ABAQUS provides the so-called Hilber-Hughes-Taylor-alpha general direct-integration method [2], which is an extension of the trapezoidal rule. This operator is implicit, that means that the integration operator matrix must be inverted, and a set of nonlinear dynamic equilibrium equations must be solved simultaneously at each time increment: this is done iteratively using Newton's method. This equation solving process is very expensive, and it is increasingly difficult

to obtain a solution since the equations are highly nonlinear. Conversely, it is to be noted that nonlinearities are usually more simply taken into account in dynamic situations than in static ones, since the inertia terms provide numerical stability to the system. This can guarantee the success of the method in all but the most extreme cases. In the context of nonlinear equations it isn't possible to establish stability results for integration operators, but nevertheless the linear stability results provide an approximate indication of the properties of the integration method also for nonlinear systems. One of the principal advantages of the Hilber-Hughes-Taylor operator is indeed that it is unconditionally stable for linear systems; this is an indication of a certain form of stability also for nonlinear and highly nonlinear systems.

5.6.2 Energy-Conserving Algorithm

The dynamic analysis of a cable with large displacements and rotations is a highly nonlinear elasto-dynamic problem, that has no known analytical solution, and for such a problem even a numerical solution is challenging. During the dynamic response, whenever the cable is fully stretched the axial stiffness dominates the cable behavior and significant high frequency effects are generated. With finite element spatial discretization, these high frequency effects may give rise to errors and instability in the numerical computations. Under these conditions, the Newmark time integration method [23] does not lead to either stable or accurate results. Furthermore, the classical Newmark family of algorithms with their variants usually fails to conserve total angular momentum for nonlinear dynamics. Since the angular momentum plays a big role on cable dynamics, this is a significant lack.

In order to overcome this lack, an algorithm that preserves the conservations law has been presented by Simo et al [27]. FEAP provides a modified version of this algorithm that, by controlling parameters, introduces numerical damping to stabilize the computations while only slightly affecting on the conservation of energy. Experience showed [10] that this algorithm with parameters of

$$\alpha = 0.55$$

$$\beta = 0.5$$

$$\gamma = 1$$

and time step

$$\Delta t = 0.005\ s$$

works successfully for the cable dynamics problem. For the sake of completeness, it must be noted that parameter values of

$$\alpha = 0.5$$

$$\beta = 0.5$$

$$\gamma = 1$$

correspond to the energy-conserving algorithm with no numerical damping.

5.6.3 Comparisons

The two time integration methods discussed above have been compared on the frequency-sweep test #130. Their horizontal reactions are shown in Figure 5-14. The present analysis is processed in FEAP, since it implements both the HHT-alpha time integration method and an energy-conserving algorithm. Dastous' model with variable bending stiffness is adopted, in order to account for both geometrical and material nonlinearities, that turn out into a higher global nonlinearity, likely to undergo unstable solutions.

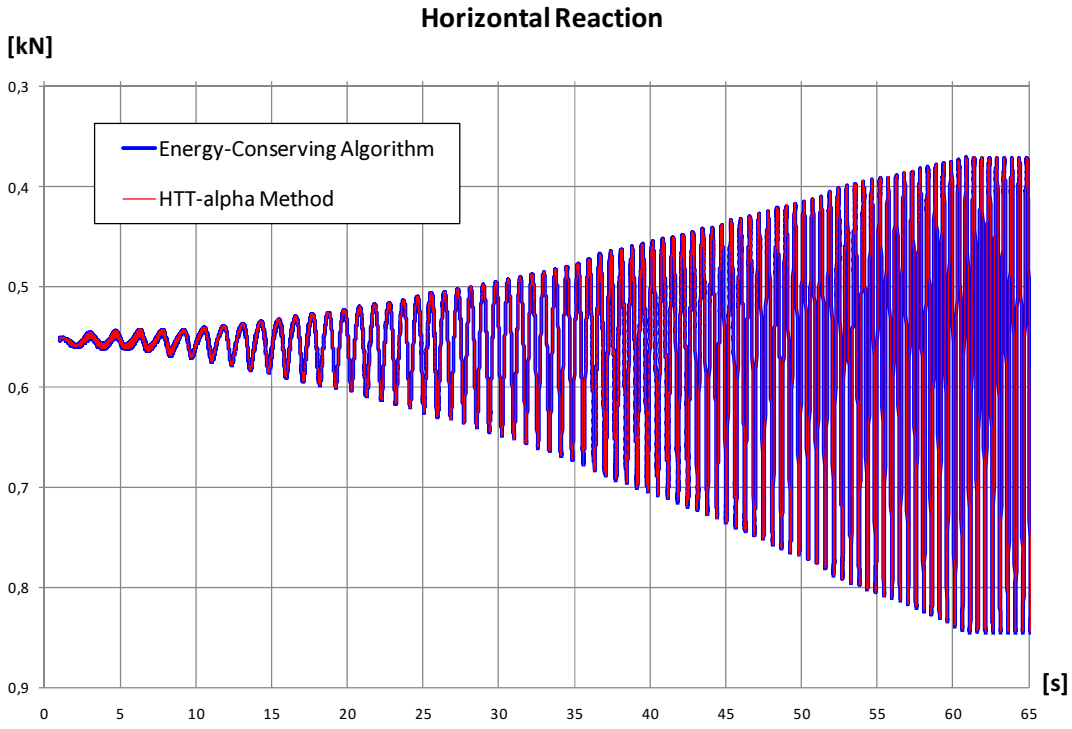

Figure 5-14: Test #130, horizontal reaction for different time-integration methods

The two solutions don't show any significant difference. Both the two methods have the capability of getting reliable and accurate solutions for these dynamic problems. Therefore, ABAQUS is as suited as FEAP for treating cable dynamics, even if it implements only the HHT-alpha method. The slight dissipation of energy for the two methods is the same, and doesn't represent a big lack of accuracy for these analyses, involving a relatively small time period.

5.7 Convergence of Solution

As mentioned earlier, being the cable dynamics highly nonlinear, it's not possible to define conditional or unconditional stability. Therefore, it isn't possible to fix a time step small enough to ensure a stable and accurate solution. Different time step must be used, and by their comparison a qualitative evaluation of the stability of the solution can be done. First of all, judging the results obtained, it's possible to see if they show sudden and very large amplification from one step to another, that could be symptom of numerical instability. It is noteworthy that it's more important to check the forces than the displacements: this is due to the fact that the finite-element program works with the displacement method. Thus, the primary unknowns solved by the program are displacements, while forces are built from those in a post-process: this means that displacements will be always more accurate than forces.

This study of accuracy is not done directly on the dynamic problem, but on the static one. This is due to different reasons. First of all, as mentioned above, the automatic time stepping is adopted for the dynamic solution, thus the convergence and the accuracy are left to the choice of the half-step residual tolerance, while the most suitable time step is computed by consequence. Furthermore, setting on purpose too big time steps, in order to obtain a non accurate solution, will require a very large of iteration by the program, because it will try unsuccessfully to achieve a convergence: therefore, the solution of this problem will require a very big computational effort. This is why this study is carried on the static part only. It is to be noted that nevertheless, if the solution is not accurate and unstable in the static part, it will be even less accurate for the dynamic part, because the affection due to the high geometrical as well as mechanical nonlinearity is more important than the improvement due to the activation of the inertia forces.

5.7.1 Time Stepping

The influence of time stepping on the stability of the solution obtained is studied for the static part common to all the sine-start test, since they present the same configuration of the cable (same own weight, same total length and span). It is decided to focus on the static part for two reasons. First, if the time stepping is not suitable to find a stable solution for the static part, the dynamic part of the analysis will be affect by consequence, since it follows the quasi-static loading procedure. Second, a dynamic analysis with a non suitable time stepping will require a lot of iterations for each step, trying to achieve the equilibrium: therefore, it requires a very big computational effort, turning in complex analyses and time wasted.

The comparisons are processed separately for the HHT-alpha time integration method implemented in ABAQUS, and the energy-conserving algorithm implemented in FEAP, because different time integration methods could need different time stepping. It is noteworthy that in a quasi-static procedure the analysis is calculated for equivalent time steps: the total load is meshed in sub-steps that are considered as time just for the sake of simplicity. In this case, the total period of the static analysis is supposed to be 1 s, applying the vertical dead load from 0 to 0.5 s and linearly moving horizontally the two ends from 0.5 to 1 s. This is valid both for Dastous' and Der Kiureghian's model, since the static part is the same: the only difference consists after that part, either in removing or not the internal forces before applying the harmonic input. Therefore, the same discussion made for the number of steps in a static analysis is valid for the dimension of the time steps in a dynamic one.

Figure 5-15 shows the horizontal reaction measured in the static part of each sine-start and frequency-sweep test for the 1796-MCM cables, solved in ABAQUS with the HHT-alpha method.

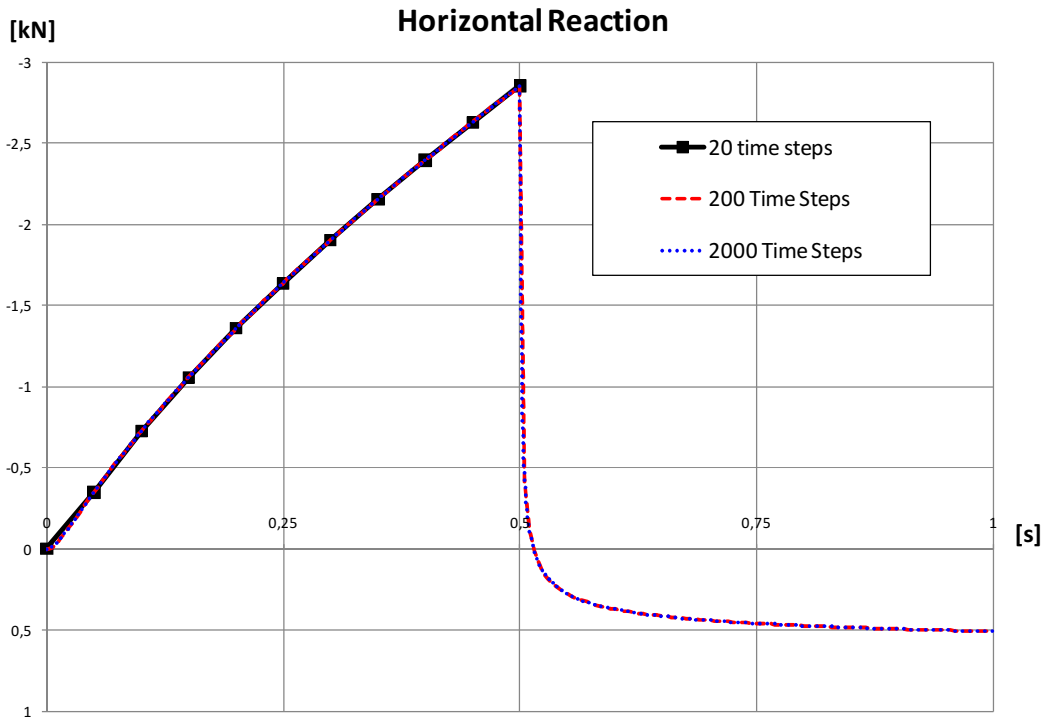

Figure 5-15: ABAQUS static part, horizontal reaction

It is to be noted that the application of the vertical dead load doesn't generate big deflections and displacements, thus also a small number of steps is sufficient to achieve the equilibrium. Conversely, when the horizontal displacements are applied at the two ends of the cable, big vertical displacements and curvatures are involved. This turns out into high nonlinearity, and requires a larger number of steps to follow the equilibrium path of the system. As a matter of fact, using only 20 steps for the whole static analysis, the equilibrium can't be achieved for the first step after applying the horizontal displacements, and the solution is lost. Increasing the order of magnitude of the steps, it is possible to achieve an equilibrium position for the system, even when very big sudden displacements and high nonlinearities are involved. Figure 5-16 presents the same study for the energy-conserving algorithm implemented in FEAP.

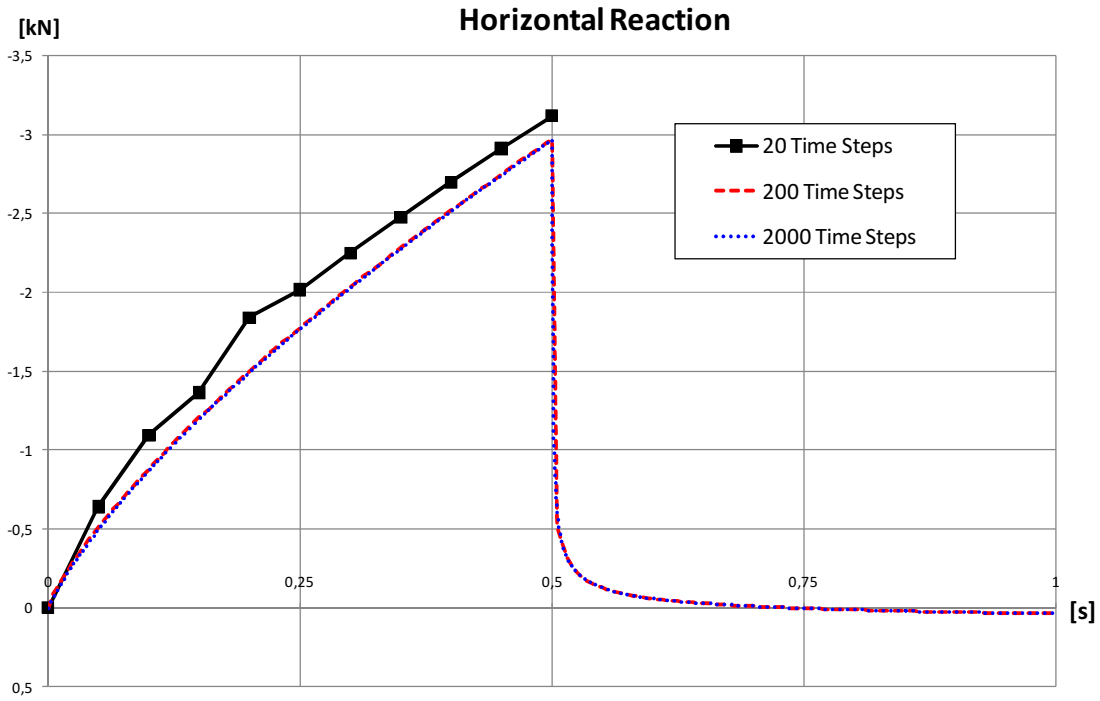

Figure 5-16: FEAP static part, horizontal reaction

It is to be noted that the value of the horizontal reactions are different from the ABAQUS graph, since in this model the variable bending stiffness is adopted: this was chosen in order to increase the possible sources of nonlinearity in the system. In this case, the total 20 steps for the static part are not sufficient, and the solution can't be obtained after applying the horizontal displacements, but it can be seen that there is a lack of accuracy also for the vertical dead load itself. This means that a larger number of steps should be required also for the first 0.5 s.

Generally, increasing by an order of magnitude the adopted time steps, a stable and accurate solution can be found. This study has a big importance, since a large number of time steps turns into a heavier computational effort, and bigger times required for the analysis. It is important to maximize the efficiency of the solution method, by choosing if possible the smallest number of steps suitable to find an accurate and stable result, in order to minimize the numerical calculations the program has to do.

5.8 Modeling of Conductor Only

In order to set a reliable analytical benchmark to model future experimental tests of electrical equipment items interconnected by flexible conductors, it is important to match the results obtained for the conductor only [4]. The geometrical as well as the material nonlinearities of the system arise from the cable, while the two equipment items, whatever they consist of, doesn't require specific studies. Conversely, it's very important to develop deep studies on the cable dynamics, to understand its behavior and accounting for all the possible different aspects regarding its motion. Since some experimental tests are already available from Dastous' testing campaign [4], supplying results for a configuration of cable common in electrical substations undergoing a harmonic motion for a large range of amplitudes and frequencies, they are used as a reference for the finite-element model. The parameters and the data for all these tests have been presented earlier in the previous chapter. Since the two cable tested (1796-MCM and 4000-MCM) differ only for some parametric value, there is no meaningful difference in modeling either one or the other: thus, it is decided to model only the 1796-MCM cable configuration, due to a bigger number of experimental tests available. All the discussions about the various issues bound to the modeling, presented earlier in this chapter, are used to refine reliable models, describing the experimental tests.

It is decided to develop two different models for every test. The first is based on Dastous' approach, with the dynamic input suddenly following the quasi-static horizontal displacement of the two ends, without removing the internal forces. Furthermore, the variable bending stiffness is used to account for material nonlinearity and provides an accurate description of the dynamic of a cable made of wrapped strand undergoing large rotations. All the data necessary for defining the variable bending stiffness for the 1796-MCM cable are presented in Table 4-4. The model is implemented in FEAP, in order to take advantage of the energy-conserving time integration method available, that leads to more stable solution also when high nonlinearities are involved. As well as for the time integration algorithm, the element formulation is a particular energy-conserving one with the capability of undergoing large displacements and rotations: otherwise, using any other formulation, the advantages of the time integration method would vanish. It is to be noted that this kind of algorithm doesn't require any half-step residual tolerance. The convergence of the solution is depending on the time stepping, that is directly plugged in by the

user. The static part is divided in 2000 steps, respectively 1000 for applying the gravity load of the cable, and 1000 for the linearly increasing horizontal displacement of the two ends. The total equivalent time period of the static procedure is up to 1 s. The time step dimension for the dynamic solution is assumed equal to 0.005 s. This requires a lot of steps, but it turns out into an acceptable numerical effort since the total period of the harmonic motion is always less than 10 s. All the damping of the system is considered to be lumped with equivalent viscous dashpots at each node of the cable, without adding any Rayleigh damping. This aims to be consistent with the real damping in the cable, which is dependent on the curvature. The value of equivalent viscous damping assumed for each dashpot is that discussed above for cable 1796-MCM:

$$10 \cdot \frac{5}{100} = 0.5\ N \cdot m \cdot s$$

This value is set to be only proportional to the rotation velocity, trying to give a realistic approximation of the physical phenomenon. The material the cable consists of, is aluminum: therefore, the IEEE recommended value for the Young's modulus was adopted (69900 MPa). The mass of the cable is accounted for by providing the density of the material (2700 kg/m^3), and the consistent mass matrix is used. For the sake of simplicity, the gravity load is converted in a vertical dead load concentrated ad each node of the cable. The value of these lumped vertical forces is:

$$P = \frac{2700 \cdot (9.1 \cdot 10^{-4} \cdot 5.52 \cdot 9.81)}{99} = 1.34\ N$$

The second model is based on Der Kiureghian's approach, with the dynamic input that is applied to the already deformed cable without any internal force. This is obtained taking the same static part common with Dastous' model, then removing all the internal forces and using only the deflected shape of the cable. In the dynamic analysis the harmonic input is applied at the two ends of the cable obtained plugging in the shape computed at the end of the static procedure. It is to be noted that the choice of removing all the internal forces has a clear explanation. Above in the chapter, it is shown how the compression forces inherent the cable can completely modify the dynamic behavior of the cable itself, shifting its natural frequencies. Since it is found from the experimental tests that the initial compression for this cable configuration is quite low (about 50 N), this value doesn't change significantly the natural frequencies of the cable. This axial force turns out just into a translation of the response curve, but it doesn't affect its general shape: thus,

this shift can be either added or removed in the post-processing, to compare the solutions without its influence. Therefore, it is preferable to begin the dynamic procedure without any internal forces, neglecting the initial compression, than having an initial value so big that turns out into a complete change of the first natural frequency of the flexible conductor, thus misunderstanding its dynamic properties. It is noteworthy that this additional step (the removal of the internal forces) is needed only if using the constant bending stiffness, turning out in a very large compression due to the horizontal motion of the two ends. Using the variable bending stiffness, accounting for the interlayer slippage and the friction forces, the initial compression in the cable is much lower, close to the real value measured from the experiments: therefore it doesn't affect so much the eigenfrequencies, and the internal forces removal is not required. Der Kiureghian's model is implemented in ABAQUS, using the HHT-alpha time integration method, since it is found to lead to solutions as accurate and stable as for the energy-conserving algorithm available in FEAP, as shown in the earlier specific paragraph. For this method, the automatic time stepping is adopted, as it is supposed to be more accurate. The half-step residual tolerance is set to a value equal to 1e4 N: this is chosen after comparing the reaction forces involved for the current cable configuration and dynamic inputs. Generally, it turns out into a bigger number of steps than those for FEAP: it means that this time integration method needs smaller time steps, in order to achieve the same accuracy for the solution. Conversely, the static part, necessary only to compute the initial shape of the cable, is divided in 2000 steps, as for FEAP: 1000 for applying the vertical dead load and 1000 for the horizontal displacement of the two ends. The Timoshenko linear element formulation is used, due to its validation from the previous study presented above. In particular, the "general section" option is used for the beams. As a matter of fact, since the cable is made of wrapped individual strands, it's not possible to define a single parameter of this cross section, from which obtaining all the geometric values of the section. Therefore, it is necessary to directly provide the program both the cross section area and the moment of inertia for bending: all the other data are not needed, since the model is only bi-dimensional. The cross-section area is set equal to the real value for the 1796-MCM cable. The moment of inertia for bending is assumed equal to that recommended by the IEEE guidelines, and discussed above. The damping, the gravity load and the Young's modulus are the same discussed for the other model. One important difference is adopted for the mass matrix. It is observed that, whether using the two lumped masses representing the load cells at the two ends of the cable, a fake first

natural mode is introduced by the solver. In order to avoid it, the two lumped masses are removed and substituted increasing the density of the two end elements of the cable: this is a way to distribute the two masses as a mass per length. Since the density of aluminum is 2700 kg/m^3 and the two lumped masses are 7.1 kg each, to be distributed along an element with a cross-section area of 910 mm^2 and a length of 55.2 mm, the increased density for the two end elements is found to be:

$$\rho^* = 2700 + \frac{7.1}{(9.1 \cdot 10^{-4}) \cdot 0.0552} = 144044 \ {}^{kg}/_{m^3}$$

This second model, even if less accurate than Dastous' one, is developed for the sake of simplicity, since it requires less computational effort, the variable flexural stiffness user-defined approach doesn't need to be plugged in, and its disadvantages are not meaningful for the further developments.

5.8.1 Sine-Start Tests

All the experimental sine-start test are made on 1796-MCM cables, with a total length equal to 5.52 m and a distance of 5.00 m between the two clamped ends. The tests differ only for the characteristics of the harmonic motion horizontally applied at the two ends, amplitude and given frequency. The quantity selected for the comparison is ΔF, the difference between the maximum and minimum horizontal reaction force measured for a given cycle of applied displacement at a given amplitude and frequency. This choice is due to the measurement made in the experiments. The precision of the sensors themselves may lack some precision when tension is low, around values close to zero. The load cells used in the experimental setup had 4500 N capacity (1000 lbs) and a precision within +/- 2% [4]. So at the observed initial tension of about 50 N this value is within 1 % of the sensor scale, meaning that the load cell may have measured an initial tension that ranges from -40 N to 140 N, if 40 N is the correct value. Therefore, this is why it is preferred to compare ΔF rather than absolute values.

The dynamic input is a harmonic displacement applied out-of-phase at the two ends of the cable in the horizontal direction. To avoid numerical instability cause by non-zero initial conditions, the sinusoidal function is multiplied by a loading ramp. The form of the motion is therefore:

$$u(t) = [1 - e^{-2\pi \cdot 0.1 \cdot f \cdot t}] \cdot A \cdot sin(2\pi \cdot f \cdot t)$$

where f is the frequency and A is the amplitude.

The duration of the input is different for each test: as a matter of fact, the term inside the square brackets governs the time needed to reach a perfectly harmonic motion, and therefore a steady response by the system. This term depends on the frequency of the input, thus every test needs a different time to reach the perfectly harmonic motion. Table 5-1 summarizes the comparisons of forces measured from the experiments on the 1796-MCM flexible conductor [4].

Table 5-1: Results of the Experimental Sine-Start Tests

Test ID	Cable	A (mm)	f (Hz)	ΔF measured (N)
#134	1796	150	1	225
#135	1796	80	2	500
#136	1796	40	3	530
#137	1796	20	3	260
#138	1796	20	5	760
#139	1796	20	1	25
#140	1796	20	2	108

Table 5-2 shows the comparisons of forces predicted by Dastous' model with the experimental tests.

Table 5-2: Comparison between Dastous' Model and the Experimental Sine-Start Tests

Test ID	Cable	A (mm)	f (Hz)	ΔF measured (N)	ΔF calculated (N)	Diff. (%)
#134	1796	150	1	225	232	3.1
#135	1796	80	2	500	531	6.2
#136	1796	40	3	530	535	0.9
#137	1796	20	3	260	262	0.8
#138	1796	20	5	760	730	-4.0
#139	1796	20	1	25	24	-4.8
#140	1796	20	2	108	125	13.6

It is observed that this model reproduces very well the measured ΔF, with a maximum error of 13.6% and an average error of 4.8% for the 7 tests compared. This leads to conclude that this model is completely adequate to accurately describe the dynamic of flexible cable usually interconnecting high-voltage substation equipment. Table 5-3 presents the same comparisons of ΔF, with the absolute values and the percentage errors, for Der Kiureghian's model with the experimental results.

Table 5-3: Comparison between Der Kiureghian's Model and the Experimental Sine-Start Tests

Test ID	Cable	A (mm)	f (Hz)	ΔF measured (N)	ΔF calculated (N)	Diff. (%)
#134	1796	150	1	225	228	-1.3
#135	1796	80	2	500	311	-37.8
#136	1796	40	3	530	505	-4.7
#137	1796	20	3	260	233	-10.4
#138	1796	20	5	760	968	27.3
#139	1796	20	1	25	25	0.0
#140	1796	20	2	108	68	-32.0

In this case, the maximum error is 37.8% and the average error is 16.2% for the 7 tests compared.

As expected, those errors are bigger than those for Dastous' model, since Der Kiureghian's one is less accurate, due to the constant flexural stiffness, not adequate to account for the material nonlinearity, and the neglect of the initial compression arising from the static procedure. This initial compression remains constant through the entire dynamic analysis, thus just shifts the curve of the reactions and doesn't affect directly the value of ΔF, that is the difference between the two peaks for a given cycle. Nevertheless, this compression can affect the natural frequencies of the cable, resulting in a different dynamic behavior. This can be observed in Figure 5-17, that presents the horizontal reactions of sine-start test #134 for the two different analytical models. Unfortunately, no time-history plots are available for the experimental tests.

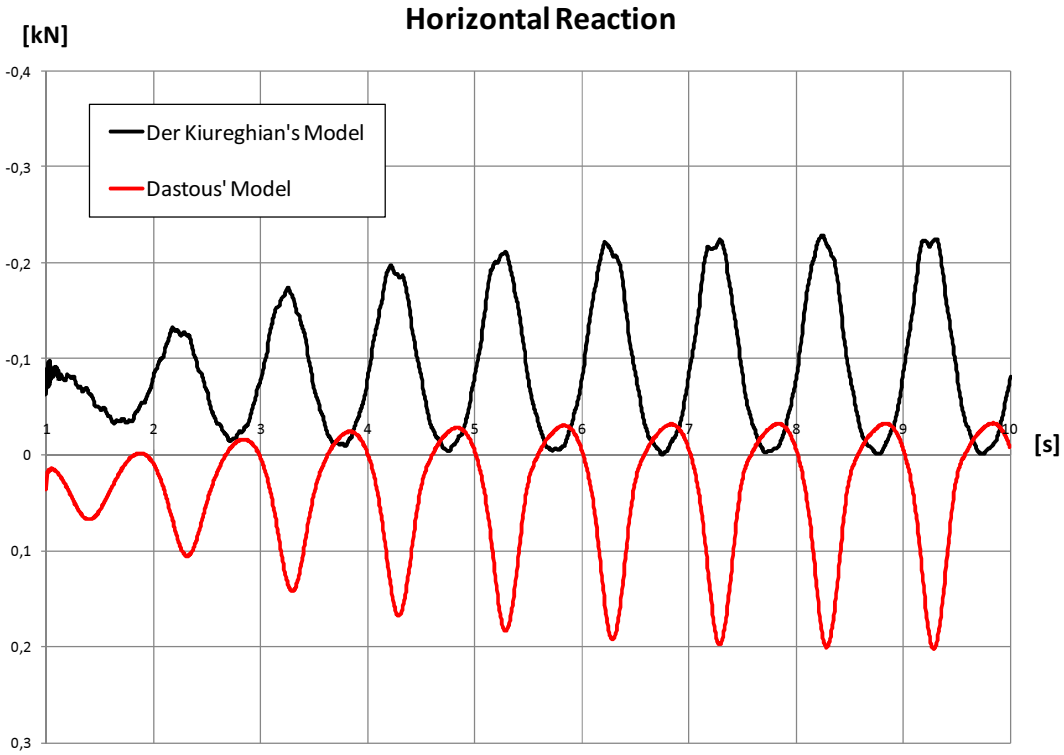

Figure 5-17: Test #134, horizontal reaction for Der Kiureghian's and Dastous' model

In the graph the positive reactions correspond to compression.

It is clear how the different value of compression (for Dastous' model) or traction (Der Kiureghian's model) can affect the natural frequencies of the system. The two curves present very similar difference between the values of the peaks, but they are completely out-of-phase. This means that their first natural frequencies are not either both bigger or both smaller than the given frequency of the input (1 Hz), but one is bigger and one is smaller. In particular, Der Kiureghian's model presents a response out-of-phase with the acceleration at the end where the response is measured: this acceleration, multiplied times the lumped mass representing the load cell, is the input force in the system. Conversely, Dastous' model response is in-phase with the input force. As discussed earlier, this is similar to the dynamic behavior of a single degree of freedom system undergoing an harmonic motion: its reaction is out-of-phase with the input force for low frequencies, but when the frequency of the input crosses the natural frequency of the system the reaction experiences a shift of 180 degrees, and thus becomes in-phase. This means that the cable analyzed with Der Kiureghian's model has a first natural frequency higher than 1 Hz, while with Dastous' model it has a first natural frequency lower than 1 Hz, which is the given frequency of the input. This difference of eigenfrequencies is explained by the presence of compression, even if not so huge, in Dastous' model. It is to be noted that, as already mentioned, due to a slack of precision of the measurement, there is uncertainty whether the cable is subjected to initial traction or compression in the experimental tests.

Increasing the given frequency of the sinusoidal input, the first natural frequency is crossed also for Der Kiureghian's model, and the response of the two models becomes the same. This can be seen in Figure 5-18 for the sine-start test #138.

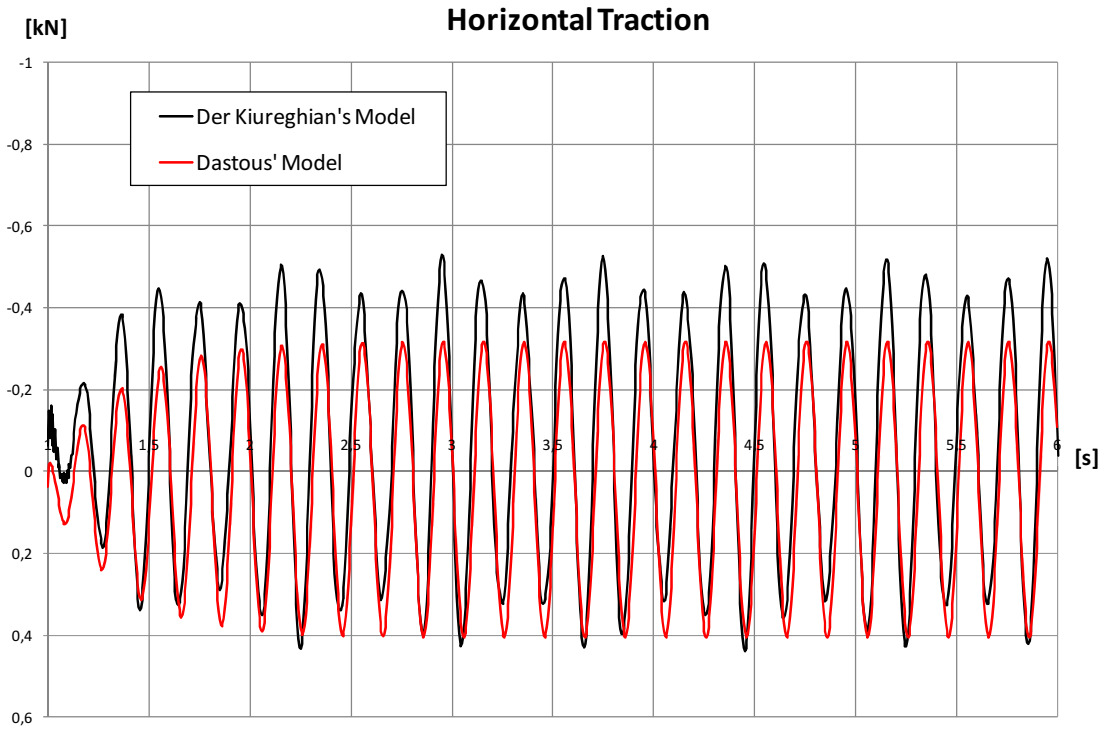

Figure 5-18: Test #138, horizontal reaction for Der Kiureghian's and Dastous' model

In this case, the given frequency of the input is equal to 5 Hz, and is bigger than the first natural frequency of both the models. Therefore, both the reactions are in-phase with the acceleration input at the same end where the reaction is computed.

The explanation for the discrepancies between the experimental results and those predicted by the two analytical models are several. First, every parameter included in the analysis has a certain influence on the solution, as discussed in the previous paragraphs of this chapter: some errors arise from the choice of these parameters. Other approximations are not involved in the finite-element models, but in the experimental tests themselves. Among them is the deformation inherently present in the actual cable, which is not a perfect straight line at first, since it was initially rolled on a wooden turret. Therefore when such a cable is installed attached at the two clamps, it may try to fight its initial curvature, varying the inherent tension. Furthermore, even though the experimental setup aimed at reproducing a perfectly harmonic motion, there was some backlash in the mechanisms (gears) transmitting the motion, and some deformation in torsion in the shaft transmitting the motion at both ends. This may have led to some additional

peak accelerations that contaminated the harmonic motion sought and therefore, may have resulted in additional forces. As a matter of fact, it is very difficult in dynamic experiments to perfectly reproduce a given motion: there is most often contamination of the signal due to the test setup itself, which is not perfect. Therefore, even the experimental analyses are not perfect.

5.8.2 Frequency-Sweep Tests

As for the sine-start tests, one of the frequency-sweep test is analyzed with both the finite-element models discussed above. It is decided to reproduce only one of them, since the time duration of the analysis, much bigger than for the sine-start test, turns out into a big computational effort and a long time required completing the solution. Furthermore, while it is necessary to run many sine-start tests to understand the response of the system under different frequencies, in this case the form of the analysis itself provides a sweep over a range of frequencies. Therefore, the response of the cable under all the frequencies comprised in the range is obtained. The experimental frequency-sweep tests differ only for the highest frequency of the range, and the amplitude of the motion. The amplitude itself affects mainly only the order of magnitude of the reactions, and only in a minor way the general dynamic behavior of the cable, that is mostly influenced by the frequency of the input. It is noteworthy that this is true only for configuration slack enough so that the applied displacement doesn't turn into a big variation in the shape of the cable. This is the case of the configuration presented in this study, showing a sag / span ratio equal to 19%. Conversely, for tighter cables, big amplitude of the harmonic motion could turn out into reaching the straight position of the cable, thus generating big changes in the shape of the cable. This means big changes of the natural frequencies of the cable during the motion itself, and developing big tractions.

In the presented case, the sine-start tests already showed that the dynamic behavior is influenced mainly by the frequency, and in a minor way by the amplitude. Therefore, the most meaningful frequency-sweep test would be #130, with a frequency range from 0.5 up to 5 Hz: this range covers up all the ranges of the other experimental frequency-sweep tests. For the sake of simplicity, only test #132 is modeled, since it has a smaller range (up to 2 Hz), requiring a smaller computational effort, but covering the frequencies that were found to be interesting as related to the first natural frequency of the cable (about 1.25 Hz). Furthermore, from Dastous' paper [7], it is known to be the test with the better agreement between experimental and

numerical results. It is noteworthy that the frequency-sweep input has duration of 60 s, that is 6 times the longest duration adopted for the sine-start tests (10 s): thus, it requires something like 15000 steps to be solved, turning out into a huge numerical effort.

The formula of the displacement input is:

$$u(t) = \left\{1 - exp\left[-2\pi \cdot 0.1\left(f_{MIN} + \frac{f_{MAX} - f_{MIN}}{2}\right)\frac{t^2}{t_{TOT}}\right]\right\} \cdot A \cdot sin\left[2\pi\left(f_{MIN} + \frac{f_{MAX} - f_{MIN}}{2}\right)\frac{t^2}{t_{TOT}}\right]$$

where f_{MIN} is the lowest frequency of the range (0.5 Hz), f_{MAX} is the highest frequency (2 Hz), A is the amplitude (80 mm), and t_{TOT} is the duration of the input (60 s).

As well as for the sine-start test, the quantity selected for the comparisons was ΔF, for the same reasons. Table 5-4 shows the horizontal reaction measured during the experimental test, and the comparison with the values predicted by Dastous' model.

Table 5-4: Comparison between Dastous' Model and the Experimental Frequency-Sweep Tests

Test ID	Cable	A (mm)	f_{MIN} (Hz)	f_{MAX} (Hz)	ΔF measured (N)	ΔF calculated (N)	Diff. (%)
#132	1796	80	0.5	2	500	503	0.6

Also in this case, it is observed that the model predicts the measured reactions with acceptable precision, albeit with a smoothing of the model response over some frequencies, as opposed to the experimental results where smaller variations were observed. This is likely to be related to the way the damping was approximated in the models. Table 5-5 presents the same comparison of reactions predicted by Der Kiureghian's model with those measured from the experiments.

Table 5-5: Comparison between Der Kiureghian's Model and the Experimental Frequency-Sweep Tests

Test ID	Cable	A (mm)	f_{MIN} (Hz)	f_{MAX} (Hz)	ΔF measured (N)	ΔF calculated (N)	Diff. (%)
#132	1796	80	0.5	2	500	330	-34%

This model provides a bigger error that can be explained looking at the whole time-history of the response, presented in Figure 5-19.

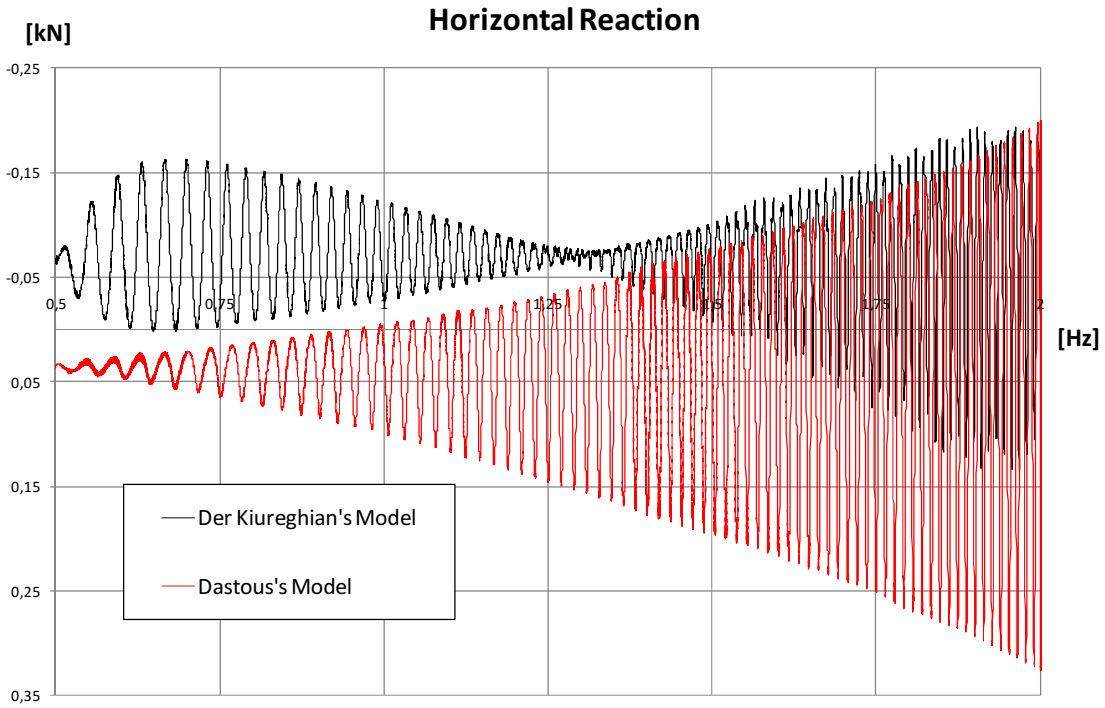

Figure 5-19: Test #132, horizontal reaction for Der Kiureghian's and Dastous' model

It is easily observed how the two models have completely different behaviors. In particular, Der Kiureghian's one shows a beat, characterizing the cross of a natural frequency. In the previous paragraphs the sources of this behavior have already been discussed. Dastous' model, that has an initial compression, doesn't cross any natural frequency, thus its reaction is always increasing. This is because the first natural frequency is shifted to a value less than 0.5 Hz (a previous hand calculation shows that it's about 0.3 Hz). This turns out into the absence of any beat, and the reaction is free to get bigger with the increase of the frequency, as it is expected to be. Conversely, Der Kiureghian's model crosses the first natural frequency, and this causes a large decrease of the total horizontal reaction, since the input force and the cable response are out-of-phase until the frequency input is lower than the first natural frequency. After the cross of the first natural frequency, the reactions begin again to increase with the input frequencies, but the difference between the positive and negative peaks is still affected by the previous decrease. In particular, comparing the ΔF for the two models around 1.25 Hz (presence of the beat), it is noted that Der Kiureghian's model shows $\Delta F \cong 0$, while Dastous' model has $\Delta F \cong 175$. Therefore, for this frequency the discrepancy between the two models is 175 N. This value is

absolutely the same that separates the final values of ΔF for a given frequency of 2 Hz. This means that the final error is completely caused by the difference in presence of the beat, and the remaining part of the time-history of ΔF just shows a shift equal to 175 N.

It is to be noted that all those discrepancies between the two models arise from the presence of initial compression due to the horizontal motion of the two ends of the cable necessary to reach the desired span.
Whether a straight cable has to be modeled, all these differences vanish.

CHAPTER 6

INTERCONNECTED EQUIPMENT: SENSITIVITY STUDY

6.1 Conductor & Two Flexible Posts

The studies presented in the previous chapter aimed to understand the dynamic behavior of a flexible stranded conductor, and how to obtain a suitable finite-element model furnishing reliable results. This is the first step to understand all the issues related to the dynamic behavior of electrical equipment items interconnected by flexible conductors. All the geometrical as well as the mechanical nonlinearities involved in this kind of problems arise mainly from the cable interconnecting the two equipment items, and not from the two standalone facilities.

As mentioned earlier, the equipment items most common in typical high-voltage electrical substation are mainly characterized by their first natural mode, that has a participant mass about 80%; therefore, they can be considered as a single degree of freedom systems, whose only degree of freedom is the horizontal displacement of the top, where the cable is attached. This means that, during a seismic event, the ground motion doesn't affect directly the cable, but it is filtered by the equipment items that transmit the input to the ends of the cable; therefore, the cable experiences something very similar to a sinusoidal displacement of its ends, which frequency is equal to the first natural frequency of the electrical item it is attached to. This reason suggests to first investigating the response of the cable subjected to harmonic sinusoidal motion of its ends, in order to look insight its dynamic behavior and set an appropriate numerical model. This was the scope of the first experimental tests made by Dastous and the Hydro-Québec Research Institute [4], as well as the analytical investigations carried on by Der Kiureghian [10] and Dastous himself [7].

Other meaningful experimental tests as well as analytical models of seismic response of electrical substation equipment interconnected by flexible conductors have been presented by Filiatrault [12, 13, 14].

The same purpose constitutes the first part of the current study. First, all the issues affecting the cable dynamics have been studied, as well as how to develop a reliable and accurate model for the stranded flexible conductor; this has been presented in the previous chapter. Next, an analytical model is created for new possible experimental tests, in this case involving both the flexible conductor and the interconnected equipment. The interconnected electrical equipment items will be dynamically tested applying either sinusoidal displacements or earthquake simulations at their bases. To do this, they will be installed on shake tables providing the dynamic motions. The dimension and geometry of the configuration are given by two different factors. First, we want to reproduce a typical high-voltage electrical substation configuration, in order to have a meaningful description of the dynamic response of such equipment undergoing an actual earthquake. Next, it is noteworthy that the configuration must match the requirements due to the characteristics of the laboratory facilities that don't allow too big dimension. Nevertheless, it is possible to create and test full-scale specimens, representing typical high-voltage electrical substation equipment items. Since those items are several, it's not possible to reproduce all their combination in interconnected equipment. Therefore, it is decided to use items that have already been tested, and whose dynamic properties are well known. In this way, all the uncertainties regarding the interconnected equipment items are removed, and the study can be focused on the flexible conductor and its influence on the global dynamic response. Once developed a validated model, the two interconnected equipment items can be changed simply varying the characteristics of the equivalent beams representing them.

It is to be noted that two basic configurations are adopted. This is chosen in order to make a broader representation of the possible configurations assumed by the cable, in typical substation. Since the big variety of field conditions, the cables have a range of sag / span ratio that goes from 0 to about 20%, depending on the structural and electrical requirements. Therefore, the only study of a single slackness configuration cannot be fully significant for the rest of the range: it is advisable to investigate the different behavior of the two configurations corresponding to the extreme values of the sag / span ratio. The first adopted configuration presents a straight cable interconnecting the two equipment items. This shape doesn't allow relative displacements between the two attachment points, thus it is expected to produce the more severe conditions on the system for a given ground motion. It is to be noted that this configuration can only be tested with a given acceleration at the bases of the two interconnected items, and not with out-of-phase

applied displacements, since no relative displacements are allowed. Conversely, the second configuration adopted is characterized by a sag / span ratio equal to 19%, that is almost the biggest common value (20%). This value is directly taken from the configuration of the 1796-MCM cable in Dastous' experiments [4]: the same ratio between total length and span is used, turning out into the same slackness ratio.

6.1.1 Tests Setup

As discussed earlier, two electrical equipment items that have already been dynamically tested are adopted as interconnected facilities. In particular, a current transformer and a transformer bushing were available with some already evaluated structural properties, since they have been subjected to seismic qualification. The structural properties of the two equipment modeled (equipment #1 and equipment #2) are inspired to their structural properties. Both the items are not considered in a standalone configuration, but installed with other structural parts representing the common installation that are present in high-voltage electrical substations. It is obvious that, since the equipment items are always installed on other structural parts, they must be tested in such a configuration; otherwise, the dynamic input they are subjected to and their global dynamic properties would be completely misunderstood. Since the study is focused only on the global behavior of the items, in order to understand the dynamic motion of the two attachment points it's not necessary to test the actual specimens for the structures they are mounted on, but it's sufficient to use adequate support structures. These structures must have equivalent dynamic properties so that the global dynamic behaviors of the as-installed equipment #1 and equipment #2 are matched. For this reason, equipment #1 is tested mounted on the top of a circular steel post. Equipment #2 is bolted at about the middle of its height on a steel plate, fixed on the top of a frame structure made of steel beams.

Figure 6-1 shows the actual test setup with the two electrical equipment items interconnected by a straight cable. This configuration is used for the base motion tests. The test setup used for the sine-start tests, considering a slack cable to allow the relative displacement between the two ends, is shown in Figure 6-2.

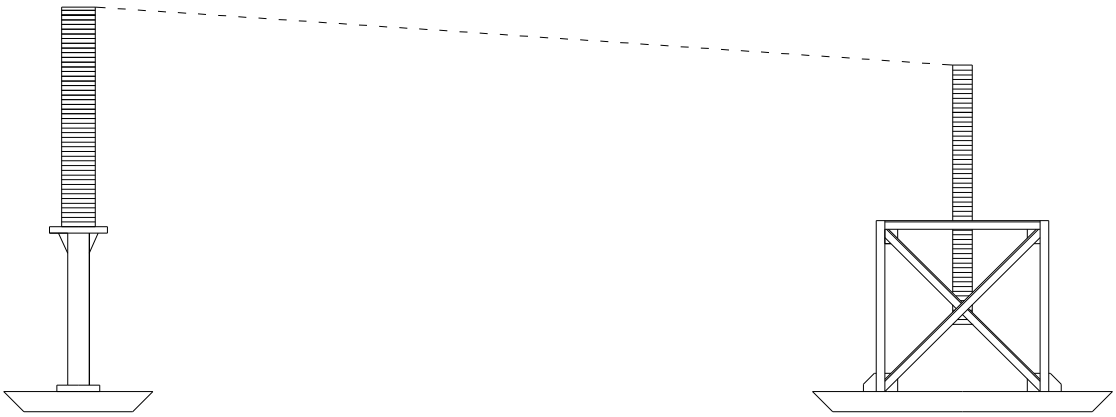

Figure 6-1: Test setup with straight cable

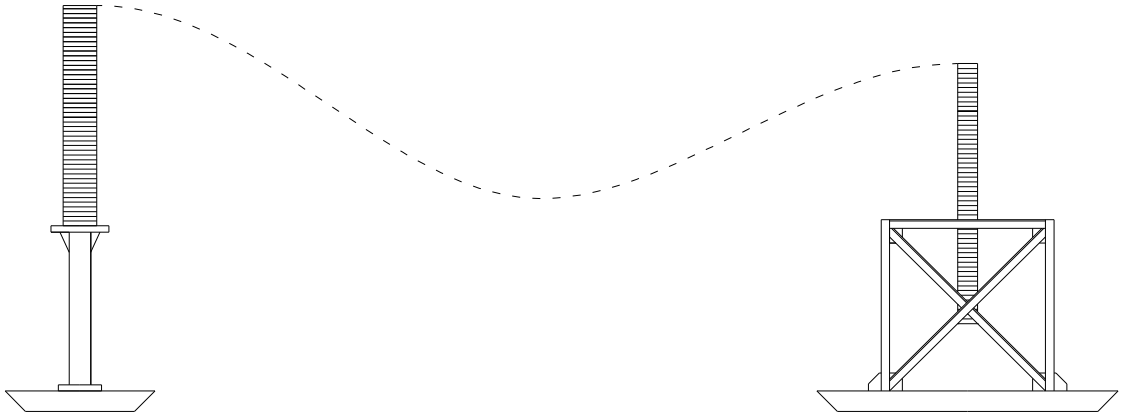

Figure 6-2: Test setup with slack cable

The geometry and the sections of the beams constituting the steel post and the support structure are completely known. The properties known for equipment #1 and equipment #2 are different.

The data available for equipment #1 comes from an impact hammer test, performed for its seismic qualification. In the qualification test, impact hammer tests were run with equipment #1 mounted on a tubular steel post bolted to floor, to determine the as-installed natural frequency. 3 accelerometers were installed at the top, and damping value was determined by curve fitting method. The first as-installed natural frequency of equipment #1 was found to be about 4 Hz,

with a negligible damping: although this structure is a single degree of freedom. Furthermore, the total height of equipment #1, its total weight and the position of its center of gravity are known.

Table 6-1 shows the geometric data for the tubular steel post.

Table 6-1: Equipment #1 Support Geometric Properties

Material	Steel
Total Height (mm)	2438.5
Inside Diameter (mm)	298.5
Outside Diameter (mm)	324

Since the steel post is symmetric, the total mass of 292.5 kg (obtained multiplying the density of steel times the volume of the post) is lumped in the middle of the post, being the center of gravity.

Table 6-2 shows the known data for equipment #1.

Table 6-2: Equipment #1 Geometric Properties

Total Height (mm)	3269
Center of Gravity from below (mm)	838
Total Mass (kg)	630
As-installed Frequency (Hz)	4

For the sake of simplicity, it is decided to model both the steel post and equipment #1 with one single beam each, with equivalent properties. This is consistent with the previous assumption that the total equipment supporting the cable is a single degree of freedom, only allowing horizontal displacement of its top. The geometric data available for the steel post are already sufficient to determine the structural properties of the equivalent beam. This beam, as every other beam in the model, has a Timoshenko linear formulation. Conversely, the equivalent parameters for equipment #1 have to be computed, since the complete geometry and the fixed-base stiffness and frequency are unknown. To do this, two beams have been modeled with a finite-element

program, one on top of the other. The beam below, representing the steel post, has the cross-section and the material of the actual equipment item, while equipment #1 is modeled with the actual height and weight, and iterative attempts for the equivalent rigidity EI are made, trying to match the as-installed frequency. Finally, the equivalent EI to be used is found to be:

$$EI_{CT,equiv} = 1.1e12\ N \cdot mm^2$$

A slightly different choice of modeling the electrical equipment items with two beams is made for equipment #2. Since the actual equipment #2 is bolted on the steel plate at a intermediate point of its height, it consists of two parts, an upper and a lower one. For this reason, it is decided to model it with two separate beams, while the whole frame support structure is modeled with only one. Due to the fact that the frame support structure is known in every single detail, but no data are directly available for the modeling of an equivalent beam, it is necessary to compute them. The final goal of this modeling is an accurate representation of the dynamic behavior of the total equipment, and not of its separated parts. Therefore, equipment #2 has been modeled first, since the data for the equivalent beam are already known from the qualification test, and then the equivalent properties of the support structure have been computed from the as-installed model. The data extracted from the qualification test for equipment #2 are shown in Table 6-3 and Table 6-4, respectively for the upper and the lower part:

Table 6-3: Upper Equipment #2 Properties

Total Height (mm)	2316.5
Center of Gravity from below (mm)	1158
Total Mass (kg)	140
Equivalent Rigidity (Nmm^2)	4.145e11

Table 6-4: Lower Equipment #2 Properties

Total Height (mm)	1511
Center of Gravity from above (mm)	755.5
Total Mass (kg)	91.5
Equivalent Rigidity (Nmm^2)	4.145e11

It is to be noted that the equivalent rigidity has been adopted equal to the mean value of those computed from a static and a dynamic test. As a matter of fact, the qualification test consisted of both a frequency extraction of the fixed-base standalone equipment #2 and a pull test in the same configuration. From the pull test, the translational stiffness for the horizontal displacement of the top of the upper equipment #2 is found to be:

$$K_{ST} = 1.05 \cdot 10^5 \ {}^{N}/_{m}$$

Therefore, the equivalent rigidity is computed considering the upper equipment #2 as a cantilever:

$$EI_{ST} = K_{ST}\frac{H^3}{3} = 1.05 \cdot 10^5 \frac{2.3165^3}{3} = 4.35 \cdot 10^5 \ {}^{N}/_{m^2}$$

From the frequency extraction, the first natural frequency of the fixed-base standalone upper bushing is 8.32 Hz. Considering the upper bushing as a cantilever with the mass lumped in the center of gravity, the computation of the stiffness is a little more complex. First, it's necessary to translate the translational mass lumped in the center of gravity into a rotational mass:

$$m_\theta = m \cdot \left(\frac{H}{2}\right)^2 = 187 \ N \cdot m \cdot s^2$$

Now, the rotational stiffness can be computed:

$$K_{DYN}^{\theta} = m_\theta \cdot \omega^2 = 187 \cdot (2\pi \cdot 8.32)^2 = 5.11 \cdot 10^5 \ N \cdot m$$

Now this rotational stiffness can be translated into the stiffness for the horizontal displacement of the top of equipment #2:

$$K_{DYN} = \frac{K_{DYN}^{\theta}}{H^2} = \frac{5.11 \cdot 10^5}{2.3165^2} = 9.52 \cdot 10^4 \ {}^{N}/_{m}$$

From this translational stiffness, the equivalent rigidity of the cantilever can be computed in the same way used for the static test:

$$EI_{DYN} = K_{DYN}\frac{H^3}{3} = 9.52 \cdot 10^4 \frac{2.3165^3}{3} = 3.94 \cdot 10^5 \ {}^{N}/_{m^2}$$

It is to be noted that the two values differs by 9.2%.

This difference can be addressed to some errors during the measurements. Since we don't know whether the static test or the dynamic test is more accurate, it is decided to adopt a value of equivalent rigidity that is the mean of the two computed values:

$$EI_{BUSH,equiv} = \frac{EI_{ST} + EI_{DYN}}{2} = \frac{4.35 \cdot 10^5 + 3.94 \cdot 10^5}{2} = 4.145 \cdot 10^5 \ N \cdot m^2$$

For the sake of symmetry, the same equivalent rigidity has been used also for the lower part of equipment #2.

No experimental investigations have been conducted on the frame support structure, thus the properties of the equivalent beam are computed from the finite-element model of the detailed structure, with the equivalent equipment #2 installed. The given data to match is the as-installed natural frequency of the system, that is 7.75 Hz. The only unknown is the equivalent rigidity of the frame support structure: its center of gravity, total mass and total height are hand-calculated from its actual geometry. As shown earlier, the two parts of the bushing are completely known. Some frequency extractions are made using the finite-element model, with iterative trial values for the equivalent EI of the frame support structure, until the as-installed frequency is matched. From this analysis, the value of the equivalent stiffness EI is found to be:

$$EI_{SUPP,equiv} = 5.0 \cdot 10^7 \; N \cdot m^2$$

Finally, all the properties of the equivalent beam representing the frame support structure are shown in Table 6-5:

Table 6-5: Frame Support Structure Properties

Total Height (mm)	2515
Center of Gravity from below (mm)	1713
Total Mass (kg)	3848
Equivalent Stiffness (Nmm^2)	5e13

The last part of the system that has to be defined is the flexible conductor interconnecting equipment #1 and equipment #2. For the sake of simplicity, the 1796-MCM cable is adopted, since its properties have already been studied in the previous experimental as well as in the analytical tests. All the properties of the cable are shown in the first column of Table 4-4. One important issue is to define its length, and the distance between the two interconnected equipment items. First, the distance between the two interconnected equipment items is selected basing on the geometry of the shake tables that will be used to run the experimental tests. The two shake tables in the seismic laboratory of the State University of New York at Buffalo don't have a fixed position but are moveable: the holes where they can be fixed have a distance

between each other of 100.5''. Therefore, considering that both equipment #1 and equipment #2 are installed in the center of each shake table, their distance can only be a multiple of 100.5''. In this case, it is decided to choose the multiple 5 of this distance:

$$horizontal\ span = 5 \cdot 100.5'' = 502.5'' = 12763.5\ mm$$

As discussed earlier in the chapter, two different configurations for the cable are adopted. For the base motion test, the cable is assumed to be straight; therefore, its initial horizontal span matches with the horizontal distance between the two interconnected equipment items. It is noteworthy that, since the two attachment points are at different heights, the total length of the cable is not the same as the horizontal span. In this case, the total length of the cable is:

$$l_{TOT} = \sqrt{(5707 - 4831.5)^2 + 12763.5^2} = 12793.5\ mm$$

The finite-element configuration plugged in the program is shown in Figure 6-3.

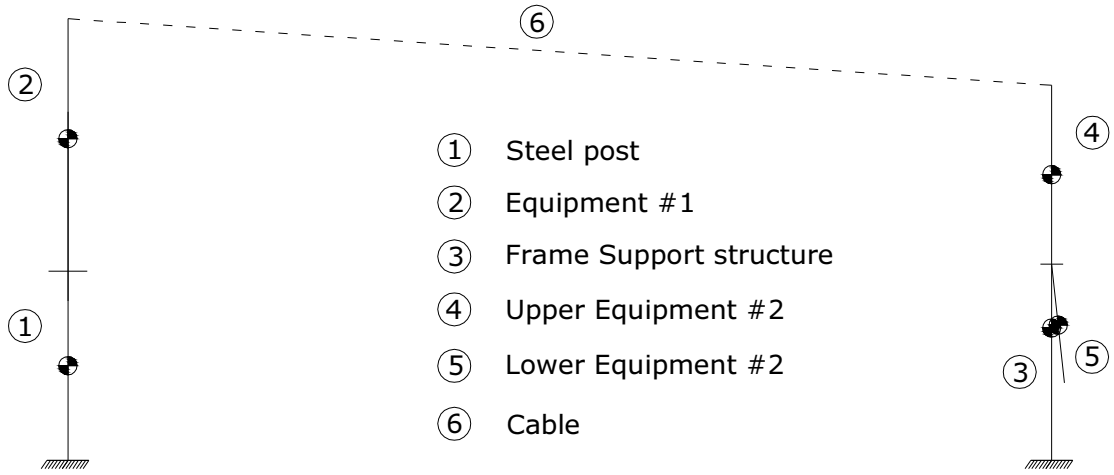

Figure 6-3: Finite-element model with straight cable

For the sine-start test, a slack configuration is mandatory to allow the relative horizontal displacements. To have the maximum allowed sag, the ratio between the initial horizontal span and the desired span is set to be the same as for Dastous' experimental tests on the 1796-MCM cable. In particular, in his previous tests this ratio was:

$$\frac{5520\ mm}{5000\ mm} = 1.104$$

In the current model the desired horizontal span is 12763.5 mm; therefore, the initial horizontal span should be:

$$12763.5 \cdot 1.104 = 14090\ mm$$

For the sake of simplicity, an initial horizontal span of 14.0 m is assumed, and the initial vertical separation between the two ends of the cable is assumed equal to the vertical separation between the two attachment points, so that there's no need to move vertically the two ends of the cable. Then, the initial shape of the cable is computed as discussed in the previous chapter. The finite-element configuration plugged in the program is shown in Figure 6-4.

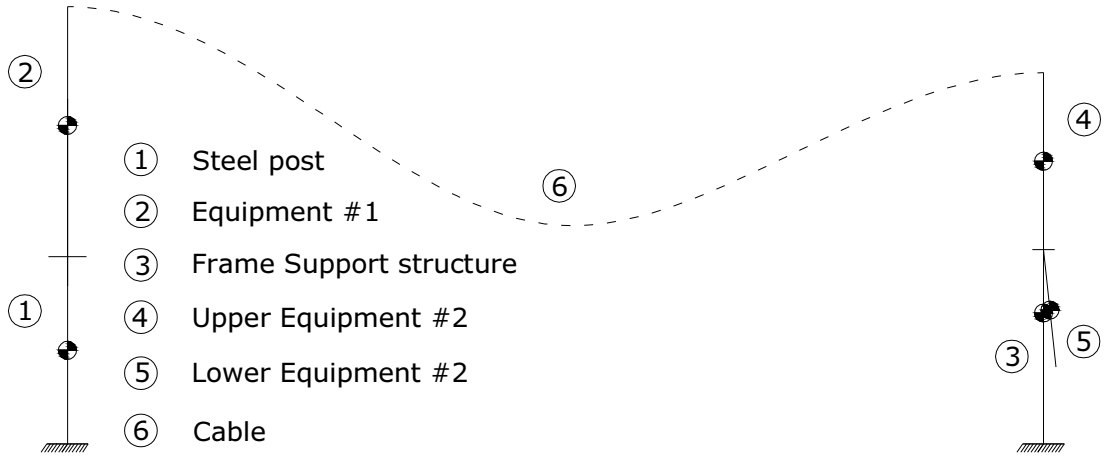

Figure 6-4: Finite-element model with slack cable

For both the models, the cable is clamped at the two ends, and the gravity load is applied as a vertical dead load. In order to have a sufficient refined mesh, it consists of 100 Timoshenko linear formulation elements. The distributed vertical dead load is applied as concentrated load at each node of the cable, with a value equal to:

$$P = \frac{2700 \cdot (9.1 \cdot 10^{-4} \cdot 14.0 \cdot 9.81)}{99} = 3.4\ N$$

After, the two ends are horizontally moved one toward the other, until the desired span is reached. At this point, the deformed shape of the cable is recorded, and then plugged in as initial configuration for the interconnected system, without any internal force. For the geometry of this system, the central sag of the cable in its initial configuration is found to be 2425 mm, corresponding to a sag / span ratio equal to 19%. This value is less than the highest value of the feasible range, assumed to be 20%. In both cases, for the straight as well for the slack cable, the

damping is modeled as lumped dashpots at each node of the cable, proportional to the rotational velocity. The equivalent viscosity of these dashpots is:

$$10 \cdot \frac{14}{100} = 1.4\ N \cdot m \cdot s$$

since the equivalent damping for unit length for the cable 1796-MCM is supposed to be $c_\theta = 10\ N \cdot s$.

For the sake of simplicity, all the dynamic analyses are run in ABAQUS using a constant bending stiffness, equal to the IEEE recommended value. Approximations and limits due to this approach will be discussed separately for the two types of tests. Nevertheless, the static step (applying the vertical dead load) is analyzed also in FEAP, accounting for both constant and variable bending stiffness, and the results are compared. The two loading steps, static and dynamic, and the parameters of the dynamic analyses will be deeply discussed in the next paragraphs.

6.1.2 Static Step

It is to be noted that is particularly interesting to observe the static behavior of the system with the straight cable, when the vertical dead load is applied. As a matter of fact, the difference between the slack cable with either constant or variable bending stiffness have already been fully developed in the previous chapter. It is known that the main differences belong to the static displacement of the two ends of the cable, when the constant stiffness provides a highly overestimated value for the flexural stiffness; therefore, the internal forces in the cable results to be unrealistically high. Conversely, the application of the vertical dead load on the already deformed cable doesn't generate big differences both in displacements and internal forces.

As shown in the previous chapter, the use of the either variable or constant ending stiffness, together with either Der Kiureghian's or Dastous' model respectively, turns out into a shift of the time-histories curves of the horizontal reactions. This is not directly due to the bending stiffness considered, but it comes from the removal of the internal forces after the static displacement of the two cable ends in Der Kiureghian's model, made before applying the vertical dead load. In such a way, this model lacks the compression forces that are present in Dastous' model. Since this compression can generate also a shift in the natural frequencies, this is the biggest limit of Der Kiureghian's approach, despite its major simplicity. Conversely, the straight cable doesn't

need any initial static displacement of its ends; therefore, Der Kiureghian's and Dastous' model completely match, and no comparison between them makes sense. For the sake of completeness, it is only to be seen the influence of the type of flexural stiffness considered on the static solution. It is noteworthy that its influence on the dynamic solution has already been deeply discussed for the slack cable. The results obtained can be extended also to the initially straight cable, since after the application of the dead load it assumes a deformed shape; therefore, it has a certain sag, even if small, and it can be considered as a slack cable. For this reason, no more dynamic comparison between the variable and constant flexural stiffness are needed.

A comparison between the different results obtained with ABAQUS, considering a constant bending stiffness, and with FEAP, considering both a variable and a constant bending stiffness, are presented. For the two models with constant bending stiffness, one run with ABAQUS and the other with FEAP, the only difference is the default tolerance used by the programs to reach the solution at each step with the Newton-Raphson method. In each model, the vertical dead load is linearly increasing applied in 2000 steps, considered as an equivalent total time period of 1 s. The results for the obtained displacements and the reaction forces are presented separately. Figure 6-5 presents the relative displacements between the two ends of the cable, that are the two attachment points.

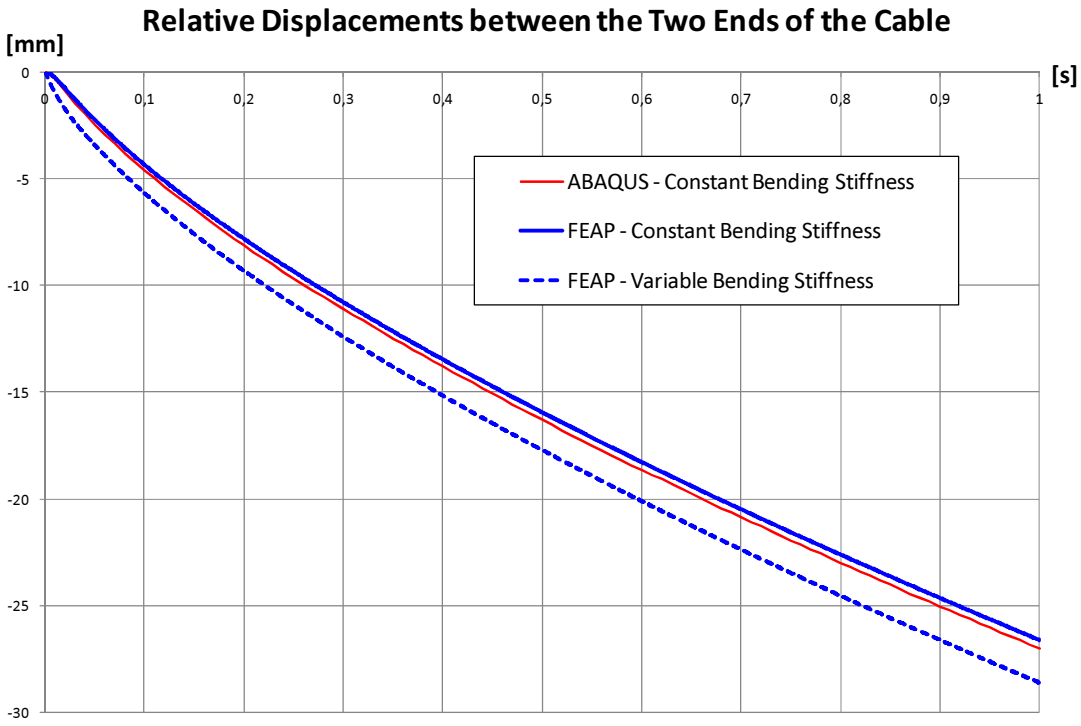

Figure 6-5: Relative displacements between the two ends of the straight cable under gravity load

It is seen that, obviously, under its own weight the cable deflects and try to close the horizontal span; therefore, the relative displacement is negative, because the tops of the two equipment items are moving one toward the other. ABAQUS and FEAP models with the same constant bending stiffness provide very similar results, without significant differences. The model accounting for variable bending stiffness shows bigger relative displacements. This is consistent with the fact that this cable is less stiff than the other, thus under the same forces turns out into bigger deformations. The same observation can be made for the vertical displacement of the middle point of the cable, shown in Figure 9-5. For short, this and the following figures for the same static step are presented in the Appendixes. Similar comparisons are made for the horizontal reaction forces at the base of equipment #1 support and of equipment #2 support. They are respectively shown in Figure 9-6 and Figure 9-7. It is to be noted that the positive values are assumed acting from the left to the right.

These results confirm what is observed for the displacements. The two models with constant bending stiffness don't show meaningful differences between them. The model accounting for

variable bending stiffness presents bigger reaction forces, coming from bigger displacements at the top of each equipment, due to the smaller stiffness of the cable. Therefore, considering constant bending stiffness can slightly underestimate the internal forces in the two equipment items. Nevertheless, the difference between the horizontal reactions obtained with the two different approaches is found to be less than 8%.

6.1.3 Sine-Start Tests

Four different sine-start tests are modeled, with different sinusoidal input and the same configuration of the system. The cable interconnecting the two electrical equipment items is assumed slack, without any internal force, and its original shape is computed as described in the previous paragraphs. The four harmonic inputs at the bases of the two equipment items are sinusoidal displacement with a loading ramp, to avoid likely instability due to non-zero initial conditions. Their formula is:

$$u(t) = [1 - e^{-2\pi \cdot 0.1 \cdot f \cdot t}] \cdot A \cdot sin(2\pi \cdot f \cdot t)$$

Given amplitude and frequency for each input are summarized in Table 6-6:

Table 6-6: Amplitudes and Frequencies of the Inputs

	Amplitude (mm)	Frequency (Hz)
Sine-Start Test #1	100	0.25
Sine-Start Test #2	100	0.84
Sine-Start Test #3	100	4.00
Sine-Start Test #4	100	7.75

The 4 frequencies have been specifically chosen, in order to test the specimens under the most severe conditions. Two frequencies, 4 Hz and 7.75 Hz, respectively correspond to the first natural frequencies of the two equipment items in the as-installed configuration; therefore, each of these motions is supposed to cause resonance in one of the two interconnected facilities. The other two frequencies correspond respectively to the first and second natural frequencies of the cable itself. These frequencies have been computed for the slack cable, in its already deflected shape without internal forces, and with a constant bending stiffness equal to the IEEE

recommended value. Since the harmonic displacements are applied out-of-phase at the bases of equipment #1 and of equipment #2, the boundary conditions used to calculate the natural frequencies of the cable are two rollers at the two ends of the cable. As a matter of fact, the two ends must be allowed to move in the horizontal direction, but must be restrained for vertical displacement and rotations. To avoid the singularity of the system, one additional horizontal restraint must be introduced: for the sake of symmetry, it is placed in the middle node of the cable. It is to be noted that these two last frequencies are not supposed to generate a resonance in the interconnected system, for two main reasons. First, due to the geometric nonlinearity, the natural frequencies of the cable vary with the motion of the cable; therefore, there are no fixed natural frequencies, but it's only possible to speak about frequencies likely to be excited. Next, since the harmonic displacements are applied at the bases of the two equipment items, the motion felt by the cable is the motion of the two attachment points, that is filtered by the two equivalent cantilever beams. Therefore, the motion of the two ends of the cable will have a frequency content more similar to the natural frequencies of the two interconnected equipment items than to the frequency content of the ground motion. Every test is analyzed with a recommended time step of 0.005 s, and a half-step residual tolerance of 1e4 N. The results are found to be stable for the first two sine-start test, since this requirement of residual tolerance never involves reducing the time step size. For sine-start test #3 and #4, the stability of the solution obtained can be validated only checking the results with the user's experience. The total time period is different for each test; it's not possible to use a same suitable period, since the lower frequencies require more time to get a steady response, due to the form of the loading ramp. The lower is the frequency, the longer is the total time period. Furthermore, the two tests with the higher frequencies must be stopped after a little time, since the resonance generates always increasing forces and displacements that are too difficult to be computed by the program.

The sine-start test #1 has a time period of 27 s; from 0 to 1 s the vertical dead load is applied, then the displacement input is applied out-of-phase at the two bases. Figure 6-6 shows the displacements experienced by the cable.

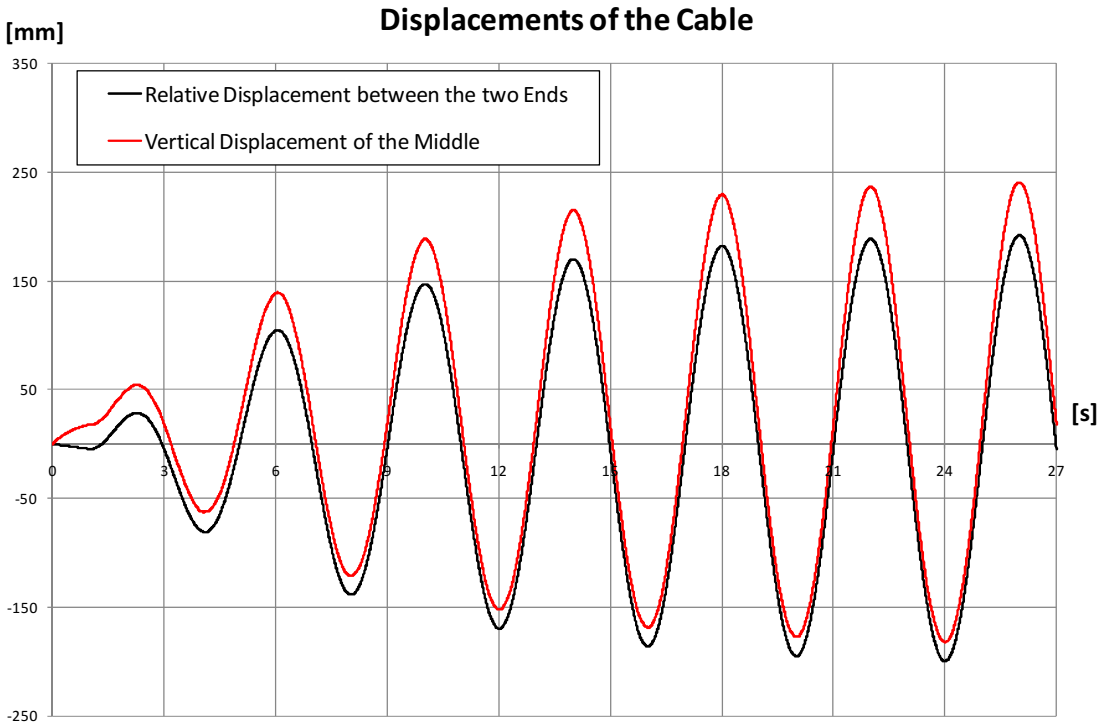

Figure 6-6: Sine-start test #1, displacement of the cable

Some observations can be made. Since the amplitude of the displacement input is equal to 100 mm and is applied out-of-phase at the two bases, the relative displacement between the two bases of the equipment items has amplitude of 200 mm. Looking at the relative displacement between the two attachment points (the black curve in the graph), it has an amplitude about 200 mm. This means that the two cantilever beams are subjected to relatively small deformations; therefore, they are not amplifying the motion they are subjected at their bases. The vertical displacement of the middle of the cable shows that, due to the slackness ratio and the vertical separation between the two attachment points, they can be even more significant than the horizontal ones. This will explain the presence of vertical forces in the system, even if the displacement input is only in the horizontal direction. Figure 6-7 presents the horizontal reactions computed at the bases of the two equipment items.

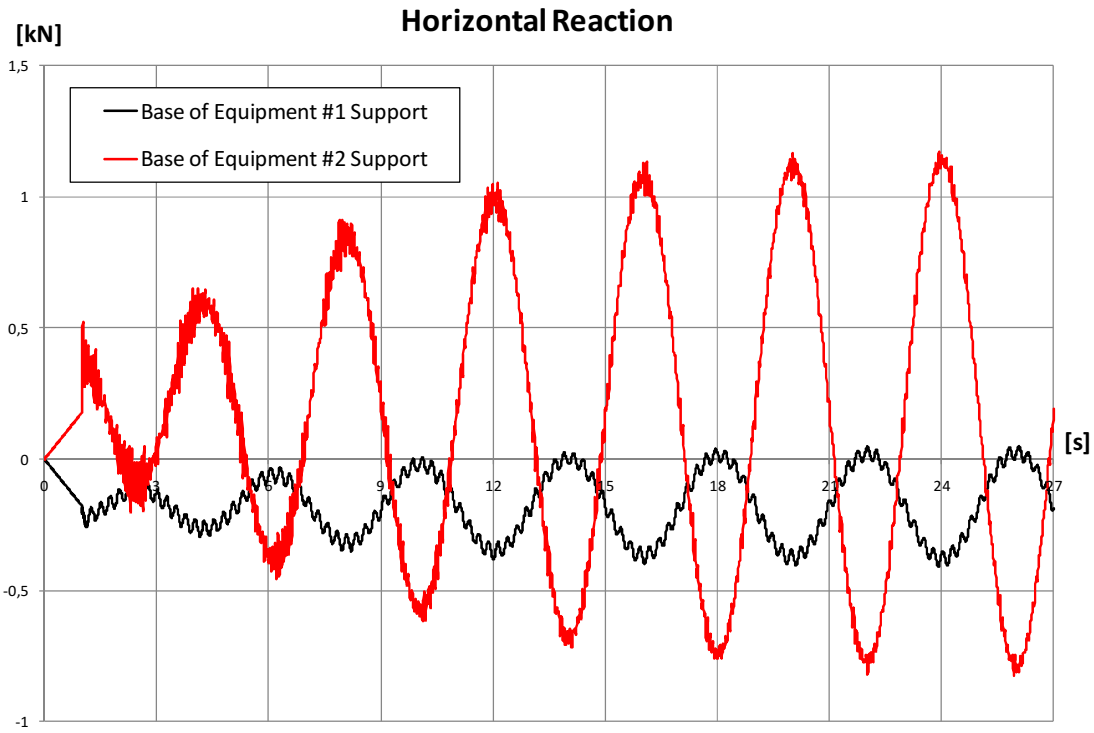

Figure 6-7: Sine-start test #1, horizontal reactions

It is noted that the base of the frame support of equipment #2 is subjected to stronger forces, that reach a maximum value of 1.17 kN pulling the top in the inside direction. This value is significantly bigger than the horizontal reaction measured under the gravity load of the cable, that is found to be 0.176 kN. The maximum value of the horizontal reaction is approximately 6.5 times the static force for the support structure of equipment #2. For the support of equipment #1, the maximum value of the absolute reaction is 0.41 kN, while the static value is again 0.176 kN (to respect the global equilibrium in the horizontal direction). This means that the maximum value of the horizontal reaction is approximately 2.3 times the static force for the support structure of equipment #1. Figure 6-8 shows the shear forces at the top of the two interconnected equipment items; the same forces, for the sake of equilibrium, are those applied at the two ends of the cable. In particular, the positive values correspond to traction in the cable.

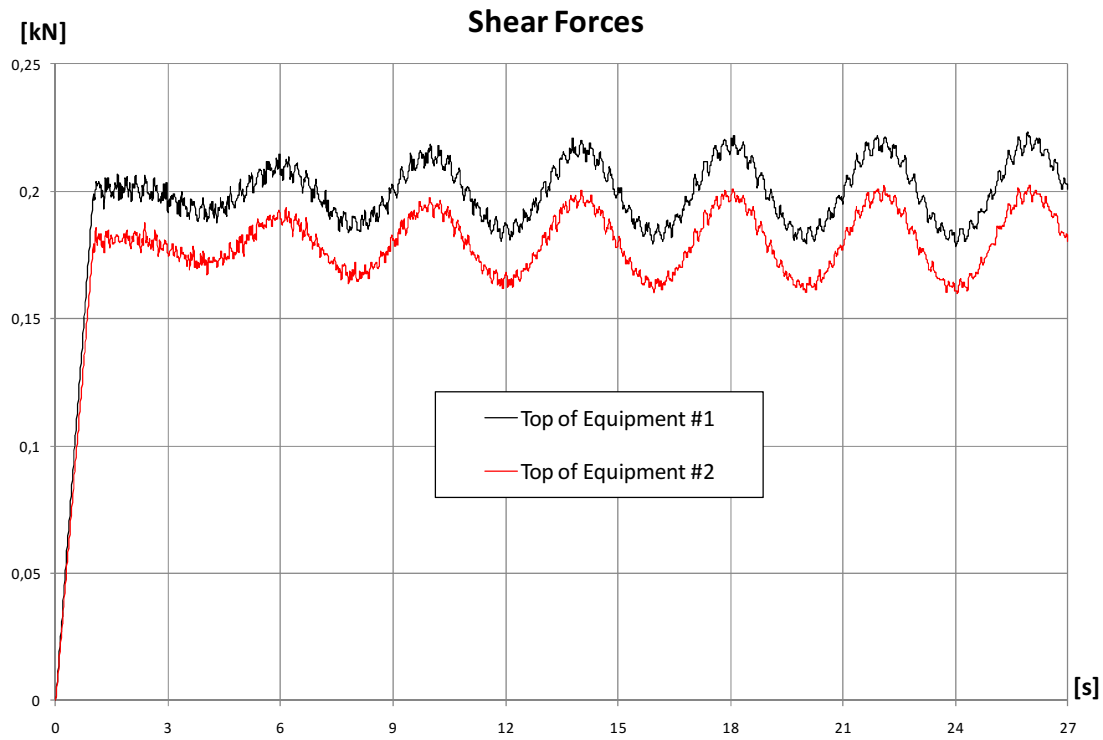

Figure 6-8: Sine-start test #1, shear forces

It's easy to explain why the difference between equipment #1 and equipment #2 for the shear forces at the top are less than for those at their bases. As a matter of fact, the acceleration inputs are the same for both, but they own very different masses. Therefore, since the support structure of equipment #2 has a much bigger mass and the same acceleration input, it is subjected to bigger shear forces, that are additional to those due to the attached cable. Conversely, it is correct that the shear forces at the two attachment points, since come directly from the motion of the cable, are more similar. Figure 6-9 shows the vertical reactions measured at the bases of the two equipment items.

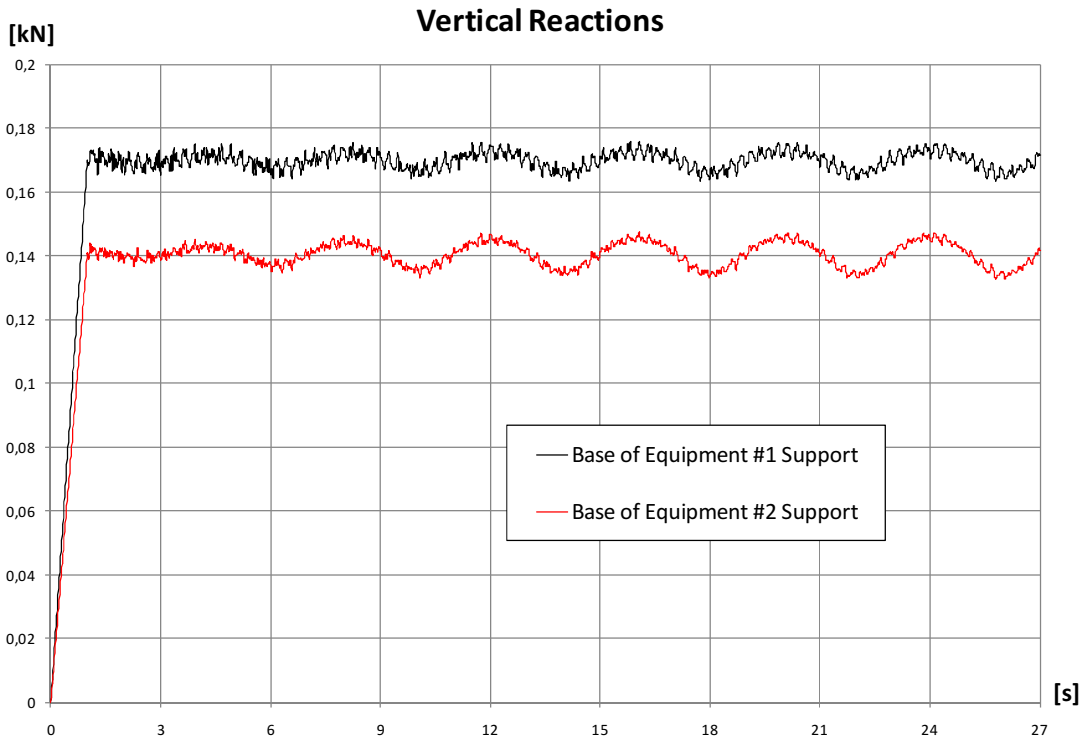

Figure 6-9: Sine-start test #1, vertical reactions

In this case, the oscillations due to the dynamic behavior are relatively small, compared to the static value descending from the gravity load of the cable. It is to be noted that these reactions neglect the gravity loads of the equipment items themselves, but take into account only the influence of the cable. This is decided since there is no vertical component of the ground motion, thus the gravity load generated by the masses of the items is a constant term through all the analysis that would only shift the two curves. Since equipment #1 and equipment #2 don't have any vertical motion, these values are not meaningful for the dynamic analysis. Only the vertical loads due to the presence of the cable are significant, to study the effects of the interaction. The bigger vertical reaction for the static load is for equipment #1, since it is the higher of the two. In this case, the dynamic input just causes amplification of these reactions about 3.5%. It is noteworthy that, neglecting the gravity loads of the two equipment items, the vertical reactions match the internal axial forces in them, since the ground motion has no vertical component. Figure 6-10 presents the moment reaction for equipment # and equipment #2.

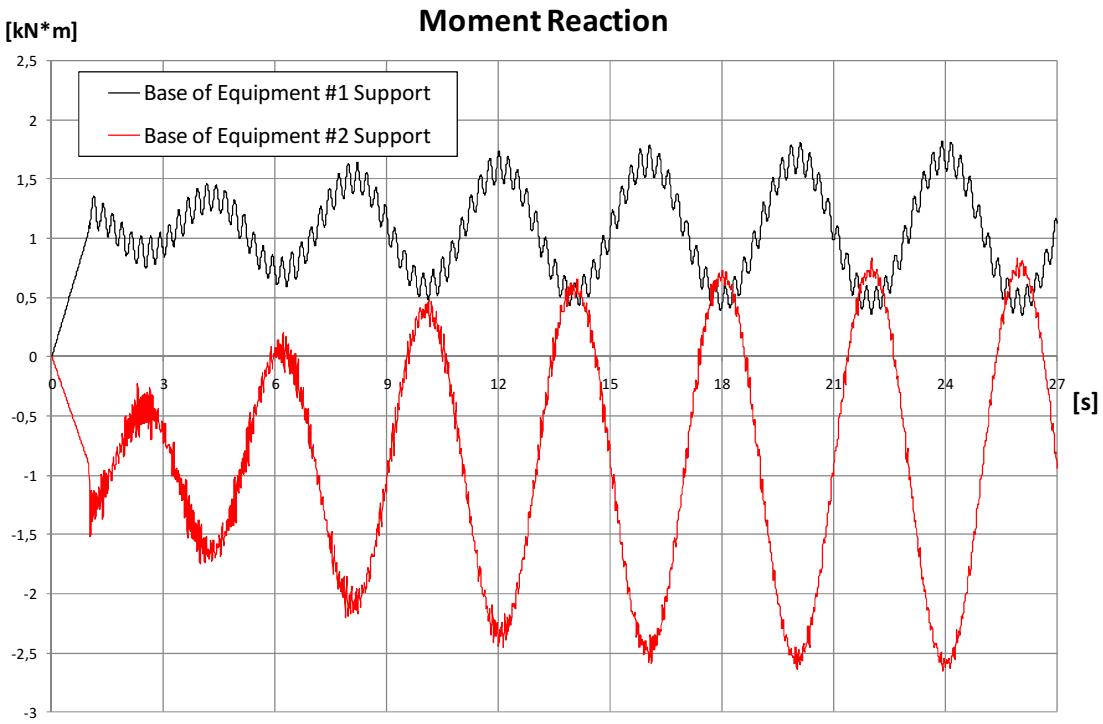

Figure 6-10: Sine-start test #1, moment reactions

The results show the same behavior observed for the horizontal reactions. In this case, the harmonic displacements cause an amplification of 2.9 times the static reaction for equipment #2, and about 1.65 times for equipment #1. The last interesting results are the internal moment at the attachment points, showed in Figure 6-11.

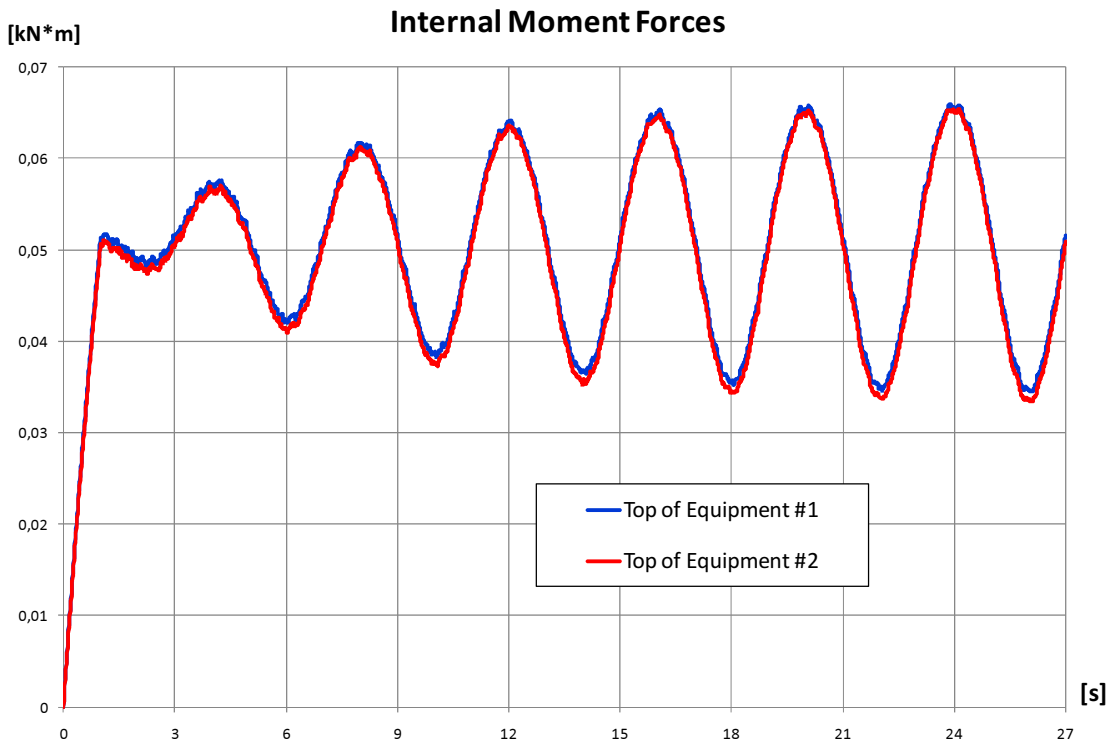

Figure 6-11: Sine-start test #1, internal moment

These moments are due to the connection between the cable and the two equipment items, that is clamped and not a pin, and to the flexural stiffness of the cable; therefore, some internal moments are transferred from the cable to equipment #1 and equipment #2, and vice versa. These moments are non negligible, even if they are about 1/20 than those at the bases, after the static loading. For these moments, the dynamic amplification is about 1.3 times the static values, for both the equipment items.

The same comparisons are presented for the other three sine-start tests. The sine-start test #2, with a given frequency equal to the second natural frequency of the cable itself, has a time period of 11 s; from 0 to 1 s the vertical dead load is applied, then the displacement input is applied out-of-phase at the two bases. For short, all the figures regarding the sine-start test #2 are presented in the Appendixes. Figure 9-8 shows the displacements experienced by the cable. For this input too, since the amplitude of the displacement input is equal to 100 mm and is applied out-of-phase at the two bases, the relative displacement between the two bases of the equipment items has amplitude of 200 mm. Looking at the relative displacement between the two attachment points

(the black curve in the graph), it has an amplitude equal to about 200 mm. This means that the two cantilever beams are subjected again to relatively small deformations; therefore, they are not strongly amplifying the motion they are subjected at their bases. The vertical displacements of the middle of the cable show that they can be are similar to the horizontal ones; as well as for the previous sine-start test, the cable is not subjected to large vertical motion. This can be confirmed by comparing the maximum dynamic vertical motion of the middle of the cable, about 280 mm, with the initial sag for the same node, that is about 2425 mm. It means that the central sag just slightly changes during the ground motion by +/- 11%. Figure 9-9 presents the horizontal reactions computed at the bases of the two equipment items. For this input too, it is noted that the base of the frame support of equipment #2 is subjected to stronger forces, that reach a maximum value of 12.34 kN pulling the top in the inside direction. This value is very significantly bigger than the horizontal reaction measured under the gravity load of the cable, found to be 0.176 kN. Since the frequency of the applied displacement is bigger than that of the previous sine-start test and the amplitude is the same, the acceleration input (the second time derivative) is much larger. In this case, the maximum value of the horizontal reaction is approximately 70 times the static force for the support structure of equipment #2. For the support of equipment #1, the maximum value of the absolute reaction is 3.27 kN, while the static value is again 0.176 kN (to respect the global equilibrium in the horizontal direction). This means that the maximum value of the horizontal reaction is approximately 18.6 times the static force for the support structure of equipment #1. Figure 9-10 shows the shear forces at the top of the two interconnected equipment items; the same forces, for the sake of equilibrium, are those applied at the two ends of the cable. In particular, the positive values correspond to traction in the cable. As discussed for the previous sine-start test, it is correct that the shear forces at the two attachment points, since come directly from the motion of the cable, are more similar, while the horizontal reactions at the bases are different from each other and are times bigger. It is to be noted that the traction in the cable doesn't experience as big dynamic amplification as the horizontal reactions at the bases of the two equipment items. Figure 9-11 shows the vertical reactions measured at the bases of the two equipment items. In this case, the oscillations due to the dynamic behavior are not so small as for the previous test, compared to the static value descending from the gravity load of the cable. It is to be noted again that these reactions neglect the gravity loads of the equipment items themselves, but take into account only the influence of the cable, for the same reason discussed

earlier. The bigger vertical reaction for the static load is that of equipment #1, since it is the higher of the two. In this case, the dynamic input causes an amplification of these reactions up to 1.47 times the static ones. It is noteworthy that, neglecting the gravity loads of the two equipment items, the vertical reactions match with the internal axial forces in them, since the ground motion has no vertical component. Figure 9-12 presents the moment reaction for equipment #1 and equipment #2. The results shows the same behavior observed for the horizontal reactions: the reactions at the base of equipment #2 support are about twice those at the base of equipment #1 support. In this case, the harmonic displacements cause an amplification of 24.9 times the static reaction for equipment #2, and about 10.8 times for equipment #1. The last interesting results are the internal moment at the attachment points, showed in Figure 9-13. These moments are non negligible, even if they are about 1/285 than those at the bases, after the static loading. As a matter of fact, while the moment reactions at the bases of equipment # and of equipment #2 can increase significantly according to the acceleration input, the internal moments in the cable have smaller variations, since its flexural stiffness is much smaller. For these moments, as well as for the previous sine-start test, the dynamic amplification is about 1.3 times the static values, for both the equipment items.

Next, the results for the sine-start test #3 are presented. This test has a given frequency of the applied displacements equal to the natural frequency of equipment #1 in the as-installed configuration. Whether applied to the standalone equipment #1 installed on the top of the steel post, it generates resonance; therefore, it is supposed to cause large amplification of the response. This sine-start test #3 was supposed to have a time period of 5 s, but the analysis is aborted by the program after about 2.13 s, due to too big forces and displacements, that don't allow finding an equilibrium position solution for the end of the time step. Nevertheless, some interesting observations can be made. As usual, from 0 to 1 s the vertical dead load is applied, and then the displacement input is applied out-of-phase at the two bases. Figure 6-12 shows the displacements experienced by the cable.

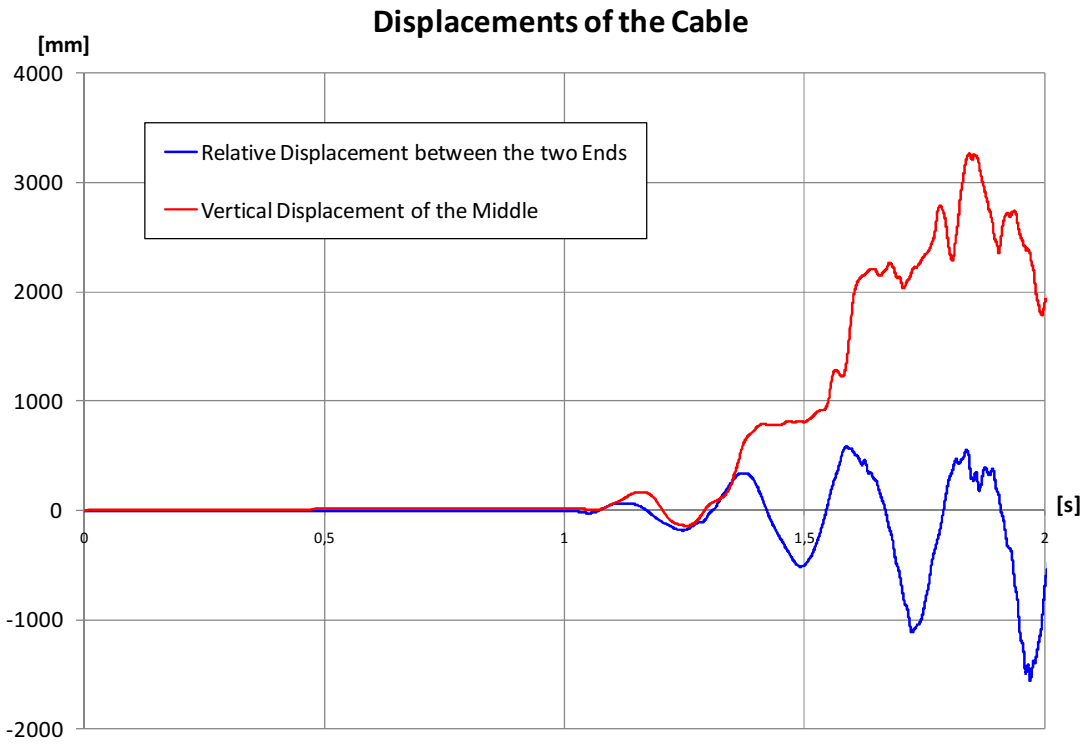

Figure 6-12: Sine-start test #3, displacement of the cable

In this case, the relative displacement between the attachment points is completely different from that between the two bases. This means that equipment #1 is experiencing an excitation close to its resonance, even if it's not a perfect resonance, since the attached cable at its top slightly changes its behavior. The top of equipment #1 is subject to very large displacements that are translated to motion of the cable, and from it to displacement at the top of equipment #2. The big motion experienced by the cable can be observed also from the vertical displacement of the middle. In this case, the peak of the displacement is about 3200 mm; it is even bigger than the initial sag, causing a motion of the cable above the straight line connecting the two attachment points. It means that the central sag changes during the ground motion by 132%. About the relative displacement between the two ends of the cable, they close their position by 1500 mm, that is 7.5 the maximum relative displacement between the bases of the two equipment items (200 mm). Figure 6-13 presents the horizontal reactions computed at the bases of the two equipment items.

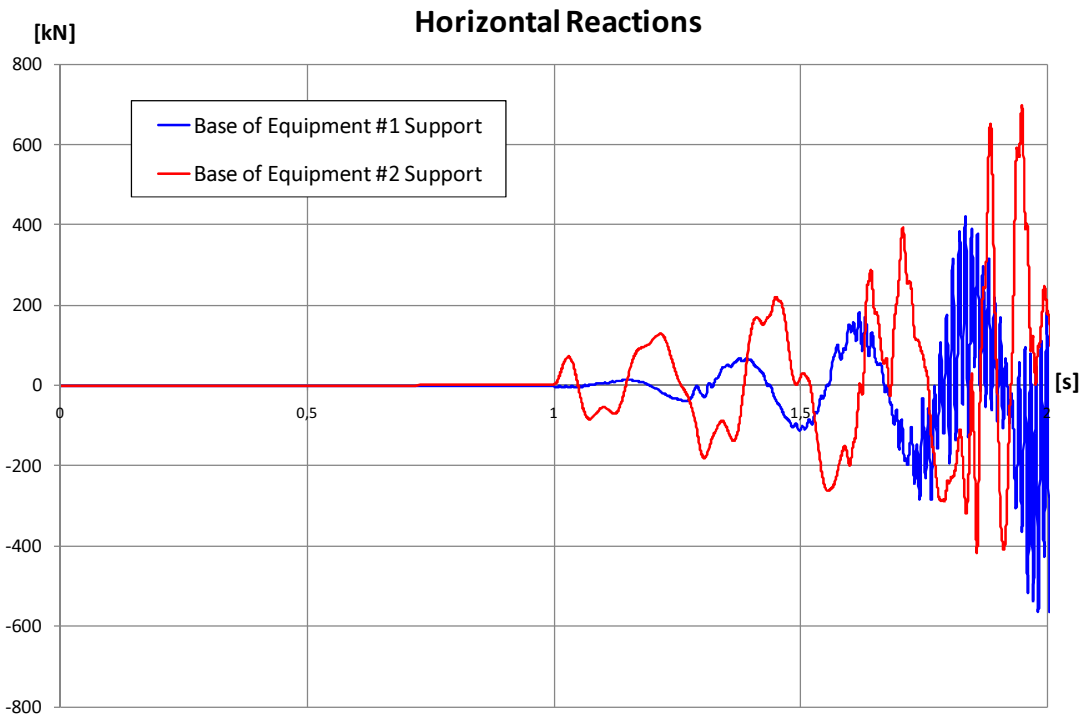

Figure 6-13: Sine-start test #3, horizontal reactions

For this input, it is to be noted that the base of the frame support and of equipment #2 are subjected to similar forces, that reach a maximum value of about 700 kN for equipment #2 and about 600 kN for equipment #1, both pulling the top in the inside direction. This is because equipment #1 is close to resonance, thus its internal forces are increasing. These values are completely from the horizontal reaction measured under the gravity load of the cable, that is found to be 0.176 kN. This can be addressed to two main reasons. First, since the frequency of the input is 4 Hz, the acceleration input is bigger than for the previous test, and thus the forces are bigger. Furthermore, one of the two equipment items is excited close to resonance. In this case, the maximum value of the horizontal reaction is approximately 4000 times the static force for the support structure of equipment #2. For the support of equipment #1, the maximum value of the horizontal reaction is approximately 3400 times the static force. Figure 6-14 shows the shear forces at the top of the two interconnected equipment items; the same forces, for the sake of equilibrium, are those applied at the two ends of the cable. In particular, the positive values correspond to traction in the cable.

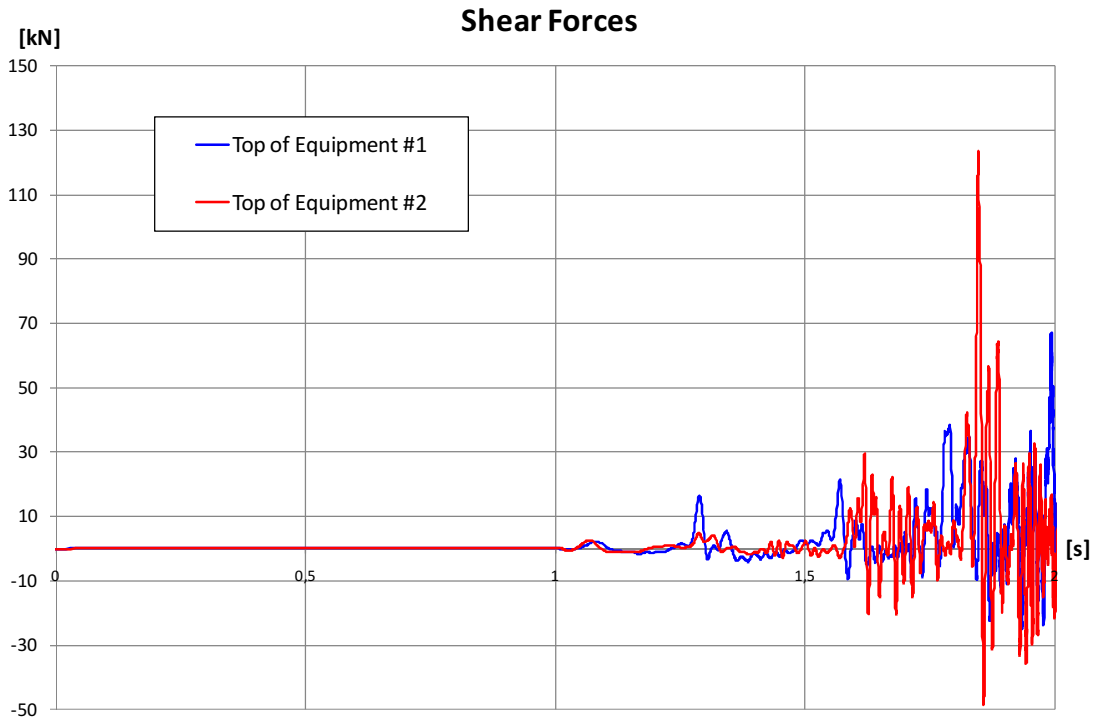

Figure 6-14: Sine-start test #3, shear forces

In this case, it is to be noted that the traction in the cable experiences very big dynamic amplification too, since its ends are subjected to very large displacements. As expected, the force at the top of equipment #1 is much bigger than the force at the top of equipment #2; this is because it is close to resonance, and has very large top displacements, that turn out into big horizontal forces, due to the inertia of the cable. Figure 6-15 shows the vertical reactions measured at the bases of the two equipment items.

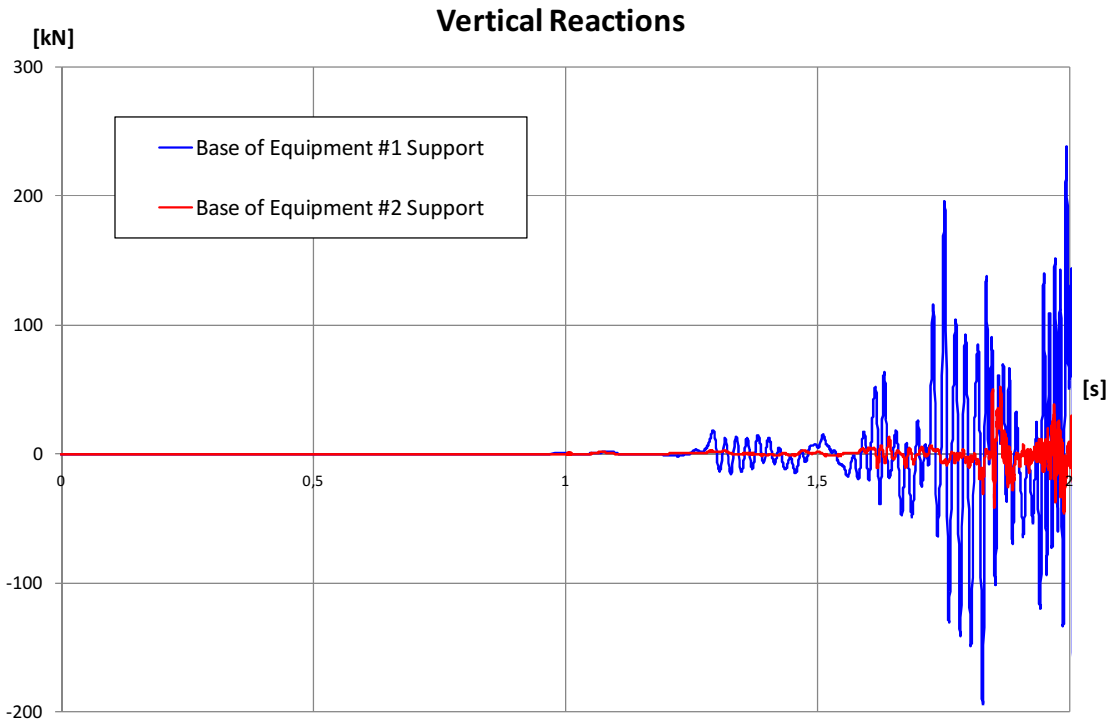

Figure 6-15: Sine-start test #3, vertical reactions

In this case, equipment #1 is subjected to strong vertical forces, due to the vertical motion of the cable, caused by the slackness and the vertical separation between the two ends. As for the previous test results, these reactions neglect the gravity loads of the equipment items themselves, but take into account only the influence of the cable, for the same reason discussed earlier. The dynamic input causes an amplification of these reactions up to 2000 times the static ones for equipment #1 that is the most severely tested. It is noteworthy that all these vertical forces are generated only by a horizontal ground motion; therefore, whether the earthquake has also a vertical component, these forces can be even bigger. In absence of any vertical motion, they are found to be smaller than the horizontal ones. Furthermore, they generate axial forces, and moments at the bases only through the geometric nonlinearity, while the horizontal forces directly generate moments and shear, that are more dangerous for the equipment items. Nevertheless, as just mentioned, the vertical forces can be very significant considering a vertical component of the ground motion; as a matter of fact, they reach meaningful values also in absence of any external force in their direction. Figure 6-16 presents the moment reaction for equipment #1 and equipment #2.

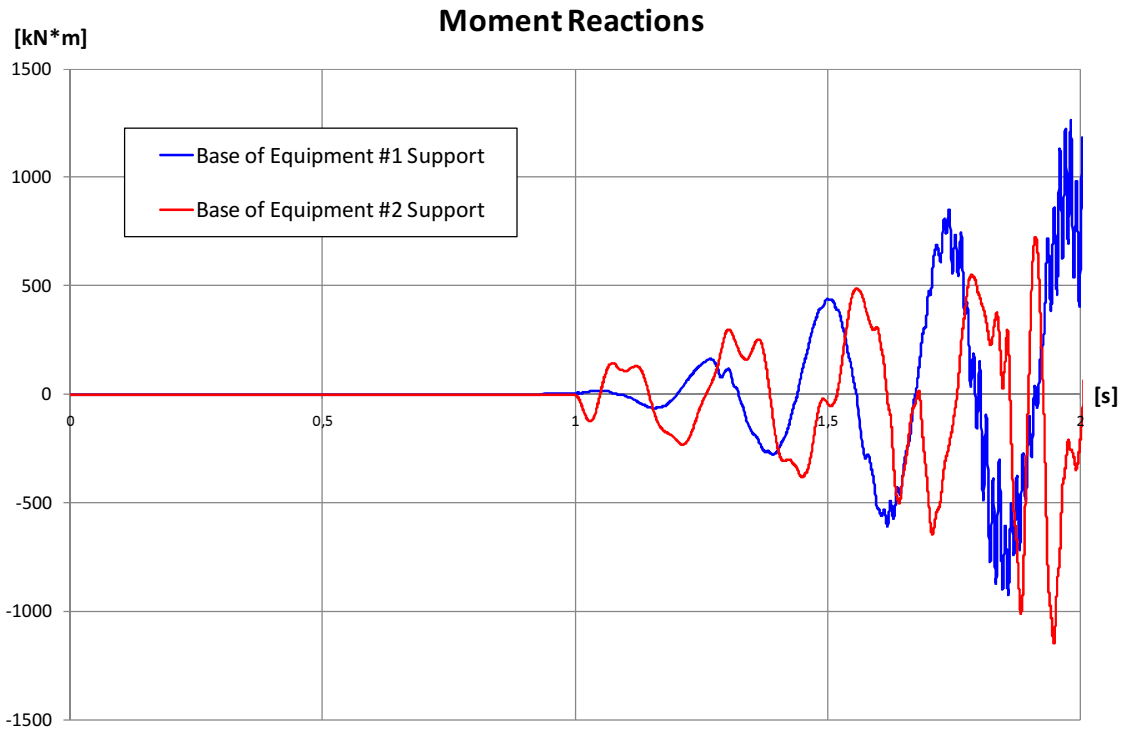

Figure 6-16: Sine-start test #3, moment reactions

The results show the same behavior observed earlier: the reactions at the base of equipment #1 support are slightly bigger than those at the base of equipment #2 support. In this case, the harmonic displacements cause an amplification of 1250 times the static reaction for equipment #2, and about 1200 times for equipment #1. As well as in the horizontal reactions, the response of equipment #1 clearly shows a harmonic behavior, with the same frequency of the displacement input: this confirms that this given frequency matches the first natural frequency of the equipment item. The last interesting results are the internal moment at the attachment points, showed in Figure 6-17.

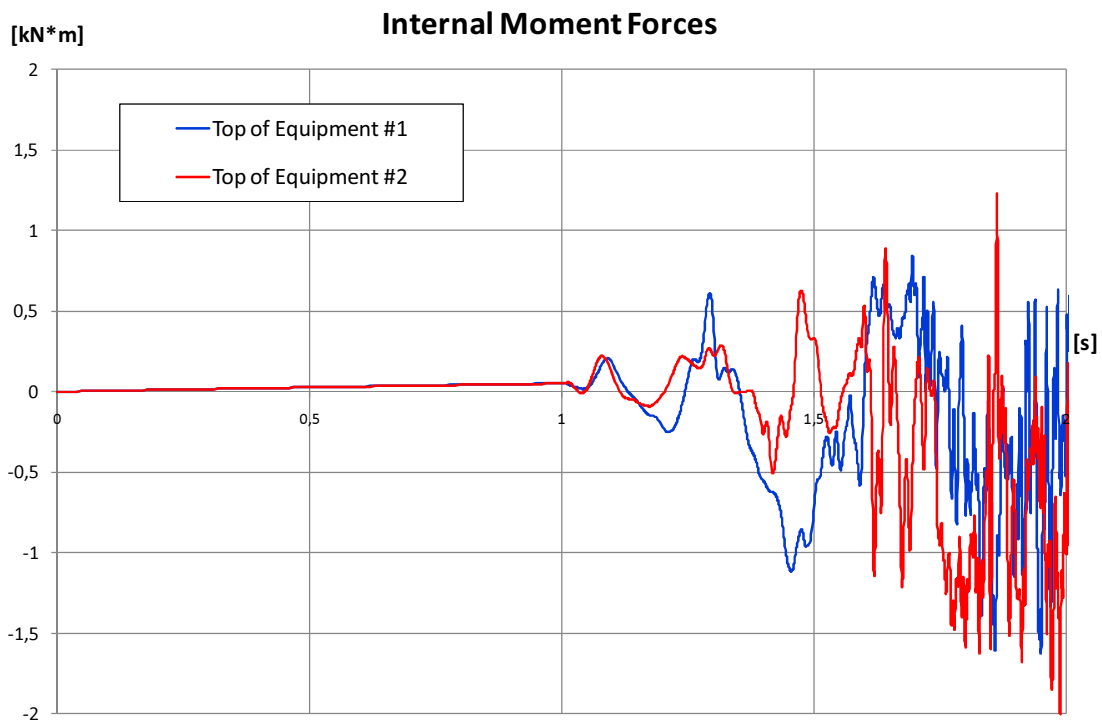

Figure 6-17: Sine-start test #3, internal moment

This time the internal moments are much smaller than the moment reactions: as discussed before, the internal moments depend on the flexural stiffness of the cable, that is quite low, thus can't increase as fast as the reactions do. Therefore, when one of the equipment items is close to resonance, these internal moments are less important. Nevertheless, they are bigger than for the previous tests, and the dynamic amplification is more than about 1.3 times the static values, for both the equipment items: in particular, it is close to 35 times.

The last presented sine-start test is #4: the fixed frequency of the displacement input is equal to the first natural frequency of equipment #2 in the as-installed configuration. This test, whether applied to the standalone equipment #2 installed on the top of the frame support structure, generates resonance; therefore, it is supposed to cause large amplification of the response of the total system. This analysis was supposed to have a time period of 5 s, but the analysis is aborted by the program after about 1.4 s, due to too big forces and displacements, that don't allow finding an equilibrium position solution for the end of the time step. In this case, it's a little more difficult to make some interesting observations, since the dynamic analysis is limited to 0.4 s,

when the displacement input has just made 4 cycles and is still in the loading ramp, thus the final amplitude is not reached yet. As a matter of fact, from 0 to 1 s the vertical dead load is applied, and only after that the displacement input is applied out-of-phase at the two bases. For short, all the figures regarding this sine-start test are presented in the Appendixes. Figure 9-14 shows the displacements experienced by the cable. The behavior is very similar to that observed for the sine-start test #3: the relative displacement between the attachment points is completely different from that between the two bases. This confirms that equipment #2 experiences an excitation close to its resonance; the only difference from resonance in its behavior is due to the restraint provided by the presence of the cable attached at its top. In this case the very large displacements at the top of equipment #2 are translated to motion of the cable, and from it to displacement at the top of equipment #1. The vertical displacement of the middle of the cable shows the big motion it experiences. The peak of the displacement is about 3600 mm; this value is even bigger than that for the resonance of equipment #1, and it is bigger than the initial sag. This causes a motion of the cable above the straight line connecting the two attachment points. The central sag changes during the ground motion by about 150%. It is to be noted that the range of frequencies of the cable likely to be excited during the motion is very large, since the geometry of the cable undergoes very big changes. In some instants, the sag of the cable is flipped from the initial one. The maximum relative displacement between the two ends of the cable is about 1200 mm, that is 6 times the maximum relative displacement between the bases of the two equipment items (200 mm). This value is smaller than for the sine-start test #3: this is because the installed equipment #2 is stiffer than equipment #1, thus its top displacement in resonance are smaller than the top displacement of equipment #1 in resonance. Figure 9-15 presents the horizontal reactions measured at the bases of the two equipment items. It is clear that equipment #2 (the red curve) is in resonance, because the reaction at its base has a harmonic shape, with very big amplitude and a frequency equal to the input one. Conversely, the reaction at the base of equipment #1 has different frequency content, since it is a combination of the ground motion and the forces at the attachment point transmitted by the cable. In this case, the maximum value of the horizontal reaction is approximately 8000 times the static force for the support structure of equipment #2, and twice those obtained when equipment #1 is in resonance. For the support of equipment #1, the maximum value of the horizontal reaction is approximately 4500 times the static force. It is to be noted that the forces are likely to get even bigger in the analysis, if it is not aborted after 0.4

s of dynamic input. Figure 9-16 shows the shear forces at the top of the two interconnected equipment items; the same forces, for the sake of equilibrium, are those applied at the two ends of the cable. In particular, the positive values correspond to traction in the cable. The shear forces at the top of equipment #1 are negligible, while those at the top of equipment #2 are very significant. This is because the forces are transmitted by equipment #2 to the cable, thus the shear forces are not caused directly by the motion of the cable, but the displacement of the top of equipment #2 restrained by the cable. This is also why, as expected, the force at the top of equipment #2 is much bigger than the force at the top of equipment #1. Figure 9-17 shows the vertical reactions measured at the bases of the two equipment items. In this case, both the electrical equipment items are subjected to strong vertical forces, due to the vertical motion of the cable, caused by the slackness and the vertical separation between the two ends. As discussed earlier, these reactions neglect the gravity loads of the equipment items themselves, but take into account only the influence of the cable. The dynamic input causes an amplification of these reactions up to 3000 times the static ones for equipment #2 that is the one experiencing resonance. As well as for the horizontal reactions, this value is supposed to increase if the solution is not aborted. For this imposed ground motion without vertical component, the vertical reactions are found to be smaller than the horizontal ones. Nevertheless, as mentioned for the previous sine-start test, the vertical forces can be very significant considering a vertical component of the ground motion; this is confirmed by the fact that they reach meaningful values also in absence of any external force in that direction. Figure 9-18 presents the moment reaction for equipment #1 and equipment #2. The behavior is the same observed for the horizontal reactions. The moments at the base of equipment #2 support are the bigger ones, and they clearly show resonance: the amplitude reaches very elevated values, and there is one dominant frequency. In this case, there is an amplification of about 2800 times the static reaction for equipment #2, and about 1300 times for equipment #1. The last interesting results are the internal moment at the attachment points, showed in Figure 9-19. As well as for the previous sine-start test, the internal moments are much smaller than the moment reactions; in this case, they are about 1/400 the moment reactions. Nevertheless, they experience a dynamic amplification about 90 times the static values, for both the equipment items.

6.1.4 Base Motion Tests

The second type of test conducted on the electrical equipment items interconnected by the flexible cable is a seismic simulation. In order to test the most severe conditions, the cable is assumed to be straight between the two attachment points. This is possible since no relative displacements between the bases of the two equipment items are needed. The configuration of the system is that already described in the previous paragraphs. The ground motion is chosen from ATC-63. The data of this recorded earthquake are presented in Table 6-7.

Table 6-7: Ground Motion Data

EQ Index	3
EQ ID	120412
PEER-NGA Record Sequence Number	1602
Owner	ERD
Lowest Useable Frequency (Hz)	0.06
Horizontal Acceleration Time History File	DUCZE/BOL090.at2
Year	1999
Recording Station	Bolu
PGA (g)	0.82

It is to be noted that, since all the analysis is bi-dimensional, only one of the two perpendicular components of the ground motion is needed. In this case, the second component is used, since it has the highest PGA. The time history of the base motion input is presented in Figure 6-18.

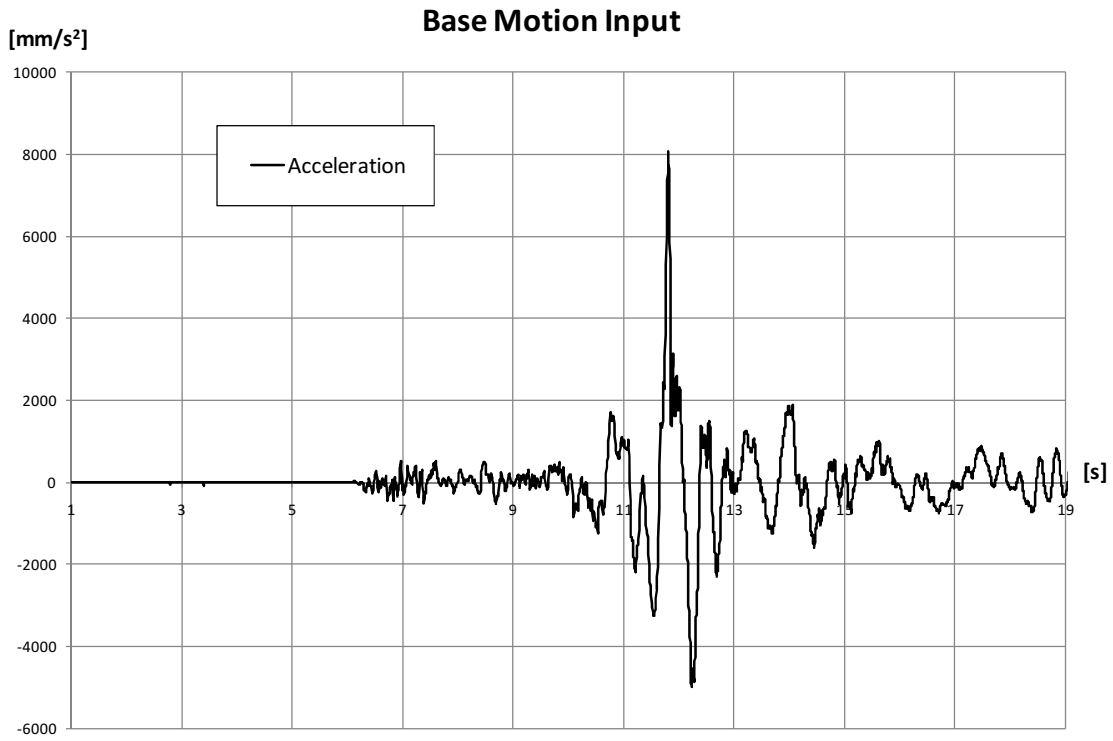

Figure 6-18: Acceleration input record

The time step of the record of the input is 0.01 s. The same value is used for the recommended size of the analysis time step, together with a residual tolerance equal to 1e4 N, that has the same order of magnitude of the expected reactions. In order to check the sensitivity of the total system to the presence of the interconnection, the same ground motion is used to test each the two electrical equipment items in their standalone configuration. Next, the comparison of their responses is made. It is to be noted that the interconnected system has non-zero initial conditions, both for displacements and forces, at the beginning of the dynamic analysis. This is because the presence of the cable undergoing its own weight introduces some reactions and displacements in the static part of the analysis; as a matter of fact, the cable deflects and pulls the two attachment points of equipment #1 and of equipment #2. Obviously, this is absent for the standalone equipment items, since there is no cable; therefore, no static analysis is needed before applying the dynamic input. For the sake of comparison, the initial values of the results for the standalone equipment items are shifted, so that they match the non-zero initial conditions for the interconnected system. In this way, it is possible to check the differences that rise from the

dynamic behavior, neglecting those only due to different static conditions. It is to be noted that in this paragraph are presented only the figures regarding the results for equipment #1, while the correspondent figures for equipment #2 are presented in the Appendixes for short. Figure 6-19 shows the comparison for the relative horizontal displacements of the attachment point at the top of equipment #1.

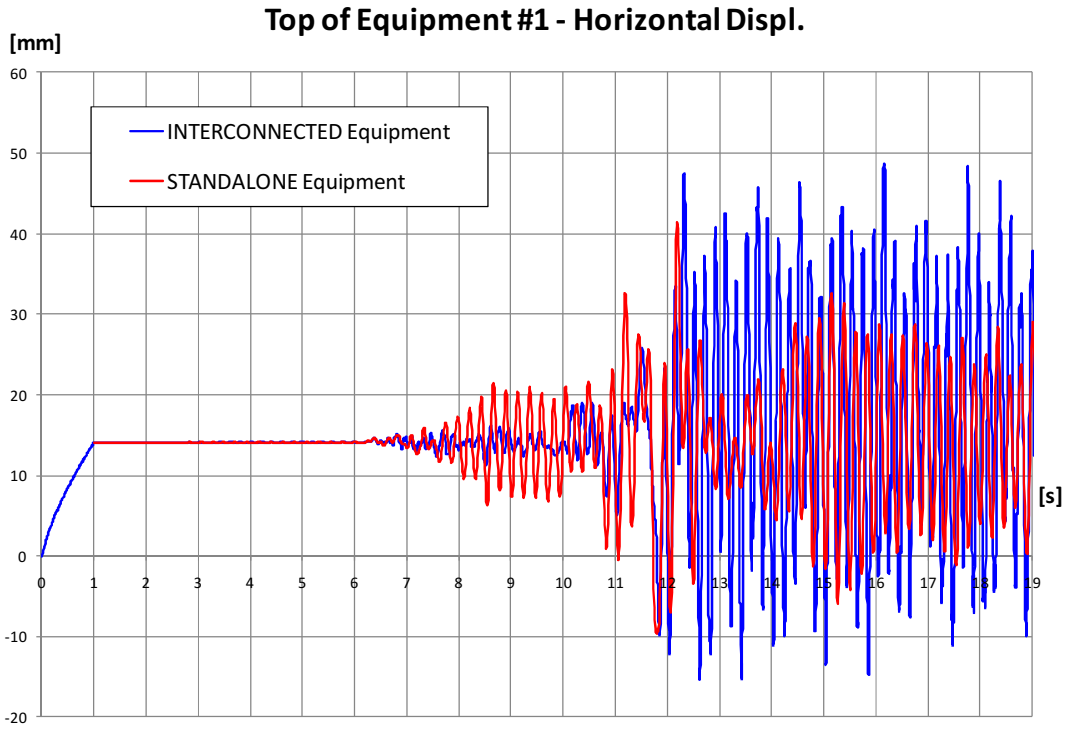

Figure 6-19: Base motion, relative horizontal displacements of the top of equipment #1

Comparing the two curves, it can be seen that the cable provides a restraint for the first seconds, when the ground motion is still relatively small. Around 12 s, after the biggest peaks of the acceleration input, the presence of the cable tends to amplify these displacements. The values of the biggest displacements for the two configurations are similar, but there is a very significant difference. In the standalone configuration, the horizontal displacements reach a peak with amplitude of about 25 mm, and then the response gets smaller and oscillates with an amplitude of 15 mm. In the interconnected configuration, after a peak with amplitude of about 30 mm, the response continues to oscillate with that amplitude, and doesn't get smaller. This is due to the

presence of the cable, that begins a very large motion and the inertia of this effect keeps the top of equipment #1 moving with large amplitudes. Figure 9-20 presents the horizontal displacements of the attachment point at the top of equipment #2. One meaningful observation can be made. The displacements experienced by the top of equipment #2 are smaller than those experienced by the top of equipment #1 in the standalone configuration; the amplitude of the peak is about 15-20 mm instead of 25. Nevertheless, considering the interconnection represented by the flexible cable, the amplitude of the displacement at the top of equipment #2 gets bigger and reaches 35-40 s; therefore, it is even bigger than equipment #1 one. Looking at the forces, the horizontal reactions measured at the base of the support of equipment #1 are shown in Figure 6-20.

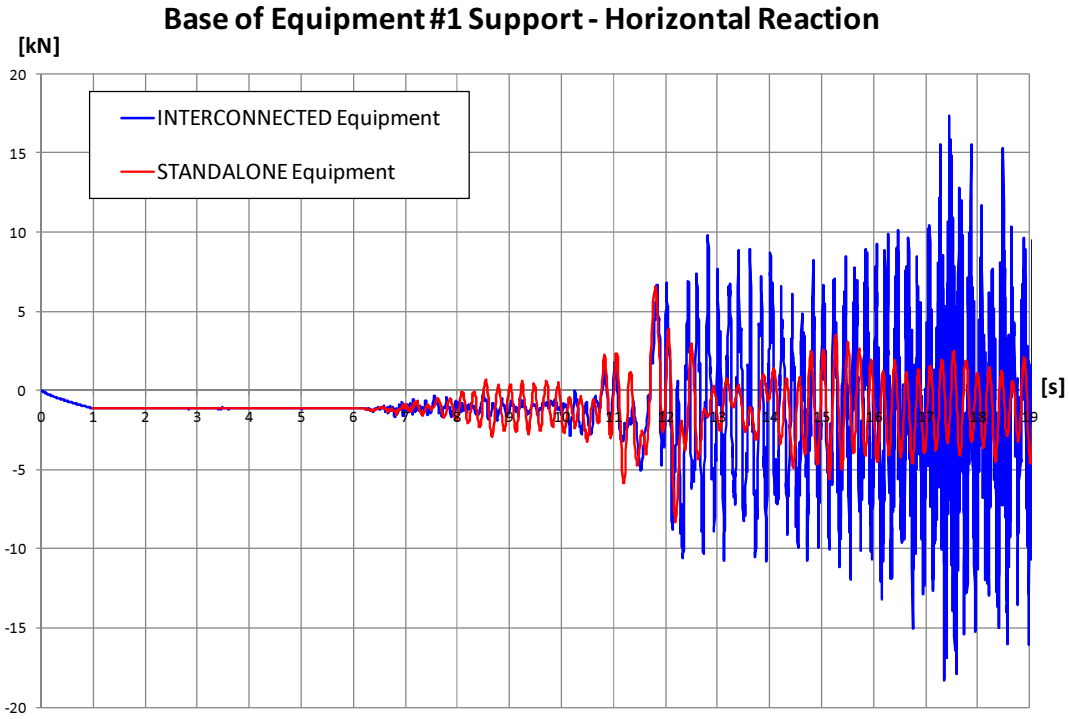

Figure 6-20: Base motion, horizontal reaction at the base of equipment #1

In this case, the reactions developed in the interconnected configurations are twice those for the standalone configuration. Furthermore, the peak of the reactions in the interconnected system doesn't match the peak of the acceleration input, but is shifted along the time axis. This means that the peak of reactions is not directly due to the input at the base, but is mainly caused by the

forces transmitted by the cable at the attachment point. Therefore, the presence of the cable doesn't change only the scale of the time history of the reaction, but the whole dynamic behavior. Figure 9-21 shows the same reactions for the other equipment item. For this equipment, the peak of the reactions in the standalone configuration (50 kN) is bigger than that in the interconnected configuration (40 kN). As expected, since equipment #2 and its frame support structure are the stiffer and heavier of the two equipment items, the reactions are mainly influenced by the dynamic behavior of the equipment itself, and less by the cable. Conversely, because of a minor dimension and a larger flexibility, equipment #1 mounted on the steel post is mainly influenced by the forces transmitted by the cable at the attachment point. Figure 6-21 presents the time history of the vertical reaction at the base of the support of equipment #1.

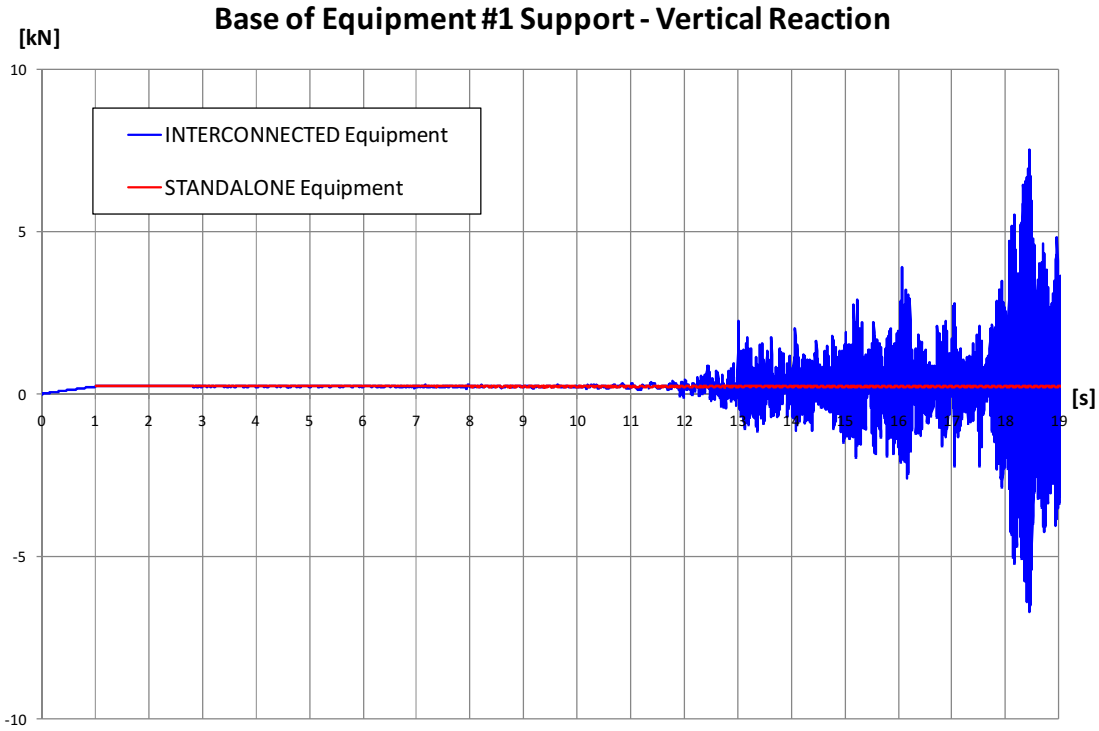

Figure 6-21: Base motion, vertical reaction at the base of equipment #1

It is to be noted that, since the ground motion has only a horizontal direction, the standalone equipment doesn't have any vertical component of motion; as for the sine-start tests, we are neglecting the static vertical forces due to the gravity load of the equipment items themselves. In this case, the presence of the cable in the interconnected configuration introduces significant

vertical forces. This is mainly due to the vertical separation between the two attachment points, since in this test the cable is straight and doesn't present vertical changes in the sag, like it happens for the slack cable. Therefore, in this case the effect of the vertical inertia of the cable is less important than the vertical separation. This separation plays a big role, since the cable mainly transmit axial forces in the direction of its axis, and smaller shear forces and moments: the vertical separation between the two ends of the cable thus provides a slope to the direction of the axial forces transmitted between the two equipment items. This is the source of the vertical component of the forces in the system. Figure 9-22 presents the same time history for equipment #2. The observations that can be made are the same already made for the other equipment. The only difference is that these reactions are 10 times smaller than those at the base of equipment #1. The difference between the two reactions is equilibrated by the effect of the vertical inertia of the cable: as a matter of fact, since the ground motion has only a horizontal component, the only element with a vertical motion is the cable. This explains another role played by the presence of the cable, through its inertia. Figure 6-22 shows the moment reaction computed at the base of the support of equipment #1.

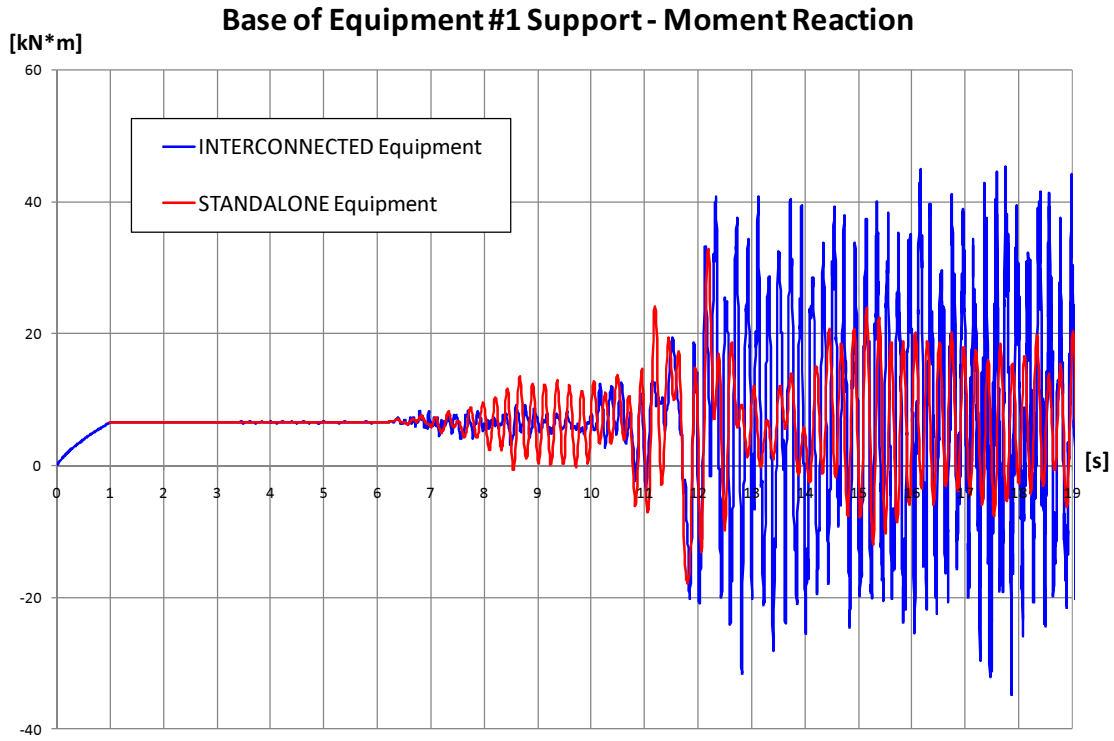

Figure 6-22: Base motion, moment reaction at the base of equipment #1

The general behavior is very similar to the time history of the horizontal reaction. It is observed that the response in the interconnected configuration is slightly bigger than the standalone configuration one, but the biggest difference is the absence of a decrease after the peak of the acceleration input. Figure 9-23 presents the same comparison for equipment #2. In this case too, the behavior is very similar to that of the horizontal reactions. This is because the two equipment items are considered as cantilevers, and the moments at their bases come from the horizontal external forces; therefore, horizontal and moment reactions are related to each other. In this case, the maximum moment at the base of equipment #2 is 1.5 times the maximum moment at the base of equipment #1. This agrees with the fact that also the horizontal forces are bigger for equipment #2. Furthermore, since equipment #2 has the more severe response in the standalone configuration, the presence of the cable provides a restraint that slightly decreases the maximum peak. It is noteworthy that a comparison for the internal moments at the top of each equipment doesn't make any sense. As a matter of fact, considering the two equipment items as cantilevers with the mass lumped in the center of gravity, the internal moment at their top will always be zero. The internal moments can only be generated by the presence of the attached cable. Nevertheless, the maximum possible internal moments will be generated when one of the elements of the interconnected system is in resonance, thus their maximum possible values have already been observed with the sine-start test. Therefore, it is not meaningful to check them for the base motion test.

The last meaningful consideration regards the sources of the moments at the vase of equipment #1 and equipment #2. It is important to understand where these moments come from, since they are the most affecting effect on the entire interconnected system. For each equipment, the moment at the base comes from three components: the seismic response of the equipment itself, the moment transmitted by the cable at the attachment point, and the moment generated by the horizontal component of the axial force transmitted by the cable at the top of the equipment. The time history of the total moment at the base of equipment #1, as well as the components coming respectively from the moment at the top of the cantilever transmitted by the cable and from the axial force of the cable are presented in Figure 6-23.

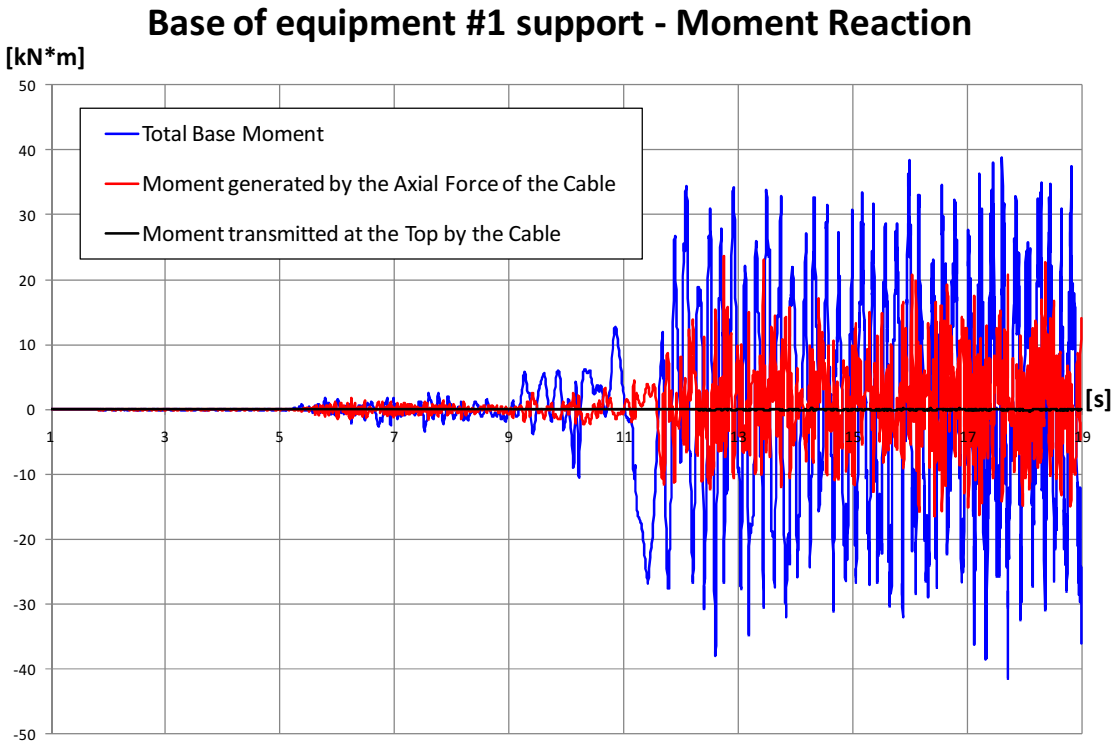

Figure 6-23: Base motion, components of the moment reaction at the base of equipment #1

In order to better understand the influences of the three components, their percentages on the total base moment are presented in Figure 6-24 for equipment #1. In particular, the maximum values and the averages of their percentage are shown in Table 6-8.

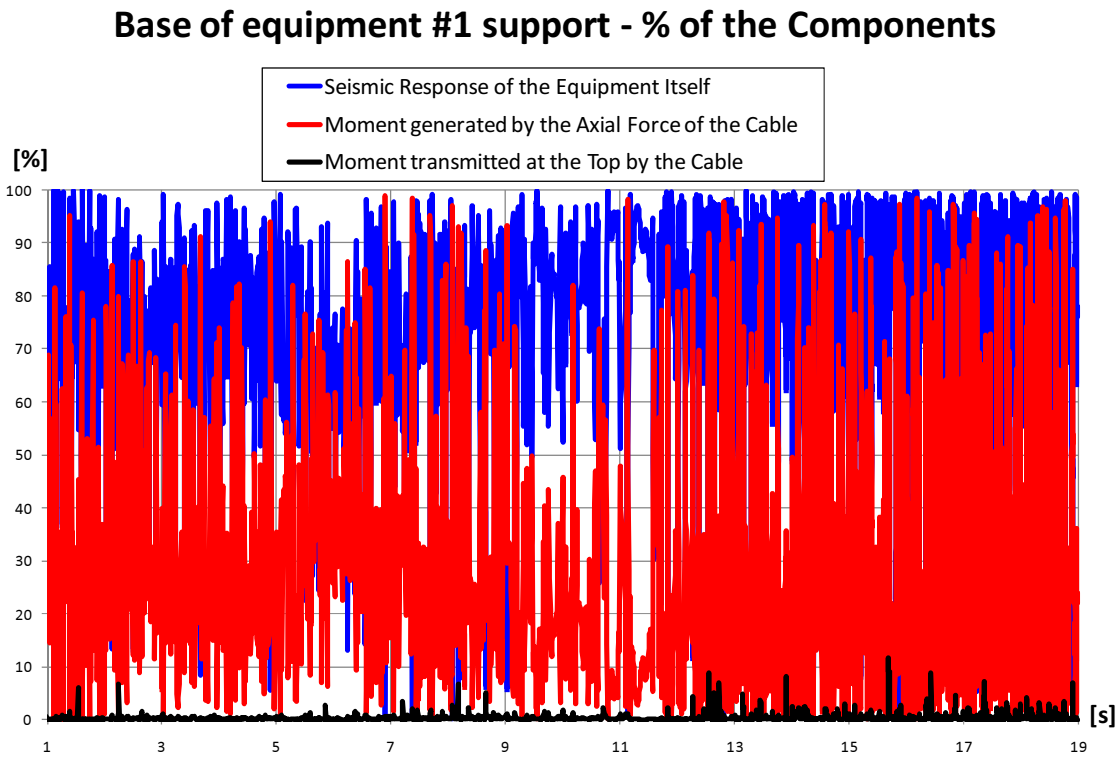

Figure 6-24: Base motion, percentages of the components of the moment reaction at the base of equipment #1

Table 6-8: Maximum and Average Values of the Components of the Moment Reaction at the Base of Equipment #1

	Maximum value (%)	Average (%)
Seismic response of the equipment itself	100	72.9
Moment generated by the axial force of the cable	98.9	26.7
Moment transmitted at the top by the cable	11.6	0.4

Very similar results are found for the moments at the base of equipment #2. For short, all the figures regarding those moments are presented in the Appendixes. The time history of the total moment at the base of equipment #2, as well as the components coming respectively from the moment at the top of the cantilever transmitted by the cable and from the axial force of the cable are presented in Figure 9-24. The percentages of the three components on the total base moment

are presented in Figure 9-25 for equipment #2. The maximum values and the averages of their percentage are shown in Table 6-9.

Table 6-9: Maximum and Average Values of the Components of the Moment Reaction at the Base of Equipment #2

	Maximum value (%)	Average (%)
Seismic response of the equipment itself	100	72.8
Moment transmitted at the top by the cable	99.7	26.9
Moment generated by the axial force of the cable	9.2	0.3

CHAPTER 7

CONCLUDING REMARKS

This study showed the current capabilities to model high voltage electrical connectors, exhibiting nonlinear vibrations when subjected to time dependent loading. The study shows the big importance of dynamic behavior of flexible connections in response to the excitation generated by earthquakes. The following remarks summarize the main issues addressed in this work.

Almost all the results showed that large forces inherent the cable might be dynamically generated, even when sufficient slack is provided to account for the differential displacement between the interconnected equipment items, indicating that it is not sufficient to seismically design connections based on static considerations only. Therefore, it is important to design flexible connections so that the range of natural frequencies at which they are likely to be excited are different from those of the equipment they are interconnecting, in order to avoid the risk of dynamic interaction and resonance between them (the natural frequencies of the interconnected electrical facilities are typically in the range 0.5 to 15 Hz).

It was found that all the models are able to adequately reproduce the shape of the cable in the static position under their own weight: this confirms what is expected, that is finite-element programs based on the displacement method provide more accurate displacements than forces. Comparisons between the model and the experimental results on the difference between the maximum and minimum horizontal traction force measured for a given cycle of applied displacement at a fixed amplitude and frequency were made for the dynamic tests.

It was observed that the model using an adequate variable bending stiffness reproduced with good accuracy the experimental results, with a maximum error of 13.6% and an average error of 4.8% for the 7 sine-start tests compared. Conversely, the model simply considering a constant bending stiffness, based on the IEEE recommendation, showed a maximum error of 37.8% and an average error of 16.2%. This underlines the important role played by the slippage of the strands each over other, and the friction forces developed throughout this process. Therefore, it could be concluded, from both the static and dynamic comparisons, that both the presented

model was sufficiently adequate to representatively predict the dynamic response for short-span flexible conductors, typically connecting high-voltage substation electrical equipment.

The sensitivity of the model to various parameters was analyzed, and the values most suitable to find good accuracy of the solution were found. These values have been used to set a valid model capable of adequately describing new possible dynamic tests on various interconnected electrical equipment items. The most important difference was found to be the compression in the cable, generated from the initial configuration of the cable. As a matter of fact, when the slackness ratio of the cable exceeds a certain quantity (0.275%), the cable is initially subjected to compression. The higher the flexural stiffness of the cable is, the higher the initial internal compression is. In particular, using a constant flexural stiffness when big rate of curvature are involved highly overvalues the computed value: therefore, unrealistic initial compressions are considered. When the compression is high enough, it causes a shift of the natural frequency, changing the dynamic properties of the cable: this involves a completely misunderstanding of the dynamic behavior of the cable. Therefore, the biggest errors in the analytical model come from the initial compression possibly caused by overestimated values of the bending stiffness: in particular the stiffness considered constant when big rate of curvature are involved, like the initial horizontal motion of the ends of the cable. Obviously, when a straight cable is considered, the slackness ratio is equal to zero, and no initial horizontal motion of the ends of the cable are needed. In this case, the cable undergoing the gravity load is only subjected to traction, and there is no compression causing any shit of the eigenfrequencies. In this case, considering either a constant or a variable bending stiffness only causes minor changes in the dynamic response of the cable.

The second part of this study was focused on the dynamic behavior of electrical equipment items interconnected by a flexible cable, and the influence of the interconnection on the response of the system. It is to be noted that the two equipment items have been chosen only since experimental data and data for the modeling were already available. Although the items used are not typical for interconnecting equipment, their dynamic characteristic are representative and it was decided to model them, in order to evaluate the interconnected cables and equipment. Furthermore, the type of interconnecting cable is more common in Québec and Canada than in the United States of America, in particular the west coast of US. However, the parameters are realistic and allow testing the modeling and the interaction issues. All the representation of the two electrical

facilities has been made through the definition of rigidity values and lumped masses for the equivalent beams: if a different kind of electrical equipment has to be modeled, this can be done very easily just modifying the single value of rigidity and lumped mass of the equivalent beam. The aluminum cable has been defined through the cross-section area and the IEEE recommended equivalent inertia, based on the number of layer and the minimum value of bending inertia: when a different kind of cable has to be modeled, the new cross-section area and equivalent flexural inertia must be plugged in. The only purpose of this study is to validate a general model, not to analyze a very specific and actual electrical system: in this way, the validated model can be very flexible, and it can be applied to a large range of electrical interconnected system.

The presence of the cable provides a restraint to the more severely tested equipment, slightly decreasing its response to the ground motion. The cable absorbs some part of the forces generated in the most affected equipment item, in this case equipment #2, and it transmits these forces to the interconnected equipment, causing a significant increase in its response. Therefore, the cable is redistributing the forces of the system from the more affected element to the less affected. This is valid for the horizontal and the moment reactions that are already present also for the two standalone equipment, since the ground motion has only a horizontal component. Conversely, in the vertical direction both the equipment items are more severely tested in the interconnected configuration, since the vertical forces are generated just by the presence of the cable, due to the vertical separation between the two ends and the vertical inertia.

Furthermore, the presence of the cable provides both the equipment items sloped forces at the attachment points, generating shear forces and internal moments also at the top of each equipment: these forces are absent in the standalone configurations, since they are cantilevers with the whole mass lumped in the center of gravity. The most affecting structural effect on the interconnected system is the moment reaction at the base of the two equipment items. This is the capacity that has to be required to the structure. Looking at this value, as the more significant, it is seen that it comes from three different sources. One component is the seismic response of the electrical equipment itself, due to its mass and its stiffness: this is not directly related to the presence of the cable. The other two components are coming from the presence of the interconnecting cable: one is the moment transmitted by the cable at the attachment point, the second is the moment generated by the horizontal component of the axial force in the cable, that

is transferred at the top of the cantilever. The moment transmitted by the cable is found to have a very small influence, with an average percentage of less than 1%: this is consistent with the small value of the flexural inertia of the cable, causing small values of the inherent moment in the cable. Conversely, the moment generated by the horizontal component of the axial force in the cable transferred at the top of the cantilever is found to have a bigger influence, with an average percentage on the total moment that is about 27%, but with peaks of the same order of magnitude of the moment due to the seismic response of the equipment itself. This underlines the big role played by the axial forces transmitted by the cable as concentrated forces at the top of the two equipment items.

It is to be noted that these values are not directly related to the comparisons made between the standalone and the interconnected responses. As a matter of fact, in some instants the concentrated force transmitted by the cable generates a moment with an opposite sign to that of the moment due to the response of the equipment itself: in this case, the presence of the cable doesn't aggravate the electrical equipment, but provides a force that fights the effects of the ground motion. Therefore, the check of the percentages themselves is not sufficient, but has to be done together with the check of the comparisons between the standalone and the interconnected seismic response, in order to understand when the cable is fighting the effects of the ground motion on the equipment items and when it aggravates their conditions.

All the considerations made can be used to set a reliable finite-element model providing accurate description for the dynamic behavior of interconnected systems that can be subjected to experimental tests. The present studies shows that the model developed in ABAQUS (Der Kiureghian's model with constant bending stiffness) is sufficiently accurate, even if less than FEAP model (Dastous' model with variable bending stiffness), but much more flexible. Therefore, it is advisable to make use of ABAQUS model that can account for a big range of equipment items and different base motions. As already mentioned, the biggest lack of this model is the overestimation of flexural stiffness when big rate of curvature are involved. Nevertheless, big rate of curvature have been observed only when one end of the cable is horizontally moved to the other, and the cable switches from an initially straight to a slack shape. All the rates of curvature observed during the dynamic motion didn't turn out in meaningful difference of flexural stiffness value between the two different models. This means that the

biggest differences between the two models are related to the initial motion of one end of the cable toward the other, in order to reach the desired span of the slack cable. It is to be noted that, whether the cable interconnecting the two equipment items is straight, this difference disappears, and both the two models provide very similar results: in this case, ABAQUS model is completely adequate to describe the dynamic behavior of the interconnected system. Conversely, when the cable interconnecting the two electrical equipment items is slack, some meaningful differences are present between ABAQUS and FEAP model. Nevertheless, as mentioned earlier, the different dynamic behavior is completely due to the initial compression value. FEAP model (Dastous' model with variable bending stiffness) provides results for the dynamic part closer to the actual ones, but it shows also a better approximation of the initial compression value; ABAQUS model (Der Kiureghian's model with constant bending stiffness) has a lack in the dynamic behavior that is proportional to the lack in the initial compression value. Therefore, a meaningful way to forecast the adequacy of ABAQUS model, when dynamic experimental tests are wanted to be modeled, is to compute the initial forces in the cable after the static steps (either compression or traction, depending on the type of cable and its slackness), and compare those with the forces experimentally measured in the cable under its own weight. If the analytical and actual values are close, it is reasonable that the finite-element model will provide an adequate approximation of the dynamic behavior of the cable; otherwise, the lack in the approximation of the dynamic behavior will be already shown by a significant difference between the analytical and actual initial forces in the cable. Therefore, the initial compression in the cable coming from the static loads is a significant parameter to evaluate the accuracy of the model for the dynamic analysis.

CHAPTER 8

REFERENCES

[1] ANSI. (2007). *National electrical safety code*, IEEE, New York, NY.

[2] Bathe, KJ and Wilson, EL (1973). "Stability and accuracy analysis of direct integration methods," *Earthquake Engineering and Structural Dynamics*, Vol. 1, pp. 283–291.

[3] Blevins, RD (1979). *Formulas for natural frequency and mode shape*, Van Nostrand Reinhold Co., New York.

[4] Dastous, J-B and Pierre, J-R (1996). "Experimental investigation on the dynamic behavior of flexible conductors between substation equipment during an earthquake," *IEEE Transactions on Power Delivery*, Vol. 11, pp. 801–807.

[5] Dastous, J-B and Paquin, J-Y (2003). "Testing and development of alternative flexible-bus geometries for interconnected substation equipment subjected to earthquakes," *IEEE Transactions on Power Delivery*, Vol. 18, pp. 772–780.

[6] Dastous, J-B, Filiatrault, A, Pierre, J-R (2003). "Estimation of displacement at interconnection points of substation equipment subjected to earthquakes," *IEEE Transactions on Power Delivery*, Vol. 19, pp. 618–628.

[7] Dastous, J-B (2005). "Nonlinear finite element analysis of stranded conductors with variable bending stiffness using the tangent stiffness method," *IEEE Transactions on Power Delivery*, Vol. 20, pp. 328–338.

[8] Dastous, J-B (2007). "Guidelines for seismic design of flexible buswork between substation equipment," *Earthquake Engineering and Structural Dynamics*, Vol. 36, pp. 191–208.

[9] Der Kiureghian, A, Sackman, JL, Hong, KJ (1999). *Interaction in interconnected electrical substation equipment subjected to earthquake ground motions*, Report No. PEER

1999/01, Pacific Earthquake Engineering Research Center, University of California, Berkeley, CA.

[10] Der Kiureghian, A, Hong, KJ, Sackman, JL (2000). *Further studies on seismic interaction in interconnected electrical substation equipment*, Report No. PEER 2000/01, Pacific Earthquake Engineering Research Center, University of California, Berkeley, CA.

[11] Der Kiureghian, A, Sackman, JL, Hong, KJ (2001). "Seismic interaction in linearly connected electrical substation equipment," *Earthquake Engineering and Structural Dynamics*, Vol. 30, pp. 327–347.

[12] Filiatrault, A and Stearns, C (2002). *Electrical substation equipment interaction—experimental flexible conductor studies*, Report No. SSRP-2002/09, University of California, San Diego, CA.

[13] Filiatrault, A and Stearns, C (2004). "Seismic response of electrical substation equipment interconnected by flexible conductors," *Journal of Structural Engineering*, *ASCE*, Vol. 130, no. 5, pp. 769-778.

[14] Filiatrault, A and Stearns, C (2005). "Flexural properties of flexible conductors interconnecting electrical substation equipment," *Journal of Structural Engineering*, *ASCE*, Vol. 131(1), pp. 151-159.

[15] Ghalibafian, H, Bhuyan, G et al (2004). "Seismic behavior of flexible conductors connecting substation equipment. Part 2: shake table tests," *IEEE Transactions on Power Delivery*, Vol. 19, pp. 1680–1687.

[16] Hibbeler, RC (1997). *Structural Analysis*, Prentice Hall Inc., Upper Saddle River, NJ.

[17] Hibbitt, HD, Karlsson, BI, Sorensen, A (1980). *ABAQUS: a finite-element code for nonlinear dynamic analysis*, Electric Power Research Institute, Palo Alto, CA.

[18] Hong, KJ, Der Kiureghian, A, Sackman, JL (2001). "Seismic interaction in cable-connected equipment items," *Journal of Engineering Mechanics*, *ASCE*, Vol. 127(11), pp. 1096–1105.

[19] Hong, KJ, Der Kiureghian, A, Sackman, JL (2005). "Bending behavior of helically wrapped cables," *Journal of Engineering Mechanics*, *ASCE*, Vol. 131(5), pp. 500–511.

[20] Ibrahimbegovic, A and Mikdad, MA (1998). "Finite rotations in dynamics of beams and implicit time-stepping schemes," *International Journal for Numerical Methods in Engineering*, Vol. 41, pp. 781–814.

[21] IEEE. (2006). *Recommended practice for seismic design of substations*, IEEE Std-693-2005, Piscataway, NJ.

[22] IEEE. (2006). *Recommended practice for the design of flexible buswork in seismically active areas*, IEEE Std-1527-2006, Piscataway, NJ.

[23] Newmark, N (1959). "A method of computation for structural dynamics," *Journal of Engineering Mechanics*, *ASCE*, Vol. 85, pp. 67–94.

[24] Noiseux, DU (1992). "Similarity laws on the internal damping of stranded cables in transverse vibration," *IEEE Transaction on Power Delivery*, Vol.7(3).

[25] Papailiou, KO (1997). "On the bending stiffness of transmission line conductors," *IEEE Transaction on Power Delivery*, Vol.12(4), pp. 1576-1588.

[26] Schiff, A (2009). Private communication.

[27] Simo, JC, Tarnow, N, Wong, KK (1992). "Exact energy-momentum conserving algorithms and symplectic schemes for nonlinear dynamics," *Computer Methods in Applied Mechanics and Engineering*, Vol. 100, pp. 63–116.

[28] Taylor, RL (2001). *FEAP Version 7.4 User Manual*, Department of Civil and Environmental Engineering, University of California at Berkeley, Berkeley, CA.

[29] Timoshenko, SP (1972). *Mechanics of Materials*, Van Nostrand Reinhold Co., New York.

[30] Zienkiewicz, OC and Taylor, RL (2000). *The finite element method* (5^{th} Edition), Vol. 1, Butterworth, London.

CHAPTER 9

APPENDIXES

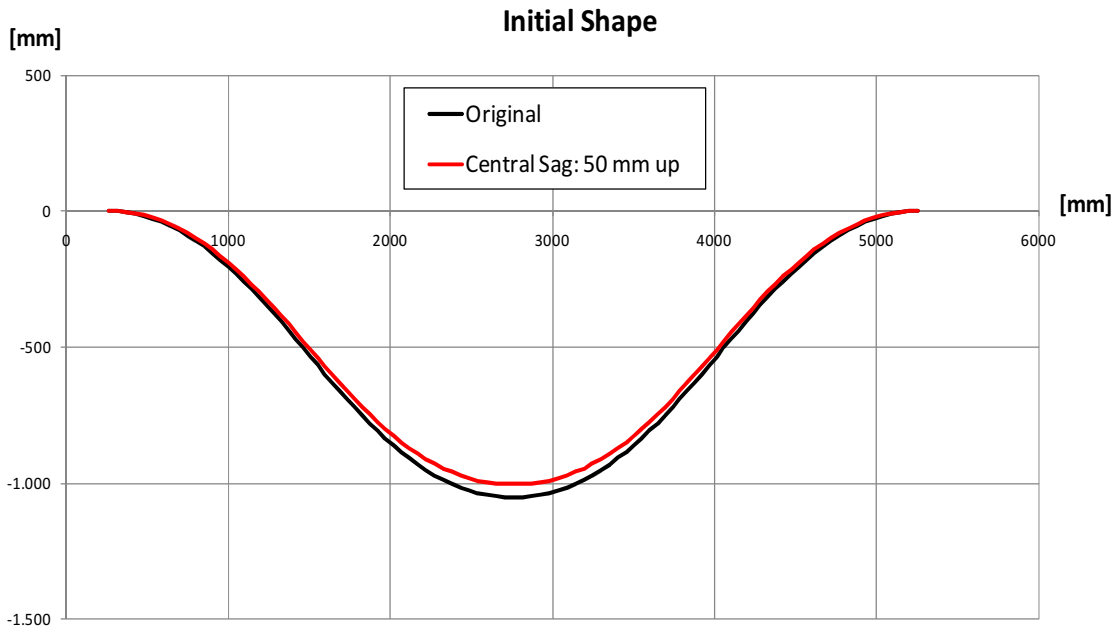

Figure 9-1: Test #135, shape of the cable with the central sag moved up by 50 mm

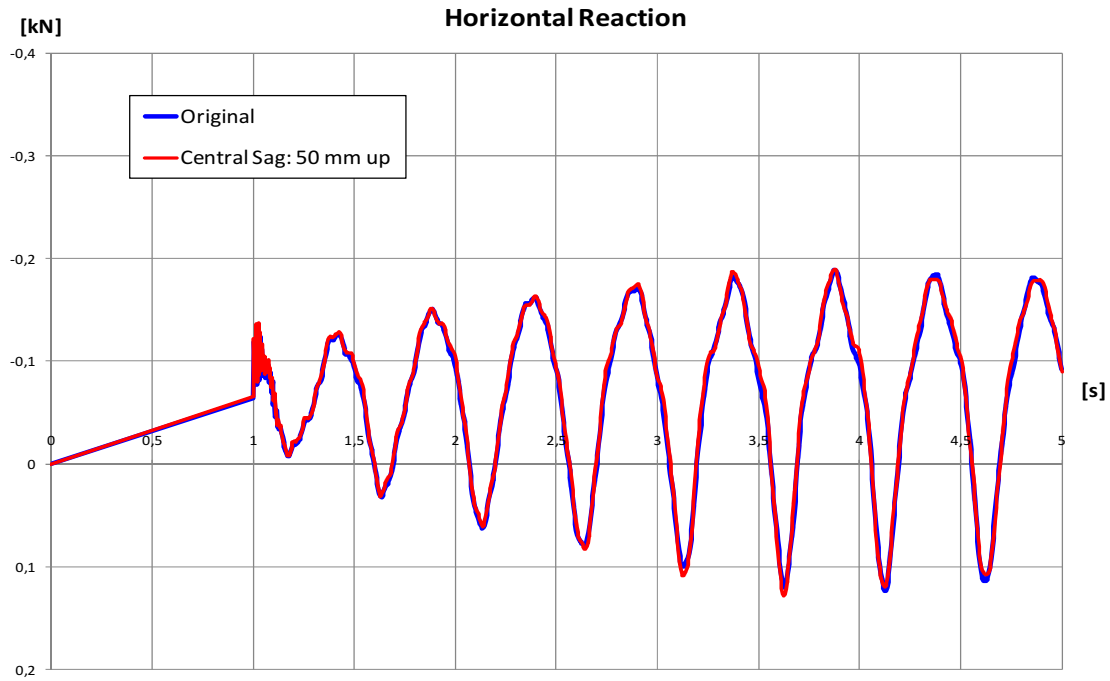

Figure 9-2: Test #135 with the central sag moved up by 50 mm, horizontal reaction

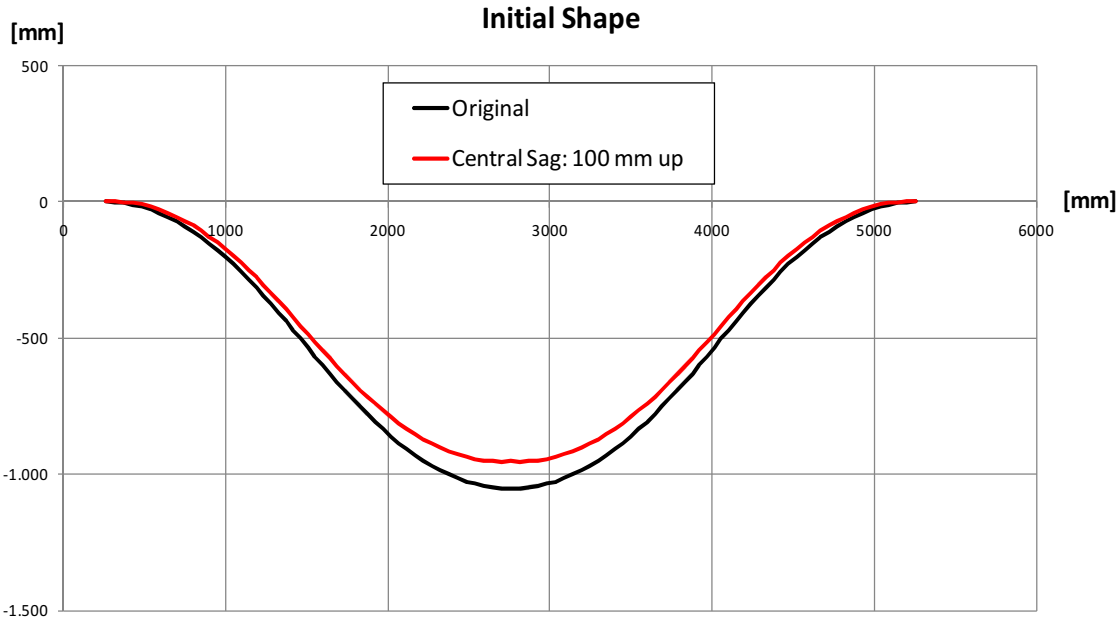

Figure 9-3: Test #135, shape of the cable with the central sag moved up by 100 mm

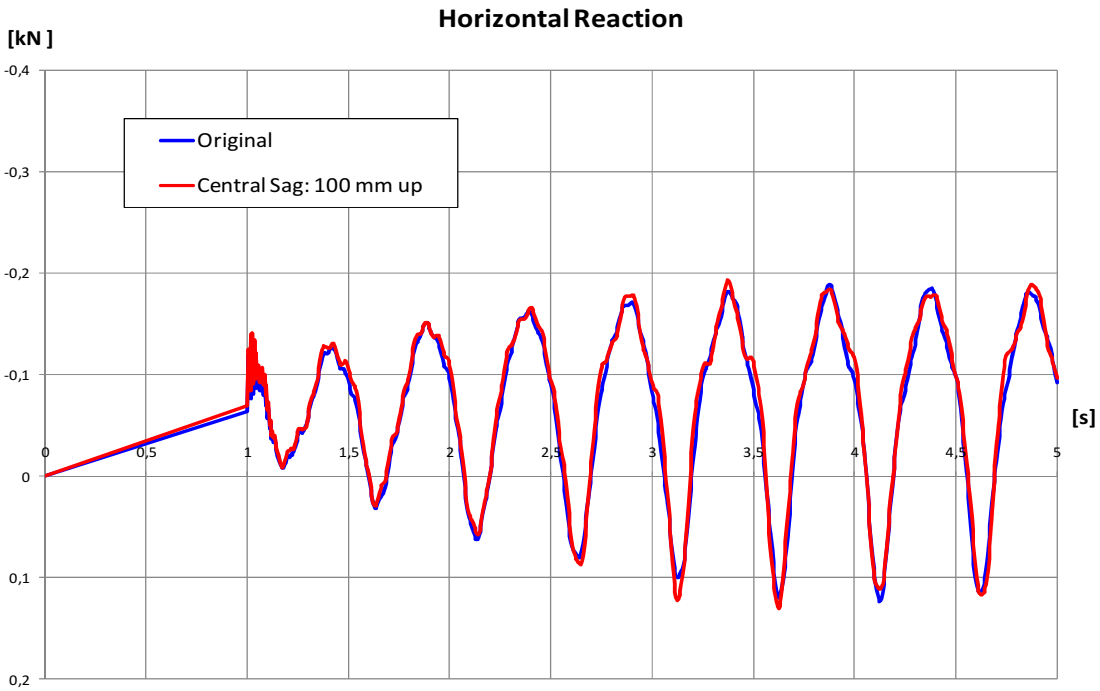

Figure 9-4: Test #135 with the central sag moved up by 100 mm, horizontal reaction

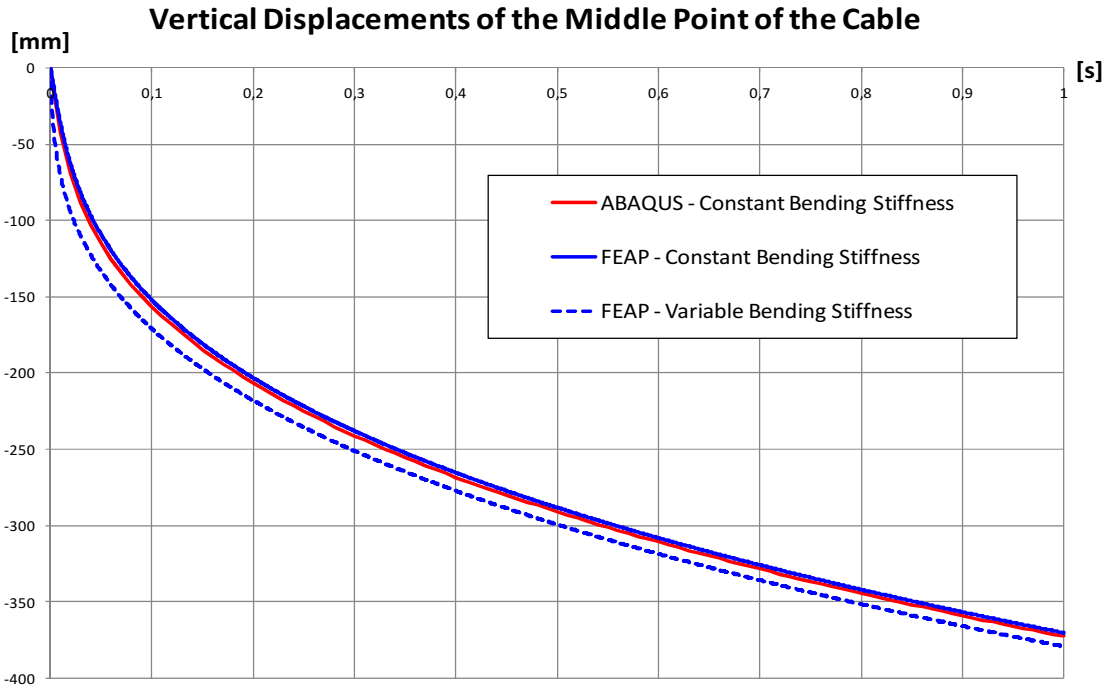

Figure 9-5: Vertical displacements of the straight cable under gravity load

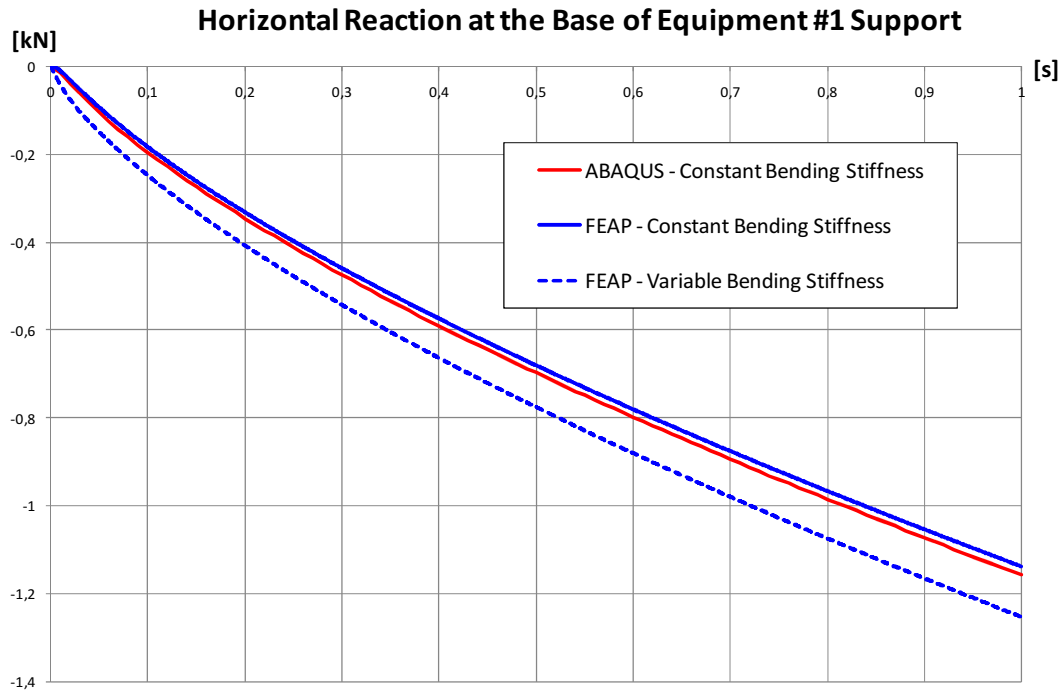

Figure 9-6: Horizontal reaction at the base of equipment #1 support for the straight cable under gravity load

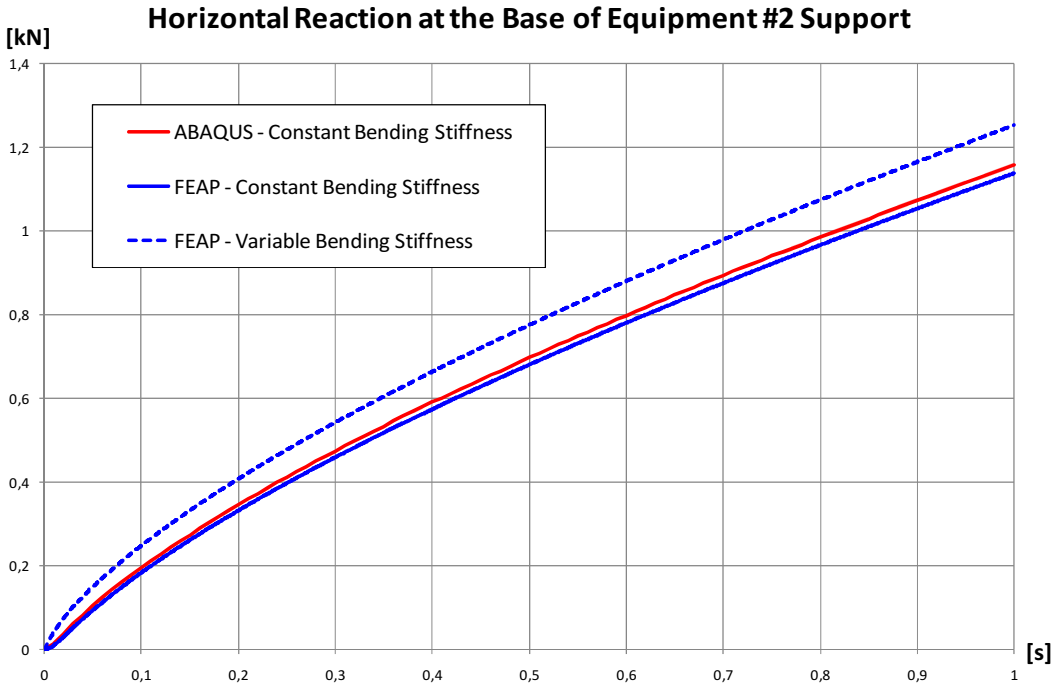

Figure 9-7: Horizontal reaction at the base of equipment #2 support for the straight cable under gravity load

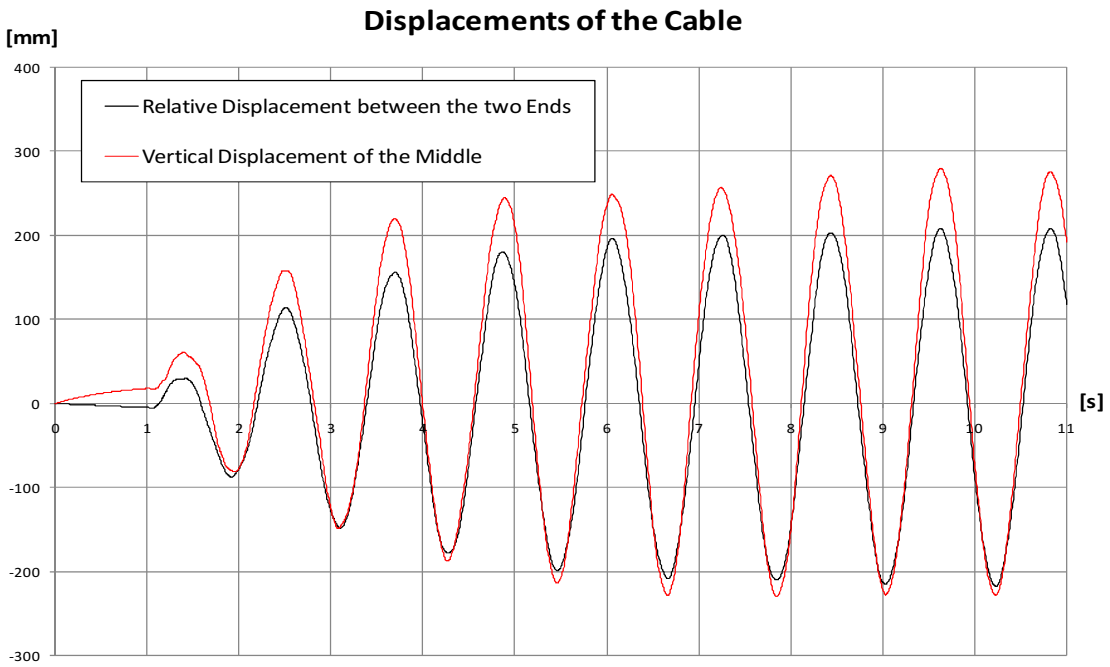

Figure 9-8: Sine-start test #2, displacement of the cable

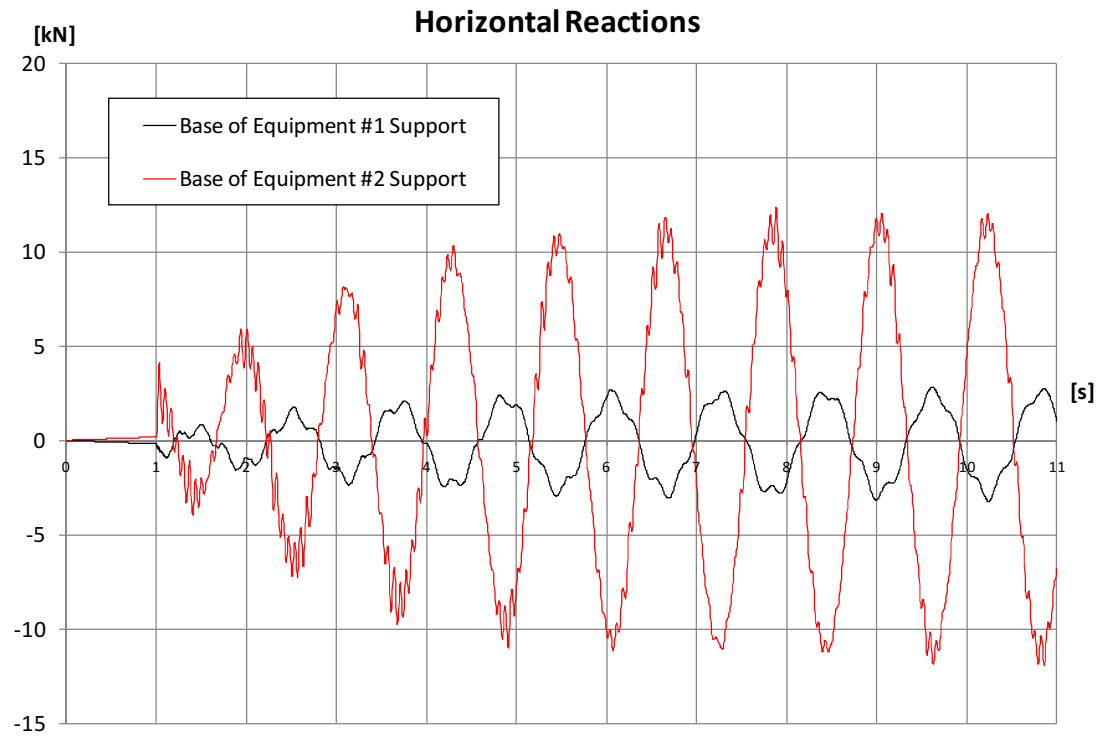

Figure 9-9: Sine-start test #2, horizontal reactions

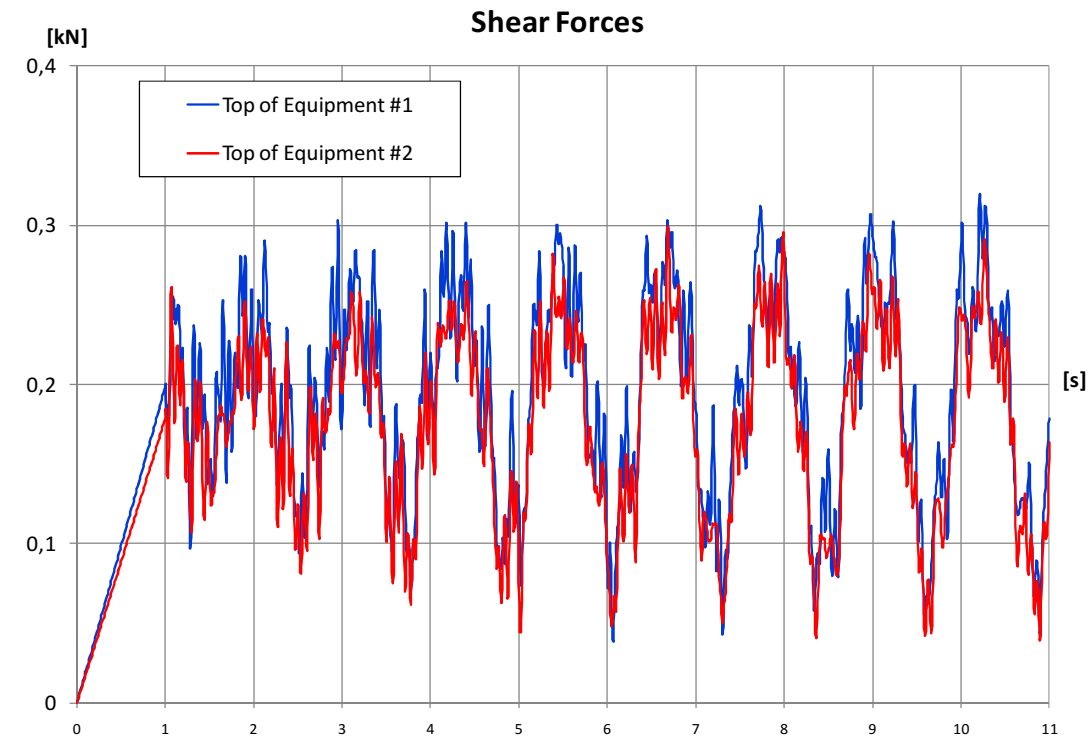

Figure 9-10: Sine-start test #2, shear forces

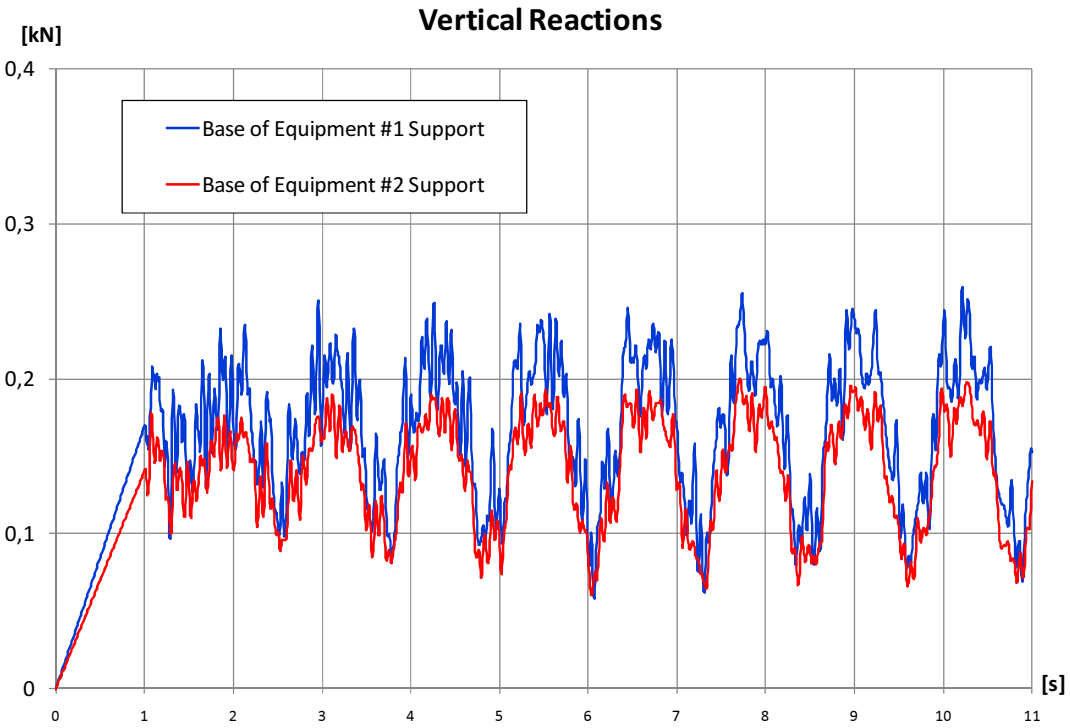

Figure 9-11: Sine-start test #2, vertical reactions

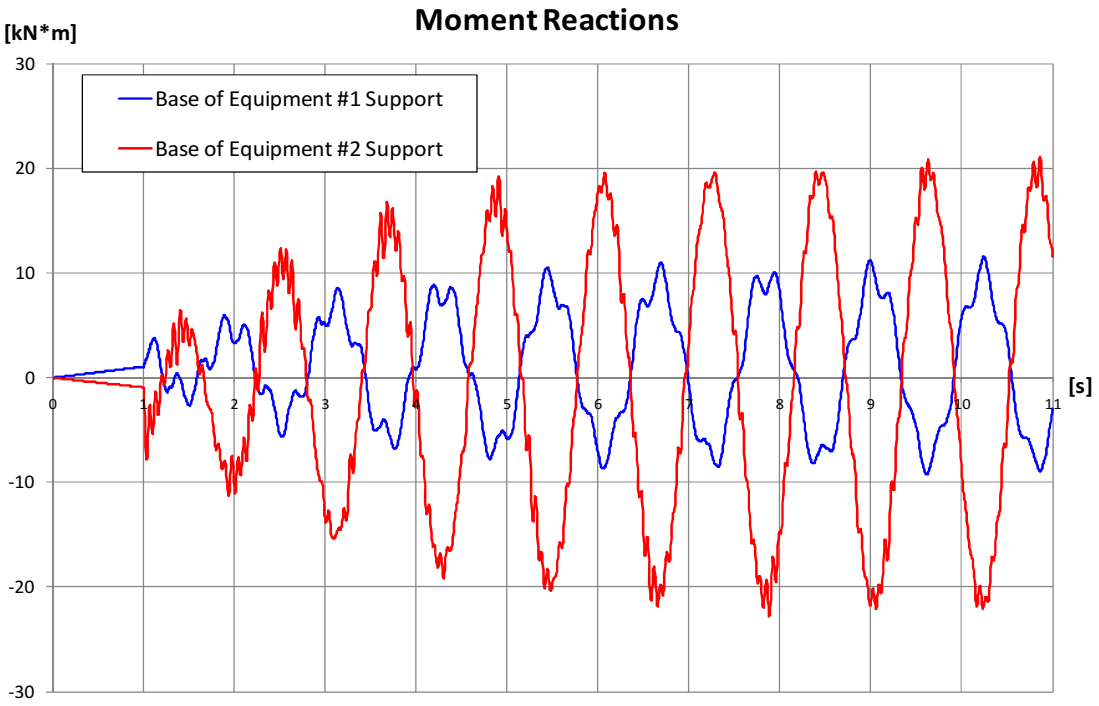

Figure 9-12: Sine-start test #2, moment reactions

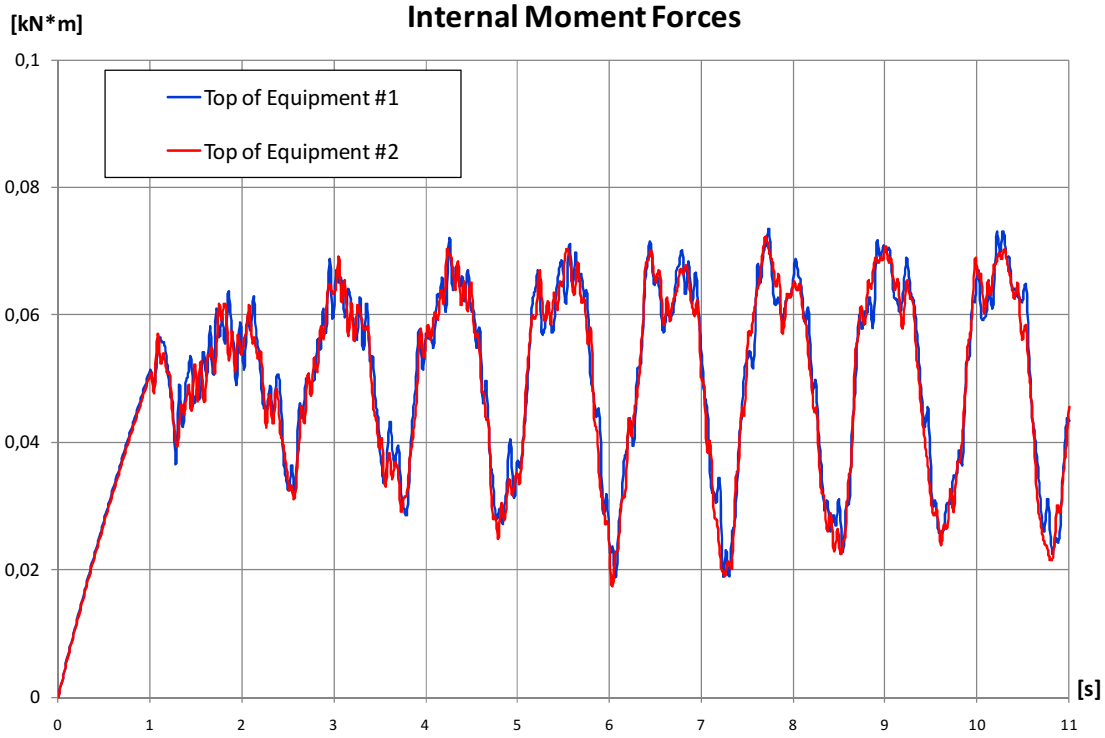

Figure 9-13: Sine-start test #2, internal moment

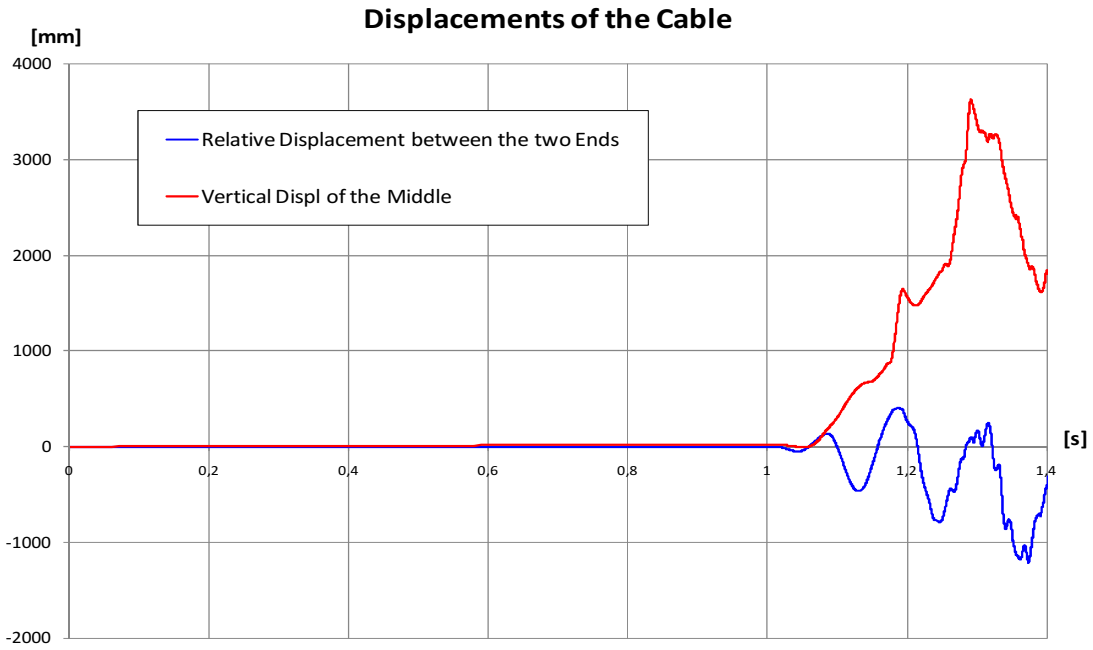

Figure 9-14: Sine-start test #4, displacement of the cable

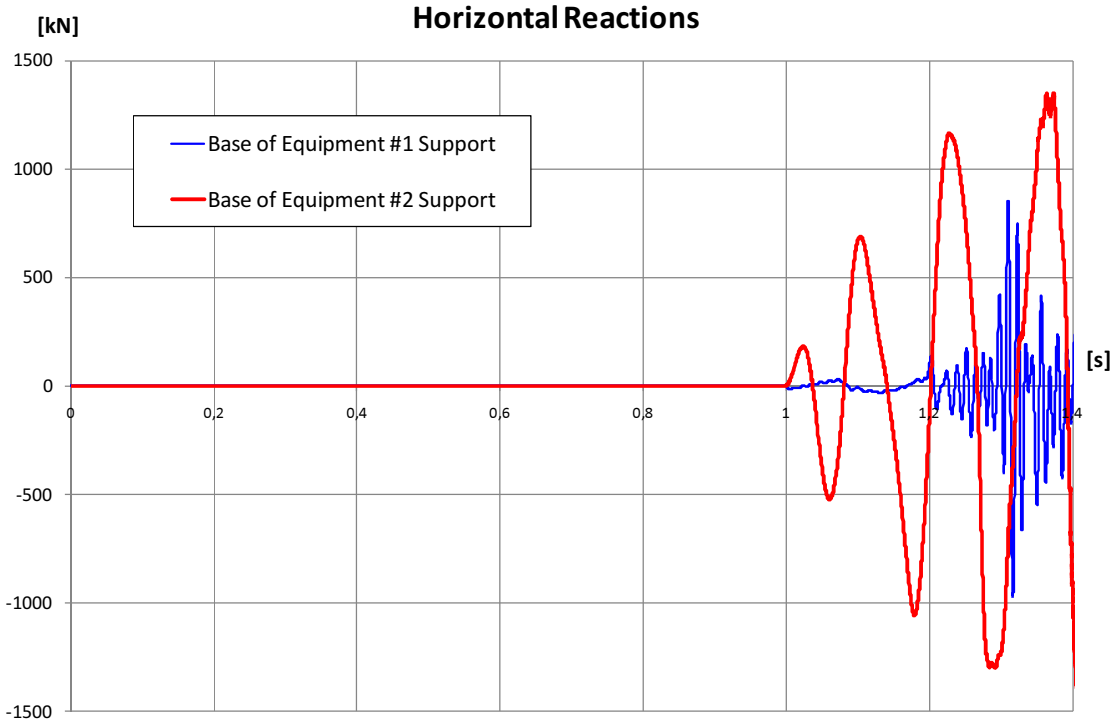

Figure 9-15: Sine-start test #4, horizontal reactions

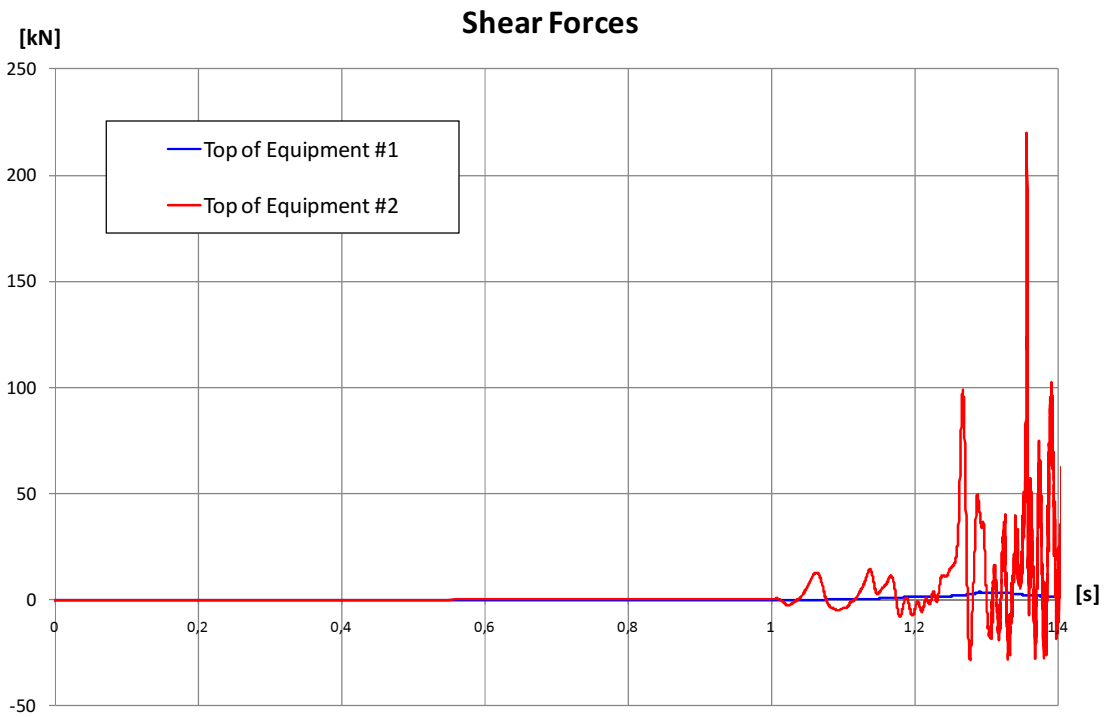

Figure 9-16: Sine-start test #4, shear forces

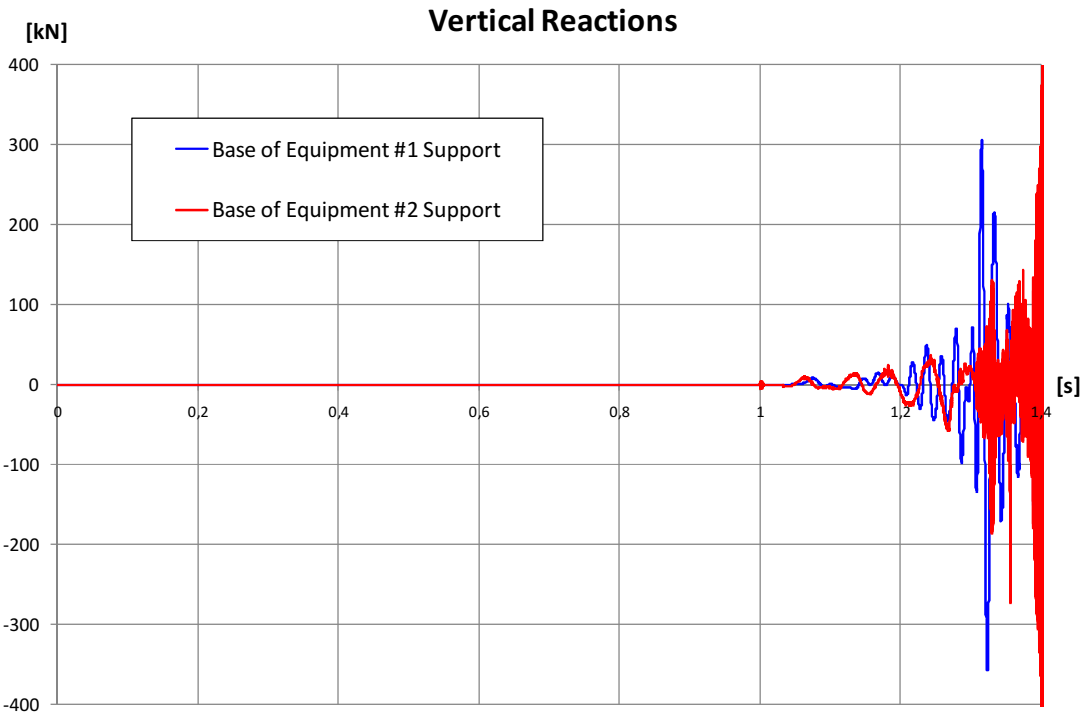

Figure 9-17: Sine-start test #4, vertical reactions

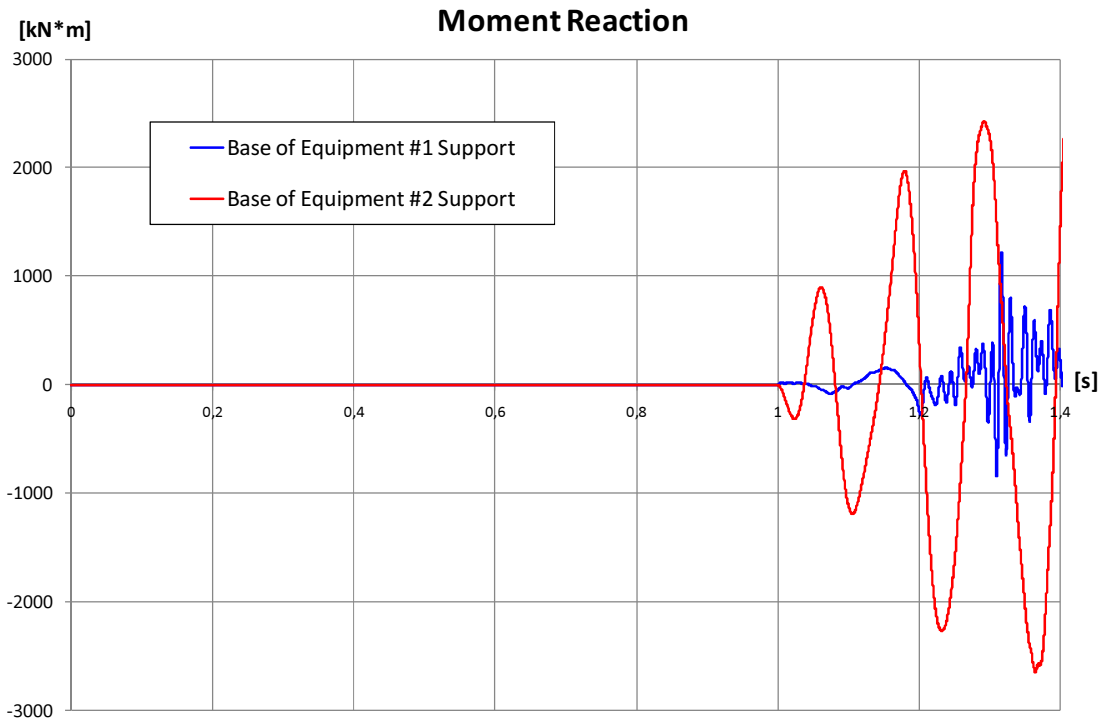

Figure 9-18: Sine-start test #4, moment reactions

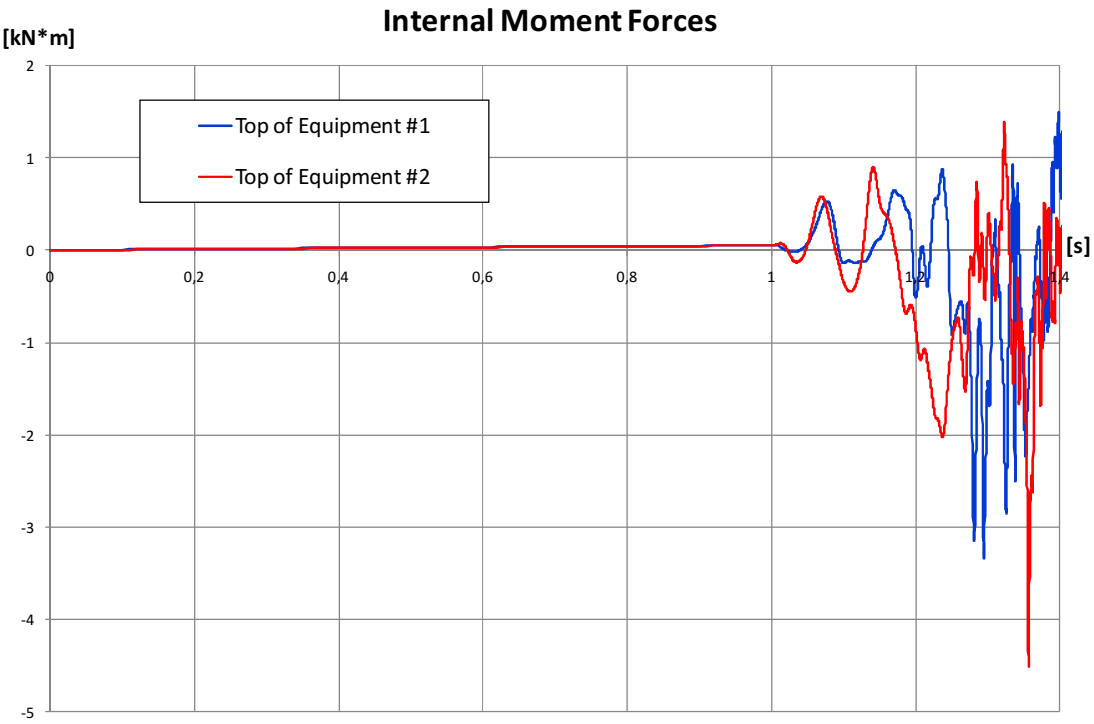

Figure 9-19: Sine-start test #4, internal moment

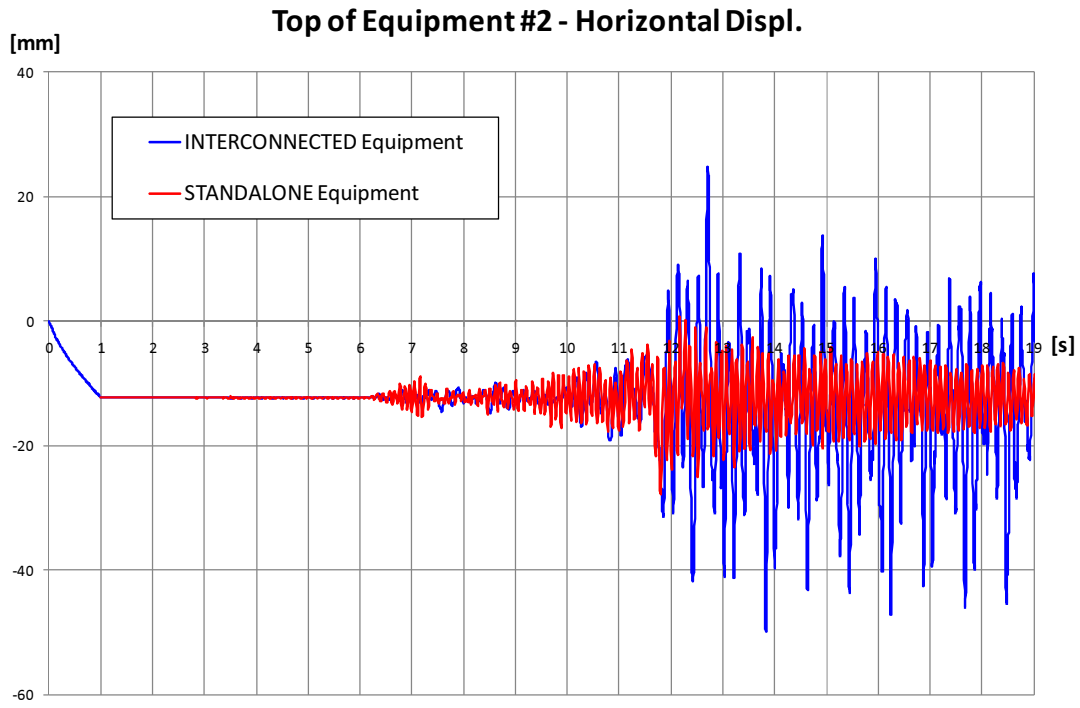

Figure 9-20: Base motion, relative horizontal displacements of the top of equipment #2

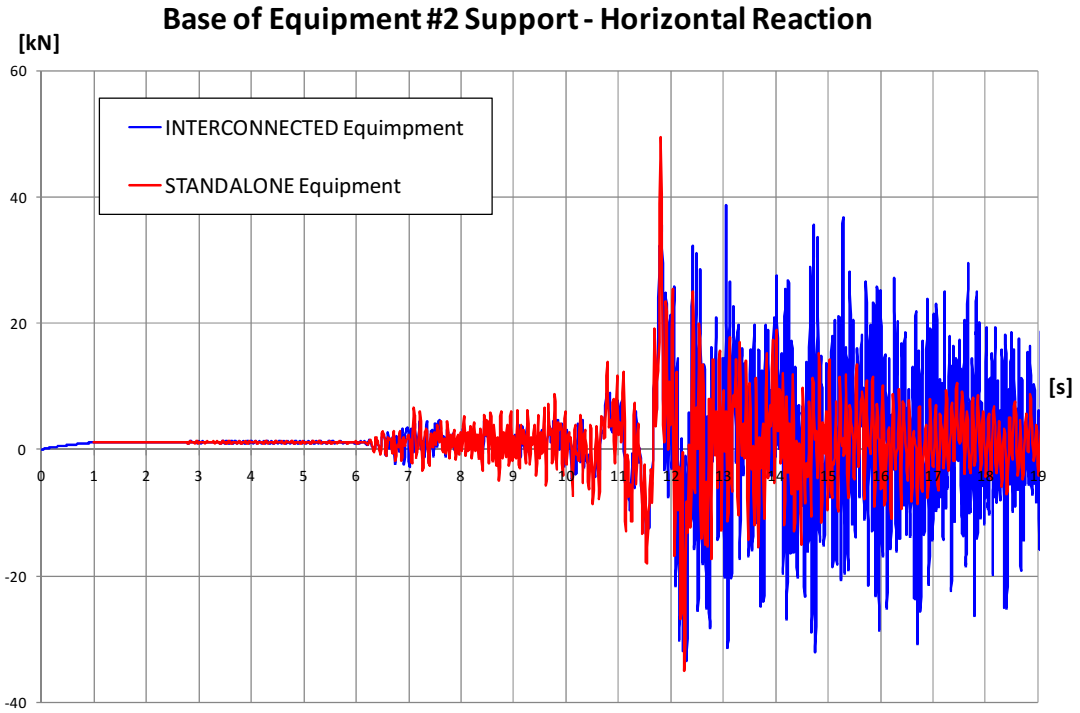

Figure 9-21: Base motion, horizontal reaction at the base of equipment #2

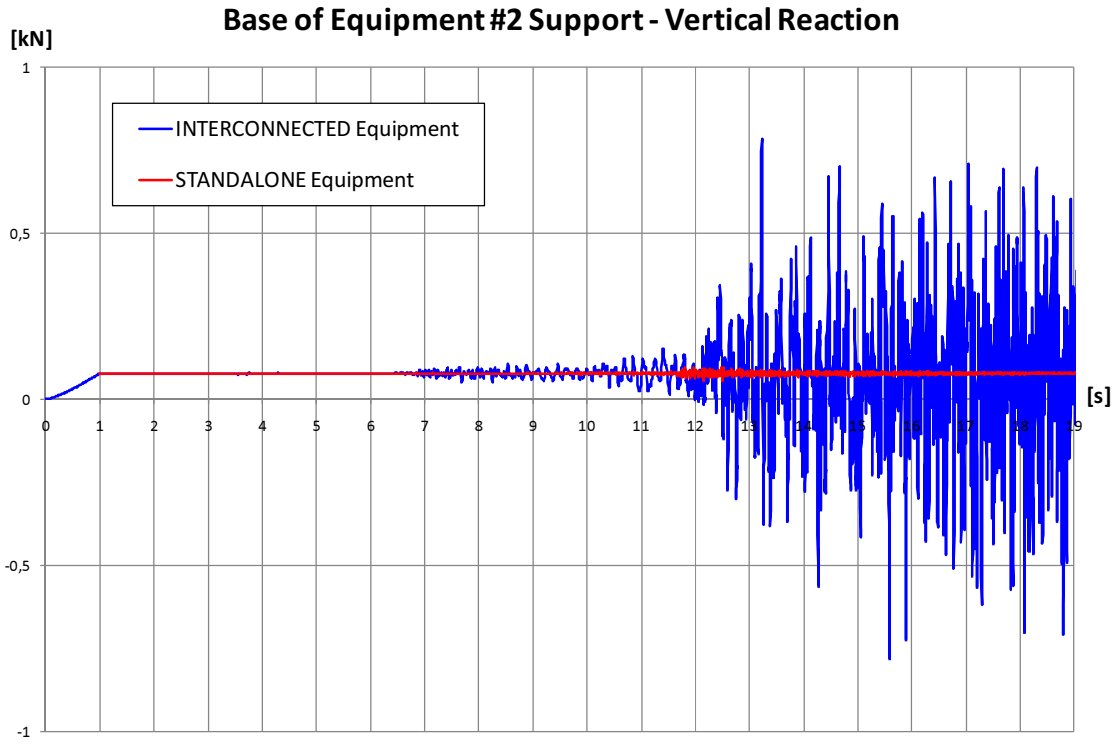

Figure 9-22: Base motion, vertical reaction at the base of equipment #2

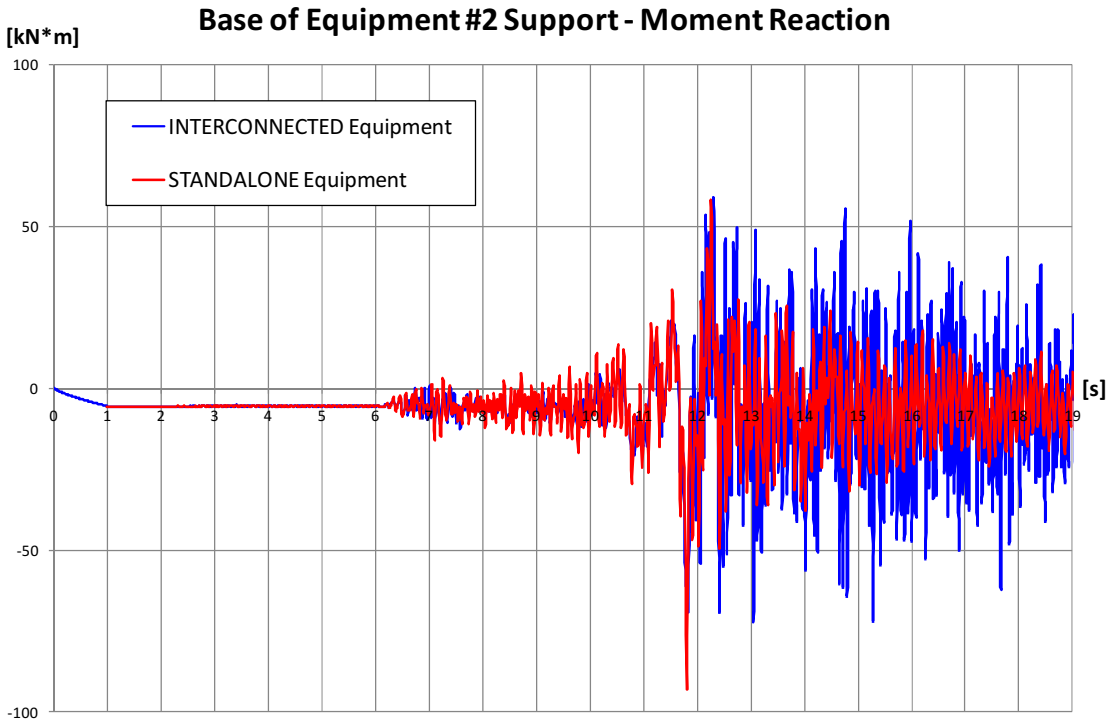

Figure 9-23: Base motion, moment reaction at the base of equipment #2

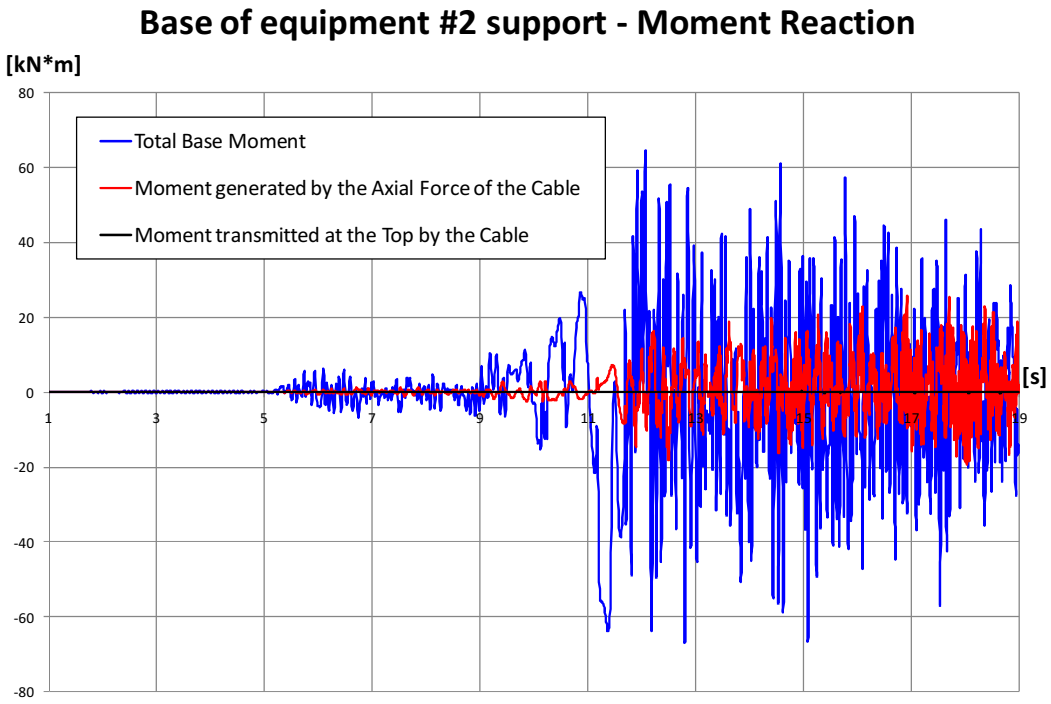

Figure 9-24: Base motion, components of the moment reaction at the base of equipment #2

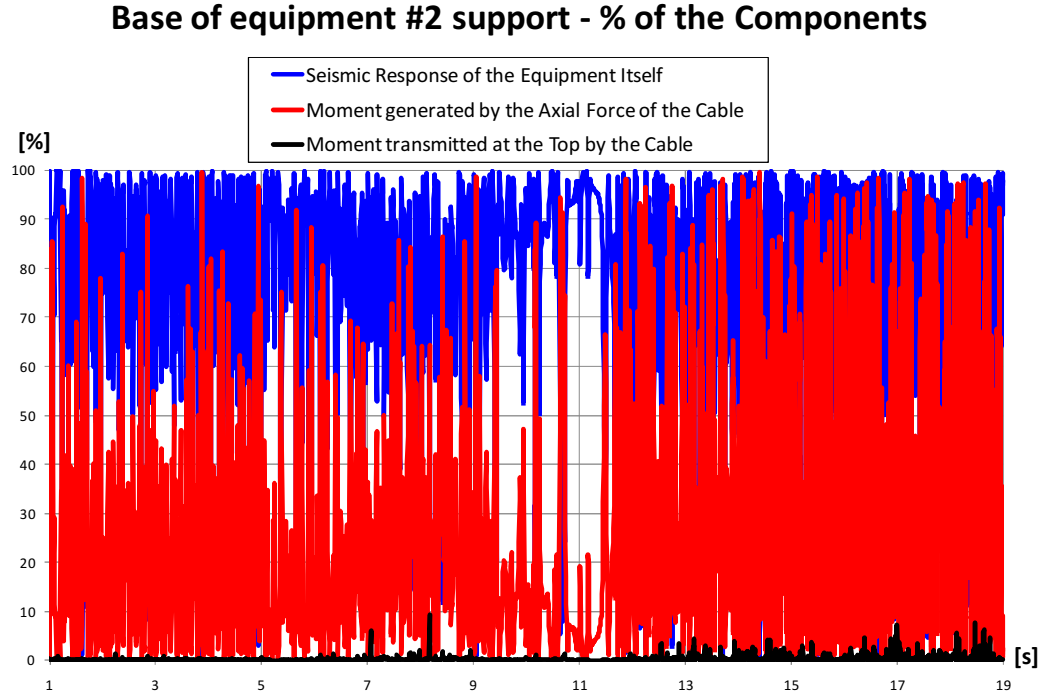

Figure 9-25: Base motion, percentages of the components of the moment reaction at the base of equipment #2